

Ali Kaveh · Majid Ilchi Ghazaan

Meta-heuristic Algorithms for Optimal Design of Real-Size Structures



Springer

Meta-heuristic Algorithms for Optimal Design of Real-Size Structures

Ali Kaveh · Majid Ilchi Ghazaan

Meta-heuristic Algorithms for Optimal Design of Real-Size Structures



Springer

Ali Kaveh
Department of Civil Engineering
Iran University of Science and Technology
Tehran
Iran

Majid Ilchi Ghazaan
Department of Civil Engineering
Iran University of Science and Technology
Tehran
Iran

ISBN 978-3-319-78779-4 ISBN 978-3-319-78780-0 (eBook)
<https://doi.org/10.1007/978-3-319-78780-0>

Library of Congress Control Number: 2018937691

© Springer International Publishing AG, part of Springer Nature 2018

This work is subject to copyright. All rights are reserved by the Publisher, whether the whole or part of the material is concerned, specifically the rights of translation, reprinting, reuse of illustrations, recitation, broadcasting, reproduction on microfilms or in any other physical way, and transmission or information storage and retrieval, electronic adaptation, computer software, or by similar or dissimilar methodology now known or hereafter developed.

The use of general descriptive names, registered names, trademarks, service marks, etc. in this publication does not imply, even in the absence of a specific statement, that such names are exempt from the relevant protective laws and regulations and therefore free for general use.

The publisher, the authors and the editors are safe to assume that the advice and information in this book are believed to be true and accurate at the date of publication. Neither the publisher nor the authors or the editors give a warranty, express or implied, with respect to the material contained herein or for any errors or omissions that may have been made. The publisher remains neutral with regard to jurisdictional claims in published maps and institutional affiliations.

Printed on acid-free paper

This Springer imprint is published by the registered company Springer International Publishing AG
part of Springer Nature
The registered company address is: Gewerbestrasse 11, 6330 Cham, Switzerland

Preface

The importance of optimization is permanently increasing in today's world due to limitations in available resources and increase in human population. Engineers always strive to design efficient structural systems which must be as economical as possible yet strong enough to withstand the most demanding functional requirements arising during their service life. The traditional trial-and-error structural design approach is not sufficient to achieve designs satisfying economical and safety criteria simultaneously.

There are a large number of developed methods that may be used to determine the solution of optimum design problems. These can be collected under two broad categories of analytical methods and numerical optimization techniques. Analytical methods are usually employed for finding minimum and maximum values of a function by using classical mathematical tools. These methods find the optimum solution as the exact solution of the system of equations which expresses the conditions for optimality. Although analytical methods are suitable tools for fundamental studies of single structural components, these are not suitable to determine the optimum solution of large-scale structural systems. Recently developed stochastic search algorithms, however, have provided an efficient tool for solving large-scale problems. These stochastic search algorithms usually make use of the ideas taken from the nature and do not require gradient computations of the objective function and constraints as is the case in mathematical programming based optimum design methods.

Structural optimization has matured from a narrow academic discipline, where researchers focused on optimum design of small idealized structural components and systems, to be the basis for modern design of complex structural systems. The present book contributes to this expanding discipline by focusing on the optimization of large-scale structures with numerous design variables. Four of the most well-known and efficient optimization algorithms are presented, and their results are compared to propose a suitable optimization technique for this class of problems. These algorithms are *Colliding Bodies Optimization*, *Enhanced Colliding Bodies Optimization*, *Vibrating Particles System* and a hybrid algorithm based on *Vibrating Particles System*, *Multi Design Variable Configurations Cascade*.

Optimization, and Upper Bound Strategy. From these four algorithms, the last one is highly suitable for large-scale problems. In the cascade optimization strategy, several optimizers can be used, one followed by another in a specified sequence, to solve a large-scale problem. In this procedure, the first optimizer starts from a user-specified design known as “cold-start”. The optimal solution achieved in the first cascade stage is called a “hot-start” and is used to initiate the second optimization stage. Accordingly, each optimization stage of the cascade procedure starts from the optimum design achieved in the previous stage. Therefore, each cascade stage except the first one initiates from a hot-start and produces a new hot-start for the next stage. In general, the optimization algorithm implemented at each stage of a cascade process may or may not be the same.

In this book, optimal design of different space structures is performed with different types of limitations such as strength, buckling, displacement, and natural frequencies. The considered structures consist of double-layer grids, barrel vaults, domes, antennas, and steel frames.

This book can be considered as an application of meta-heuristic algorithms to optimal design of skeletal structures. The present book is addressed to those scientists, engineers, and students who wish to explore the potentials of newly developed meta-heuristics. The concepts presented in this book are not only applicable to skeletal structures and finite element models but can equally be used for designing other systems such as hydraulic and electrical networks. The author and his graduate students have been involved in various developments and applications of different meta-heuristic algorithms to structural optimization in the last two decades. This book contains part of this research suitable for various aspects of optimization for skeletal structures. This book is likely to be of interest to civil, mechanical, and electrical engineers who use optimization methods for design, as well as to those students and researchers in structural optimization who will find it to be necessary professional reading.

In Chap. 1, a short introduction is provided for the development of optimization and different meta-heuristic algorithms. Chapter 2 presents an explanation of the meta-heuristic algorithms utilized in this book. In Chap. 3, optimal design of well-known structural optimization benchmark problems is discussed. Chapter 4 considers optimum design of large-scale special truss structures. Chapter 5 deals with optimal design of large-scale double-layer grids. Chapter 6 provides optimal design of large-scale barrel vaults. Chap. 7 deals with optimal design of dome structures. Chapter 8 discusses optimal design of steel lattice transmission line towers. Chapter 9 provides optimum seismic design of 3D steel frames. Appendix A provides the computer codes developed for configuration processing of the structures.

We would like to take this opportunity to acknowledge a deep sense of gratitude to a number of colleagues and friends who, in different ways, have helped in the preparation of this book. Professor Ch. Bucher encouraged and supported the first author to write this book. Our special thanks are due to Ms. Silvia Schilgerius, the senior editor of the Applied Sciences of Springer, for her constructive comments, editing, and unfailing kindness in the course of the preparation of this book.

My sincere appreciation is extended to our Springer colleague Mr. J. Komala for excellent typesetting of the book.

We would like to thank Dr. A. Zolghadr for proofreading of this book. We would like to thank the publishers who permitted some of our papers to be utilized in the preparation of this book, consisting of Springer Verlag, Elsevier, and Wiley. Our warmest gratitude is due to our family for their continued support in the course of preparing this book.

Every effort has been made to render the book error free. However, the authors would appreciate any remaining errors being brought to their attention through the following email addresses:

alikaveh@iust.ac.ir

majilchi@civileng.iust.ac.ir

Tehran, Iran

April 2018

Ali Kaveh
Majid Ilchi Ghazaan

Contents

1	Introduction	1
1.1	Structural Optimization Using Meta-heuristic Algorithms	1
1.2	Goals and Organization of the Present Book	3
References		4
2	Optimization Algorithms Utilized in This Book	7
2.1	Introduction	7
2.2	Colliding Bodies Optimization Algorithm	7
2.2.1	Theory of Collision Between Two Bodies	8
2.2.2	Presentation of CBO	9
2.3	The Enhanced Colliding Bodies Optimization Algorithm	11
2.4	Vibrating Particles System Algorithm	13
2.4.1	Damped Free Vibration	13
2.4.2	Presentation of VPS	15
2.5	The MDVC-UVPS Algorithm	18
2.5.1	The Multi-Design Variable Configurations Cascade Optimization	18
2.5.2	The Upper Bound Strategy	19
2.5.3	Presentation of MDVC-UVPS	20
References		21
3	Optimal Design of Usual-Size Skeletal Structures	23
3.1	Introduction	23
3.2	Numerical Examples with Frequency Constraints	24
3.2.1	A 72-Bar Space Truss Problem	24
3.2.2	A Spatial 120-Bar Dome-Shaped Truss Problem	25
3.2.3	A 200-Bar Planar Truss Problem	28

3.3	Numerical Examples with Strength Constraints	32
3.3.1	A Spatial 120-Bar Dome-Shaped Truss Problem	32
3.3.2	A 3-Bay 15-Story Frame Problem	34
3.3.3	A 3-Bay 24-Story Frame Problem	40
3.4	Concluding Remarks	40
	References	43
4	Optimal Design of Large-Scale Special Truss Structures	45
4.1	Introduction	45
4.2	Optimum Design Problem of Steel Trusses	45
4.3	Design Examples	47
4.3.1	A Spatial 582-Bar Tower Truss	47
4.3.2	A Spatial 942-Bar Tower Truss	50
4.3.3	A Spatial 2386-Bar Tower Truss	50
4.4	Concluding Remarks	55
	References	63
5	Optimal Design of Double-Layer Grids	65
5.1	Introduction	65
5.2	Optimal Design of Double-Layer Grids	66
5.3	Design Problems	67
5.3.1	A 520-Bar Double-Layer Grid	69
5.3.2	A 672-Bar Double-Layer Grid	69
5.3.3	A 800-Bar Double-Layer Grid	74
5.3.4	A 1016-Bar Double-Layer Grid	75
5.3.5	A 1520-Bar Double-Layer Grid	77
5.4	Concluding Remarks	80
	References	83
6	Optimal Design of Double-Layer Barrel Vault Space Structures	85
6.1	Introduction	85
6.2	Optimal Design of Double-Layer Barrel Vaults	86
6.3	Design Examples	87
6.3.1	A 384-Bar Double-Layer Barrel Vault	89
6.3.2	A 693-Bar Double-Layer Barrel Vault	89
6.3.3	A 1536-Bar Double-Layer Barrel Vault	92
6.4	Concluding Remarks	98
	References	98
7	Optimal Design of Dome-Shaped Trusses	101
7.1	Introduction	101
7.2	Frequency Constraint Optimization Problem	102
7.3	Design Examples	103

7.3.1	A 600-Bar Dome Truss	104
7.3.2	A 1180-Bar Dome Truss	107
7.3.3	A 1410-Bar Dome Truss	115
7.4	Concluding Remarks	121
	References	122
8	Optimal Design of Steel Lattice Transmission Line Towers	123
8.1	Introduction	123
8.2	Optimal Design of Transmission Line Towers	124
8.3	Design Problems	124
8.3.1	A 47-Bar Power Transmission Tower	125
8.3.2	A 160-Bar Power Transmission Tower	129
8.3.3	A 244-Bar Power Transmission Tower	133
8.4	Concluding Remarks	135
	References	137
9	Optimal Seismic Design of 3D Steel Frames	139
9.1	Introduction	139
9.2	Optimum Design Problem of Steel Space Frame	140
9.2.1	Design Constraints	141
9.2.2	The Objective Function	142
9.3	Design Examples	143
9.3.1	A Four-Story 132-Member Steel Frame	145
9.3.2	A Four-Story 428-Member Steel Frame	146
9.3.3	A Twelve-Story 276-Member Steel Frame	150
9.4	Concluding Remarks	151
	References	154
	Appendix A: Configuration Processing	157

Chapter 1

Introduction



1.1 Structural Optimization Using Meta-heuristic Algorithms

The action of making the best or most effective use of a situation or resource is called optimization. Optimization problems are studied in different fields and various steps need to be taken to achieve an optimal solution for a problem. These steps are as follows: The parameters of the problem, which can be either continuous or discrete, should be recognized. The objective function(s) and the constraints of the problem have to be identified. At the end, a suitable optimizer should be chosen and employed to solve the problem.

Structural optimization is a critical and challenging field that has received considerable attention by engineers and researchers. These optimization problems can be classified as follows: (1) obtaining optimal size of structural members (sizing optimization); (2) finding the optimal form for the structure (shape optimization); and (3) achieving optimal size and connectivity between structural members (topology optimization). The main concept of this book is to propose a suitable optimization technique for size optimization of real-size structures where the search space has a large size and a great number of design constraints must be controlled.

In the past, the most commonly used optimization techniques were gradient-based algorithms which utilized gradient information to search the solution space near an initial starting point [1, 2]. In general, gradient-based methods converge faster and can obtain solutions with higher accuracy compared to stochastic approaches. However, the acquisition of gradient information can be either costly or even impossible to obtain the minima. Moreover, these kinds of algorithms only guarantee convergence to local minima. Furthermore, a good starting point is quite vital for a successful execution of these methods. In many optimization problems, prohibited zones, side limits, and non-smooth or non-convex functions should be taken into consideration. As a result, these non-convex optimization problems cannot be solved easily by these methods.

On the other hand, other types of optimization methods, known as meta-heuristic algorithms, do not suffer the abovementioned restrictions. These methods are suitable for global search due to their capability of exploring and finding promising regions in the search space in an affordable computational time. Meta-heuristic algorithms tend to perform well for most of the optimization problems [3, 4]. This is because these methods refrain from simplifying or making assumptions about the original problem. Evidence of this is provided by their successful applications to a vast variety of fields, such as engineering, physics, chemistry, art, economics, marketing, genetics, operations research, robotics, social sciences, and politics.

A heuristic method can be considered as a procedure that is likely to discover a very good feasible solution, but not necessarily an optimal solution, for a considered specific problem. No guarantee can be provided about the quality of the solution obtained, but a well-designed heuristic method usually can provide a solution that is at least nearly optimal. The procedure also should be sufficiently efficient to deal with very large problems. Heuristic methods are often considered as *iterative algorithms*, where each iteration involves conducting a search for a new solution that might be better than the best solution found previously. After a reasonable time when the algorithm is terminated, the solution it provides is the best one that was found during all iterations. A meta-heuristic is formally defined as an iterative generation process which guides a subordinate heuristic by combining intelligently different concepts for exploring (global search) and exploiting (local search) the search space; learning strategies are used to structure information in order to find efficiently near-optimal solutions [5–7].

Since the 1970s, many meta-heuristic algorithms have been developed and applied to different optimization problems. In terms of the source of inspiration, meta-heuristics can be generally classified into three categories:

1. Evolutionary algorithms: They mimic the concepts of evolution in nature like Genetic Algorithm (GA) [8], Differential Evolution (DE) [9], Evolutionary Strategy (ES) [10], Evolutionary Programming (EP) [11, 12], and Biogeography-Based Optimization (BBO) algorithm [13].
2. Swarm algorithms: these techniques mimic the processes of decentralized, self-organized systems, which can be either natural or artificial in nature like Ant Colony Optimization (ACO) [14], Particle Swarm Optimization (PSO) [15], Artificial Bee Colony (ABC) algorithm [16], Cuckoo Search (CS) algorithm [17], Firefly Algorithm (FA) [18], Bat Algorithm (BA) [19], Dolphin Echolocation (DE) [20], and Cyclical Parthenogenesis Algorithm (CPA) [21].
3. Physical algorithms: These methods are inspired by the physical laws like Simulated Annealing (SA) [22], Charged System Search (CSS) [23], Ray Optimization (RO) [24], Water Evaporation Optimization (WEO) [25], and Thermal Exchange Optimization (TEO) [26].

A complete explanation of various recently developed meta-heuristic algorithms and their applications can be found in Kaveh [27, 28].

1.2 Goals and Organization of the Present Book

Sizing optimization problems are very popular design problems and can be found frequently in literature. The contribution of this book is concerned with size optimization of real-size structures with numerous design variables. Various types of structures with different design constraints are studied. Four efficient optimization algorithms will be presented and their results are compared to propose a suitable optimization technique for this class of problems.

The remaining chapters of this book are organized in the following manner:

Chapter 2 presents the rules of the optimization algorithms employed in this book. These algorithms consist of Colliding Bodies Optimization (CBO) [29], Enhanced Colliding Bodies Optimization (ECBO) [30], Vibrating Particles System (VPS) [31], and a hybrid algorithm called MDVC-UVPS [32].

Chapter 3 presents a comparison between the results obtained by proposed algorithms and some well-known state-of-the-art meta-heuristics for usual-size skeletal structures. Four truss design examples and two frame design examples with continuous and discrete sizing variables are studied in this chapter. Different types of constraints (i.e., natural frequency constraints and strength and displacement constraints) are considered for benchmarks.

Chapter 4 presents optimal design of three spatial tower trusses. The examples have 582, 942, and 2386 elements and contain 32, 76, and 220 variables, respectively. All of the structures are designed according to AISC-ASD provisions [33] and the cross-sectional areas of the bar elements are selected from W-shape profile list.

Chapter 5 deals with the design optimization of five double-layer grids with different configurations. The examples contain larger square on square, square on larger square, square on square, square on diagonal, and diagonal on diagonal double-layer grids. Strength and slenderness limitations are imposed according to AISC-LRFD provisions [34].

Chapter 6 deals with size optimization of three double-layer barrel roof structures. These examples consist of a 384-bar double-layer barrel vault, a 693-bar double-layer barrel vault, and a 1536-bar double-layer barrel vault. The structures are subjected to stress, stability, and displacement limitations according to the provisions of AISC-ASD [31]. The design variables are the cross-sectional areas of the bar elements which are selected from steel pipe sections.

Chapter 7 examines the abilities of the proposed methods for size optimization of dome-shaped trusses. Three dome truss design examples with 600, 1180, and 1410 elements are studied in this chapter. Two different constraint cases are considered for each example (i.e., natural frequency constraints and strength and displacement constraints).

Chapter 8 presents the application of the proposed algorithms for optimization of steel lattice transmission line towers. Three benchmark structural examples including 47-bar, 160-bar, and 244-bar power transmission towers are studied in this chapter. The design variables are the cross-sectional areas of the bar elements

and in all problems, solution candidates are allowed to select discrete values from a permissible list of cross sections.

Chapter 9 deals with the optimization of 3D steel frames under seismic loads based on response spectra. Three irregular steel frame problems (i.e., four-story 132-member, four-story 428-member, and twelve-story 276-member steel frames) are considered to evaluate the performance of the proposed algorithms. The frames are designed according to the LRFD-AISC design criteria [35]. Load combinations recommended by ASCE 7-10 [36] are considered and the frames are Intermediate Moment Frames (IMF).

References

1. Majid KI (1974) Optimum design of structures. Newness-Butterworth, UK
2. Kirsch U (1993) Structural optimization: fundamentals and applications. Springer, Berlin
3. Gonzalez TF (ed) (2007) Handbook of approximation algorithms and metaheuristics. Computer and information science series. Chapman & Hall/CRC, Boca Raton, FL
4. Yang X-S (2010) Nature-inspired metaheuristic algorithms, 2nd edn. Luniver Press, UK
5. Glover F, Kochenberger GA (eds) (2003) Handbook of metaheuristics. Kluwer Academic Publishers, Dordrecht
6. Voß S, Martello S, Osman IH, Roucairol C (eds) (1999) Metaheuristics: advances and trends in local search paradigms for optimization. Kluwer Academic Publishers, Norwell, MA
7. Osman IH, Laporte G (1996) Metaheuristics: a bibliography. Ann Oper Res 63:513–623
8. Goldberg DE, Holland JH (1988) Genetic algorithms and machine learning. Mach Learn 3:95–99
9. Storn R, Price K (1997) Differential evolution—a simple and efficient heuristic for global optimization over continuous spaces. J Global Optim 11:341–359
10. Rechenberg I (1973) Evolution strategy: optimization of technical systems by means of biological evolution, vol 104. Fromman-Holzboog, Stuttgart, pp 15–16
11. Fogel LJ, Owens AJ, Walsh MJ (1966) Artificial intelligence through simulated evolution. Wiley, Hoboken
12. Yao X, Liu Y, Lin G (1999) Evolutionary programming made faster. Evol Comput IEEE Trans 3:82–102
13. Simon D (2008) Biogeography-based optimization. Evol Comput IEEE Trans 12:702–713
14. Colomni A, Dorigo M, Maniezzo V (1991) Distributed optimization by ant colonies. In: Proceedings of the first European conference on artificial life, pp 134–142
15. Eberhart RC, Kennedy J (1995) A new optimizer using particle swarm theory. In: Proceedings of the sixth international symposium on micro machine and human science, pp 39–43
16. Karaboga D, Basturk B (2007) A powerful and efficient algorithm for numerical function optimization: artificial bee colony (ABC) algorithm. J Global Optim 39:459–471
17. Yang XS, Deb S (2009) Cuckoo search via Lévy flights. In: Nature & biologically inspired computing, pp 210–214
18. Yang XS (2010) Engineering optimization: an introduction with metaheuristic applications, Wiley, PP. 221–230
19. Yang XS (2010) A new metaheuristic bat-inspired algorithm. In: Nature inspired cooperative strategies for optimization (NISCO 2010). Springer, Berlin, 65–74
20. Kaveh A, Farhoudi N (2013) A new optimization method: dolphin echolocation. Adv Eng Software 59:53–70
21. Kaveh A, Zolghadr A (2017) Cyclical parthenogenesis algorithm for guided modal strain energy based structural damage detection. Appl Soft Comput 57:250–264

22. Kirkpatrick S, Gelatt CD, Vecchi MP (1983) Optimization by simulated annealing. *Science* 220(4598):671–680
23. Kaveh A, Talatahari S (2010) A novel heuristic optimization method: charged system search. *Acta Mech* 213(3):267–289
24. Kaveh A, Khayatazarad M (2012) A new meta-heuristic method: ray optimization. *Comput Struct* 112:283–294
25. Kaveh A, Bakhshpoori T (2016) Water evaporation optimization: a novel physically inspired optimization algorithm. *Comput Struct* 167:69–85
26. Kaveh A, Dadras A (2017) A novel meta-heuristic optimization algorithm: thermal exchange optimization. *Adv Eng Softw* 110:69–84
27. Kaveh A (2017) Advances in metaheuristic algorithms for optimal design of structures, 2nd edn. Springer International Publishing, Switzerland
28. Kaveh A (2017) Applications of metaheuristic optimization algorithms in civil engineering. Springer, Switzerland
29. Kaveh A, Mahdavi VR (2014) Colliding bodies optimization: a novel meta-heuristic method. *Comput Struct* 139:18–27
30. Kaveh A, Ilchi Ghazaan M (2014) Enhanced colliding bodies optimization for design problems with continuous and discrete variables. *Adv Eng Softw* 77:66–75
31. Kaveh A, Ilchi Ghazaan M (2017) Vibrating particles system algorithm for truss optimization with multiple natural frequency constraints. *Acta Mech* 228(1):307–322
32. Kaveh A, Ilchi Ghazaan M (2018) A new hybrid meta-heuristic algorithm for optimal design of large-scale dome structures. *Eng Optimiz* 50(2):235–252
33. American Institute of Steel Construction (AISC) (1989) Manual of steel construction: allowable stress design, Chicago, USA
34. American Institute of Steel Construction (AISC) (1994) Manual of steel construction load resistance factor design, USA
35. AISC 360-10 (2010). Specification for structural steel buildings. American Institute of Steel Construction, Chicago, Illinois 60601-1802, USA
36. ASCE 7-10 (2010) Minimum design loads for building and other structures

Chapter 2

Optimization Algorithms Utilized in This Book



2.1 Introduction

The main features and rules of the optimization algorithms utilized in this book are explained in this chapter. These algorithms consist of Colliding Bodies Optimization (CBO) [1], Enhanced Colliding Bodies Optimization (ECBO) [2], Vibrating Particles System (VPS) [3], and a hybrid algorithm called MDVC-UVPS [4]. All of the algorithms considered here are recently developed and are multi-agent meta-heuristic methods. These algorithms start with a set of randomly selected candidate solutions of the optimization problem and according to a series of simple rules, mainly inspired by the nature, the existing solutions are perturbed iteratively in order to improve their cost function values. Many other recently developed meta-heuristic algorithms and their applications can be found in the recently published books of Kaveh [5, 6].

2.2 Colliding Bodies Optimization Algorithm

Colliding Bodies Optimization (CBO) is an efficient meta-heuristic algorithm which is recently introduced by Kaveh and Mahdavi [1]. CBO is based on the governing physical laws of one-dimensional collision between two bodies which states that when an object collides with another one, they move toward minimum energy levels. CBO algorithm is simple in concept, depends on no internal parameters, and does not require memory for saving the best-so-far solutions.

2.2.1 Theory of Collision Between Two Bodies

Collisions between bodies are governed by the laws of momentum and energy. When a collision occurs in an isolated system between two objects (Fig. 2.1), the total momentum of the system of objects is conserved. Provided that there are no net external forces acting upon the objects, the total momentum of the objects before the collision equals the total momentum of the objects after the collision.

Conservation of total momentum can be expressed by the following equation:

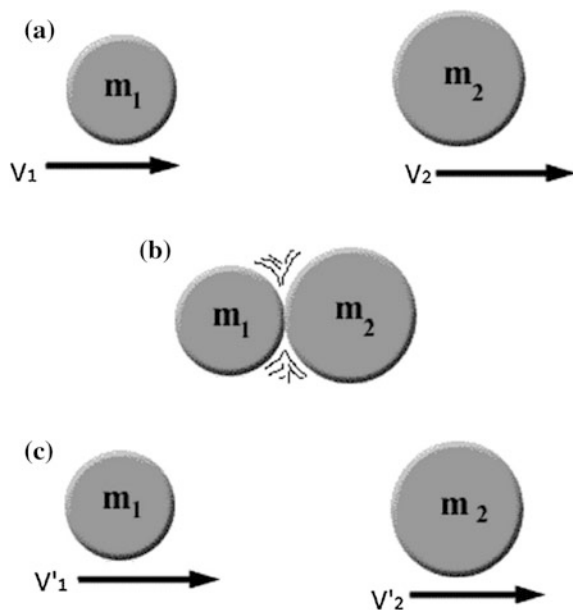
$$m_1 v_1 + m_2 v_2 = m_1 v'_1 + m_2 v'_2 \quad (2.1)$$

Likewise, the conservation of the total kinetic energy is expressed as

$$\frac{1}{2} m_1 v_1^2 + \frac{1}{2} m_2 v_2^2 = \frac{1}{2} m_1 v'_1^2 + \frac{1}{2} m_2 v'_2^2 + Q \quad (2.2)$$

where v_1 is the initial velocity of the first object before impact, v_2 is the initial velocity of the second object before impact, v'_1 is the final velocity of the first object after impact, v'_2 is the final velocity of the second object after impact, m_1 is the mass of the first object, m_2 is the mass of the second object, and Q is the loss of kinetic energy due to the impact [7].

Fig. 2.1 The collision between two bodies, **a** before collision, **b** at the time of collision, and **c** after collision



The formulas for the velocities after a one-dimensional collision are

$$v'_1 = \frac{(m_1 - \varepsilon m_2)v_1 + (m_2 + \varepsilon m_1)v_2}{m_1 + m_2} \quad (2.3)$$

$$v'_2 = \frac{(m_2 - \varepsilon m_1)v_2 + (m_1 + \varepsilon m_2)v_1}{m_1 + m_2} \quad (2.4)$$

where ε is the Coefficient Of Restitution (COR) of the two colliding bodies, defined as the ratio of the relative velocity of separation to the relative velocity of approach:

$$\varepsilon = \frac{|v'_2 - v'_1|}{|v_2 - v_1|} = \frac{v'}{v} \quad (2.5)$$

According to the coefficient of restitution, there are two special cases of any collision as follows:

1. A perfectly elastic collision is defined as the one in which there is no loss of kinetic energy in the collision ($Q = 0$ and $\varepsilon = 1$). In reality, any macroscopic collision between objects will convert some kinetic energy to internal energy and other forms of energy. In this case, after collision, the velocity of separation is high.
2. An inelastic collision is the one in which part of the kinetic energy is changed to some other forms of energy in the collision. Momentum is conserved in inelastic collisions (as it is for elastic collisions), but one cannot track the kinetic energy through the collision since some of it will be converted to other forms of energy. In this case, the coefficient of restitution is not equal to one ($Q \neq 0$ and $\varepsilon < 1$), and after collision the velocity of separation is low.

For most of the real objects, the value of ε is between 0 and 1.

2.2.2 *Presentation of CBO*

In CBO, each solution candidate is considered as a Colliding Body (CB) and these massed objects are composed of two main equal groups, i.e., stationary and moving objects, where the moving objects move to follow stationary objects and a collision occurs between pairs of objects. This is done for two purposes: (i) to improve the positions of moving objects; and (ii) to push stationary objects toward better positions. After the collision, the new positions of colliding bodies are updated based on their new velocities using the collision laws as discussed in the previous subsection. The procedure of CBO can be outlined as follows and its pseudocode is provided in Fig. 2.2.

Step 1 The initial positions of all colliding bodies are determined randomly in the search space.

procedure CBO

Initialize algorithm parameters

Initial positions are created randomly

The values of objective function and masses are evaluated

while maximum iterations is not fulfilled

Stationary and moving groups are created

for each CB

The velocity before the collision is evaluated by Eq. (2.7) or Eq. (2.8)

The velocity after the collision is evaluated by Eq. (2.9) or Eq. (2.10)

New location is updated by Eq. (2.12) or Eq. (2.13)

end for

The values of objective function and masses are evaluated

end while
end procedure

Fig. 2.2 Pseudocode of the CBO algorithm

Step 2 Each CB has a specified mass defined as

$$m_k = \frac{\frac{1}{\text{fit}(k)}}{\sum_{i=1}^n \frac{1}{\text{fit}(i)}}, \quad k = 1, 2, \dots, n \quad (2.6)$$

where $\text{fit}(i)$ represents the objective function value of the i th CB and n is the number of colliding bodies. In order to select pairs of objects for collision, CBs are sorted according to their mass in an decreasing order and they are divided into two equal groups: (i) stationary group and (ii) moving group (see Fig. 2.3). Moving objects collide with stationary objects to improve their positions and push stationary objects toward better positions.

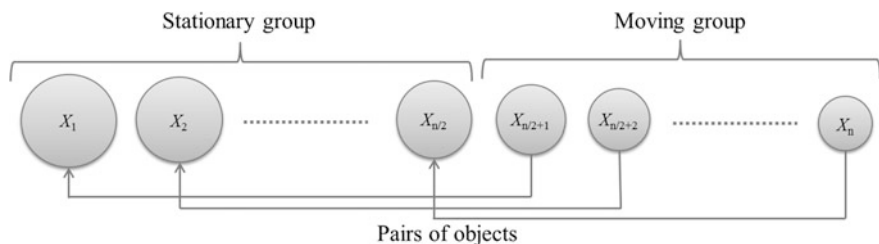


Fig. 2.3 The pairs of objects for collision

Step 3 The velocity of stationary bodies before collision is zero and moving objects move toward stationary objects:

$$v_i = 0, \quad i = 1, 2, \dots, \frac{n}{2} \quad (2.7)$$

$$v_i = x_{i-\frac{n}{2}} - x_i, \quad i = \frac{n}{2} + 1, \frac{n}{2} + 2, \dots, n \quad (2.8)$$

Step 4 The velocities of stationary and moving bodies after the collision (v'_i) are evaluated by

$$v'_i = \frac{(m_i + \frac{n}{2} + \varepsilon m_{i+\frac{n}{2}}) v_{i+\frac{n}{2}}}{m_i + m_{i+\frac{n}{2}}} \quad i = 1, 2, \dots, \frac{n}{2} \quad (2.9)$$

$$v'_i = \frac{\left(m_i - \varepsilon m_{i-\frac{n}{2}}\right) v_i}{m_i + m_{i-\frac{n}{2}}} \quad i = \frac{n}{2} + 1, \frac{n}{2} + 2, \dots, n \quad (2.10)$$

ε is the coefficient of restitution that decreases linearly from unit to zero. Thus, it is stated as

$$\varepsilon = 1 - \frac{\text{iter}}{\text{iter}_{\max}} \quad (2.11)$$

where iter is the current iteration number and iter_{\max} is the total number of iterations for optimization process.

Step 5 The new position of each stationary CB is

$$x_i^{new} = x_{i-\frac{n}{2}} + \text{rand} \circ v'_i, \quad i = \frac{n}{2} + 1, \frac{n}{2} + 2, \dots, n \quad (2.12)$$

where x_i^{new} , x_i , and v'_i are the new position, previous position, and the velocity after the collision of the i th CB, respectively. rand is a random vector uniformly distributed in the range of $[-1, 1]$ and the sign “ \circ ” denotes an element-by-element multiplication. The new position of each moving CB is calculated by

$$x_i^{new} = x_{i-\frac{n}{2}} + \text{rand} \circ v'_i, \quad i = \frac{n}{2} + 1, \frac{n}{2} + 2, \dots, n \quad (2.13)$$

Step 6 The optimization process is terminated after a fixed number of iterations. If this criterion is not satisfied, go to Step 2 for a new round of iteration.

2.3 The Enhanced Colliding Bodies Optimization Algorithm

In order to get faster and more reliable solutions, Enhanced Colliding Bodies Optimization (ECBO) is developed [2]. Memory which saves a number of the best-so-far solutions is used in ECBO to improve the algorithm's performance.

A mechanism is also defined to change some components of CBs randomly to afford a chance for the CBs to escape from local minima and prevent probable premature convergence. The steps of this technique are outlined in the following and its pseudocode is provided in Fig. 2.4.

- Step 1 The initial position vectors of all CBs are created randomly in the search space.
- Step 2 The value of mass for each CB is evaluated according to Eq. (2.6).
- Step 3 Colliding Memory (CM) is utilized to save a number of historically best CB vectors and their related mass and objective function values. Solution vectors which are saved in CM are added to the population and the same number of current worst CBs are deleted. Finally, CBs are sorted according to their objective function values in an increasing order. Using this mechanism can improve the algorithm's performance without increasing the computational cost.
- Step 4 CBs are composed of two main equal groups, i.e., stationary and moving groups. The pairs of CBs for collision are selected according to Fig. 2.3.
- Step 5 The velocity of stationary bodies before the collision is zero (Eq. (2.7)). Besides, moving objects move toward stationary objects and their velocities before the collision are calculated by Eq. (2.8).

```

procedure ECBO
    Initialize algorithm parameters
    Initial positions are created randomly
    The values of objective function and masses are evaluated
    while maximum iterations is not fulfilled
        Colliding memory is updated
        The population is updated
        Stationary and moving groups are created
        for each CB
            The velocity before the collision is evaluated by Eq. (2.7) or Eq. (2.8)
            The velocity after the collision is evaluated by Eq. (2.9) or Eq. (2.10)
            New location is updated by Eq. (2.12) or Eq. (2.13)
            If  $rn_j < pro$ 
                 $k \leftarrow \text{random\_int}(1, m)$       /*  $m$  is the number of variables */
                kth dimension is regenerated randomly in its allowable range
            end if
        end for
        The values of objective function and masses are evaluated
    end while
end procedure

```

Fig. 2.4 Pseudocode of the ECBO algorithm

- Step 6 The velocities of stationary and moving bodies after collision are evaluated by Eqs. (2.9) and (2.10), respectively.
- Step 7 The new position of each CB is calculated by Eqs. (2.12) and (2.13).
- Step 8 To improve the exploration capabilities of the standard CBO and to prevent premature convergence, a stochastic approach is employed in ECBO. A parameter like ***Pro*** within (0, 1) is introduced to specify whether a component of each CB must be changed or not. For each colliding body, ***Pro*** is compared with r_n ($i = 1, 2, \dots, n$) which is a random number uniformly distributed within (0, 1). If $r_n < pro$, one dimension of the i th CB is selected randomly and its value is regenerated by

$$x_i^j = x_{\min}^j + \text{random} (x_{\max}^j - x_{\min}^j) \quad (2.14)$$

where x_i^j is the j th variable of the i th CB. x_{\min}^j and x_{\max}^j are the minimum and maximum limits of the j th variable. In order to protect the structures of CBs, only one dimension is changed.

- Step 9 The process of optimization is terminated after a predefined maximum number of objective function evaluations. If it is not fulfilled, go to Step 2 for a new round of iteration.

2.4 Vibrating Particles System Algorithm

Vibrating Particles System (VPS) algorithm is a population-based algorithm which simulates free vibration of single degree of freedom systems with viscous damping [3]. Similar to other multi-agent methods, VPS has a number of individuals (or particles) consisting of the variables of the problem. The solution candidates gradually approach to their equilibrium positions which are determined using a combination of the current population and the historically best position in order to maintain a proper balance between diversification and intensification.

2.4.1 Damped Free Vibration

A vibration is the oscillating motion of a particle or a body about a position of equilibrium. In general, there are two types of vibrations: (1) free vibration and (2) forced vibration. When the motion is maintained by the restoring forces only, the vibration is said to be a free vibration and when a force is applied to the system, the resulting motion is described as a forced vibration. In the study of a vibrating system, the effects of friction can be neglected resulting in an undamped vibration. However, all vibrations are actually damped to some degree by friction forces.

These forces can be caused by dry friction, or Coulomb friction, between rigid bodies, by fluid friction when a rigid body moves in a fluid, or by internal friction between the molecules of a seemingly elastic body. In this section, the free vibration of single degree of freedom systems with viscous damping is studied. The viscous damping is caused by fluid friction at low and moderate speeds. Viscous damping is characterized by the fact that the friction force is directly proportional and opposite to the velocity of the moving body [8].

The vibrating motion of a body or system of mass m having viscous damping can be characterized by a block and a spring of constant k as it is shown in Fig. 2.5. The effect of damping is provided by the dashpot connected to the block, and the magnitude of the friction force exerted on the plunger by the surrounding fluid is equal to $c\dot{x}$ (c is the coefficient of viscous damping, and its value depends on the physical properties of the fluid and the construction of the dashpot). If the block is displaced a distance x from its equilibrium position, the equation of motion can be expressed as

$$m\ddot{x} + c\dot{x} + kx = 0 \quad (2.15)$$

Before presenting the solutions for this differential equation, the critical damping coefficient c_c is defined as

$$c_c = 2m\omega_n \quad (2.16)$$

$$\omega_n = \sqrt{\frac{k}{m}} \quad (2.17)$$

where ω_n is the natural circular frequency of the vibration.

Depending on the value of the coefficient of viscous damping, three different cases of damping can be distinguished: (1) over-damped system ($c > c_c$), (2) critically damped system ($c = c_c$), and (3) under-damped system ($c < c_c$). The solutions of over-damped and critically damped systems correspond to a non-vibratory motion. Therefore, the system only oscillates about its equilibrium position when $c < c_c$.

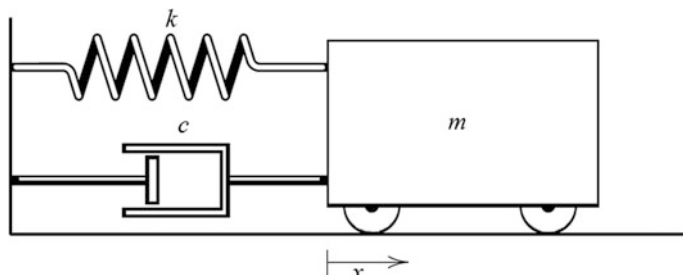


Fig. 2.5 Free vibration of a system with damping

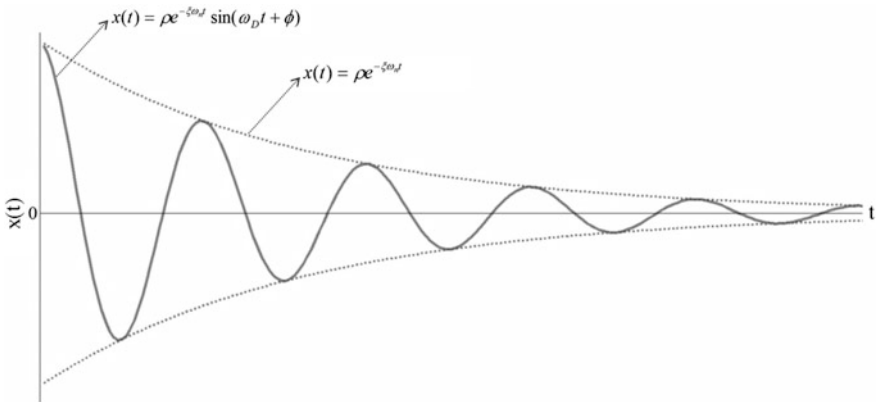


Fig. 2.6 Vibrating motion of under-damped system

The solution of Eq. (2.15) for under-damped system is as follows:

$$x(t) = \rho e^{-\xi\omega_n t} \sin(\omega_D t + \phi) \quad (2.18)$$

$$\omega_D = \omega_n \sqrt{1 - \xi^2} \quad (2.19)$$

$$\xi = \frac{c}{2m\omega_n} \quad (2.20)$$

where ρ and ϕ are constants generally determined from the initial conditions of the problem. ω_D and ξ are damped natural frequency and damping ratio, respectively. Equation (2.18) is shown in Fig. 2.6, and the effect of damping ratio on vibratory motion is illustrated in Fig. 2.7.

2.4.2 Presentation of VPS

In the VPS, the position of each particle is updated by learning from the historically best position of the entire population, a good particle, and a bad particle. By controlling the weights of these terms, a proper balance between the diversification and the intensification inclinations can be achieved. The VPS procedure can be outlined as follows and its pseudocode is provided in Fig. 2.8.

- Step 1 The initial positions of all particles are determined randomly in search space.
- Step 2 The objective function value is calculated for each particle.
- Step 3 For each particle, three equilibrium positions with different weights are defined that the particle tends to approach: (1) the best position achieved so far across the entire population (HB), (2) a good particle (GP), and

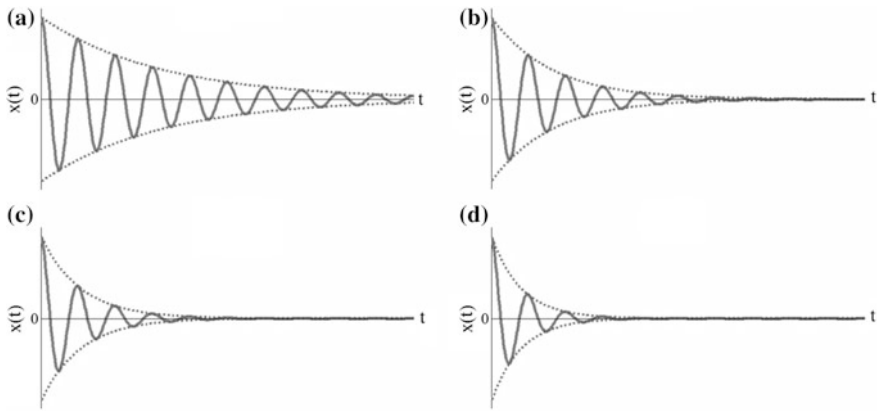


Fig. 2.7 Free vibration of systems with four levels of damping: **a** $\xi = 5\%$, **b** $\xi = 10\%$, **c** $\xi = 15\%$, and **d** $\xi = 20\%$

procedure VPS

 Initialize algorithm parameters

 Initial positions are created randomly

 The values of objective function are evaluated and *HB* is stored

while maximum iterations is not fulfilled

for each particle

 The GP and BP are chosen

if $P < \text{rand}$

$w_3 = 0$ and $w_2 = 1 - w_1$

end if

for each component

 New location is obtained by Eq. (2.22)

end for

 Violated components are regenerated by harmony search-based handling approach

end for

 The values of objective function are evaluated and *HB* is updated

end while

end procedure

Fig. 2.8 Pseudocode of the VPS algorithm

(3) a bad particle (BP). In order to select the GP and BP for each candidate solution, the current population is sorted according to their objective function values in an increasing order, and then GP and BP are chosen randomly from the first and second half, respectively.

Figure 2.7 shows the important effect of damping level in the vibration. In order to model this phenomenon in the optimization algorithm, a descending function that is proportional to the number of iterations is proposed as follows:

$$D = \left(\frac{\text{iter}}{\text{iter}_{\max}} \right)^{-\alpha} \quad (2.21)$$

where iter is the current iteration number and iter_{\max} is the total number of iterations for optimization process. α is a constant and Fig. 2.9 shows the effect of this parameter on D .

According to the mentioned concepts, the positions are updated by

$$x_i^j = w_1.[D.A.\text{rand } 1 + \text{HB}^j] + w_2.[D.A.\text{rand } 2 + \text{GP}^j] + w_3.[D.A.\text{rand } 3 + \text{BP}^j] \quad (2.22)$$

$$A = [w_1.(\text{HB}^j - x_i^j)] + [w_2.(\text{GP}^j - x_i^j)] + [w_3.(\text{BP}^j - x_i^j)] \quad (2.23)$$

$$w_1 + w_2 + w_3 = 1 \quad (2.24)$$

where x_i^j is the j th variable of particle i . w_1 , w_2 , and w_3 are three parameters to measure the relative importance of HB, GP, and BP, respectively. Here, rand1, rand2, and rand3 are random numbers uniformly distributed in the range of [0,1]. The effects of A and D parameters in Eq. (2.22) are similar to that of ρ and $e^{-\xi\omega_n t}$ in Eq. (2.18), respectively. Also, the value of $\sin(\omega_D t + \phi)$ is considered as unity ($x(t) = \rho e^{-\xi\omega_n t}$ is shown in Fig. 2.6 by dotted line).

A parameter like p within (0, 1) is defined to specify whether the effect of BP must be considered in updating position or not. For each particle, p is compared

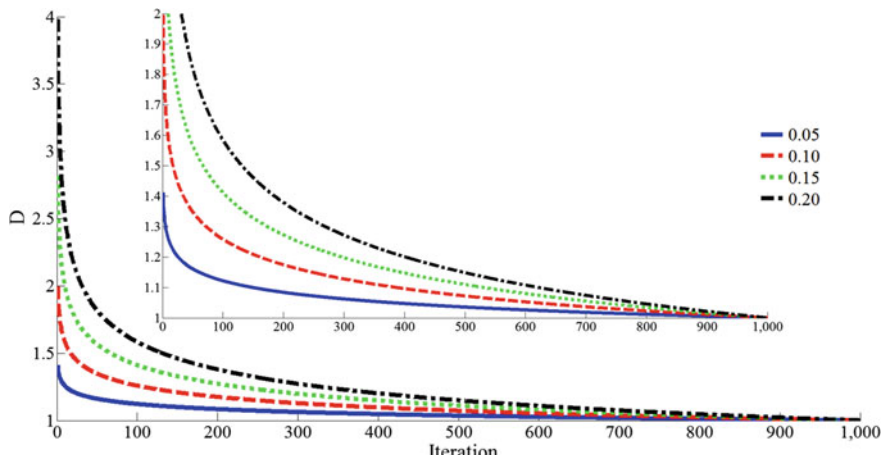


Fig. 2.9 The influence of α on function D

with $rand$ (a random numbers uniformly distributed in the range of $[0,1]$) and if $p < rand$, then $w_3 = 0$ and $w_2 = 1-w_1$.

Three essential concepts consisting of self-adaptation, cooperation, and competition are considered in this algorithm. Particles move toward HB so the self-adaptation is provided. Any particle has the chance to have influence on the new position of the other one, so the cooperation between the particles is supplied. Because of the p parameter, the influence of GP (good particle) is more than that of BP (bad particle), and therefore the competition is provided.

Step 4 The particle moves in the search space to find a better result and may violate the side constraints. If any component of the system violates a boundary, it must be regenerated by harmony search-based side constraint handling approach [9]. In this technique, there is a possibility like *HMCR* (harmony memory considering rate) that specifies whether the violating component must be changed with the corresponding component of the historically best position of a random particle or it should be determined randomly in the search space. Moreover, if the component of a historically best position is selected, there is a possibility like *PAR* (pitch adjusting rate) that specifies whether this value should be changed with the neighboring value or not.

Step 5 Steps 2 through 4 are repeated until a termination criterion is fulfilled. Any terminating condition can be incorporated; however, in this book, the optimization process is terminated after a fixed number of iterations.

2.5 The MDVC-UVPS Algorithm

MDVC-UVPS is a hybrid algorithm based on VPS, Multi-Design Variable Configurations cascade optimization (Multi-DVC) and Upper Bound Strategy (UBS) [4]. The VPS is used as the main engine of the hybrid algorithm; Multi-DVC cascade optimization is utilized to handle the large number of variables and UBS is employed to reduce the computational time. The reason for selecting VPS for hybridization is that CBO, ECBO, and VPS algorithms have been used previously for optimal design of many structures, and the VPS has shown its superiority compared to CBO and ECBO (Kaveh [5, 6]). This will be further clarified by the examples of the subsequent chapter.

2.5.1 *The Multi-Design Variable Configurations Cascade Optimization*

The cascade optimization strategy is proposed to use several optimizers, one followed by another in a specified sequence, to solve a large-scale problem [10]. In this procedure, the first optimizer starts from a user-specified design known as

“cold-start”. The optimal solution achieved in the first cascade stage is called a “hot-start” and is used to initiate the second optimization stage. Accordingly, each optimization stage of the cascade procedure starts from the optimum design achieved in the previous stage. Therefore, each cascade stage except the first one initiates from a hot-start and produces a new hot-start for the next stage. In general, the optimization algorithm implemented at each stage of a cascade process may or may not be the same [11, 12].

In the multi-DVC cascade optimization, a series of appropriate Design Variable Configurations (DVCs) for the optimization problem under consideration is constructed to use a different configuration at each cascade optimization stage. The coarsest DVC which avoids confusing the employed optimizer with huge design spaces is utilized in the first stage of the cascade procedure. Therefore, the areas of appropriate design variable values are identified by detecting near-optimum solutions among the relatively limited design options provided. As the number of design variables processed in the cascade stages becomes larger, more detailed representation of the full design space is offered and the optimizer is given the opportunity to improve the quality of the optimal solution reached. In the final cascade stages utilizing the finest DVC, relatively small adjustments to an already good-quality design occur in an effort to identify (or at least approach) the globally optimum design. In summary, the first optimization stage of the cascade procedure serves the purpose of basic design space exploration, while the last stages aim at fine-tuning the achieved optimal solution.

2.5.2 *The Upper Bound Strategy*

An upper bound strategy is proposed as a simple, yet efficient strategy, to reduce the total number of structural analyses through avoiding unnecessary analyses during the course of optimization. The key issue in the UBS is to detect those candidate designs which have no chance to surpass the best design found so far during the iterations of the optimum design process. After identifying those non-improving designs, they are directly excluded from the structural analysis stage, resulting in a significant saving in the computational effort. The current best design can usually be considered as the upper bound for the forthcoming candidates to eliminate unnecessary structural analysis and associated fitness computations for those candidates that have no chance of surpassing the best solution. Basically, the key feature in this approach is to define the penalized weight of the current best solution found during the previous iterations as an upper bound for the net weight of the newly generated candidate solutions. Thus, any new candidate solution with a net weight greater than this upper bound will not be analyzed and this will reduce the computational burden of the optimization algorithm [13].

2.5.3 *Presentation of MDVC-UVPS*

According to the above concepts, the following steps are provided to introduce the MDVC-UVPS algorithm. Pseudocode of this algorithm is provided in Fig. 2.10.

Step 1 A series of design variable configurations are constructed and sorted according to the size in an increasing order. The coarsest DVC is utilized in the first stage of the cascade procedure and the initial positions of all

```

procedure MDVC-UVPS
    Initialize algorithm parameters
    A series of design variable configurations are defined
    The coarsest DVC is selected and initial positions are created randomly based on it
    The values of objective function are evaluated and HB is stored
    while maximum iterations is not fulfilled
        The upper bound is selected
        for each particle
            The GP and BP are chosen
            if P<rand
                 $w_3=0$  and  $w_2=1-w_1$ 
            end if
            for each component
                New location is obtained by Eq. (2.22)
            end for
            Violated components are regenerated by harmony search-based handling
            approach
            Net weight is computed
            if net weight > upper bound
                The position of particle is replaced to its historically best solution
            else
                The objective function value is calculated
            end if
        end for
        if the termination criterion of current DVC is fulfilled
            The next DVC is used
            The population is updated
        end for
        HB is updated
    end while
end procedure

```

Fig. 2.10 Pseudocode of the MDVC-UVPS algorithm

particles are randomly set based on this configuration. The objective function values are calculated for the initial population.

- Step 2 Since the benchmark examples utilized in this book are large size problems, the value of the so far best design is not selected as the upper bound. In order to select it, the median of the historically best objective function values is chosen.
- Step 3 New positions are determined by Eq. (2.22) and violated components are regenerated by the harmony search-based handling approach.
- Step 4 Net weight of each solution candidate is computed (note that it is not necessary to consider design constraints). Any particle with a net weight greater than upper bound will not be analyzed and its position is replaced to its historically best design. Other particles should be analyzed and their objective function values should be calculated (design constraints are considered for these particles).
- Step 5 The optimization process in each stage except the last one is terminated after a fixed number of iterations with no improvement. If this criterion is satisfied, the next DVC is used in the new stage and particles are initialized based on the finally attained optimum design of the previous stage. In the new population, the *HB* is one of the particles and the other ones are randomly selected from the neighboring region of *HB* by the normal distribution with the mean HB^j and the standard deviation $\frac{x_{\max}^j - x_{\min}^j}{C}$ (x_{\min}^j and x_{\max}^j are the minimum and maximum limits of the j th variable and C is a constant). After a predefined number of iterations, the cascade process is terminated.

References

1. Kaveh A, Mahdavi VR (2014) Colliding bodies optimization: a novel meta-heuristic method. *Comput Struct* 139:18–27
2. Kaveh A, Ilchi Ghazaan M (2014) Enhanced colliding bodies optimization for design problems with continuous and discrete variables. *Adv Eng Softw* 77:66–75
3. Kaveh A, Ilchi Ghazaan M (2017) Vibrating particles system algorithm for truss optimization with multiple natural frequency constraints. *Acta Mech* 228(1):307–322
4. Kaveh A, Ilchi Ghazaan M (2018) A new hybrid meta-heuristic algorithm for optimal design of large-scale dome structures. *Eng Optimiz* 50(2):235–252
5. Kaveh A (2017) Advances in metaheuristic algorithms for optimal design of structures, 2nd edn. Springer International Publishing, Switzerland
6. Kaveh A (2017) Applications of metaheuristic optimization algorithms in civil engineering. Springer, Switzerland
7. Tolman RC (1979) The principles of statistical mechanics. Clarendon Press, Oxford (Reissued)
8. Beer FP, Johnston ER Jr, Mazurek DF, Cornwell P, Self BP (2013) Vector mechanics for engineers. McGraw-Hill, New York, USA
9. Kaveh A, Talatahari S (2010) A novel heuristic optimization method: charged system search. *Acta Mech* 213(3):267–289

10. Patnaik SN, Coroneos RM, Hopkins DA (1997) A cascade optimization strategy for solution of difficult design problems. *Int J Numer Methods Eng* 40:2257–2266
11. Charmpis DC, Lagaros ND, Papadrakakis M (2005) Multi-database exploration of large design spaces in the framework of cascade evolutionary structural sizing optimization. *Comput Methods Appl Mech Eng* 194:3315–3330
12. Lagaros ND (2014) A general purpose real-world structural design optimization computing platform. *Struct Multidiscip Optim* 49(6):1047–1066
13. Kazemzadeh Azad S, Hasançebi O, Kazemzadeh Azad S (2013) Upper bound strategy for metaheuristic based design optimization of steel frames. *Adv Eng Softw* 57:19–32

Chapter 3

Optimal Design of Usual-Size Skeletal Structures



3.1 Introduction

Sizing optimization of truss and frame structures are frequent structural design problems that are subjected to various constraints such as displacements, stress, buckling, and natural frequencies. A great number of papers has been published in literature, where different meta-heuristic search algorithms have been applied to this class of problems [1, 2]. The aim of this chapter is to examine the ability of the CBO, ECBO and VPS which have been utilized in the next chapters for comparison with MDVC-UVPS. The results of well-known state-of-the-art meta-heuristics are also provided and compared here. The reason for selecting VPS for hybridization is that the VPS has shown its superiority compared to CBO and ECBO for optimal design of many structures, Kaveh [1, 2].

There are many design constraints that should be fulfilled in structural optimization. In the literature, the benchmark design examples usually studied with displacements, stress, and buckling constraints or displacements and frequencies constraints. Therefore, we decided to follow the same path in this book. Structural design examples with frequency constraints are studied in the next section and after that, benchmark examples with strength constraints are optimized.

The optimization problem can formally be stated as

$$\begin{array}{ll} \text{Find} & \{X\} = [x_1, x_2, \dots, x_{ng}] \\ \text{to minimize} & W(\{X\}) = \sum_{i=1}^{ng} x_i \sum_{j=1}^{nm(i)} \rho_j L_j \\ \text{subjected to:} & \begin{cases} g_j(\{X\}) \leq 0, & j = 1, 2, \dots, nc \\ x_{i\min} \leq x_i \leq x_{i\max} \end{cases} \end{array} \quad (3.1)$$

where $\{X\}$ is the vector containing the design variables; $W(\{X\})$ presents the weight of the structure; ng is the number of design groups; $nm(i)$ is the number of members for the

i th group; and ρ_j and L_j denote the material density and the length of the j th member, respectively. $x_{i\min}$ and $x_{i\max}$ are the lower and upper bounds of the design variable x_i , respectively. $g_j(\{X\})$ denotes design constraints, and nc is the number of the constraints.

For constraints handling, a penalty approach is utilized. For this purpose, the objective function (Eq. (3.1)) is redefined as follows:

$$P(\{X\}) = (1 + \varepsilon_1 \cdot v)^{\varepsilon_2} \times W(\{X\}) \quad (3.2)$$

where $P(\{X\})$ is the penalized cost function or the objective function to be minimized and v denotes the sum of the violations of the design constraints. Here, ε_1 is set to unity, and ε_2 is calculated by

$$\varepsilon_2 = 1.5 + 1.5 \times \frac{\text{iter}}{\text{iter}_{\max}} \quad (3.3)$$

where iter is the current iteration number, and iter_{max} is the total number of iterations for optimization process [3].

3.2 Numerical Examples with Frequency Constraints

3.2.1 A 72-Bar Space Truss Problem

The schematic of a 72-bar space truss is shown in Fig. 3.1 as the first design example. The elements are divided into 16 groups, considering the symmetry. The material density is 2767.99 kg/m³ and the elastic modulus is 68.95 GPa for all the members. Four nonstructural masses of 2268 kg are attached to the nodes 1 through 4. The allowable minimum cross-sectional area of all elements is set to 0.645 cm². This example has two frequency constraints. The first frequency is required to be $f_1 = 4$ Hz and the third frequency is required to satisfy $f_3 \geq 6$ Hz.

The optimized designs found by CSS-BBBC (hybridization of Charged System Search and Big Bang-Big Crunch with trap recognition capability) [4], HALC-PSO (transplants a Harmony search-based mechanism to Particle Swarm Optimization with an Aging Leader and Challengers) [5], TWO (Tug of War Optimization) [6], CBO [7], EBO [7], and VPS [8] are compared in Table 3.1. The CSS-BBBC obtained the lightest design; however, the best designs of all methods are approximately identical. Besides, the elastic modulus of 69.8 GPa was used in [4] that generally results in lighter structures. The average optimized weight and the standard deviation on average weight of the VPS are less than those of all other methods. Frequency constraints are satisfied by all methods (see Table 3.2). The VPS requires 4720 structural analyses to find the optimum solution while HALC-PSO, CBO, and ECBO require 8000, 4000, and 14,800 structural analyses, respectively.

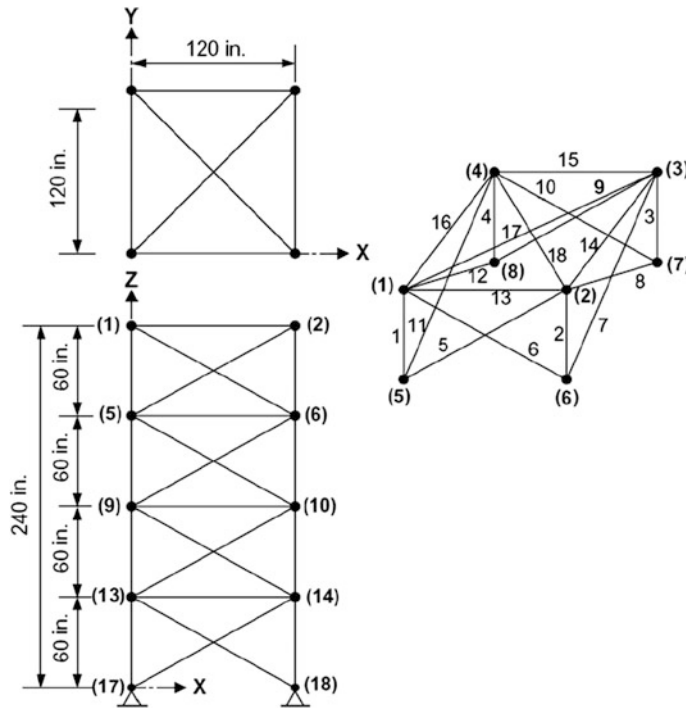


Fig. 3.1 Schematic of a spatial 72-bar truss

3.2.2 A Spatial 120-Bar Dome-Shaped Truss Problem

Figure 3.2 shows the schematic of a 120-bar dome truss. The members are categorized into seven groups considering the symmetry. The material density is 7971.810 kg/m^3 and the modulus of elasticity is 210 GPa for all elements. Nonstructural masses are attached to all free nodes as follows: 3000 kg at node 1, 500 kg at nodes 2–13, and 100 kg at the remaining nodes. Element cross-sectional areas can vary between 1 and 129.3 cm^2 . The frequency constraints are as

$$f_1 \geq 9 \text{ Hz} \text{ and } f_2 \geq 11 \text{ Hz}$$

The comparison of the outcomes of different algorithms can be seen in Table 3.3. The VPS [8] yields the least weight. The best weight of this method is 8888.74 kg while it is 9046.34 kg for CSS-BBBC [4], 8889.96 kg for the HALC-PSO [5], 8890.69 kg for the CBO [7] and 8896.50 kg for the ECBO [7]. Moreover, it can be seen that the lightest average optimized weight is found by the VPS technique. Table 3.4 reports the natural frequencies of the optimized

Table 3.1 Performance comparison of the 72-bar space truss problem

Design variable	Members in the group	Areas (cm ²)					
		CSS-BBBC [4]	HALC-PSO [5]	TWO [6]	CBO [7]	ECBO [7]	VPS [8]
1	1–4	2.854	3.3437	3.380	3.7336	3.5498	3.5017
2	5–12	8.301	7.8688	8.086	7.9355	7.8356	7.9340
3	13–16	0.645	0.6450	0.647	0.6450	0.645	0.6450
4	17–18	0.645	0.6450	0.646	0.6450	0.645	0.6450
5	19–22	8.202	8.1626	8.890	8.3765	8.1183	8.0215
6	23–30	7.043	7.9502	8.136	8.0889	8.1338	7.9826
7	31–34	0.645	0.6452	0.654	0.6450	0.645	0.6450
8	35–36	0.645	0.6450	0.647	0.6450	0.6450	0.6450
9	37–40	16.328	12.2668	13.097	12.9491	12.6231	12.8175
10	41–48	8.299	8.1845	8.101	8.0524	8.0971	8.1129
11	49–52	0.645	0.6451	0.663	0.6450	0.6450	0.6450
12	53–54	0.645	0.6451	0.646	0.6450	0.645	0.6450
13	55–58	15.048	17.9632	16.483	16.6629	17.3908	17.3362
14	59–66	8.268	8.1292	7.873	8.0557	8.0634	8.1010
15	67–70	0.645	0.6450	0.651	0.645	0.645	0.6450
16	71–72	0.645	0.6450	0.657	0.645	0.645	0.6450
Weight (kg)		327.507	327.77	328.83	327.740	327.653	327.649
Average optimized weight (kg)		N/A	327.99	336.1	328.20	327.76	327.670
Standard deviation on average weight (kg)		N/A	0.19	5.8	0.54	0.06	0.018

Table 3.2 Natural frequencies (Hz) evaluated at the optimum designs of the 72-bar space truss problem

Frequency number	Natural frequencies (Hz)					
	CSS-BBBC [4]	HALC-PSO [5]	TWO [6]	CBO [7]	ECBO [7]	VPS [8]
1	4.000	4.000	4.000	4.000	4.000	4.0000
2	4.000	4.000	4.000	4.000	4.000	4.0002
3	6.004	6.000	6.000	6.000	6.000	6.0000
4	6.2491	6.230	6.259	6.267	6.246	6.2428
5	8.9726	9.041	9.082	9.101	9.071	9.0698

structures, and it is clear that none of the frequency constraints are violated. The HALC-PSO, CBO, ECBO, and VPS algorithms obtain the optimal solution after 17,000, 3,700, 7700, and 6860 analyses, respectively.

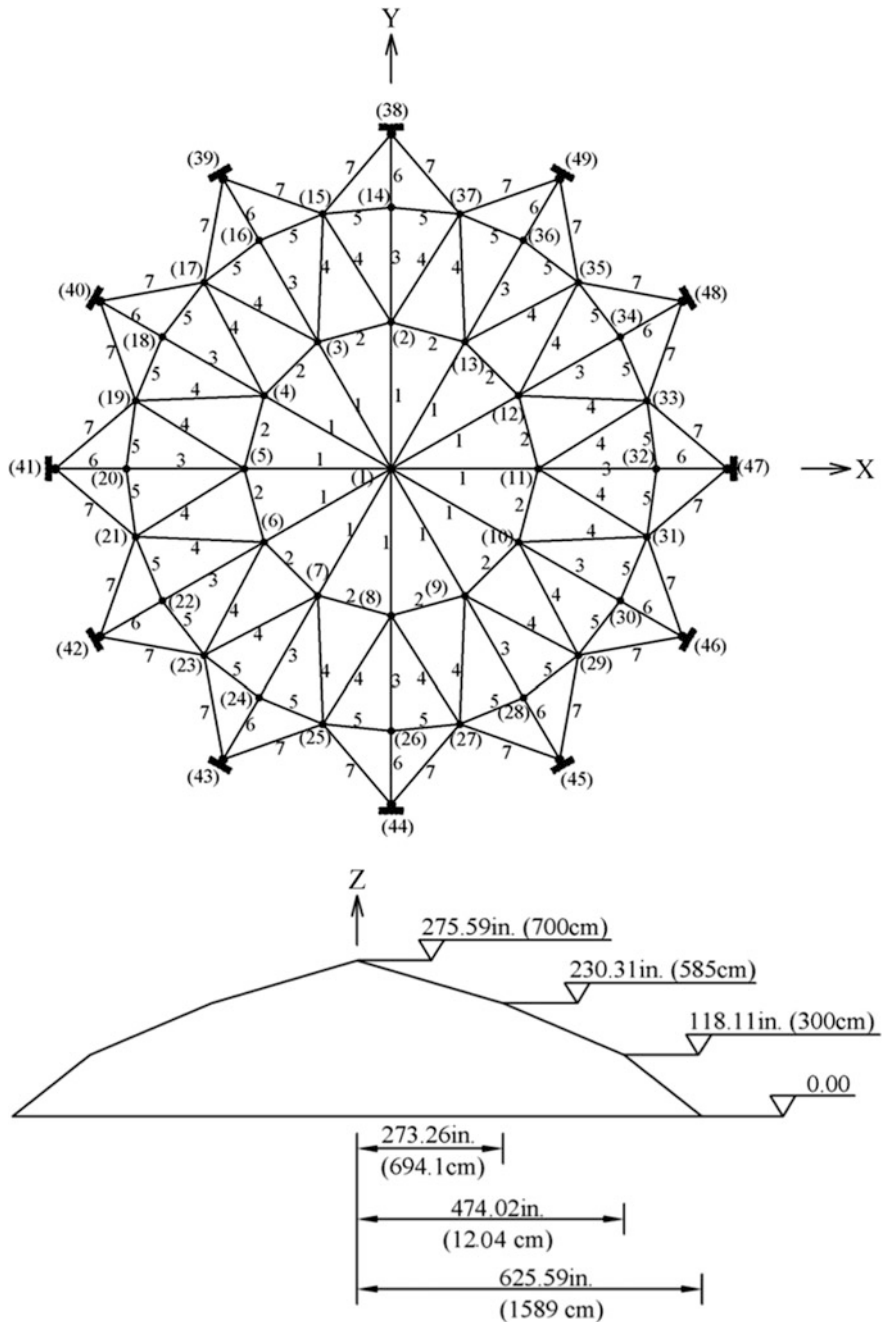


Fig. 3.2 Schematic of the spatial 120-bar dome-shaped truss

Table 3.3 Performance comparison of the spatial 120-bar dome-shaped truss problem

Design variable	Areas (cm ²)				
	CSS-BBBC [4]	HALC-PSO [5]	CBO [7]	ECBO [7]	VPS [8]
1	17.478	19.8905	19.7738	19.8290	19.6836
2	49.076	40.4045	40.6757	41.4037	40.9581
3	12.365	11.2057	11.6056	11.0055	11.3325
4	21.979	21.3768	21.4601	21.2971	21.5387
5	11.190	9.8669	9.8104	9.4718	9.8867
6	12.590	12.7200	12.2866	13.0176	12.7116
7	13.585	15.2236	15.1417	15.2840	14.9330
Weight (kg)	9046.34	8889.96	8890.69	8896.50	8888.74
Average optimized weight (kg)	N/A	8900.39	8945.64	8920.16	8896.04
Standard deviation on average weight (kg)	N/A	6.38	38.33	20.12	6.65

Table 3.4 Natural frequencies (Hz) evaluated at the optimum designs of the spatial 120-bar dome-shaped truss problem

Frequency number	Natural frequencies (Hz)				
	CSS-BBBC [4]	HALC-PSO [5]	CBO [7]	ECBO [7]	VPS [8]
1	9.000	9.000	9.000	9.001	9.0000
2	11.007	11.000	11.000	11.001	11.0000
3	11.018	11.000	11.000	11.003	11.0000
4	11.026	11.010	11.010	11.010	11.0096
5	11.048	11.050	11.049	11.052	11.0491

3.2.3 A 200-Bar Planar Truss Problem

The last structural optimization problem solved in this class is the optimal design of a 200-bar planar truss schematized in Fig. 3.3. Due to the symmetry, the elements are divided into 29 groups. The modulus of elasticity and the material density of members are 210 GPa and 7860 kg/m³, respectively. Nonstructural masses of 100 kg are attached to the upper nodes. A lower bound of 0.1 cm² is assumed for the cross-sectional areas. The first three natural frequencies of the structure must satisfy the following limitations ($f_1 \geq 5$ Hz, $f_2 \geq 10$ Hz, $f_3 \geq 15$ Hz).

Table 3.5 presents the results of the optimal designs utilizing CSS-BBBC [4], HALC-PSO [5], CBO-PSO (a hybrid of CBO and PSO algorithms) [9], CBO [7], ECBO [7], and VPS [3]. The weight of the best result obtained by VPS is

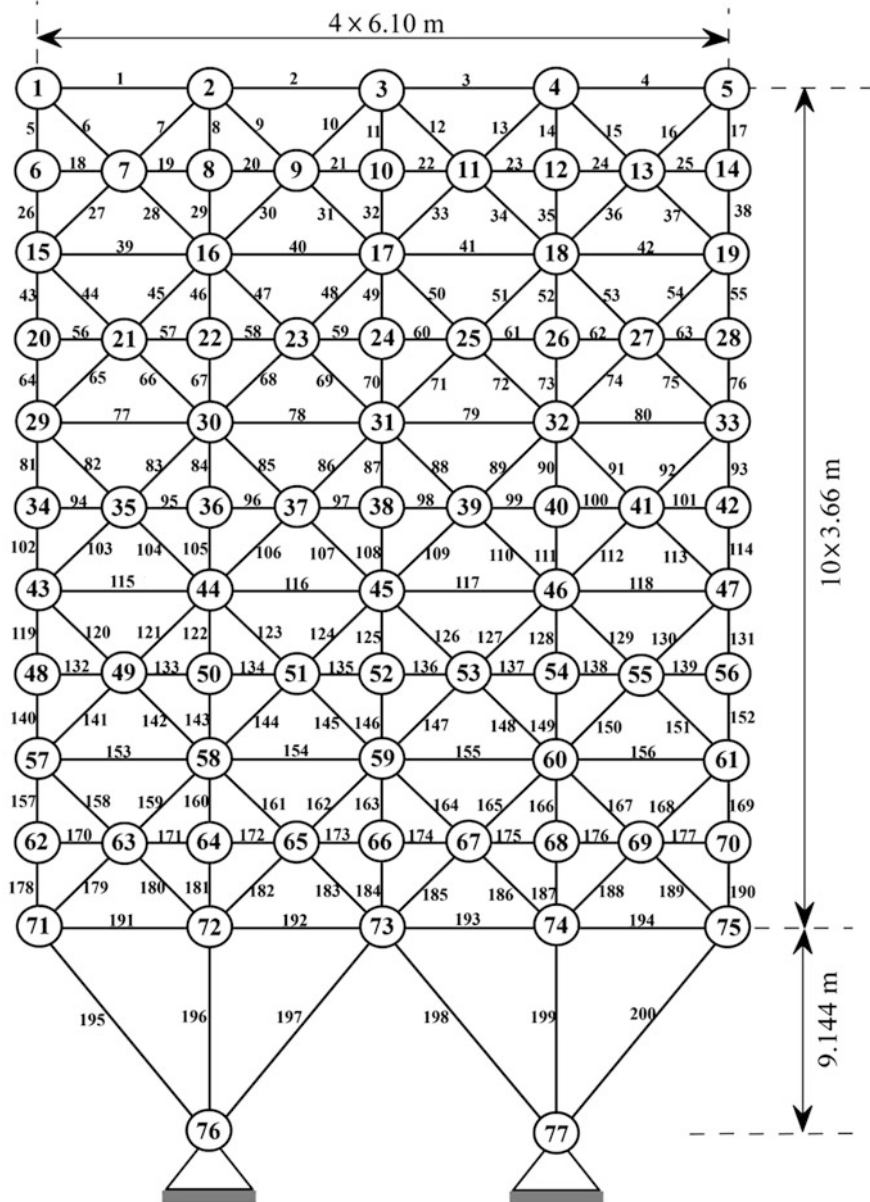


Fig. 3.3 Schematic of the 200-bar planar truss

2156.62 kg that is the best among the compared methods. The average optimized weight of the HALC-PSO is 2157.14 kg, which is less than those of all other methods. Table 3.6 reports the natural frequencies of the optimized structures, and

Table 3.5 Performance comparison of the 200-bar planar truss problem

Element group	Members in the group	Areas (cm ²)						VPS [3]
		CSS-BBBC [4]	HALC-PSO [5]	CBO-PSO [9]	CBO [7]	ECBO [7]		
1	1,2,3,4	0.2934	0.3072	0.2797	0.3059	0.2993	0.3031	
2	5,8,11,14,17	0.5561	0.4545	0.6968	0.4476	0.4497	0.4496	
3	19,20,21,22,23,24	0.2952	0.1000	0.1000	0.1000	0.1000	0.1000	0.1002
4	18,25,56,63,94,101,132,139,170,177	0.1970	0.1000	0.1000	0.1001	0.1000	0.1000	0.1000
5	26,29,32,35,38	0.8340	0.5080	0.5796	0.4944	0.5137	0.5086	
6	6,7,9,10,12,13,15,16,27,28,30,31,33, 34,36,37	0.6455	0.8276	0.8213	0.8369	0.7914	0.8204	
7	39,40,41,42	0.1770	0.1023	0.1279	0.1001	0.1013	0.1000	
8	43,46,49,52,55	1.4796	1.4357	1.0152	1.5514	1.4129	1.4210	
9	57,58,59,60,61,62	0.4497	0.1007	0.1000	0.1000	0.1019	0.1002	
10	64,67,70,73,76	1.4556	1.5528	1.5647	1.5286	1.6460	1.5900	
11	44,45,47,48,50,51,53,54,65,66,68,69, 71,72,74,75	1.2238	1.1529	1.6465	1.1547	1.1532	1.1530	
12	77,78,79,80	0.2739	0.1522	0.2296	0.1000	0.1000	0.1277	
13	81,84,87,90,93	1.9174	2.9564	2.9007	2.9980	3.1850	2.9160	
14	95,96,97,98,99,100	0.1170	0.1003	0.1000	0.1017	0.1034	0.1009	
15	102,105,108,111,114	3.5535	3.2242	3.0133	3.2475	3.3126	3.2826	
16	82,83,85,86,88,89,91,92,103,104,106, 107,109,110,112,113	1.3360	1.5839	1.6142	1.5213	1.5920	1.5856	
17	115,116,117,118	0.6289	0.2818	0.2755	0.3996	0.2238	0.2794	
18	119,122,125,128,131	4.8335	5.0696	5.0951	4.7557	5.1227	5.0680	
19	133,134,135,136,137,138	0.6062	0.1033	0.1000	0.1002	0.1050	0.1004	

(continued)

Table 3.5 (continued)

Element group	Members in the group	Areas (cm ²)	CSS-BBBC [4]	HALC-PSO [5]	CBO-PSO [9]	CBO [7]	ECBO [7]	VPS [3]
20	140,143,146,149,152	5.4393	5.4657	5.5172	5.1359	5.3707	5.4760	
21	120,121,123,124,126,127,129,130,141,142,144,145,147,148,150,151	1.8435	2.0975	2.2032	2.1181	2.0645	2.1169	
22	153,154,155,156	0.8955	0.6598	0.8659	0.9200	0.5443	0.6939	
23	157,160,163,166,169	8.1759	7.6585	7.6477	7.3084	7.6497	7.6912	
24	171,172,173,174,175,176	0.3209	0.1444	0.1000	0.1185	0.1000	0.1332	
25	178,181,184,187,190	10.98	8.0520	8.1273	7.6901	7.6754	7.9972	
26	158,159,161,162,164,165,167,168,179,180,182,183,185,186,188,189	2.9489	2.7889	2.9665	3.0895	2.7178	2.7859	
27	191,192,193,194	10.5243	10.4770	10.2386	10.6462	10.8141	10.4331	
28	195,197,198,200	20.4271	21.3257	20.6364	20.7190	21.6349	21.2289	
29	196,199	19.0983	10.5111	11.6468	11.7463	10.3520	10.7392	
Weight (kg)		2298.61	2156.73	2195.469	2161.15	2158.08	2156.62	
Average optimized weight (kg)		N/A	2157.14	N/A	2447.52	2159.93	2159.46	
Standard deviation on average weight (kg)		N/A	0.2413	N/A	301.29	1.57	2.79	

Table 3.6 Natural frequencies (Hz) evaluated at the optimum designs of the 200-bar planar truss problem

Frequency number	Natural frequencies (Hz)					
	CSS-BBBC [4]	HALC-PSO [5]	CBO-PSO	CBO [7]	ECBO [7]	VPS [3]
1	5.010	5.000	5.003	5.000	5.000	5.0000
2	12.911	12.254	12.281	12.221	12.189	12.2086
3	15.416	15.044	15.125	15.088	15.048	15.0153
4	17.033	16.718	16.613	16.759	16.643	16.6946
5	21.426	21.461	21.331	21.419	21.342	21.4046

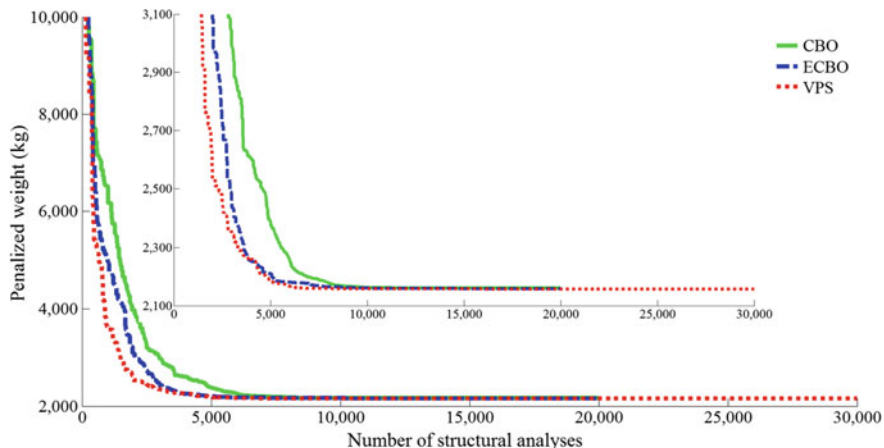


Fig. 3.4 Convergence curves for the 200-bar planar truss problem

it is clear that none of the frequency constraints are violated. Comparison of the convergence rates between CBO, ECBO, and VPS is illustrated in Fig. 3.4. The VPS requires 16,420 structural analyses to find the optimum solution while HALC-PSO, CBO-PSO, CBO, and ECBO require 13,000, 9000, 10,500, and 14,700 structural analyses, respectively. It should be noted that the designs found by VPS at 9,000th, 10,500th, 13,000th, and 14,700th analyses are 2158.35, 2158.06, 2157.74, and 2157.72 kg, respectively.

3.3 Numerical Examples with Strength Constraints

3.3.1 A Spatial 120-Bar Dome-Shaped Truss Problem

The schematic and element grouping of a spatial 120-bar dome truss are shown in Fig. 3.5. This structure is divided into seven groups of elements because of symmetry (for the sake of clarity, not all the element groups are numbered in Fig. 3.5).

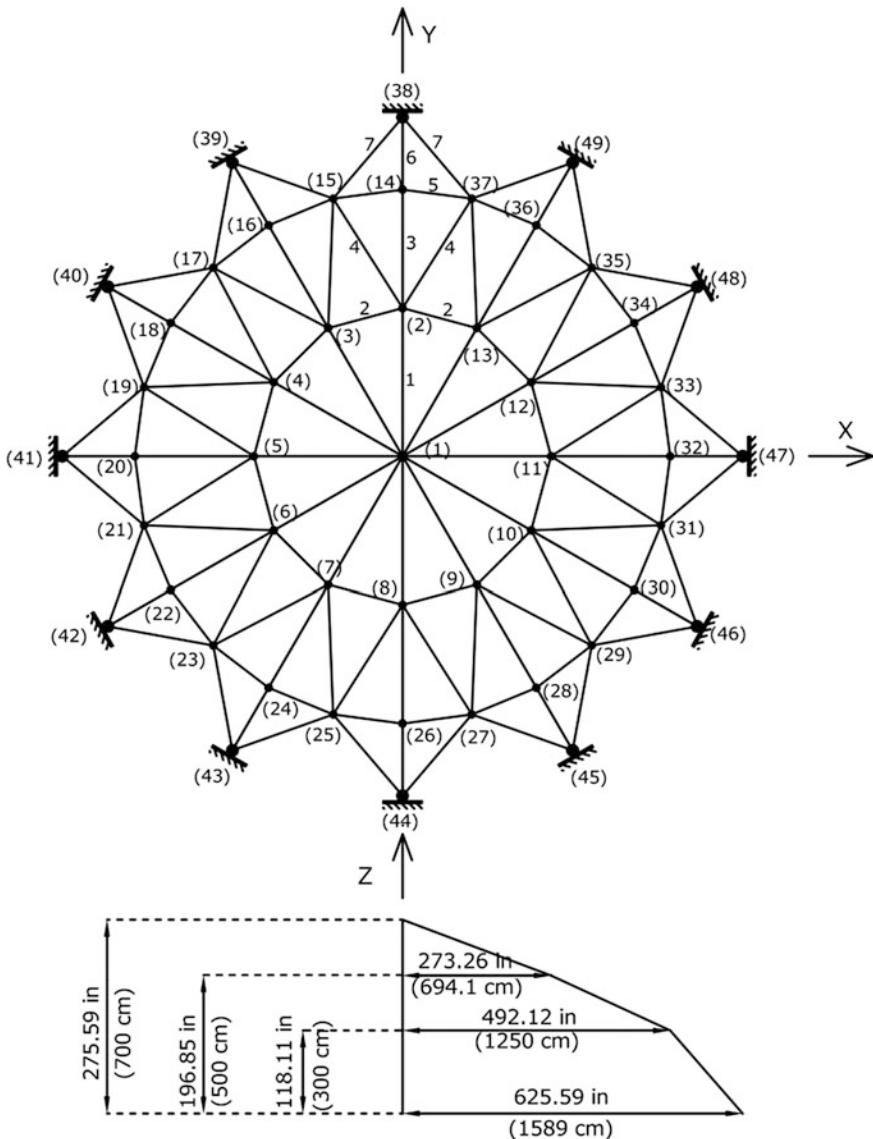


Fig. 3.5 Schematic of the spatial 120-bar dome-shaped truss

The modulus of elasticity is 30,450 ksi (210 GPa) and the material density is 0.288 lb/in.³ (7971.810 kg/m³). The yield stress of steel is taken as 58.0 ksi (400 MPa). The dome is considered to be subjected to vertical loading at all the unsupported joints. These loads are taken as -13.49 kips (-60 kN) at node 1, -6.744 kips (-30 kN) at nodes 2 through 14, and -2.248 kips (-10 kN) at the remaining nodes. Element cross-sectional areas can vary between 0.775 in.²

(5 cm^2) and 20.0 in.^2 (129.032 cm^2). Displacement limitations of $\pm 0.1969 \text{ in.}$ ($\pm 5 \text{ mm}$) are imposed on all nodes in x , y , and z coordinate directions. Constraints on member stresses are imposed according to the provisions of the AISC [10] as follows:

The allowable tensile stresses for tension members are calculated as

$$\sigma_i^+ = 0.6F_y \quad (3.4)$$

where F_y is the yield strength.

The allowable stress limits for compression members are calculated depending on two possible failure modes of the members known as elastic and inelastic buckling. Therefore

$$\sigma_i^- = \begin{cases} \left[\left(1 - \frac{\lambda_i^2}{2C_c^2} \right) F_y \right] / \left[\frac{5}{3} + \frac{3\lambda_i}{8C_c} - \frac{\lambda_i^3}{8C_c^3} \right] & \text{for } \lambda_i < C_c \\ \frac{12\pi^2 E}{23\lambda_i^2} & \text{for } \lambda_i \geq C_c \end{cases} \quad (3.5)$$

where E is the modulus of elasticity; λ_i is the slenderness ratio ($\lambda_i = kl_i/r_i$); C_c denotes the slenderness ratio dividing the elastic and inelastic buckling regions ($C_c = \sqrt{2\pi^2 E/F_y}$); k is the effective length factor (k is set equal to 1 for all truss members); L_i is the member length; and r_i is the minimum radius of gyration.

This truss is optimized by MPSO (Multistage Particle Swarm Optimization) [11], TWO (Tug of War Optimization) [12], WEO (Water Evaporation Optimization) [13], CBO, ECBO, and VPS [3]. Comparison of the optimal designs is given in Table 3.7. It can be seen that the lightest design (i.e., 33,249.98 lb) and the best average optimized weight (i.e., 33,253.56 lb) are found by the VPS method. Figure 3.6 compares the convergence curves of the best results obtained by the CBO, ECBO, and VPS. The VPS converges to the optimum solution after 8280 analyses. The MPSO, TWO, WEO, CBO, and ECBO obtain the optimal solution after 15,000, 16,000, 19,510, 12,080, and 19,800 analyses, respectively.

3.3.2 A 3-Bay 15-Story Frame Problem

The schematic of a 3-bay 15-story frame is represented in Fig. 3.7. The applied loads and the numbering of the member groups are also shown in this figure. The modulus of elasticity is 29 Msi (200 GPa) and the yield stress is 36 ksi (248.2 MPa). The effective length factors of the members are calculated as $k_x \geq 0$ for a sway-permitted frame and the out-of-plane effective length factor is specified as $k_y = 1.0$. Each column is considered as non-braced along its length, and the non-braced length for each beam member is specified as one-fifth of the span length. Limitation on displacement and strength are imposed according to the provisions of the AISC [14] as follows:

Table 3.7 Performance comparison of the spatial 120-bar dome-shaped truss problem

Element group	Optimal cross-sectional areas (in. ²)					ECBO	VPS [3]
	MSPSO [11]	TWO [12]	WEO [13]	CBO			
1	3.0244	3.0247	3.0243	3.0260		3.0234	3.0244
2	14.7804	14.7261	14.7943	14.8237		14.8569	14.7536
3	5.0567	5.1338	5.0618	5.1576		4.8649	5.0789
4	3.1359	3.1369	3.1358	3.1310		3.1319	3.1371
5	8.4830	8.4545	8.4870	8.3350		8.5716	8.4829
6	3.3104	3.2946	3.2886	3.3872		3.3967	3.3012
7	2.4977	2.4956	2.4967	2.4938		2.5042	2.4963
Weight (lb)	33,251.22	33,250.31	33,250.24	33,256.15		33,268.56	33,249.98
Average optimized weight (lb)	33,257.29	33,282.64	33,255.55	33,284.19		33,303.53	33,253.56
Standard deviation on average weight (lb)	4.29	25.38	N/A	31.40		26.958	4.36

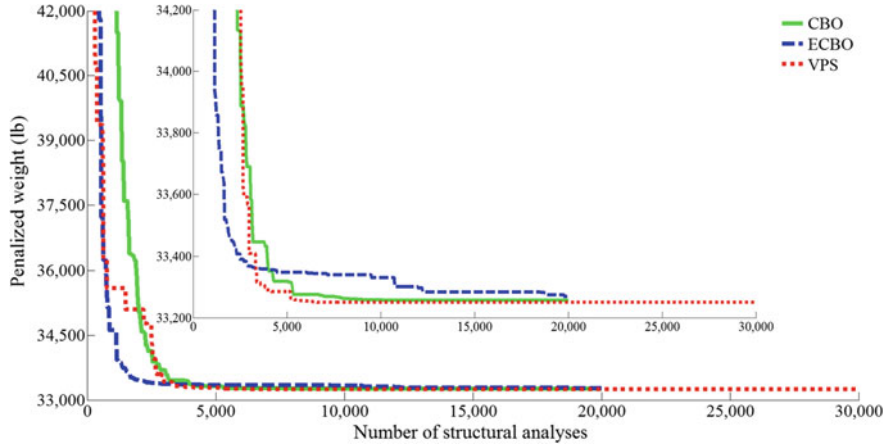


Fig. 3.6 Convergence curves for the spatial 120-bar dome-shaped truss problem

(a) Maximum lateral displacement

$$\frac{\Delta_T}{H} - R \leq 0 \quad (3.6)$$

where Δ_T is the maximum lateral displacement, H is the height of the frame structure, and R is the maximum drift index which is equal to 1/300.

(b) The inter-story displacements

$$\frac{d_i}{h_i} - R_I \leq 0, \quad i = 1, 2, \dots, ns \quad (3.7)$$

where d_i is the inter-story drift, h_i is the story height of the i th floor, ns is the total number of stories, and R_I is the inter-story drift index (1/300).

(c) Strength constraints

$$\begin{cases} \frac{P_u}{2\phi_c P_n} + \frac{M_u}{\phi_b M_n} - 1 \leq 0, & \text{for } \frac{P_u}{\phi_c P_n} < 0.2 \\ \frac{P_u}{\phi_c P_n} + \frac{8M_u}{9\phi_b M_n} - 1 \leq 0, & \text{for } \frac{P_u}{\phi_c P_n} \geq 0.2 \end{cases} \quad (3.8)$$

where P_u is the required strength (tension or compression); P_n is the nominal axial strength (tension or compression); ϕ_c is the resistance factor ($\phi_c = 0.9$ for tension,

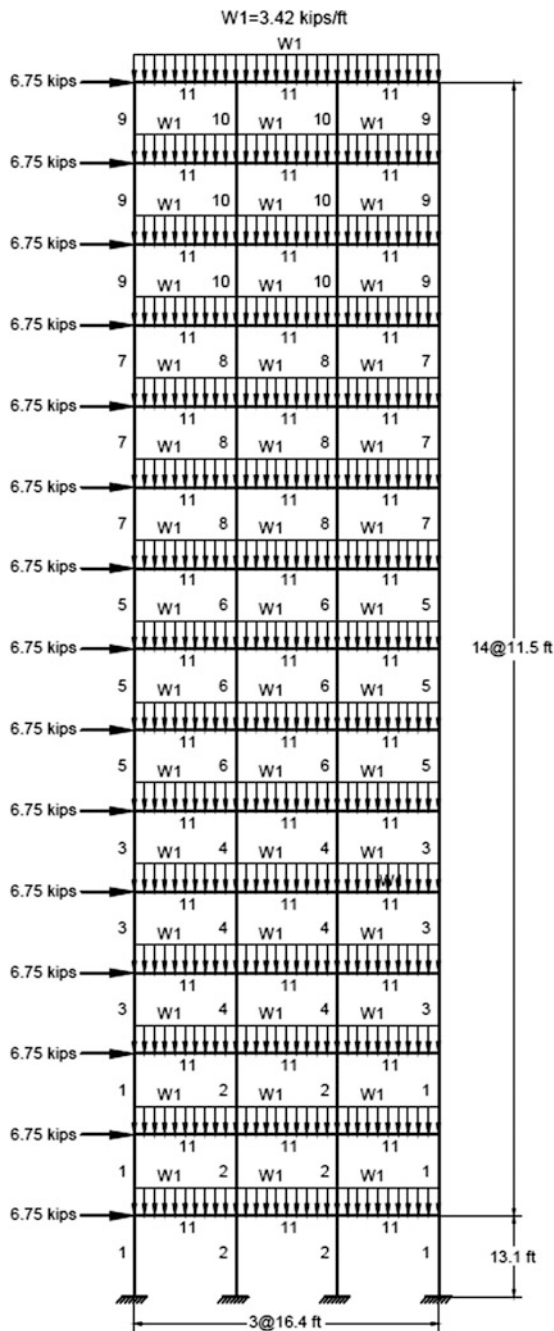


Fig. 3.7 Schematic of the 3-bay 15-story frame

$\phi_c = 0.85$ for compression); M_u is the required flexural strengths; M_n is the nominal flexural strengths; and ϕ_b denotes the flexural resistance reduction factor ($\phi_b = 0.90$).

The nominal tensile strength for yielding in the gross section is calculated by

$$P_n = A_g \cdot F_y \quad (3.9)$$

The nominal compressive strength of a member is computed as

$$P_n = A_g \cdot F_{cr} \quad (3.10)$$

where

$$\begin{cases} F_{cr} = \left(0.658\lambda_c^2\right)F_y, & \text{for } \lambda_c \leq 1.5 \\ F_{cr} = \left(\frac{0.877}{\lambda_c^2}\right)F_y, & \text{for } \lambda_c > 1.5 \end{cases} \quad (3.11)$$

$$\lambda_c = \frac{kl}{r\pi} \sqrt{\frac{F_y}{E}} \quad (3.12)$$

where A_g is the cross-sectional area of a member, and k is the effective length factor that is calculated by Dumonteil [15]:

$$k = \sqrt{\frac{1.6G_A G_B + 4.0(G_A + G_B) + 7.5}{G_A + G_B + 7.5}} \quad (3.13)$$

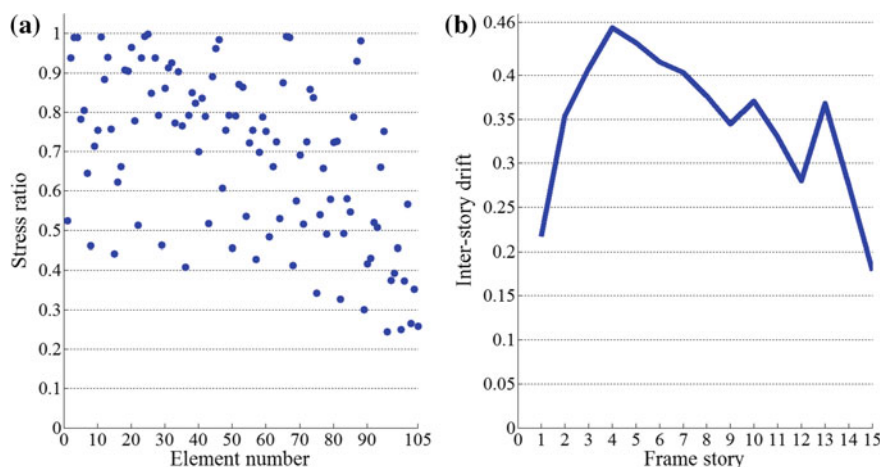
where G_A and G_B are stiffness ratios of columns and girders at the two end joints A and B of the column section, respectively.

Additionally, in this example, the sway of the top story is limited to 9.25 in. (23.5 cm).

Table 3.8 presents the comparison of the results of different algorithms. The VPS algorithm yields the least weight for this example, which is 86,985 lb. The other design weights are 92,723 lb by CSS [16], 93,315 lb by ES-DE (Eagle Strategy with Differential Evolution) [17], 91,248 lb by DSOS (Discrete Symbiotic Organisms Search) [18], 93,795 lb by CBO [19] and 86,986 lb by ECBO [19]. The best design of VPS has been achieved in 19,600 analyses. The CSS, ES-DE, CBO, and ECBO require 5,000, 10,000, 9520, and 9000 structural analyses to find the optimum solutions, respectively. It should be noted that the proposed method achieved about 92,000 lb (the best weight among the other methods except ECBO) after 10,800 structural analyses. Element stress ratio and inter-story drift evaluated at the best design optimized by VPS are shown in Fig. 3.8. The maximum stress ratio is 99.88% and the maximum inter-story drift is 45.41.

Table 3.8 Performance comparison of the 3-bay 15-story frame problem

Element group	Optimal W-shaped sections					
	CSS [16]	ES-DE [17]	DSOS [18]	CBO [19]	ECBO [19]	VPS [3]
1	W21 × 147	W18 × 106	W16 × 100	W24 × 104	W14 × 99	W14 × 90
2	W18 × 143	W36 × 150	W32 × 152	W40 × 167	W27 × 161	W36 × 170
3	W12 × 87	W12 × 79	W12 × 79	W27 × 84	W27 × 84	W14 × 82
4	W30 × 108	W27 × 114	W27 × 114	W27 × 114	W24 × 104	W24 × 104
5	W18 × 76	W30 × 90	W21 × 93	W21 × 68	W14 × 61	W21 × 68
6	W24 × 103	W10 × 88	W12 × 79	W30 × 90	W30 × 90	W18 × 86
7	W21 × 68	W18 × 71	W21 × 55	W8 × 48	W14 × 48	W21 × 48
8	W14 × 61	W18 × 65	W14 × 61	W21 × 68	W14 × 61	W14 × 61
9	W18 × 35	W8 × 28	W14 × 22	W14 × 34	W14 × 30	W12 × 30
10	W10 × 33	W12 × 40	W14 × 43	W8 × 35	W12 × 40	W10 × 39
11	W21 × 44	W21 × 48	W21 × 48	W21 × 50	W21 × 44	W21 × 44
Weight (lb)	92,723	93,315	91,248	93,795	86,986	86,985
Average optimized weight (lb)	N/A	98,531	N/A	98,738	88,410	90,066
Standard deviation on average weight (lb)	N/A	3294	N/A	N/A	N/A	2533

**Fig. 3.8** Constraint margins for the best design obtained by VPS for the 3-bay 15-story frame problem: **a** element stress ratio and **b** inter-story drift

3.3.3 A 3-Bay 24-Story Frame Problem

The last structural optimization problem solved in this chapter is the weight minimization of a 3-bay 24-story frame shown in Fig. 3.9. Frame members are collected in 20 groups (16 column groups and 4 beam groups). Each of the four beam element groups is chosen from all 267 W shapes, while the 16 column element groups are limited to W14 sections. The material has a modulus of elasticity equal to $E = 29,732$ Msi (205 GPa) and a yield stress of $f_y = 33.4$ ksi (230.3 MPa). The effective length factors of the members are calculated as $k_x \geq 0$ for a sway-permitted frame and the out-of-plane effective length factor is specified as $k_y = 1.0$. All columns and beams are considered as non-braced along their lengths. Similar to the previous example, the frame is designed following the LRFD-AISC specification and uses an inter-story drift displacement constraint (AISC [14]).

This steel frame structure was optimized by CSS [16], ES-DE [17] and DSOS [18], CBO [19], ECBO [19], and VPS [3]. Table 3.9 presents a comparison between these results. The lightest design (i.e., 201,618 lb) is found by ECBO algorithm and after that, the best design belongs to VPS (i.e., 202,998 lb). Figure 3.10 shows the convergence curves of the best results found by CBO, ECBO, and VPS. The best design has been achieved at 16,220 analyses by VPS and it obtained a weight of 209,532 lb after 8800 analyses, which is the best result compared to the weight achieved by the other method. The CSS, ES-DE, DSOS, CBO, and ECBO get the optimal solution after 5500, 12,500, 7500, 8280, and 15,360 analyses, respectively.

3.4 Concluding Remarks

In this chapter, the CBO, ECBO, and VPS algorithms are examined in the context of size optimization of skeletal structure designed for minimum weight. Four trusses and two frames subjected to different constraints are employed, and their final results are compared with results of the state-of-the-art algorithms from literature. The VPS achieved the lightest designs for most of the benchmarks and after that, ECBO performed better among the compared methods. The small values of the standard deviation on average weights prove the robustness of these techniques. Moreover, they show appropriate convergence rates. Although the results found by CBO are not better than ECBO and VPS but it has no internal parameter to adjust. Therefore, it can be performed more easily on various problems. Generally, comparison of the results proves the efficiency of the proposed algorithms and shows that they are suitable methods for comparison with the MDVC-UVPS.

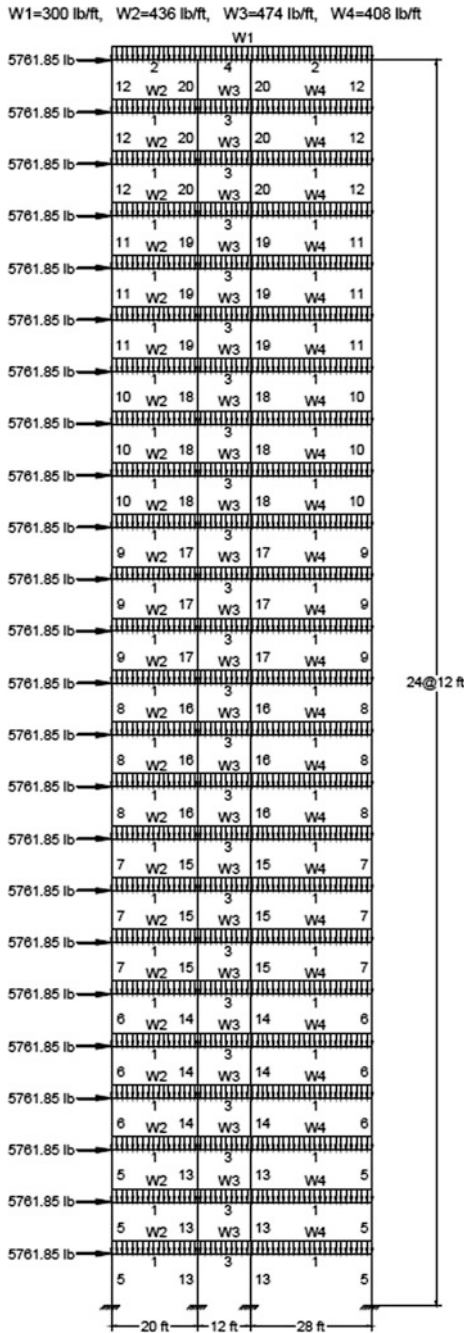


Fig. 3.9 Schematic of the 3-bay 24-story frame

Table 3.9 Performance comparison of the 3-bay 24-story frame problem

Element group	Optimal W-shaped sections					
	CSS [16]	ES-DE [17]	DSOS [18]	CBO [19]	ECBO [19]	VPS [3]
1	W30 × 90	W30 × 90	W30 × 90	W27 × 102	W30 × 90	W30 × 90
2	W21 × 50	W21 × 55	W21 × 62	W8 × 18	W6 × 15	W8 × 18
3	W21 × 48	W21 × 48	W21 × 48	W24 × 55	W24 × 55	W21 × 48
4	W12 × 19	W10 × 45	W21 × 55	W6 × 8.5	W6 × 8.5	W6 × 8.5
5	W14 × 176	W14 × 145	W14 × 176	W14 × 132	W14 × 145	W14 × 176
6	W14 × 145	W14 × 109	W14 × 109	W14 × 120	W14 × 132	W14 × 145
7	W14 × 109	W14 × 99	W14 × 120	W14 × 145	W14 × 99	W14 × 99
8	W14 × 90	W14 × 145	W14 × 82	W14 × 82	W14 × 90	W14 × 82
9	W14 × 74	W14 × 109	W14 × 61	W14 × 61	W14 × 74	W14 × 82
10	W14 × 61	W14 × 48	W14 × 99	W14 × 43	W14 × 38	W14 × 38
11	W14 × 34	W14 × 38	W14 × 34	W14 × 38	W14 × 38	W14 × 30
12	W14 × 34	W14 × 30	W14 × 38	W14 × 22	W14 × 22	W14 × 30
13	W14 × 145	W14 × 99	W14 × 120	W14 × 99	W14 × 99	W14 × 90
14	W14 × 132	W14 × 132	W14 × 109	W14 × 109	W14 × 99	W14 × 99
15	W14 × 109	W14 × 109	W14 × 90	W14 × 82	W14 × 99	W14 × 99
16	W14 × 82	W14 × 68	W14 × 90	W14 × 90	W14 × 82	W14 × 90
17	W14 × 68	W14 × 68	W14 × 82	W14 × 74	W14 × 68	W14 × 61
18	W14 × 43	W14 × 68	W14 × 38	W14 × 61	W14 × 61	W14 × 61
19	W14 × 34	W14 × 61	W14 × 38	W14 × 30	W14 × 30	W14 × 34
20	W14 × 22	W14 × 22	W14 × 22	W14 × 22	W14 × 22	W14 × 26
Weight (lb)	212,364	212,492	209,795	215,874	201,618	202,998
Average optimized weight (lb)	215,226	N/A	N/A	225,071	209,644	212,289
Standard deviation on average weight (lb)	2448	N/A	N/A	N/A	N/A	8292

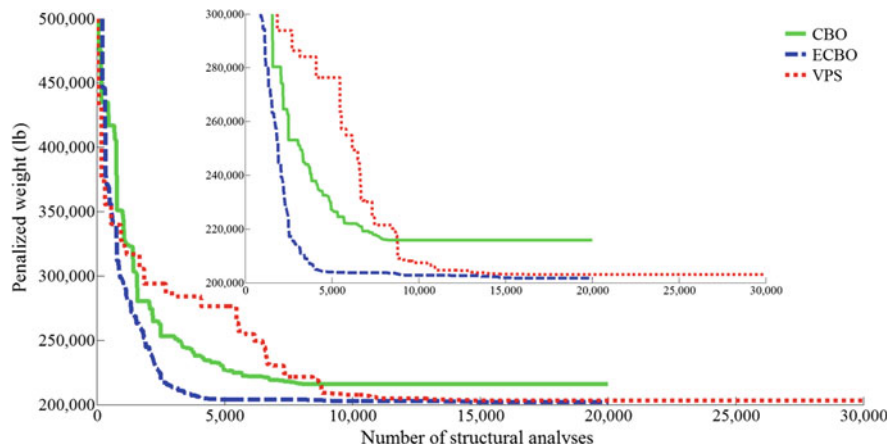


Fig. 3.10 Convergence curves for the 3-bay 24-story frame problem

References

1. Kaveh A (2017) Advances in metaheuristic algorithms for optimal design of structures, 2nd edn. Springer, Switzerland
2. Kaveh A (2017) Applications of metaheuristic optimization algorithms in civil engineering. Springer, Switzerland
3. Kaveh A, Ilchi Ghazaan M (2017) A new meta-heuristic algorithm: vibrating particles system. Sci Iranica, Trans A, Civil Eng 24(2):551–566
4. Kaveh A, Zolghadr A (2012) Truss optimization with natural frequency constraints using a hybridized CSS–BBCB algorithm with trap recognition capability. Comput Struct 102–103:14–27
5. Kaveh A, Ilchi Ghazaan M (2015) Hybridized optimization algorithms for design of trusses with multiple natural frequency constraints. Adv Eng Softw 79:137–147
6. Kaveh A, Zolghadr A (2017) Truss shape and size optimization with frequency constraints using Tug of war optimization. Asian J Civil Eng 7(2):311–333
7. Kaveh A, Ilchi Ghazaan M (2014) Enhanced colliding bodies algorithm for truss optimization with frequency constraints. J Comput Civil Eng 29(6)
8. Kaveh A, Ilchi Ghazaan M (2017) Vibrating particles system algorithm for truss optimization with multiple natural frequency constraints. Acta Mech 228(1):307–322
9. Kaveh A, Mahdavi VR (2015) A hybrid CBO–PSO algorithm for optimal design of truss structures with dynamic constraints. Appl Soft Comput 34:260–273
10. American Institute of Steel Construction (AISC) (1989) Manual of steel construction: allowable stress design
11. Talatahari S, Kheirollahi M, Farahmandpour C, Gandomi AH (2013) A multi-stage particle swarm for optimum design of truss structures. Neural Comput Appl 23:1297–1309
12. Kaveh A, Zolghadr A (2016) A novel metaheuristic algorithm: tug of war optimization. Int J Optim Civil Eng 6(4):469–492
13. Kaveh A, Bakhshpoori T (2016) Water evaporation optimization: a novel physically inspired optimization algorithm. Comput Struct 167:69–85
14. American Institute of Steel Construction (AISC) (2001) Manual of steel construction: load and resistance factor design
15. Dumonteil P (1992) Simple equations for effective length factors. Eng J AISC 29(3):111–115

16. Kaveh A, Talatahari S (2012) Charged system search for optimal design of frame structures. *Appl Soft Comput* 12:382–393
17. Talatahari S, Gandomi AH, Yang XS, Deb S (2015) Optimum design of frame structures using the eagle strategy with differential evolution. *Eng Struct* 91:16–25
18. Talatahari S (2016) Symbiotic organisms search for optimum design of and grillage system. *Asian J Civil Eng* 17(3):299–313
19. Kaveh A, Ilchi Ghazaan M (2015) A comparative study of CBO and ECBO for optimal design of skeletal structures. *Comput Struct* 153:137–147

Chapter 4

Optimal Design of Large-Scale Special Truss Structures



4.1 Introduction

A truss is a two- or three-dimensional structure composed of linear members connected at nodes to sustain concentrated loads with the members being subjected to tension or compression. Optimum design problems of steel trusses are known as benchmarks in the field of structural optimization due to the presence of many design variables, large search spaces, and multiple constraints. Truss optimization problems can be classified in three categories: (1) size optimization (obtaining the optimal cross sections of the structural members); (2) shape optimization (finding the optimal form of the structure); and (3) topology optimization (achieving the optimal size and connectivity of the structural members). Truss structures can be considered as a suitable means to investigate the efficiency of optimization algorithms. This branch of structural optimization has been extensively developed in the last three decades [1–16].

In this chapter, sizing optimization of large-scale tower trusses is studied. Steel truss members are adopted from a predetermined list of available sections; therefore, a discrete optimization is performed in order to obtain the optimum or a near optimum solution. These types of structures are typically considered as high-rise and large-scale structures composed of several hundred elements. These towers have important applications in telecommunication and broadcasting industries.

4.2 Optimum Design Problem of Steel Trusses

The aim of optimizing a structure is generally to find a set of design variables corresponding to the minimum weight structure while satisfying certain constraints. Truss structures are often designed to carry multiple loading conditions under static constraints on the nodal displacements, stresses in the members, and critical

buckling loads. The mathematical formulation of a structural optimization problem can be expressed as follows:

$$\begin{aligned} \text{Find } & \{X\} = [x_1, x_2, \dots, x_{ng}] \\ \text{to minimize } & W(\{X\}) = \sum_{i=1}^{ng} x_i \sum_{j=1}^{nm(i)} \rho_j L_j \\ \text{subjected to : } & \begin{cases} g_j(\{X\}) \leq 0, j = 1, 2, \dots, nc \\ x_{i\min} \leq x_i \leq x_{i\max} \end{cases} \end{aligned} \quad (4.1)$$

where $\{X\}$ is a vector containing the design variables; $W(\{X\})$ presents the weight of the structure; ng is the number of design groups; $nm(i)$ is the number of members for the i th group; and ρ_j and L_j denote the material density and the length of the j th member, respectively. $x_{i\min}$ and $x_{i\max}$ are the lower and upper bounds of the design variable x_i , respectively. $g_j(\{X\})$ denotes the set of design constraints, and nc is the number of constraints.

For constraint handling, a penalty approach is utilized. For this purpose, the objective function (Eq. 4.1) is redefined as follows:

$$P(\{X\}) = (1 + \varepsilon_1 v)^{\varepsilon_2} \times W(\{X\}) \quad (4.2)$$

where $P(\{X\})$ is the penalized cost function or the objective function to be minimized and v denotes the sum of the violations of the design constraints. Here, ε_1 is set to unity, and ε_2 is calculated by

$$\varepsilon_2 = 1.5 + 1.5 \times \frac{iter}{iter_{\max}} \quad (4.3)$$

where $iter$ is the current iteration number, and $iter_{\max}$ is the total number of iterations for the optimization process.

The constraint conditions for truss structures studied here are briefly explained in the following. Limitations on stress and stability of truss elements are imposed according to the provisions of the ASD-AISC [17] as follows.

The allowable tensile stress for tension members are calculated by

$$\sigma_i^+ = 0.6F_y \quad (4.4)$$

where F_y stands for the yield strength.

The allowable stress limits for compression members are calculated depending on two possible failure modes of the members known as elastic and inelastic buckling. Thus

$$\sigma_i^- = \begin{cases} \left[\left(1 - \frac{\lambda_i^2}{2C_c^2} \right) F_y \right] / \left(\frac{5}{3} + \frac{3\lambda_i}{8C_c} - \frac{\lambda_i^2}{8C_c^3} \right) & \text{for } \lambda_i < C_c \\ \frac{12\pi^2 E}{23\lambda_i^2} & \text{for } \lambda_i \geq C_c \end{cases} \quad (4.5)$$

where E is the modulus of elasticity; λ_i is the slenderness ratio ($\lambda_i = kl_i/r_i$); C_c denotes the slenderness ratio dividing the elastic and inelastic buckling regions ($C_c = \sqrt{2\pi^2 E/F_y}$); k is the effective length factor (k is set to 1 for all truss members); l_i is the member length; and r_i is the minimum radius of gyration.

According to the provisions of ASD-AISC, the maximum slenderness ratios are limited to 300 and 200 for tension and compression members, respectively. Nodal displacements in all coordinate directions must be less than ± 3.15 in. (i.e., ± 8 cm).

4.3 Design Examples

In this section, three tower truss optimization benchmark problems are optimized using CBO, ECBO, VPS, and MDVC-UVPS algorithms. These optimization examples are as follows:

- A spatial 582-bar tower truss
- A spatial 942-bar tower truss
- A spatial 2386-bar tower truss.

4.3.1 A Spatial 582-Bar Tower Truss

The schematic of the 582-bar tower truss is shown in Fig. 4.1. The members of the truss are grouped into 32 independent sizing variables considering its symmetry about x - and y -axes. A single load case is considered consisting of lateral loads of 1.12 kips (5.0 kN) applied in both x - and y -directions and vertical loads of -6.74 kips (-30 kN) applied in z -direction to all free nodes of the tower. A discrete set of standard steel sections selected from the list of W-shape profiles is considered for the sizing variables based on the cross-sectional areas and radii of gyration. Cross-sectional areas of the elements can vary between 6.16 and 215 in.² (i.e., between 39.74 and 1387.09 cm²). Limitations on stress and stability of truss elements and nodal displacements are defined in Sect. 4.2.

This problem is optimized in three stages by MDVC-UVPS. The number of design variables in stages 1, 2, and 3 is 8, 15, and 32, respectively. Table 4.1 presents the design variables configurations. Table 4.2 presents the results obtained by CBO [18], ECBO [18], VPS, and MDVC-UVPS. The best design obtained by MDVC-UVPS is better than those of the other methods (1,295,038 in.³). The best volumes found by CBO, ECBO, and VPS are 1,334,994, 1,296,776, and 1,304,569 in.³, respectively. MDVC-UVPS is the most robust optimizer, achieving the lowest average volume over the independent optimization runs. The CBO,

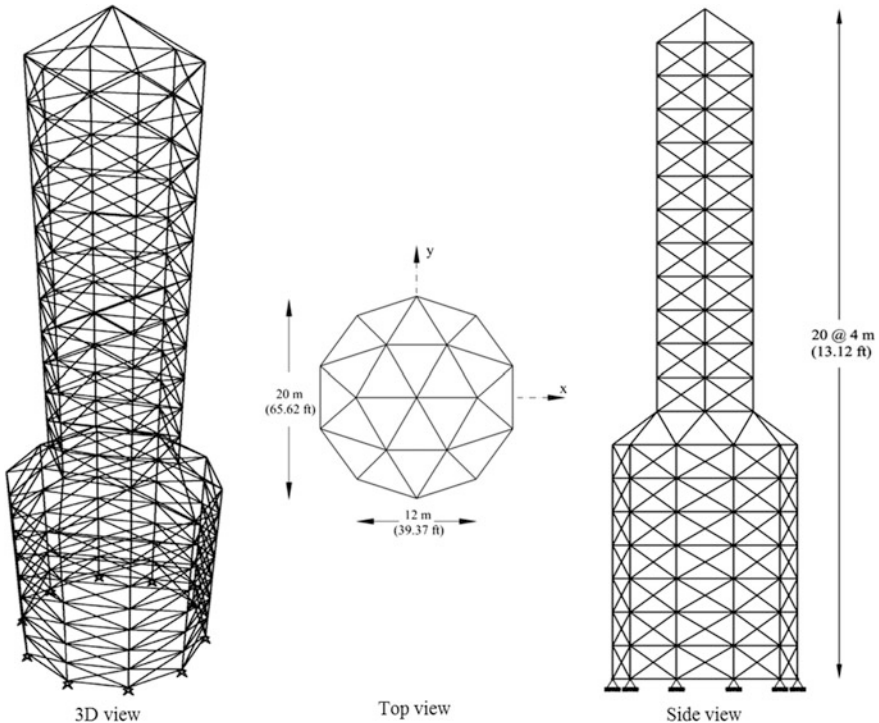


Fig. 4.1 Schematic of the 582-bar tower truss

Table 4.1 Design variable configurations utilized for the 582-bar tower problem

	Number of design variables in stages	Design variables in the group (design variable configurations)
Stage 1	8	[1 6 9]; [2 4 7 10]; [3 5 8 11]; [12 13 14]; [19 22 25 28 31]; [32]; [15 17 20 23 26 29]; [16 18 21 24 27 30]
Stage 2	15	[1 6 9]; [2 4]; [7 10]; [3 5]; [8 11]; [12]; [13]; [14]; [19 22 25]; [28 31]; [32]; [15 17 20]; [23 26 29]; [16 18 21]; [24 27 30]

ECBO, VPS, and MDVC-UVPS algorithms obtained the optimal solutions after 17,700, 19,700, 17,540, and 15,480 analyses, respectively. Stress ratios and nodal displacements in all directions evaluated for the best design optimized by MDVC-UVPS are shown in Fig. 4.2. The maximum stress ratio and the maximum nodal displacement obtained by MDVC-UVPS are 99.88% and 3.1493 in. respectively.

Table 4.2 Performance comparison for the spatial 582-bar tower truss problem

Element group	Optimal W-shaped sections			
	CBO [18]	ECBO [18]	VPS	MDVC-UVPS
1	W8 × 21	W8 × 21	W8 × 21	W8 × 21
2	W14 × 82	W14 × 90	W14 × 90	W14 × 90
3	W8 × 28	W8 × 24	W8 × 24	W8 × 24
4	W12 × 50	W14 × 61	W21 × 62	W14 × 61
5	W8 × 24	W8 × 24	W8 × 24	W8 × 24
6	W8 × 21	W8 × 21	W8 × 21	W8 × 21
7	W12 × 53	W10 × 49	W10 × 39	W10 × 45
8	W12 × 26	W8 × 24	W8 × 24	W8 × 24
9	W8 × 21	W8 × 21	W8 × 24	W8 × 21
10	W14 × 48	W14 × 43	W10 × 33	W14 × 43
11	W8 × 24	W8 × 24	W8 × 24	W8 × 24
12	W14 × 61	W12 × 72	W14 × 74	W10 × 68
13	W14 × 82	W12 × 72	W10 × 77	W12 × 72
14	W12 × 50	W10 × 54	W10 × 49	W10 × 49
15	W14 × 74	W12 × 65	W10 × 77	W14 × 82
16	W8 × 40	W8 × 31	W8 × 31	W8 × 31
17	W12 × 53	W10 × 60	W21 × 62	W21 × 62
18	W6 × 25	W8 × 24	W8 × 24	W8 × 24
19	W8 × 21	W8 × 21	W10 × 22	W8 × 21
20	W8 × 40	W14 × 43	W10 × 49	W14 × 38
21	W8 × 24	W8 × 24	W8 × 24	W8 × 24
22	W8 × 21	W8 × 21	W8 × 21	W8 × 21
23	W12 × 26	W8 × 21	W10 × 22	W6 × 25
24	W12 × 26	W8 × 24	W8 × 24	W8 × 24
25	W10 × 22	W8 × 21	W8 × 21	W8 × 21
26	W10 × 22	W8 × 21	W8 × 21	W8 × 21
27	W6 × 25	W8 × 24	W8 × 24	W8 × 24
28	W8 × 21	W8 × 21	W8 × 21	W8 × 21
29	W8 × 21	W8 × 21	W10 × 22	W8 × 21
30	W8 × 24	W8 × 24	W8 × 24	W8 × 24
31	W8 × 21	W8 × 21	W10 × 22	W8 × 21
32	W6 × 25	W8 × 24	W8 × 24	W8 × 24
Volume (in. ³)	1,334,994	1,296,776	1,304,569	1,295,038
Average optimized volume (in. ³)	1,345,429	1,306,728	1,324,086	1,302,422
Standard deviation on average volume (in. ³)	9116	7536	12,218	4347

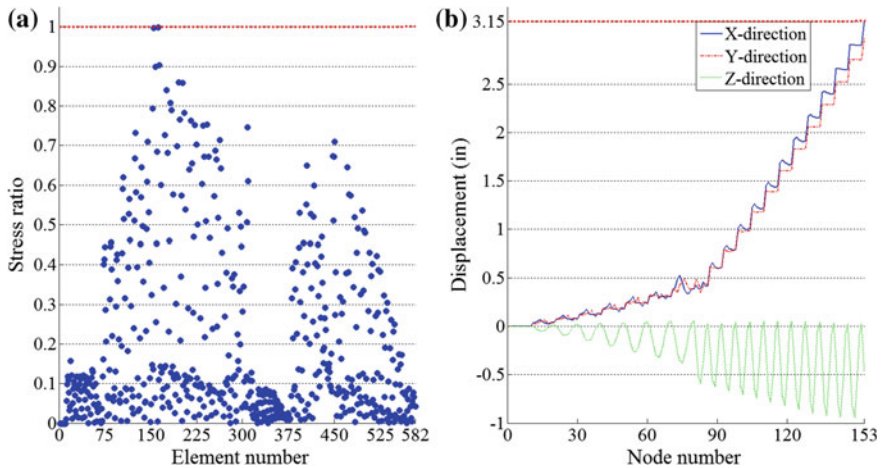


Fig. 4.2 Constraint margins for the best design obtained by MDVC-UVPS algorithm for the 582-bar tower truss problem: **a** element stress ratio and **b** nodal displacements

4.3.2 A Spatial 942-Bar Tower Truss

Figure 4.3 shows the schematic of a 942-bar tower truss. This example has been investigated by many researchers considering 59 design variables [19]. In this study, the design variables are increased to 76, and the performance constraints, material properties, and other conditions are the same as those of the first example. Figure 4.4 shows the member groups. Three stages with 16, 28, and 76 design variables are considered to solve this problem using MDVC-UVPS. The design variable configurations are shown in Table 4.3.

The optimized designs found by different algorithms are compared in Table 4.4. The volume of the best result obtained by the hybrid algorithm is 3,263,387 in.³ that is the best among the compared methods. The average optimized volume and the standard deviation on average volume obtained by MDVC-UVPS are less than those of all other considered methods. This algorithm requires 14,587 structural analyses to find the optimum solution, while CBO [20], ECBO [20], and VPS [21] require 29,600, 19,960, and 26,180 structural analyses, respectively. The amount of saving in structural analyses in each iteration of the MDVC-UVPS is shown in Fig. 4.5.

4.3.3 A Spatial 2386-Bar Tower Truss

The schematic of a 2386-bar tower truss is shown in Fig. 4.6. This example is studied here for the first time. The performance constraints, material properties, and other conditions are the same as those of the first example. The elements are divided

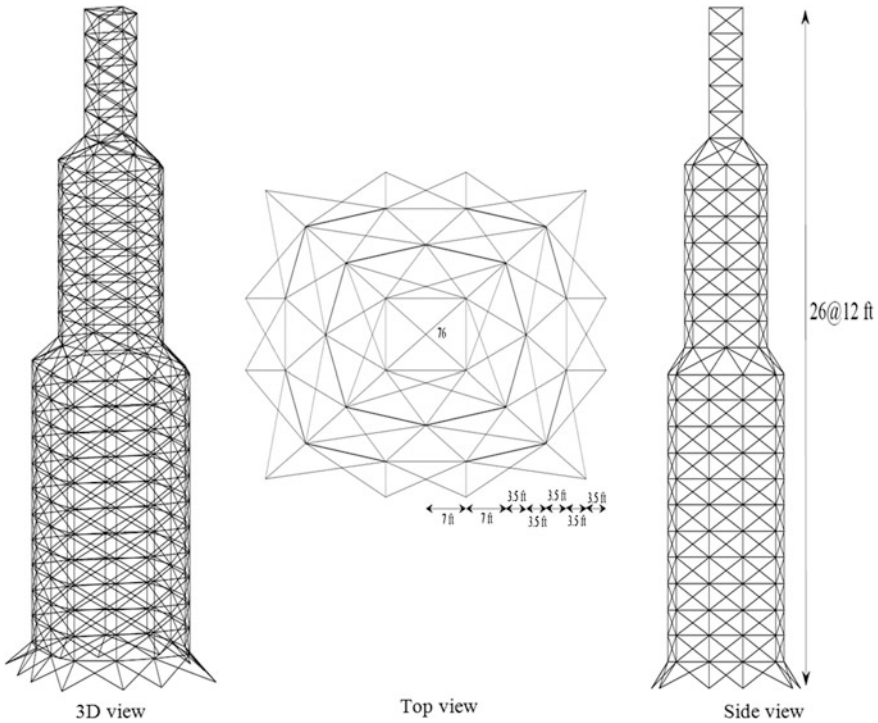


Fig. 4.3 Schematic of the 942-bar tower truss

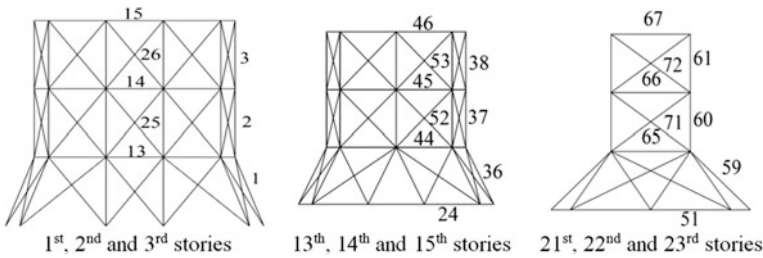


Fig. 4.4 Member groups of 942-bar tower truss

into 220 groups and member groups are presented in Fig. 4.7. Four stages are considered to optimize this example using MDVC-UVPS. The number of design variable in stages 1, 2, 3, and 4 is 21, 42, 84, and 220, respectively. Table 4.5 lists the design variable configurations.

Table 4.6 presents the optimum designs obtained by the proposed algorithms. The lightest design (i.e., 12,165,572 in.³) is achieved by MDVC-UVPS algorithm

Table 4.3 Design variable configurations utilized for the 942-bar tower problem

	Number of design variables in stages	Design variables in the group (design variable configurations)
Stage 1	16	[1]; [2–6]; [7–12]; [13–18]; [19–24]; [25–29]; [30–35]; [36]; [37–43]; [44–51]; [52–58]; [59]; [60–64]; [65–70]; [71–75]; [76]
Stage 2	28	[1]; [2 3]; [4–6]; [7–9]; [10–12]; [13–15]; [16–18]; [19–21]; [22–24]; [25 26]; [27–29]; [30–32]; [33–35]; [36]; [37–39]; [40–43]; [44–47]; [48–51]; [52–54]; [55–58]; [59]; [60 61]; [62–64]; [65–67]; [68–70]; [71 72]; [73–75]; [76]

Table 4.4 Performance comparison for the spatial 942-bar tower truss problem

Element group	Optimal W-shaped sections			
	CBO [20]	ECBO [20]	VPS [21]	MDVC-UVPS
1	W14 × 145	W12 × 190	W12 × 170	W12 × 170
2	W36 × 280	W36 × 230	W36 × 260	W14 × 257
3	W24 × 250	W40 × 199	W44 × 262	W24 × 279
4	W14 × 257	W24 × 229	W30 × 235	W33 × 241
5	W33 × 241	W36 × 150	W36 × 245	W40 × 249
6	W44 × 262	W30 × 173	W24 × 229	W14 × 211
7	W30 × 211	W24 × 250	W40 × 199	W24 × 192
8	W33 × 201	W27 × 258	W14 × 193	W24 × 192
9	W24 × 176	W14 × 159	W40 × 174	W14 × 176
10	W24 × 162	W30 × 191	W24 × 162	W40 × 174
11	W21 × 147	W18 × 158	W14 × 145	W12 × 136
12	W12 × 136	W18 × 119	W18 × 119	W24 × 131
13	W33 × 221	W24 × 250	W12 × 279	W36 × 230
14	W6 × 25	W14 × 30	W8 × 21	W8 × 24
15	W10 × 54	W8 × 21	W10 × 22	W8 × 21
16	W8 × 21	W8 × 21	W12 × 26	W10 × 22
17	W10 × 22	W8 × 21	W10 × 22	W8 × 21
18	W8 × 21	W8 × 21	W10 × 22	W10 × 22
19	W10 × 22	W8 × 21	W10 × 22	W8 × 21
20	W8 × 21	W8 × 21	W10 × 22	W10 × 22
21	W8 × 21	W8 × 21	W6 × 25	W8 × 21
22	W10 × 22	W8 × 21	W8 × 24	W8 × 21
23	W10 × 22	W8 × 21	W10 × 22	W8 × 21
24	W14 × 145	W24 × 117	W14 × 145	W21 × 147
25	W14 × 34	W12 × 50	W8 × 31	W12 × 30
26	W8 × 24	W14 × 30	W8 × 24	W6 × 25
27	W8 × 24	W10 × 33	W8 × 24	W6 × 25

(continued)

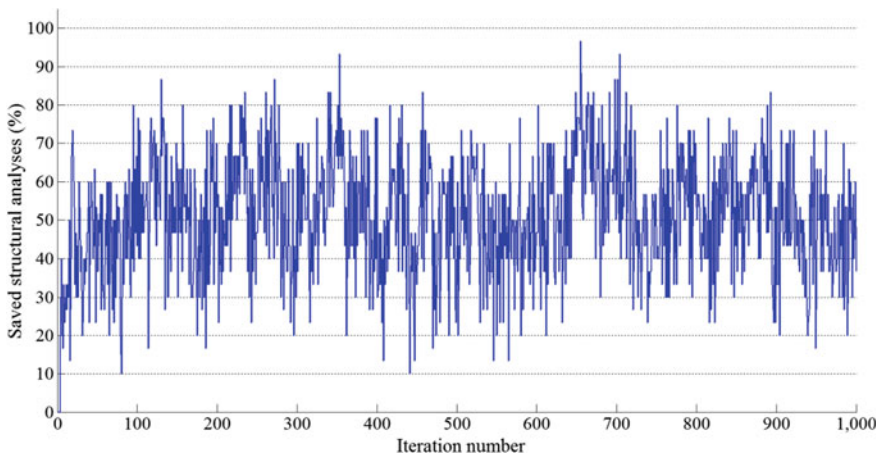
Table 4.4 (continued)

Element group	Optimal W-shaped sections			
	CBO [20]	ECBO [20]	VPS [21]	MDVC-UVPS
28	W6 × 25	W6 × 25	W8 × 24	W8 × 24
29	W12 × 79	W8 × 31	W12 × 26	W8 × 24
30	W10 × 22	W8 × 31	W10 × 22	W10 × 22
31	W6 × 25	W8 × 21	W8 × 21	W10 × 22
32	W10 × 22	W12 × 26	W10 × 22	W10 × 22
33	W8 × 21	W8 × 21	W8 × 21	W10 × 22
34	W6 × 25	W8 × 21	W10 × 22	W10 × 22
35	W10 × 22	W8 × 21	W8 × 21	W10 × 22
36	W14 × 90	W18 × 86	W16 × 89	W12 × 87
37	W40 × 174	W30 × 191	W30 × 211	W12 × 170
38	W21 × 147	W30 × 116	W14 × 109	W36 × 150
39	W12 × 136	W27 × 178	W24 × 131	W21 × 147
40	W10 × 100	W24 × 131	W21 × 101	W24 × 104
41	W14 × 74	W18 × 86	W10 × 88	W16 × 100
42	W14 × 82	W10 × 88	W10 × 77	W21 × 93
43	W14 × 61	W21 × 62	W12 × 50	W21 × 62
44	W24 × 117	W12 × 136	W27 × 114	W18 × 119
45	W8 × 31	W8 × 21	W10 × 22	W8 × 21
46	W6 × 25	W8 × 21	W10 × 22	W10 × 22
47	W12 × 30	W8 × 21	W10 × 22	W8 × 21
48	W12 × 26	W8 × 21	W6 × 25	W6 × 25
49	W8 × 21	W8 × 21	W10 × 22	W10 × 22
50	W10 × 22	W8 × 21	W8 × 40	W8 × 21
51	W18 × 76	W27 × 94	W12 × 58	W21 × 62
52	W8 × 24	W10 × 22	W6 × 25	W8 × 24
53	W8 × 24	W6 × 25	W10 × 22	W8 × 24
54	W8 × 24	W8 × 21	W10 × 22	W10 × 22
55	W10 × 22	W8 × 21	W10 × 22	W8 × 21
56	W10 × 22	W8 × 21	W10 × 22	W8 × 21
57	W8 × 24	W8 × 21	W8 × 21	W8 × 21
58	W10 × 22	W8 × 21	W10 × 22	W8 × 21
59	W14 × 48	W21 × 62	W14 × 43	W12 × 50
60	W21 × 111	W12 × 152	W24 × 117	W12 × 96
61	W12 × 87	W14 × 120	W18 × 119	W21 × 93
62	W10 × 60	W12 × 65	W14 × 38	W14 × 48
63	W6 × 25	W14 × 30	W10 × 77	W14 × 38
64	W8 × 24	W8 × 21	W14 × 61	W8 × 24
65	W10 × 22	W8 × 21	W10 × 22	W8 × 21
66	W14 × 34	W8 × 21	W10 × 22	W8 × 21

(continued)

Table 4.4 (continued)

Element group	Optimal W-shaped sections			
	CBO [20]	ECBO [20]	VPS [21]	MDVC-UVPS
67	W24 × 146	W8 × 21	W8 × 21	W8 × 21
68	W12 × 58	W8 × 21	W10 × 22	W10 × 22
69	W8 × 21	W8 × 21	W10 × 22	W12 × 26
70	W8 × 21	W8 × 21	W10 × 22	W10 × 22
71	W8 × 24	W8 × 24	W8 × 31	W8 × 21
72	W8 × 24	W8 × 24	W10 × 22	W8 × 21
73	W8 × 24	W8 × 21	W12 × 26	W10 × 22
74	W16 × 36	W8 × 21	W10 × 22	W10 × 22
75	W10 × 22	W8 × 21	W8 × 21	W8 × 21
76	W6 × 25	W8 × 21	W8 × 28	W14 × 30
Volume (in. ³)	3,414,157	3,376,968	3,296,202	3,263,387
Average optimized volume (in. ³)	3,601,976	3,429,516	3,346,822	3,276,876
Standard deviation on average volume (in. ³)	47,864	45,121	41,617	13,823

**Fig. 4.5** Saving in structural analyses using the MDVC-UVPS algorithm for the 942-bar tower truss problem

after 13,385 analyses. The best design obtained by the CBO [20], ECBO [20], and VPS [21] is 15,587,709 in.³, 14,086,857 in.³, and 12,989,713 in.³, respectively. These values are found after 29,970, 29,670, and 29,980 analyses. MDVC-UVPS is also the most robust optimizer, achieving the lowest average design over the independent optimization runs. Convergence history diagrams are depicted in

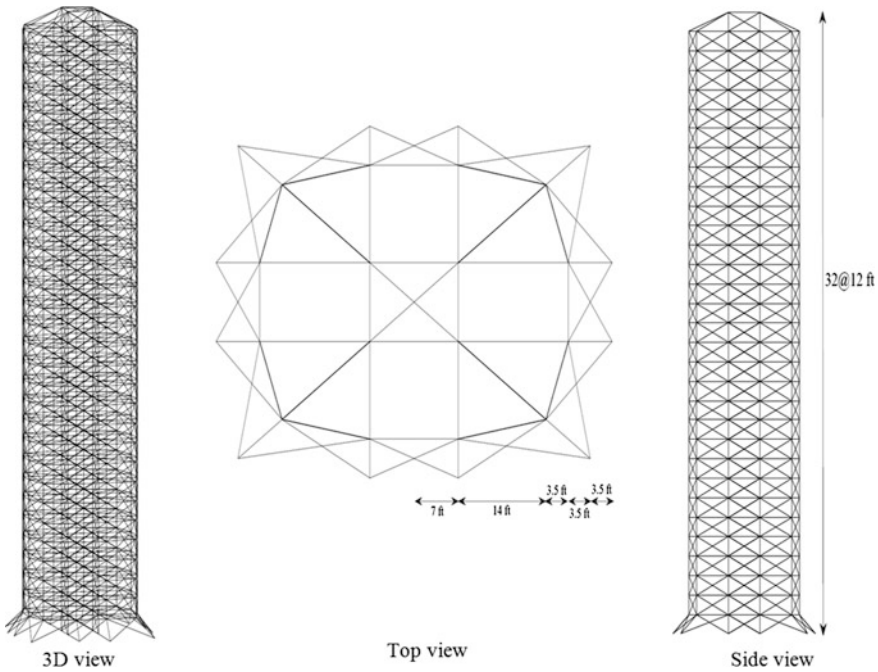


Fig. 4.6 Schematic of the 2386-bar tower truss

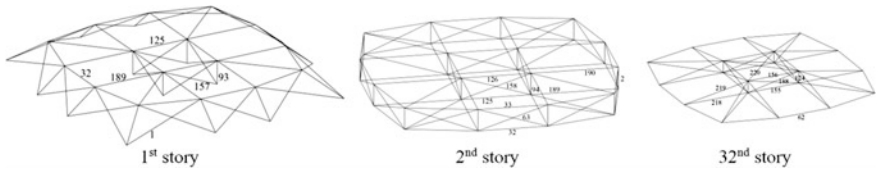


Fig. 4.7 Member groups of the 2386-bar tower truss

Fig. 4.8 and demonstrate that the intermediate designs found by MDVC-UVPS are always better than those found by the other considered algorithms.

4.4 Concluding Remarks

Truss structures are often designed to carry multiple loading conditions under static constraints on the nodal displacements, stresses in the members, and critical buckling loads. This class of problems is highly nonlinear and also widely studied in the field of practical structural engineering. In this chapter, three tower trusses with a large number of design variables are studied to test and verify the efficiency

Table 4.5 Design variable configurations utilized for the 2386-bar tower problem

	Number of design variables in stages	Design variables in the group (design variable configurations)
Stage 1	21	[1–10]; [11–20]; [21–31]; [32–41]; [42–51]; [52–62]; [63–72]; [73–82]; [83–92]; [93–103]; [104–113]; [114–124]; [125–135]; [136–146]; [147–156]; [157–167]; [168–178]; [179–188]; [189–199]; [200–210]; [211–220]
Stage 2	42	[1:4]; [5:10]; [11:15]; [16:20]; [21:25]; [26:31]; [32:36]; [37:41]; [42:46]; [47:51]; [52:56]; [57:62]; [63:67]; [68:72]; [73:77]; [78:82]; [83:87]; [88:92]; [93:97]; [98:103]; [104:108]; [109:113]; [114:118]; [119:124]; [125:129]; [130:135]; [136:140]; [141:146]; [147:151]; [152:156]; [157:161]; [162:167]; [168:172]; [173:178]; [179:183]; [184:188]; [189:193]; [194:199]; [200:204]; [205:210]; [211:215]; [216:220]
Stage 3	84	[1]; [2–4]; [5–7]; [8–10]; [11 12]; [13–15]; [16 17]; [18–20]; [21 22]; [23–25]; [26–28]; [29–31]; [32 33]; [34–36]; [37 38]; [39–41]; [42 43]; [44–46]; [47 48]; [49–51]; [52 53]; [54–56]; [57–59]; [60–62]; [63 64]; [65–67]; [68 69]; [70–72]; [73 74]; [75–77]; [78 79]; [80–82]; [83 84]; [85–87]; [88 89]; [90–92]; [93 94]; [95–97]; [98–100]; [101–103]; [104 105]; [106–108]; [109 110]; [111–113]; [114 115]; [116–118]; [119–121]; [122–124]; [125 126]; [127–129]; [130–132]; [133–135]; [136 137]; [138–140]; [141–143]; [144–146]; [147 148]; [149–151]; [152 153]; [154–156]; [157 158]; [159–161]; [162–164]; [165–167]; [168 169]; [170–172]; [173–175]; [176–178]; [179 180]; [181–183]; [184 185]; [186–188]; [189 190]; [191–193]; [194–196]; [197–199]; [200 201]; [202–204]; [205–207]; [208–210]; [211 212]; [213–215]; [216 217]; [218–220]

Table 4.6 Performance comparison for the spatial 23862-bar tower truss problem

Element group	Optimal W-shaped sections			
	CBO [20]	ECBO [20]	VPS [21]	MDVC-UVPS
1	W14 × 605	W14 × 730	W14 × 665	W14 × 730
2	W14 × 730	W14 × 730	W14 × 605	W14 × 730
3	W14 × 730	W14 × 730	W14 × 665	W14 × 730
4	W14 × 605	W14 × 665	W14 × 665	W14 × 730
5	W14 × 730	W14 × 730	W14 × 605	W14 × 730
6	W14 × 605	W14 × 730	W14 × 665	W14 × 730
7	W40 × 249	W14 × 730	W14 × 665	W14 × 730
8	W14 × 730	W40 × 215	W14 × 665	W14 × 730
9	W14 × 665	W14 × 665	W14 × 605	W14 × 730
10	W14 × 665	W14 × 500	W14 × 665	W14 × 730
11	W14 × 665	W12 × 279	W14 × 665	W14 × 455
12	W27 × 194	W33 × 318	W14 × 426	W14 × 455
13	W27 × 194	W14 × 605	W14 × 665	W14 × 455

(continued)

Table 4.6 (continued)

Element group	Optimal W-shaped sections			
	CBO [20]	ECBO [20]	VPS [21]	MDVC-UVPS
14	W14 × 730	W14 × 730	W14 × 426	W14 × 455
15	W30 × 235	W14 × 455	W14 × 605	W14 × 455
16	W33 × 241	W33 × 221	W14 × 550	W14 × 370
17	W12 × 136	W44 × 335	W36 × 245	W36 × 328
18	W12 × 279	W14 × 426	W33 × 291	W12 × 279
19	W27 × 258	W33 × 221	W33 × 263	W33 × 291
20	W12 × 230	W24 × 229	W30 × 292	W12 × 279
21	W30 × 235	W14 × 145	W33 × 221	W30 × 191
22	W36 × 150	W12 × 252	W18 × 158	W24 × 192
23	W36 × 328	W27 × 194	W18 × 158	W12 × 136
24	W14 × 211	W36 × 245	W12 × 136	W27 × 94
25	W27 × 258	W27 × 161	W14 × 109	W24 × 131
26	W10 × 54	W33 × 118	W44 × 335	W14 × 61
27	W24 × 146	W33 × 201	W18 × 86	W27 × 94
28	W27 × 161	W8 × 21	W14 × 30	W12 × 65
29	W14 × 34	W14 × 90	W10 × 33	W12 × 26
30	W10 × 39	W8 × 21	W8 × 21	W10 × 45
31	W8 × 28	W8 × 35	W14 × 61	W16 × 36
32	W14 × 730	W30 × 211	W14 × 605	W14 × 500
33	W12 × 79	W14 × 120	W14 × 120	W10 × 112
34	W8 × 21	W16 × 67	W10 × 22	W8 × 24
35	W18 × 97	W10 × 100	W14 × 30	W8 × 24
36	W12 × 79	W12 × 26	W10 × 22	W6 × 25
37	W14 × 176	W8 × 31	W6 × 25	W10 × 22
38	W10 × 112	W33 × 118	W10 × 22	W10 × 22
39	W12 × 45	W10 × 68	W10 × 22	W10 × 22
40	W10 × 60	W8 × 21	W12 × 26	W10 × 22
41	W10 × 22	W8 × 35	W10 × 22	W10 × 22
42	W14 × 82	W14 × 74	W10 × 22	W10 × 22
43	W14 × 159	W8 × 24	W12 × 26	W8 × 21
44	W14 × 159	W14 × 120	W12 × 26	W8 × 21
45	W21 × 62	W8 × 24	W8 × 24	W8 × 21
46	W12 × 53	W10 × 39	W8 × 21	W8 × 21
47	W36 × 359	W16 × 36	W6 × 25	W8 × 21
48	W14 × 132	W8 × 21	W10 × 49	W8 × 21
49	W10 × 45	W8 × 21	W8 × 21	W8 × 21
50	W8 × 21	W12 × 40	W10 × 22	W8 × 21
51	W14 × 74	W14 × 34	W12 × 26	W8 × 21
52	W14 × 43	W12 × 26	W10 × 22	W8 × 21
53	W12 × 26	W8 × 21	W10 × 22	W8 × 21

(continued)

Table 4.6 (continued)

Element group	Optimal W-shaped sections			
	CBO [20]	ECBO [20]	VPS [21]	MDVC-UVPS
54	W8 × 21	W8 × 21	W10 × 22	W8 × 21
55	W12 × 106	W8 × 21	W12 × 26	W8 × 21
56	W14 × 34	W8 × 21	W10 × 22	W8 × 21
57	W8 × 40	W8 × 21	W8 × 31	W8 × 21
58	W10 × 22	W8 × 24	W10 × 22	W8 × 21
59	W8 × 21	W14 × 34	W6 × 25	W8 × 21
60	W21 × 62	W10 × 22	W10 × 22	W8 × 21
61	W8 × 21	W16 × 36	W10 × 22	W8 × 21
62	W12 × 45	W8 × 35	W8 × 21	W8 × 21
63	W14 × 176	W33 × 318	W10 × 112	W18 × 97
64	W27 × 114	W12 × 136	W16 × 89	W16 × 100
65	W18 × 158	W21 × 147	W10 × 68	W10 × 54
66	W21 × 101	W18 × 86	W12 × 79	W12 × 65
67	W12 × 50	W10 × 88	W10 × 60	W16 × 67
68	W36 × 300	W14 × 82	W14 × 61	W16 × 67
69	W21 × 111	W12 × 152	W14 × 43	W14 × 61
70	W14 × 159	W10 × 49	W16 × 67	W16 × 67
71	W10 × 54	W10 × 60	W21 × 62	W10 × 54
72	W12 × 87	W12 × 136	W12 × 58	W12 × 50
73	W33 × 241	W16 × 89	W14 × 61	W12 × 50
74	W33 × 263	W14 × 90	W21 × 62	W12 × 53
75	W30 × 116	W14 × 38	W16 × 36	W14 × 48
76	W12 × 106	W12 × 65	W10 × 68	W10 × 33
77	W24 × 146	W14 × 90	W10 × 60	W10 × 49
78	W24 × 192	W12 × 65	W14 × 34	W8 × 40
79	W16 × 67	W30 × 116	W14 × 43	W10 × 45
80	W12 × 50	W14 × 90	W8 × 35	W14 × 43
81	W27 × 94	W18 × 76	W21 × 62	W16 × 36
82	W10 × 68	W14 × 48	W12 × 45	W8 × 40
83	W14 × 61	W10 × 68	W12 × 26	W8 × 31
84	W16 × 36	W8 × 28	W12 × 50	W8 × 24
85	W12 × 65	W10 × 60	W6 × 25	W14 × 34
86	W8 × 24	W14 × 38	W10 × 22	W12 × 26
87	W12 × 72	W10 × 45	W10 × 22	W8 × 31
88	W12 × 40	W12 × 50	W10 × 22	W16 × 36
89	W8 × 21	W14 × 82	W16 × 36	W8 × 28
90	W12 × 65	W8 × 40	W6 × 25	W10 × 22
91	W12 × 26	W10 × 22	W12 × 26	W10 × 22
92	W8 × 21	W8 × 21	W10 × 22	W10 × 22
93	W8 × 21	W8 × 21	W10 × 22	W8 × 21

(continued)

Table 4.6 (continued)

Element group	Optimal W-shaped sections			
	CBO [20]	ECBO [20]	VPS [21]	MDVC-UVPS
94	W10 × 22	W12 × 40	W8 × 21	W8 × 21
95	W8 × 21	W12 × 40	W14 × 82	W8 × 21
96	W14 × 61	W8 × 21	W10 × 22	W8 × 21
97	W12 × 58	W10 × 39	W12 × 79	W8 × 21
98	W12 × 30	W14 × 30	W21 × 93	W8 × 24
99	W14 × 43	W14 × 48	W14 × 30	W14 × 30
100	W10 × 39	W10 × 88	W10 × 22	W10 × 22
101	W18 × 97	W12 × 50	W14 × 48	W8 × 24
102	W18 × 76	W14 × 34	W8 × 24	W10 × 22
103	W10 × 39	W14 × 43	W12 × 26	W10 × 22
104	W27 × 84	W12 × 65	W8 × 31	W10 × 22
105	W12 × 87	W12 × 53	W12 × 26	W10 × 22
106	W30 × 116	W12 × 26	W12 × 45	W21 × 62
107	W12 × 87	W8 × 21	W14 × 38	W8 × 24
108	W8 × 31	W6 × 25	W14 × 38	W6 × 25
109	W14 × 82	W10 × 39	W10 × 22	W10 × 45
110	W14 × 30	W8 × 28	W10 × 39	W14 × 48
111	W12 × 53	W10 × 39	W16 × 89	W8 × 28
112	W14 × 34	W8 × 21	W14 × 34	W14 × 74
113	W8 × 21	W10 × 22	W8 × 21	W12 × 26
114	W8 × 40	W10 × 49	W14 × 38	W8 × 21
115	W12 × 30	W10 × 33	W12 × 30	W8 × 21
116	W12 × 40	W8 × 31	W10 × 22	W8 × 21
117	W8 × 24	W10 × 22	W8 × 28	W8 × 21
118	W8 × 24	W8 × 21	W6 × 25	W8 × 21
119	W10 × 22	W8 × 28	W12 × 58	W10 × 22
120	W10 × 22	W14 × 30	W24 × 279	W10 × 22
121	W8 × 28	W12 × 26	W14 × 38	W14 × 43
122	W14 × 34	W10 × 49	W8 × 31	W6 × 25
123	W12 × 40	W8 × 21	W10 × 22	W8 × 31
124	W10 × 49	W18 × 86	W10 × 22	W10 × 77
125	W36 × 260	W33 × 118	W18 × 158	W10 × 22
126	W10 × 22	W8 × 21	W8 × 21	W10 × 22
127	W6 × 25	W10 × 22	W21 × 182	W10 × 22
128	W8 × 21	W12 × 26	W8 × 31	W12 × 40
129	W16 × 36	W10 × 22	W10 × 22	W10 × 22
130	W8 × 28	W8 × 24	W14 × 48	W10 × 22
131	W14 × 74	W8 × 21	W16 × 36	W10 × 22
132	W10 × 45	W8 × 21	W12 × 30	W10 × 22
133	W10 × 33	W8 × 21	W8 × 21	W10 × 22

(continued)

Table 4.6 (continued)

Element group	Optimal W-shaped sections			
	CBO [20]	ECBO [20]	VPS [21]	MDVC-UVPS
134	W10 × 22	W8 × 21	W8 × 21	W10 × 22
135	W10 × 22	W8 × 21	W10 × 22	W10 × 22
136	W14 × 38	W12 × 26	W10 × 22	W8 × 21
137	W12 × 26	W10 × 22	W10 × 49	W12 × 26
138	W12 × 50	W10 × 22	W12 × 106	W8 × 21
139	W10 × 45	W8 × 21	W10 × 22	W12 × 26
140	W8 × 21	W10 × 22	W6 × 25	W12 × 26
141	W8 × 21	W8 × 21	W10 × 22	W8 × 21
142	W6 × 25	W8 × 21	W10 × 22	W8 × 21
143	W12 × 50	W8 × 21	W10 × 22	W8 × 21
144	W8 × 31	W8 × 21	W10 × 22	W8 × 21
145	W8 × 21	W14 × 30	W12 × 30	W8 × 21
146	W8 × 21	W10 × 22	W12 × 40	W8 × 21
147	W14 × 30	W8 × 21	W14 × 550	W10 × 22
148	W8 × 21	W8 × 21	W10 × 22	W10 × 22
149	W8 × 24	W8 × 21	W6 × 25	W10 × 22
150	W8 × 21	W14 × 34	W10 × 22	W10 × 22
151	W10 × 22	W10 × 22	W10 × 22	W10 × 22
152	W14 × 30	W12 × 30	W8 × 24	W6 × 25
153	W8 × 21	W8 × 21	W12 × 26	W14 × 30
154	W21 × 101	W10 × 22	W8 × 28	W14 × 38
155	W14 × 43	W8 × 24	W8 × 31	W12 × 26
156	W36 × 230	W27 × 146	W12 × 79	W27 × 94
157	W12 × 53	W14 × 48	W10 × 22	W8 × 21
158	W10 × 22	W8 × 21	W10 × 22	W8 × 21
159	W14 × 38	W14 × 34	W8 × 24	W8 × 21
160	W10 × 54	W8 × 21	W10 × 45	W8 × 21
161	W14 × 30	W10 × 22	W33 × 201	W8 × 21
162	W8 × 21	W6 × 25	W14 × 34	W8 × 21
163	W10 × 22	W8 × 21	W12 × 65	W8 × 21
164	W12 × 30	W8 × 24	W12 × 30	W8 × 21
165	W8 × 28	W10 × 22	W10 × 22	W8 × 21
166	W8 × 21	W8 × 24	W10 × 22	W8 × 21
167	W8 × 21	W8 × 21	W6 × 25	W8 × 21
168	W10 × 22	W8 × 21	W8 × 28	W10 × 33
169	W14 × 34	W14 × 34	W14 × 30	W14 × 30
170	W10 × 22	W10 × 22	W8 × 24	W10 × 22
171	W8 × 21	W8 × 31	W10 × 22	W10 × 22
172	W8 × 21	W6 × 25	W8 × 21	W10 × 22
173	W8 × 21	W10 × 22	W12 × 26	W8 × 21

(continued)

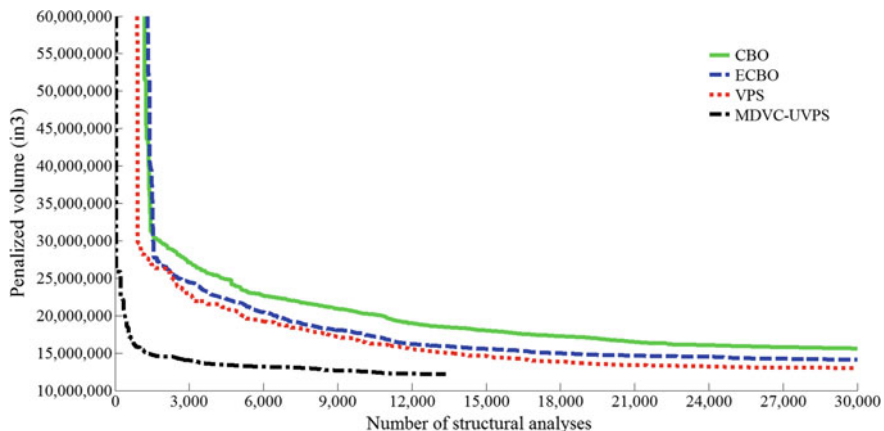
Table 4.6 (continued)

Element group	Optimal W-shaped sections			
	CBO [20]	ECBO [20]	VPS [21]	MDVC-UVPS
174	W8 × 28	W8 × 21	W8 × 21	W8 × 21
175	W8 × 21	W6 × 25	W10 × 22	W8 × 21
176	W8 × 21	W8 × 24	W10 × 22	W8 × 21
177	W8 × 21	W8 × 21	W8 × 24	W8 × 21
178	W10 × 22	W8 × 21	W12 × 45	W8 × 21
179	W8 × 21	W8 × 21	W8 × 24	W8 × 24
180	W8 × 21	W8 × 21	W14 × 38	W8 × 24
181	W8 × 21	W8 × 21	W10 × 22	W8 × 21
182	W8 × 24	W10 × 22	W12 × 26	W8 × 21
183	W8 × 21	W6 × 25	W10 × 22	W8 × 21
184	W8 × 21	W8 × 21	W12 × 58	W8 × 21
185	W6 × 25	W8 × 21	W14 × 34	W8 × 21
186	W8 × 21	W14 × 30	W10 × 22	W10 × 77
187	W12 × 26	W10 × 22	W6 × 25	W16 × 36
188	W14 × 605	W14 × 605	W14 × 605	W30 × 326
189	W10 × 22	W16 × 36	W8 × 21	W10 × 22
190	W8 × 28	W8 × 24	W8 × 24	W10 × 22
191	W8 × 21	W14 × 38	W10 × 22	W10 × 22
192	W12 × 26	W8 × 21	W10 × 22	W10 × 22
193	W8 × 21	W10 × 22	W8 × 24	W10 × 22
194	W8 × 21	W8 × 21	W12 × 26	W8 × 21
195	W10 × 22	W8 × 21	W10 × 22	W8 × 21
196	W10 × 22	W8 × 21	W10 × 22	W8 × 21
197	W10 × 22	W8 × 28	W6 × 25	W8 × 21
198	W8 × 21	W8 × 21	W12 × 30	W8 × 21
199	W8 × 21	W8 × 21	W8 × 24	W8 × 21
200	W8 × 21	W10 × 22	W10 × 22	W8 × 21
201	W8 × 21	W12 × 26	W10 × 22	W8 × 21
202	W8 × 21	W8 × 21	W12 × 26	W8 × 21
203	W10 × 22	W8 × 21	W10 × 22	W8 × 21
204	W8 × 21	W6 × 25	W10 × 22	W8 × 21
205	W14 × 48	W10 × 22	W8 × 24	W8 × 21
206	W8 × 28	W8 × 21	W6 × 25	W8 × 21
207	W12 × 26	W10 × 22	W8 × 21	W8 × 21
208	W8 × 21	W8 × 21	W8 × 24	W8 × 21
209	W8 × 21	W8 × 21	W12 × 26	W8 × 21
210	W6 × 25	W8 × 21	W10 × 22	W8 × 21
211	W8 × 21	W8 × 21	W12 × 26	W8 × 21
212	W8 × 21	W6 × 25	W10 × 22	W8 × 21
213	W8 × 21	W8 × 21	W10 × 22	W8 × 21

(continued)

Table 4.6 (continued)

Element group	Optimal W-shaped sections			
	CBO [20]	ECBO [20]	VPS [21]	MDVC-UVPS
214	W8 × 28	W8 × 21	W10 × 22	W8 × 21
215	W10 × 22	W8 × 21	W8 × 24	W8 × 21
216	W8 × 21	W8 × 21	W10 × 22	W10 × 49
217	W12 × 26	W12 × 26	W8 × 21	W10 × 49
218	W10 × 22	W8 × 31	W10 × 22	W10 × 49
219	W12 × 53	W12 × 58	W12 × 53	W10 × 49
220	W14 × 211	W14 × 99	W27 × 178	W10 × 49
Volume (in. ³)	15,587,709	14,086,857	12,989,713	12,165,572
Average optimized volume (in. ³)	16,314,541	15,556,672	13,371,681	12,435,451
Standard deviation on average volume (in. ³)	390,632	343,118	267,601	145,629

**Fig. 4.8** Convergence curves for the 2386-bar tower truss problem

of MDVC-UVPS. In the first example, the design found by ECBO, VPS, and MDVC-UVPS is approximately identical and is about 3% lighter than the result obtained by the CBO. In the second one, the design obtained by MDVC-UVPS is 4.5, 3.5, and 1% lighter than the best designs achieved by CBO, ECBO, and VPS, respectively. These values are 28, 15, and 6.5% for the last example. The average optimized design and the standard deviation on average design of the hybrid algorithm are less than those of all other compared methods for all of the examples. Moreover, this algorithm comes close to the optimum design rapidly.

References

1. Lee KS, Geem ZW (2004) A new structural optimization method based on the harmony search algorithm. *Comput Struct* 82:781–798
2. Camp CV (2007) Design of space trusses using Big Bang-Big Crunch optimization. *J Struct Eng* 133:999–1008
3. Rahami H, Kaveh A, Gholipour Y (2008) Sizing, geometry and topology optimization of trusses via force method and genetic algorithm. *Eng Struct* 30:2360–2369
4. Lamberti L (2008) An efficient simulated annealing algorithm for design optimization of truss structures. *Comput Struct* 86:1936–1953
5. Kaveh A, Talatahari S (2009) A particle swarm ant colony optimization for truss structures with discrete variables. *J Constr Steel Res* 65:1558–1568
6. Li LJ, Huang ZB, Liu F (2009) A heuristic particle swarm optimization method for truss structures with discrete variables. *Comput Struct* 87:435–443
7. Wu CY, Tseng KY (2010) Truss structure optimization using adaptive multi-population differential evolution. *Struct Multidiscip Optim* 42(4):575–590
8. Dede T, Bekiroglu S, Ayvaz Y (2011) Weight minimization of trusses with genetic algorithm. *Appl Soft Comput* 11:2565–2575
9. Gandomi AH, Talatahari S, Yang XS, Deb S (2013) Design optimization of truss structures using cuckoo search algorithm. *Struct Des Tall Spec* 22(17):1330–1349
10. Kaveh A, Mahdavi VR (2014) Colliding bodies optimization method for optimum discrete design of truss structures. *Comput Struct* 139:43–53
11. Kaveh A, Ilchi Ghazaan M (2014) Enhanced colliding bodies optimization for design problems with continuous and discrete variables. *Adv Eng Softw* 77:66–75
12. Ahrari A, Atai AA, Deb K (2014) Simultaneous topology, shape and size optimization of truss structures by fully stressed design based on evolution strategy. *Eng Optimiz* 47(8):37–41
13. Hasançebi O, Kazemzadeh Azad S (2015) Adaptive dimensional search: a new metaheuristic algorithm for discrete truss sizing optimization. *Comput Struct* 154:1–16
14. Bekdaş G, Nigdeli SM, Yang XS (2015) Sizing optimization of truss structures using flower pollination algorithm. *Appl Soft Comput* 37:322–331
15. Ho-Huu V, Nguyen-Thoi T, Vo-Duy T, Nguyen-Trang T (2016) An adaptive elitist differential evolution for optimization of truss structures with discrete design variables. *Comput Struct* 165:59–75
16. Kaveh A, Bakhshpoori T (2016) A new metaheuristic for continuous structural optimization: water evaporation optimization. *Struct Multidiscip Optim* 54(1):23–43
17. American Institute of Steel Construction (AISC) (1989) Manual of steel construction: allowable stress design, Chigago, USA
18. Kaveh A, Ilchi Ghazaan M (2014) Enhanced colliding bodies optimization for design problems with continuous and discrete variables. *Adv Eng Softw* 77:66–75
19. Hasançebi O (2008) Adaptive evolution strategies in structural optimization: enhancing their computational performance with applications to large-scale structures. *Comput Struct* 86:119–132
20. Kaveh A, Ilchi Ghazaan M (2016) Optimum design of large-scale truss towers using cascade optimization. *Acta Mech* 227(9):2645–2656
21. Kaveh A, Ilchi Ghazaan M (2017) MATLAB codes for vibrating particles system algorithm. *Int J Optim Civil Eng* 7(3):355–366

Chapter 5

Optimal Design of Double-Layer Grids



5.1 Introduction

Double-layer grids belong to the category of space structures and consist of two planar networks of members forming the top and bottom layers parallel to each other and interconnected by vertical and inclined web members. Double-layer grids are characterized by ball joints with no moment or torsional resistance; therefore, all members can only resist tension or compression. Even in the case of connection by comparatively rigid joints, the influence of bending or torsional moment is insignificant. A wide variety of double-layer grids can be formed either by altering the direction of the top and bottom layers with respect to each other or by changing the relative positions of the nodal points of the top and bottom layers. Additional variations can also be introduced by utilizing layers of different sizes [1]. Double-layer grids are ideally suited for covering exhibition pavilions, assembly halls, swimming pools, hangars, churches, bridge decks, and many types of industrial buildings in which large unobstructed areas are required.

In the past decades, a number of meta-heuristic algorithms have been developed and used for structural optimization problems, e.g., see Kaveh [2]. Double-layer grids have a great number of structural elements, and therefore optimization techniques can be rewardingly employed to achieve economic and efficient designs of them. Here, five different types of double-layer grids are studied and optimized utilizing the colliding bodies optimization (CBO) [3], enhanced colliding bodies optimization (ECBO) [4], vibrating particles system (VPS) [5], and a hybrid algorithm called MDVC-UVPS [6]. The cross-section areas of the grid elements are considered as discrete design variables and all of them are selected from a list of tube sections available in AISC-LRFD [7]. Strength, stability, and displacement constraints are considered for each example.

5.2 Optimal Design of Double-Layer Grids

Here, the aim of the optimization problem is to find a set of design variables that result in a double-layer grid with the minimum weight while satisfying certain constraints. This can be expressed as

$$\begin{aligned} \text{Find } \{X\} &= [x_1, x_2, \dots, x_{ng}] \\ \text{to minimize } W(\{X\}) &= \sum_{i=1}^{ng} x_i \sum_{j=1}^{nm(i)} \rho_j L_j \\ \text{subjected to : } &\quad \begin{cases} g_j(\{X\}) \leq 0, & j = 1, 2, \dots, nc \\ x_{i\min} \leq x_i \leq x_{i\max} \end{cases} \end{aligned} \quad (5.1)$$

where $\{X\}$ is the vector containing the design variables; ng is the number of design groups; $W(\{X\})$ presents the weight of the structure; $nm(i)$ is the number of members for the i th group; ρ_j and L_j denote the material density and the length of the j th member, respectively. $x_{i\min}$ and $x_{i\max}$ are the lower and upper bounds of the design variable x_i , respectively. $g_j(\{X\})$ denotes design constraints; and nc is the number of constraints.

For handling the constraints, a penalty approach is utilized. For this purpose, the objective function (Eq. 5.1) is redefined as follows:

$$P(\{X\}) = (1 + \varepsilon_1 v)^{\varepsilon_2} \times W(\{X\}) \quad (5.2)$$

where $P(\{X\})$ is the penalized cost function or the objective function to be minimized and v denotes the sum of the violations of the design constraints. Here, ε_1 is set to unity and ε_2 is calculated by

$$\varepsilon_2 = 1.5 + 1.5 \times \frac{\text{iter}}{\text{iter}_{\max}} \quad (5.3)$$

where iter is the current iteration number and iter_{\max} is the total number of iterations for the optimization process.

The constraint conditions for grid structures are briefly explained in the following.

Displacement constraint:

$$\delta_i \leq \delta_i^{\max}, \quad i = 1, 2, \dots, nn \quad (5.4)$$

Tension member constraint [7]:

$$p_u \leq p_r; \quad p_r = \min \begin{cases} \phi_t F_y A_g; & \phi_t = 0.9 \\ \phi_t F_u A_e; & \phi_t = 0.75 \end{cases} \quad (5.5)$$

Compression member constraint [7]:

$$p_u \leq p_r; \quad p_r = \phi_c F_{cr} A_g; \quad \phi_c = 0.85$$

$$F_{cr} = \begin{cases} (0.658 \frac{F_y}{F_e}) F_y; & \frac{KL}{r} \leq 4.71 \sqrt{\frac{E}{F_y}} \\ 0.877 F_e; & \frac{KL}{r} > 4.71 \sqrt{\frac{E}{F_y}} \end{cases}; \quad F_e = \frac{\pi^2 E}{(\frac{KL}{r})^2} \quad (5.6)$$

Slenderness ratio constraints [7]:

$$\frac{KL}{r} \leq 200; \quad \text{for compression members} \quad (5.7)$$

$$\frac{KL}{r} \leq 300; \quad \text{for tension members}$$

where δ_i and δ_i^{\max} are the displacement and allowable displacement for the i th node; nn is the number of nodes; P_u is the required strength (tension or compression); P_r is the nominal axial strength (tension or compression); A_g and A_e are the gross cross-sectional area and the effective net cross-sectional area of a member; k is the effective length factor taken equal to 1; L is the length of member; and r is the radius of gyration.

5.3 Design Problems

Design optimization of five double-layer grids with different configurations are investigated in this section. These examples include the following:

- A 520-bar double-layer grid (larger square on square)
- A 672-bar double-layer grid (square on larger square)
- A 800-bar double-layer grid (square on square)
- A 1016-bar double-layer grid (square on diagonal)
- A 1520-bar double-layer grid (diagonal on diagonal).

A span of 40×40 m is considered for all examples and the height is equal to 3 m. All connections are assumed to be ball jointed. The design variables are the cross-sectional areas of the bar elements which are selected from the list of steel pipe sections from AISC-LRFD [7]. These pipe sections are shown in Table 5.1. ST, EST, and DEST abbreviations stand for standard weight, extra strong, and double-extra strong, respectively. The modulus of elasticity, the yield stress, and the density of steel are taken as 205 GPa, 248.2 MPa, and 7833.413 kg/m^3 , respectively. Strength and slenderness limitations are according to AISC-LRFD provisions [7] as discussed earlier and displacement limitations of span/600 were imposed on all nodes in the vertical direction.

Table 5.1 The steel pipe sections

No.	Type	Nominal diameter (in.)	Area (cm ²)	Gyration radius (cm)
1	^a ST	½	1.6129	0.662432
2	^b EST	½	2.064512	0.635
3	ST	¾	2.129028	0.846582
4	EST	¾	2.774188	0.818896
5	ST	1	3.161284	1.066038
6	EST	1	4.129024	1.034542
7	ST	1¼	4.322572	1.371346
8	ST	1½	5.16128	1.582166
9	EST	1¼	5.677408	1.331214
10	EST	1½	6.903212	2.003806
11	ST	2	6.903212	1.53543
12	EST	2	9.548368	1.945132
13	ST	2½	10.96772	2.41681
14	ST	3	14.387068	2.955798
15	EST	2½	14.5161	2.346452
16	^c DEST	2	17.161256	1.782572
17	ST	3½	17.290288	3.395726
18	EST	3	19.483832	2.882646
19	ST	4	20.451572	3.835908
20	EST	3½	23.741888	3.318002
21	DEST	2½	25.999948	2.143506
22	ST	5	27.74188	4.775454
23	EST	4	28.451556	3.749548
24	DEST	3	35.290252	2.65811
25	ST	6	35.999928	5.700014
26	EST	5	39.419276	4.675124
27	DEST	4	52.25796	3.490976
28	ST	8	54.19344	7.462012
29	EST	6	54.19344	5.577332
30	DEST	5	72.90308	4.379976
31	ST	10	76.77404	9.342628
32	EST	8	82.58048	7.309358
33	ST	12	94.19336	11.10361
34	DEST	6	100.64496	5.236464
35	EST	10	103.87076	9.216898
36	EST	12	123.87072	11.028934
37	DEST	8	137.41908	7.004812

^aST standard weight^bEST extra strong^cDEST double-extra strong

Each example has been solved 20 times independently, and 1000 iterations are considered as the terminal condition. A population of 20 particles is considered for each algorithm and the other algorithm parameters are set the same as the values proposed in [4–6]. The optimization algorithms are coded in MATLAB and the structures are analyzed using the direct stiffness method by our own codes.

5.3.1 A 520-Bar Double-Layer Grid

The larger square on square double-layer grid contains 520 members and 165 nodes shown in Fig. 5.1. The bottom layer is simply supported at the nodes illustrated in Fig. 5.2a. Each top layer joint is subjected to a concentrated vertical load of 46 kN. Cross-sectional areas of the members are categorized into 20 groups as shown in Fig. 5.2. In order to optimize this structure by MDVC-UVPS, two stages are considered. The design variable configuration utilized for the first stage is listed as follows: [1], [2 4], [3 5], [6 8], [7 9], [10 11], [12 13], [14 15], [16], [17 18], and [19 20].

The results found by CBO, ECBO, VPS, and MDVC-UVPS algorithms are summarized in Table 5.2. VPS achieves the lightest design (i.e., 60,018 kg). MDVC-UVPS has better performance in terms of the average optimized weight and standard deviation on average weights which are 63,130, and 1932 kg, respectively. The best designs obtained by CBO, ECBO, and MDVC-UVPS are 64,513, 61,119, and 61,456 kg, respectively. The maximum stress ratios for the best designs of the CBO, ECBO, VPS, and MDVC-UVPS are 94.39, 96.76, 96.90, and 98.33%, respectively. Convergence histories are depicted in Fig. 5.3. The required number of structural analyses to achieve the best design by CBO, ECBO, VPS, and MDVC-UVPS are 3400, 19,820, 19,560, and 2804 analyses, respectively.

5.3.2 A 672-Bar Double-Layer Grid

Figure 5.4 shows the 3D view of a square on larger square grid. This structure has 672 members and 205 nodes and the bottom layer is simply supported at the nodes shown in Fig. 5.5a. Each top layer joint is subjected to a concentrated vertical load

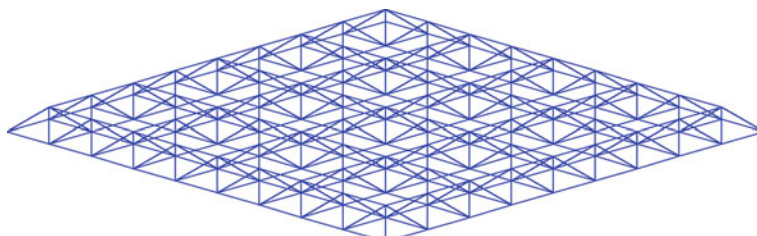


Fig. 5.1 3D view of the 520-bar double-layer grid problem

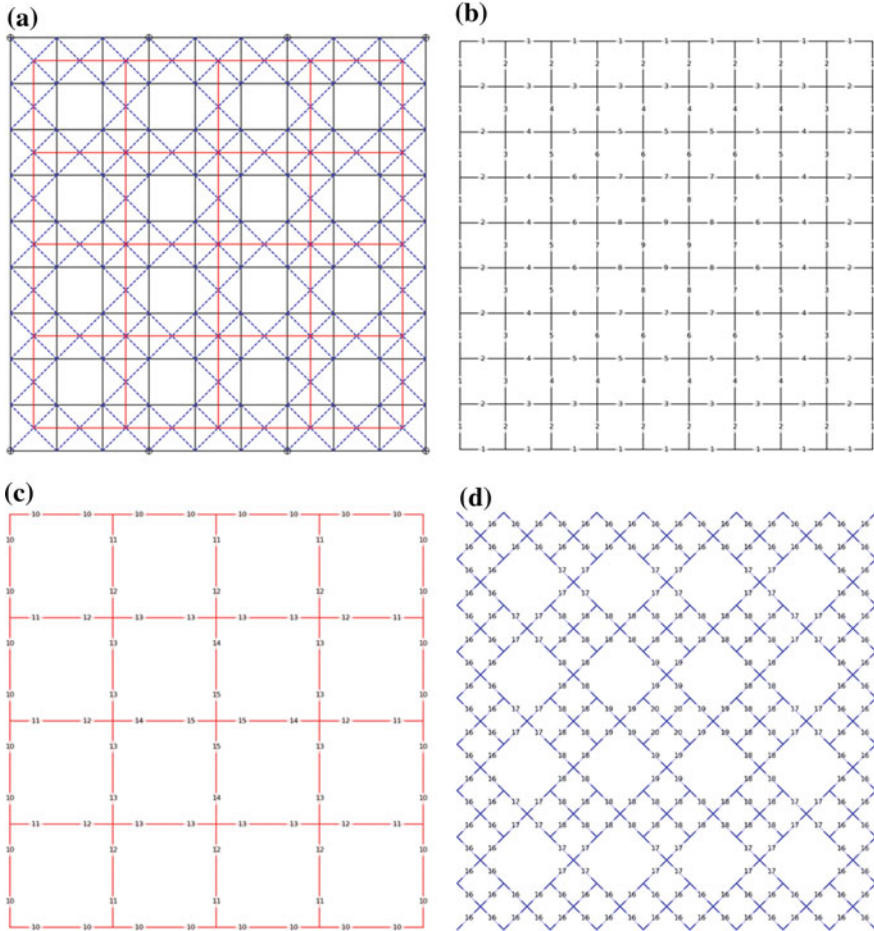


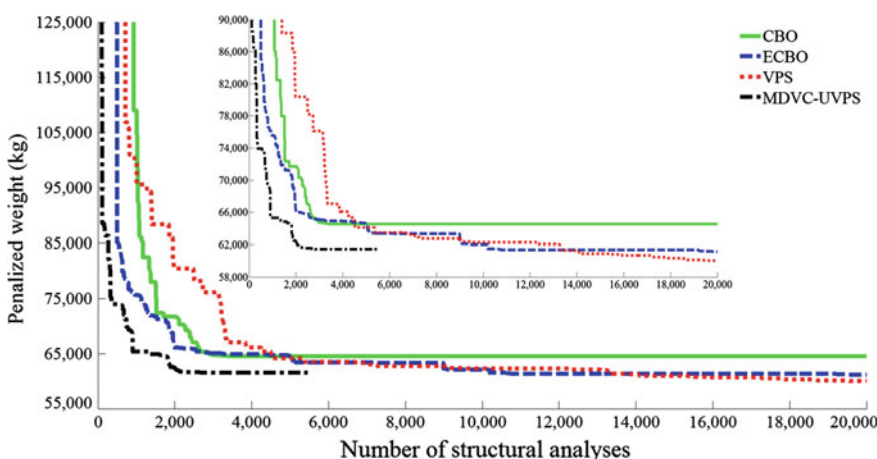
Fig. 5.2 Top view of the 520-bar double-layer grid problem and member groups: **a** all members with simple supports, **b** bottom layer members, **c** top layer members, and **d** web members

of 30 kN. The cross-sectional areas of the members are categorized into 22 groups as depicted in Fig. 5.5. In order to optimize this structure by MDVC-UVPS, two stages are considered. The design variable configuration utilized for the first stage is listed as follows: [1 2], [3 4], [5 6], [7 8], [9], [10 12], [11 13], [14 16], [15 17], [18 19], [20 21], and [22].

Table 5.3 lists the optimal designs found by different methods. MDVC-UVPS obtained the lightest design compared to other methods that is 53,552 kg. Moreover, the average optimized weight and the standard deviation on average weight of MDVC-UVPS (58,589 and 3626 kg) are less than those of all other methods. The best designs found by the CBO, ECBO, and VPS are 55,621, 54,569, and 53,704 kg, respectively. The maximum stress ratios for the best designs of the

Table 5.2 Performance comparison for the 520-bar double-layer grid problem

Element group	Sections			
	CBO	ECBO	VPS	MDVC-UVPS
1	EST 4	ST 4	ST 5	ST 6
2	EST 4	ST 5	ST 5	EST 4
3	ST 4	DEST 3	ST 3½	EST 4
4	ST 4	ST 3½	ST 3½	ST 3
5	DEST 5	EST 5	EST 4	ST 6
6	ST 3½	ST 3½	EST 3	EST 4
7	EST 3½	EST 5	DEST 2½	EST 4
8	EST 4	DEST 4	EST 5	DEST 4
9	EST 6	ST 8	EST 6	EST 6
10	EST 6	EST 6	ST 8	EST 8
11	EST 10	EST 5	EST 5	ST 5
12	EST 8	DEST 5	DEST 5	EST 6
13	EST 8	ST 12	EST 12	ST 10
14	ST 10	DEST 6	DEST 6	EST 12
15	DEST 8	DEST 8	DEST 6	DEST 8
16	ST 6	ST 6	ST 6	ST 5
17	ST 4	ST 4	ST 4	ST 4
18	ST 3½	ST 3½	ST 3½	ST 4
19	EST 3	ST 3	ST 3½	ST 5
20	ST 3½	ST 2½	ST 2½	ST 5
Weight (kg)	64,513	61,119	60,018	61,456
Average optimized weight (kg)	66,906	63,463	63,360	63,130
Standard deviation on average weight (kg)	7167	4052	2446	1932

**Fig. 5.3** Convergence curves for the 520-bar double-layer grid problem

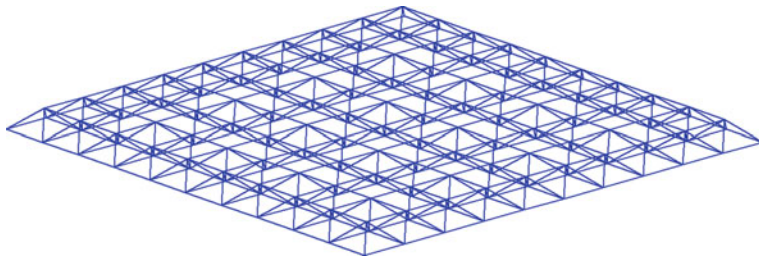


Fig. 5.4 3D view of the 672-bar double-layer grid problem

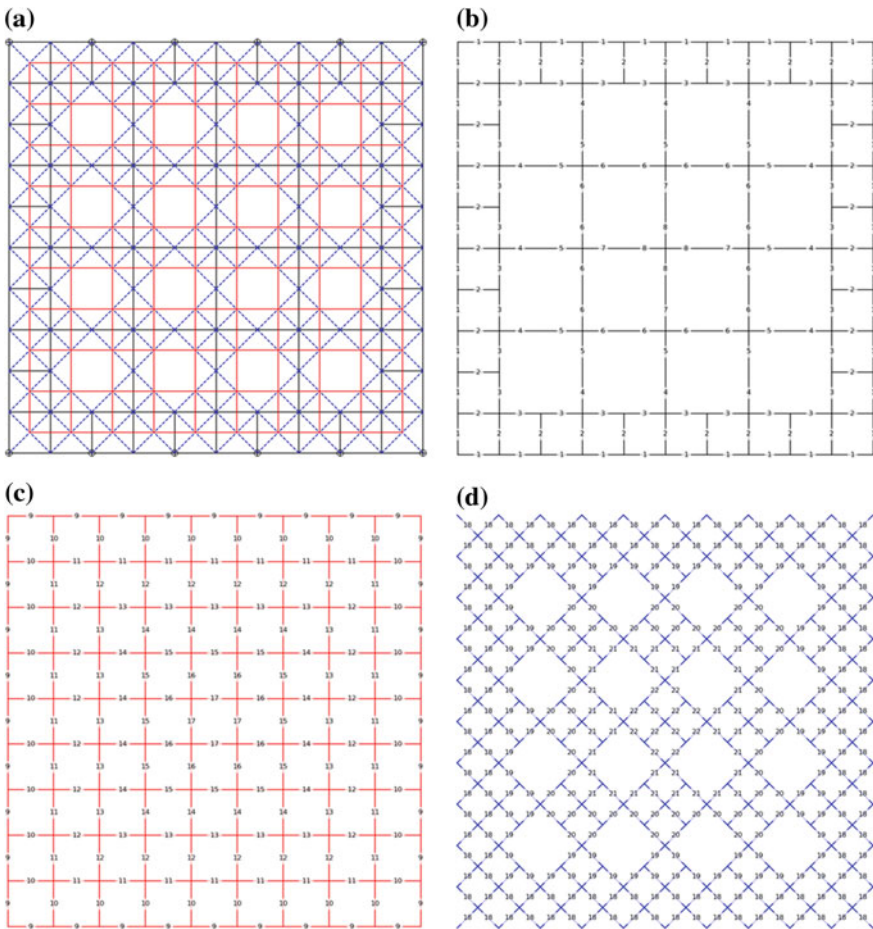


Fig. 5.5 Top view of the 672-bar double-layer grid problem and member groups: **a** all members with simple supports, **b** bottom layer members, **c** top layer members, and **d** web members

Table 5.3 Performance comparison for the 672-bar double-layer grid problem

Element group	Sections			
	CBO	ECBO	VPS	MDVC-UVPS
1	ST 4	ST 4	ST 5	ST 4
2	ST 6	ST 5	ST 4	ST 5
3	ST 2½	ST 3½	ST 4	ST 3½
4	ST 2½	EST 1½	EST 1½	EST 1½
5	ST 2½	ST 4	ST 6	ST 3
6	EST 6	EST 4	EST 6	DEST 4
7	EST 4	EST 6	EST 6	DEST 4
8	EST 6	DEST 4	DEST 5	EST 6
9	EST 5	ST 6	EST 5	ST 6
10	ST 4	ST 3½	ST 3½	ST 3½
11	ST 6	EST 6	ST 5	DEST 4
12	EST 5	EST 4	EST 4	ST 5
13	EST 5	DEST 4	EST 6	EST 6
14	DEST 4	DEST 4	ST 6	EST 5
15	EST 8	EST 6	DEST 4	DEST 4
16	DEST 4	DEST 4	EST 6	EST 5
17	ST 5	DEST 5	ST 8	DEST 5
18	ST 4	ST 4	ST 4	ST 4
19	ST 4	ST 4	ST 3½	ST 3½
20	ST 3½	ST 3½	ST 3½	ST 3½
21	ST 3½	ST 3	ST 3½	EST 2½
22	ST 2½	ST 2½	ST 2½	ST 2½
Weight (kg)	55,621	54,569	53,704	53,552
Average optimized weight (kg)	62,287	59,164	60,850	58,589
Standard deviation on average weight (kg)	9853	5597	5985	3626

CBO, ECBO, VPS, and MDVC-UVPS are 96.59, 95.73, 99.96, and 98.91%, respectively. Convergence histories are demonstrated in Fig. 5.6. It should be noted that MDVC-UVPS requires 3772 structural analyses to find the optimum solution while CBO, ECBO, and VPS require 4640, 14,480, and 19,640 structural analyses, respectively.

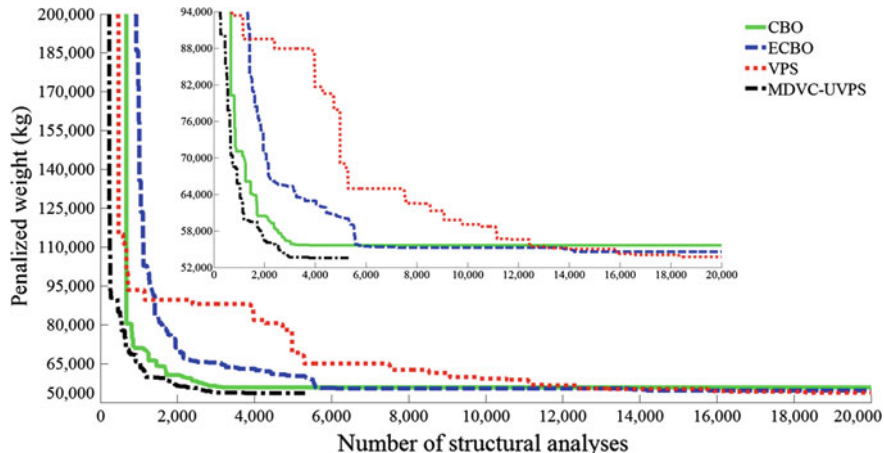


Fig. 5.6 Convergence curves for the 672-bar double-layer grid problem

5.3.3 A 800-Bar Double-Layer Grid

The design of square on square double-layer grid shown in Fig. 5.7 is considered as the third example. This structure has 800 members and 221 nodes and the bottom layer is simply supported at the nodes illustrated in Fig. 5.8a. Each top layer joint is subjected to a concentrated vertical load of 30 kN. Cross-sectional areas of the members are categorized into 24 groups as shown in Fig. 5.8. In order to optimize this structure by MDVC-UVPS, two stages are considered. The design variable configuration utilized for the first stage is listed as follows: [1], [2 4], [3 5], [6 8], [7 9], [10], [11], [12 14], [13 15], [16 18], [17 19], [20 21 22], and [23 24].

Table 5.4 summarizes the results obtained by CBO, ECBO, VPS, and MDVC-UVPS methods. MDVC-UVPS has better performance in terms of the best weight, average optimized weight, and standard deviation on average weight which are 53,590, 57,679, and 3524 kg, respectively. The best designs obtained by CBO, ECBO, and VPS are 55,714, 53,673, and 53.714 kg, respectively. The maximum stress ratios for the best designs of the CBO, ECBO, VPS, and MDVC-UVPS are

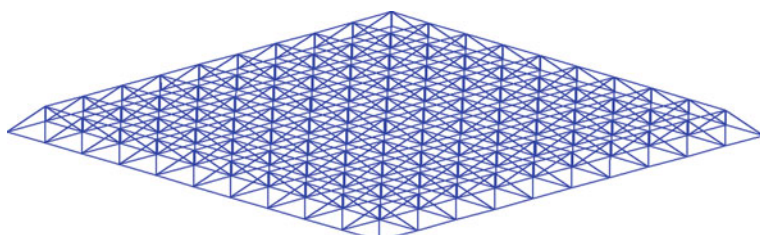


Fig. 5.7 3D view of the 800-bar double-layer grid problem

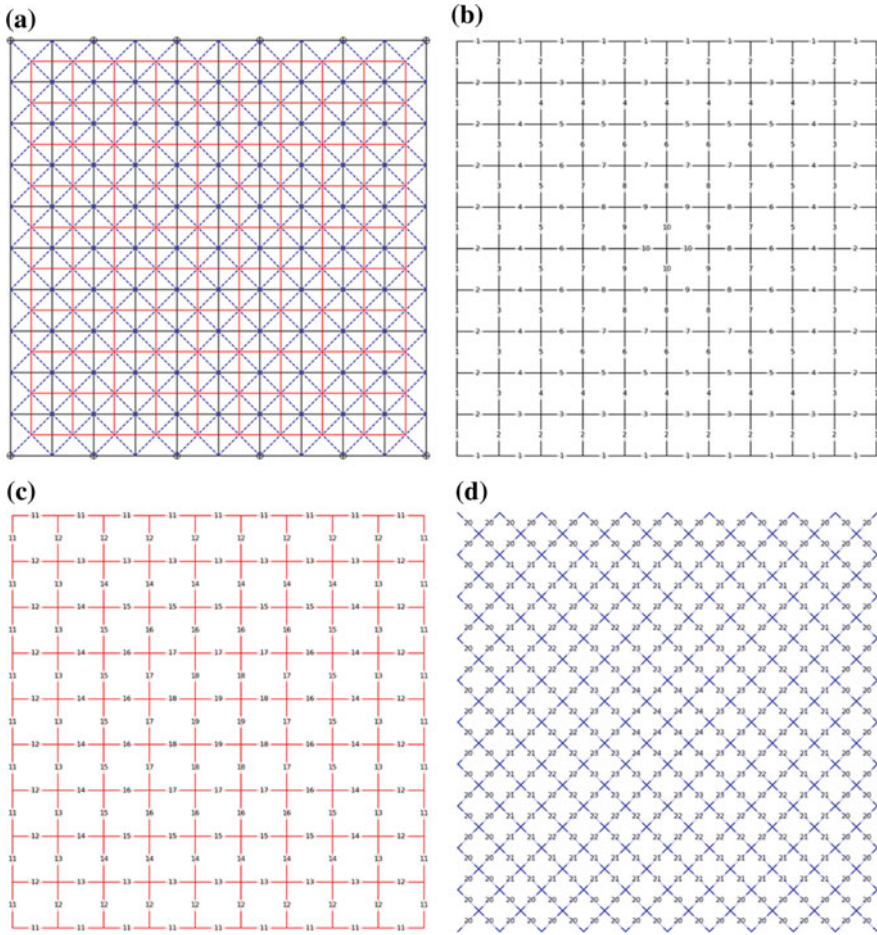


Fig. 5.8 Top view of the 800-bar double-layer grid problem and member groups: **a** all members with simple supports, **b** bottom layer members, **c** top layer members, and **d** web members

99.94, 93.86, 91.87, and 94.71%, respectively. Convergence histories are depicted in Fig. 5.9. The required number of structural analyses to achieve the best design by CBO, ECBO, VPS, and MDVC-UVPS are 11,520, 16,860, 15,600, and 5122 analyses, respectively.

5.3.4 A 1016-Bar Double-Layer Grid

Figure 5.10 shows the 3D view of a square on the diagonal grid. This grid has 1016 members and 320 nodes and simple support conditions are employed for the bottom layer at the nodes demonstrated in Fig. 5.11a. Each top layer joint is subjected to a concentrated vertical load of 30 kN. The elements are divided into

Table 5.4 Performance comparison for the 800-bar double-layer grid problem

Element group	Sections			
	CBO	ECBO	VPS	MDVC-UVPS
1	EST 3½	ST 4	ST 4	ST 4
2	ST 6	ST 5	ST 5	ST 5
3	ST 2	EST 2	EST 1½	ST 1½
4	ST 3½	ST 3	EST 3	ST 3
5	ST 2½	EST 2	ST 3½	ST 2½
6	ST 3	ST 2	EST 1½	ST 2
7	EST 3	EST 3½	ST 5	ST 3
8	ST 2½	ST 3	ST 4	DEST 2
9	EST 3	EST 3½	EST 3	ST 5
10	ST 5	ST 3	ST 2	DEST 3
11	ST 8	EST 5	ST 6	DEST 4
12	ST 3½	ST 3½	ST 3½	ST 3½
13	ST 4	ST 6	ST 6	ST 6
14	ST 5	ST 6	ST 6	ST 5
15	ST 6	ST 6	ST 6	ST 5
16	ST 6	ST 6	ST 6	ST 6
17	DEST 4	EST 5	EST 6	DEST 4
18	EST 5	EST 6	EST 5	DEST 4
19	EST 5	DEST 4	DEST 4	DEST 5
20	EST 3½	ST 4	ST 4	ST 4
21	ST 3½	ST 3½	ST 3½	ST 3½
22	ST 3	ST 3½	ST 3	ST 3
23	ST 2½	ST 2½	ST 2½	ST 2½
24	ST 2½	ST 2½	ST 2½	ST 2½
Weight (kg)	55,714	53,673	53,714	53,590
Average optimized weight (kg)	61,464	58,953	57,912	57,679
Standard deviation on average weight (kg)	10,127	4643	4102	3524

25 groups and the member groups are presented in Fig. 5.11. Two stages with 11 and 25 variables are considered by MDVC-UVPS algorithm. The first DVC is as follows: [1 2], [3 4 5], [6 7 8], [9 10 11], [12], [13 15], [14 16], [17 19], [18 20], [21 22 23], and [24 25].

Table 5.5 presents the optimum designs obtained by proposed algorithms. The lightest design (i.e., 65,826 kg) is achieved by MDVC-UVPS algorithm after 4234 analyses. The best designs obtained by CBO, ECBO, and VPS are 74,849, 67,839, and 67,229 kg, respectively. These values are found after 9760, 15,760, and 15,220 analyses. MDVC-UVPS obtains the lost values of average optimized weight and standard deviation on average weight which are equal to 70,488, and 5018 kg, respectively. The maximum values of the stress ratio for CBO, ECBO,

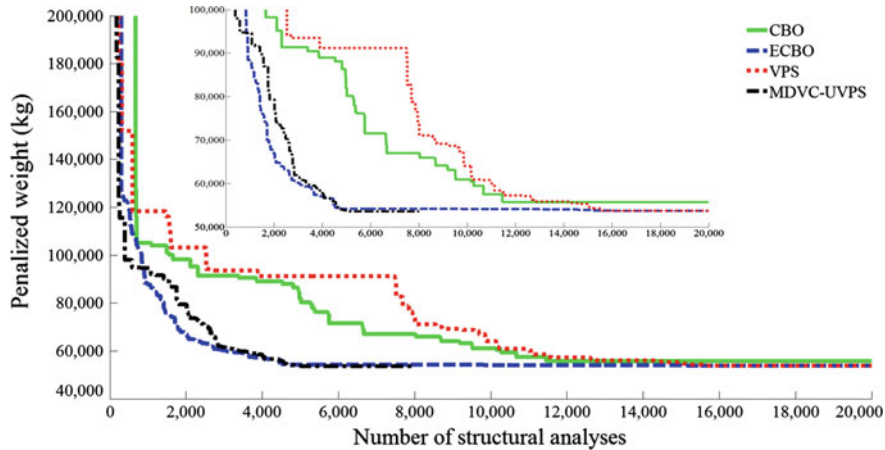


Fig. 5.9 Convergence curves for the 800-bar double-layer grid problem

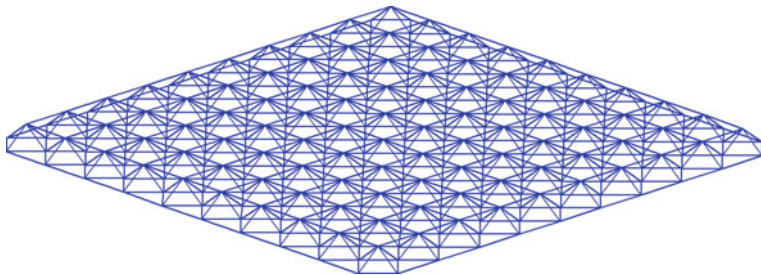


Fig. 5.10 3D view of the 1016-bar double-layer grid problem

VPS, and MDVC-UVPS are 93.01, 93.99, 96.07, and 97.10%, respectively. Convergence history diagrams are depicted in Fig. 5.12.

5.3.5 A 1520-Bar Double-Layer Grid

Figure 5.13 shows the 3D view of a diagonal on diagonal grid. This structure has 1520 members and 401 nodes and the bottom layer is simply supported at the nodes shown in Fig. 5.14a. Each top layer joint is subjected to a concentrated vertical load of 16 kN. The cross-sectional areas of the members are categorized into 31 groups as depicted in Fig. 5.14. In order to optimize this structure by MDVC-UVPS, two stages are considered. The design variable configuration

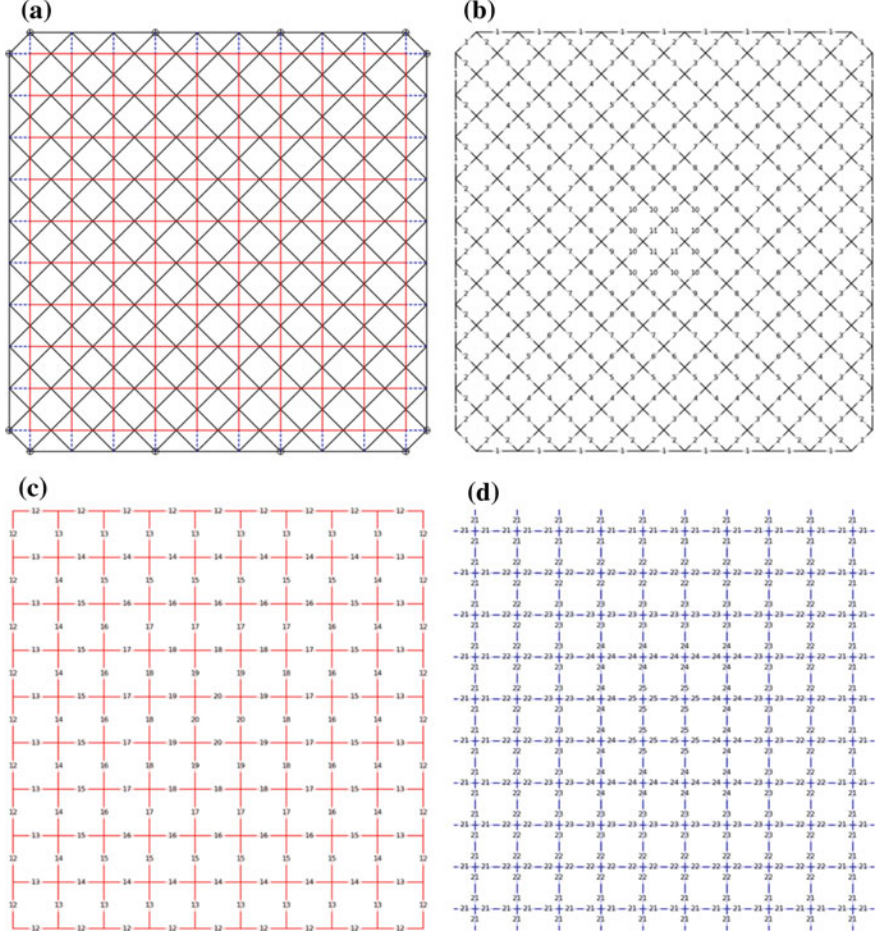


Fig. 5.11 Top view of the 1016-bar double-layer grid problem and member groups: **a** all members with simple supports, **b** bottom layer members, **c** top layer members, and **d** web members

utilized for the first stage is listed as follows: [1 2], [3 4 5], [6 7 8], [9 10 11], [12], [13 14], [15 16], [17 18], [19 20], [21], [22], [23 24 25], [26 27 28], and [29 30 31].

Table 5.6 presents a comparison between the results of the optimal designs found by different methods. MDVC-UVPS obtained the lightest design compared to other methods that is 79,571 kg. Moreover, the average optimized weight and the standard deviation on the average weight of MDVC-UVPS (85,398 and 4407 kg) are less than those of all other methods. The best designs found by the CBO, ECBO, and VPS are 93,174, 82,254, and 82,357 kg, respectively. The maximum

Table 5.5 Performance comparison for the 1016-bar double-layer grid problem

Element group	Sections			
	CBO	ECBO	VPS	MDVC-UVPS
1	EST 5	EST 5	ST 6	DEST 4
2	DEST 3	EST 5	ST 5	DEST 3
3	ST 3½	ST 3	ST 3½	ST 3½
4	ST 2½	ST 3½	ST 2½	ST 2½
5	ST 2½	ST 2½	ST 4	ST 3
6	ST 2	ST 2	EST 1	EST 1½
7	ST 2	DEST 2	EST 2	EST 1½
8	ST 2½	DEST 2	DEST 2	EST 2½
9	DEST 2½	EST 2	EST 3	ST 3½
10	DEST 2½	ST 6	DEST 2½	DEST 2
11	ST 1½	ST 2	EST 12	DEST 2½
12	DEST 5	EST 8	DEST 5	EST 8
13	EST 3½	EST 3½	ST 4	EST 4
14	EST 3½	ST 5	ST 5	ST 4
15	EST 4	ST 4	ST 5	ST 5
16	ST 6	EST 5	DEST 4	ST 4
17	ST 5	ST 5	EST 4	ST 6
18	EST 4	EST 5	EST 4	ST 6
19	EST 5	EST 5	EST 4	EST 6
20	ST 8	ST 8	DEST 4	EST 6
21	ST 6	ST 5	ST 6	ST 5
22	ST 3	ST 3	ST 3½	ST 3½
23	EST 6	EST 2½	EST 2½	EST 2½
24	ST 3½	ST 5	ST 2½	ST 2½
25	EST 1½	ST 4	EST 1½	ST 2½
Weight (kg)	74,849	67,839	67,229	65,826
Average optimized weight (kg)	79,422	73,042	72,366	70,488
Standard deviation on average weight (kg)	8154	9158	5545	5018

stress ratio for the best designs of the CBO, ECBO, VPS, and MDVC-UVPS are 99.59, 99.40, 99.94, and 99.92%, respectively. Convergence histories are demonstrated in Fig. 5.15. It should be noted that MDVC-UVPS requires 3142 structural analyses to find the optimum solution while CBO, ECBO, and VPS require 4360, 18,000, and 12,120 structural analyses, respectively.

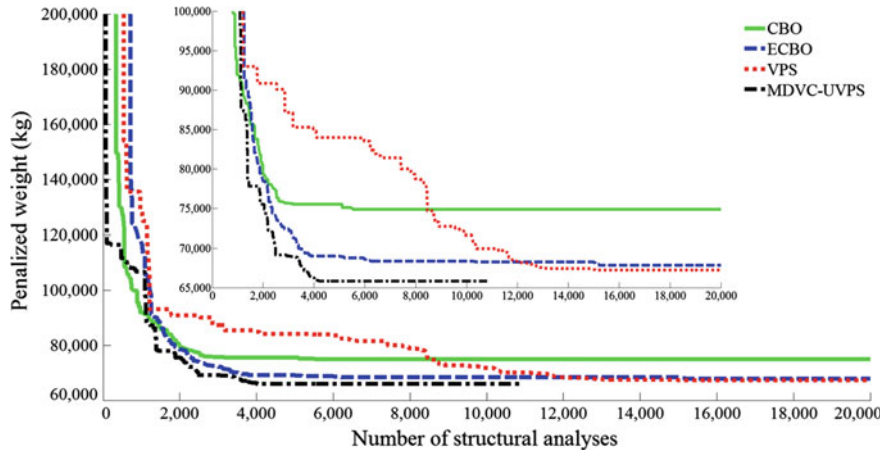


Fig. 5.12 Convergence curves for the 1016-bar double-layer grid problem

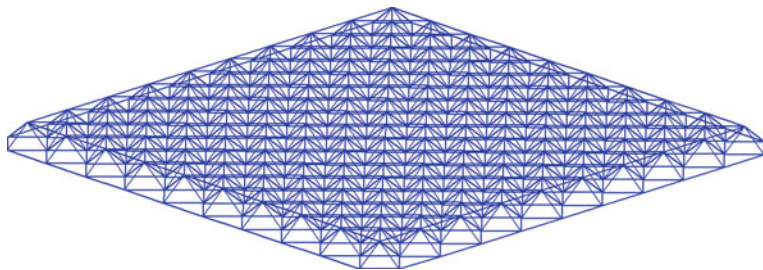


Fig. 5.13 3D view of the 1520-bar double-layer grid problem

5.4 Concluding Remarks

Optimal design of larger square on square, square on larger square, square on square, square on diagonal, and diagonal on diagonal double-layer grids using four meta-heuristic algorithms are studied. Strength and stability constraints of AISC-LRFD specifications and some displacement limitations are imposed on these grids. The diagonal on diagonal type has more connections and members and the optimum weight achieved for this configuration is heavier than those of other grids. The lightest designs are found for the square on larger square and square on square grids. For the utilized algorithms, MDVC-UVPS achieved the best designs for four of the five cases. This algorithm had also better performance in terms of the average optimized weight and standard deviation on average weight. Convergence history diagrams are depicted for all design problems confirming the superiority of the MDVC-UVPS algorithm.

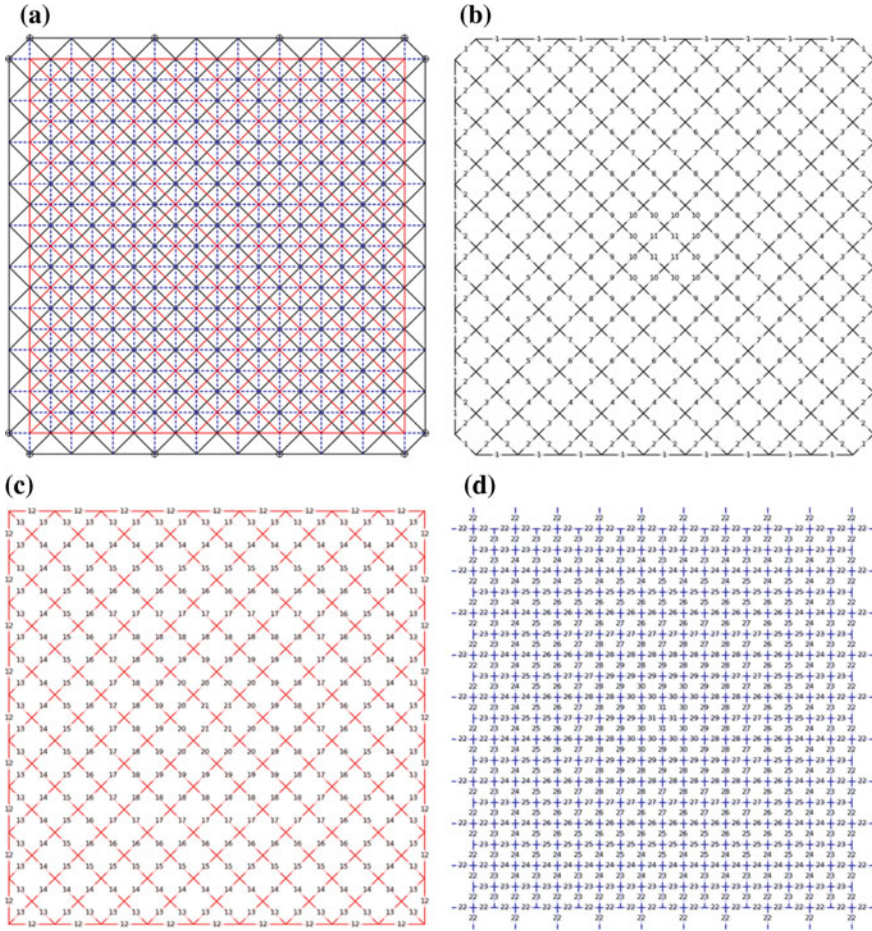


Fig. 5.14 Top view of the 1520-bar double-layer grid problem and member groups: **a** all members with simple supports, **b** bottom layer members, **c** top layer members, and **d** web members

Table 5.6 Performance comparison for the 1520-bar double-layer grid problem

Element group	Sections			
	CBO	ECBO	VPS	MDVC-UVPS
1	EST 5	DEST 5	EST 5	ST 6
2	ST 5	EST 5	ST 5	DEST 3
3	ST 2½	ST 2½	EST 2½	ST 2½
4	EST 1½	EST 1½	EST 1½	ST 2½
5	ST 1½	ST 2	ST 1½	ST 2½
6	EST 1¼	ST 2	ST 1¼	EST 2½
7	ST 3	EST 2½	ST 8	EST 2½
8	ST 4	EST 3	EST 5	EST 2½

(continued)

Table 5.6 (continued)

Element group	Sections			
	CBO	ECBO	VPS	MDVC-UVPS
9	ST 5	DEST 2½	EST 3½	EST 4
10	EST 10	EST 4	DEST 3	DEST 3
11	ST 6	ST 6	EST 5	DEST 3
12	DEST 6	DEST 5	EST 10	DEST 6
13	EST 4	ST 2½	ST 2½	ST 3½
14	ST 3½	ST 3½	ST 2½	ST 3½
15	ST 3	ST 4	EST 2½	ST 3½
16	ST 4	ST 5	ST 3	EST 3
17	EST 10	DEST 2½	ST 4	DEST 2½
18	EST 3	EST 3½	DEST 3	DEST 3
19	DEST 2½	ST 6	DEST 3	EST 5
20	EST 4	DEST 5	DEST 4	ST 6
21	DEST 6	EST 6	EST 10	ST 10
22	EST 5	EST 5	ST 6	ST 6
23	EST 3½	ST 3	ST 2½	ST 2½
24	ST 3	ST 2½	EST 2½	ST 2½
25	ST 2½	ST 2½	ST 3	ST 2½
26	EST 1½	EST 1½	EST 1½	EST 2
27	ST 3	EST 2	ST 2½	EST 2
28	ST 2½	EST 2	ST 3	EST 2
29	ST 2½	ST 2½	ST 2½	EST 1½
30	ST 3	EST 1½	ST 1½	EST 2
31	ST 3½	EST 2	ST 4	ST 2½
Weight (kg)	93,174	82,254	82,357	79,571
Average optimized weight (kg)	97,823	90,752	89,607	85,398
Standard deviation on average weight (kg)	9226	5995	5188	4407

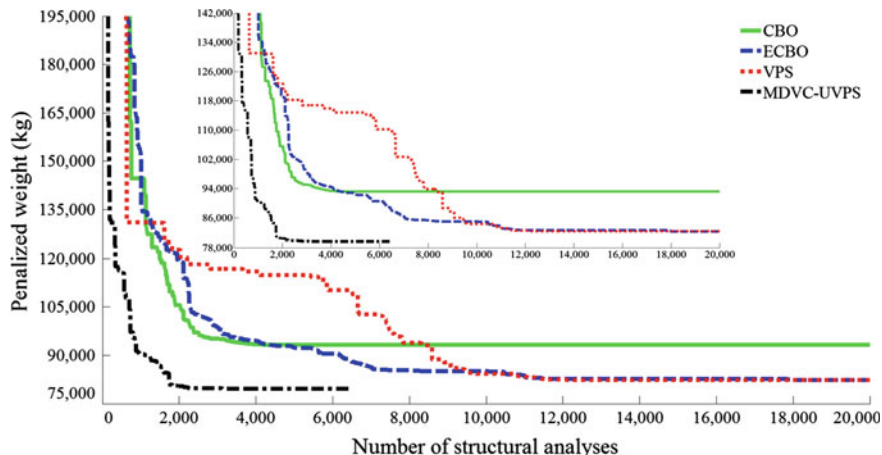


Fig. 5.15 Convergence curves for the 1520-bar double-layer grid problem

References

1. Lan TT (2005) Space frame structures. Handbook of structural engineering. CRC Press, Boca Raton, FL
2. Kaveh A (2017) Advances in metaheuristic algorithms for optimal design of structures, 2nd edn. Springer, Switzerland
3. Kaveh A, Mahdavi VR (2014) Colliding bodies optimization: a novel meta-heuristic method. Comput Struct 139:18–27
4. Kaveh A, Ilchi Ghazaan M (2014) Enhanced colliding bodies optimization for design problems with continuous and discrete variables. Adv Eng Softw 77:66–75
5. Kaveh A, Ilchi Ghazaan M (2016) Vibrating particles system algorithm for truss optimization with multiple natural frequency constraints. Acta Mech 228(1):307–332
6. Kaveh A, Ilchi Ghazaan M (2018) A new hybrid meta-heuristic algorithm for optimal design of large-scale dome structures. Eng Optimiz 50(2):235–252
7. American Institute of Steel Construction (AISC) (1994) Manual of steel construction load resistance factor design. USA

Chapter 6

Optimal Design of Double-Layer Barrel Vault Space Structures



6.1 Introduction

The brick architecture of the Orient and the masonry construction of the Romans provide numerous examples of the structural use of barrel vaults. During recent years, architects and engineers have rediscovered the advantages of barrel vaults as viable and often highly suitable forms for covering not only low-cost industrial buildings, warehouses, large-span hangars, and indoor sports stadiums, but also large cultural and leisure centers. The impact of industrialization on production of prefabricated barrel vaults has proved to be the most significant factor leading to lower cost for these structures [1].

Barrel vaults are given different names depending on the way their surface is formed. The earlier types of barrel vaults were constructed as single-layer structures. Nowadays, with the increase of the spans, double-layer systems are often preferred. While the members of single-layer barrel vaults are mainly under the action of flexural moments, those of double-layer barrel vaults are almost exclusively under the action of axial forces and the elimination of bending moments leads to a full utilization of strength of all the elements. Double-layer barrel vaults are generally statically indeterminate. In such systems, due to the rigidity, the risk of instability can almost be eliminated. The use of this type of barrel vaults enhances the stiffness of the vault structure and provides structural systems of great potential, capable of having spans in excess of 100 m [2, 3].

In the recent decades, different meta-heuristic algorithms have been developed and applied to structural optimization problems. The growing popularity of these techniques arises from (i) the lack of dependency on gradient information; (ii) inherent capability to deal with both discrete and continuous design variables; and (iii) incorporating global search features to produce reasonable solutions for complicated problems [4]. Double-layer barrel vaults have a great number of structural elements, and utilizing optimization techniques has a considerable influence on their economy and efficient structural configuration. For optimal design of

double-layer barrel vaults, Kaveh and Eftekhar presented an improved hybrid Big Bang-Big Crunch (IBBBC) algorithm [5]. In another study optimal design of some single-layer barrel vaults and a double arch barrel vault were investigated by Kaveh et al. [6]. In several studies, the optimal design of a practical model of a braced barrel vault has been studied by various researchers. Hasançebi and Çarbaş used ant colony search method [7], Hasançebi et al. employed a reformulation of the ant colony optimization [8] and Hasançebi and Kazemzadeh Azad utilized a reformulation of Big Bang-Big Crunch algorithm and adaptive dimensional search method [4, 9, 10].

In this chapter, three double-layer barrel roof structures are optimized to investigate the performance of the CBO [11], ECBO [12], VPS [13] and MDVC-UVPS [14] meta-heuristic algorithms. The structures are subjected to stress, stability, and displacement limitations according to the provisions of AISC-ASD [15]. The design variables are the cross-sectional areas of the bar elements which are selected from a list of steel pipe sections.

6.2 Optimal Design of Double-Layer Barrel Vaults

Typically in practical design optimization of skeletal structures, the goal is to find a minimum cost or weight design by selecting the cross-sectional areas of structural elements from a list of available sections such that the final design satisfies strength and serviceability requirements determined by standard design codes. Size optimization of a skeletal structure with its members being collected in ng design groups can be formulated as follows:

$$\begin{aligned} \text{Find} \quad & \{X\} = [x_1, x_2, \dots, x_{ng}] \\ \text{to minimize} \quad & W(\{X\}) = \sum_{i=1}^{ng} x_i \sum_{j=1}^{nm(i)} \rho_j L_j \\ \text{subjected to:} \quad & \begin{cases} g_j(\{X\}) \leq 0, & j = 1, 2, \dots, nc \\ x_{i\min} \leq x_i \leq x_{i\max} \end{cases} \end{aligned} \quad (6.1)$$

where $\{X\}$ is the vector containing the design variables; $W(\{X\})$ presents the weight of the structure; $nm(i)$ is the number of members for the i th group; ρ_j and L_j denote the material density and the length of the j th member, respectively. $x_{i\min}$ and $x_{i\max}$ are the lower and upper bounds of the design variable x_i , respectively. $g_j(\{X\})$ denotes design constraints; and nc is the number of constraints.

For constraint handling, a penalty approach is utilized. For this purpose, the objective function (Eq. 6.1) is redefined as follows:

$$P(\{X\}) = (1 + \varepsilon_1 \cdot v)^{\varepsilon_2} \times W(\{X\}) \quad (6.2)$$

where $P(\{X\})$ is the penalized cost function or the objective function to be minimized and v denotes the sum of the violations of the design constraints. Here, ε_1 is set to unity and ε_2 is calculated by:

$$\varepsilon_2 = 1.5 + 1.5 \times \frac{\text{iter}}{\text{iter}_{\max}} \quad (6.3)$$

where iter is the current iteration number and iter_{max} is the total number of iterations for optimization process.

The constraint conditions for barrel vaults studied here are briefly explained in the following. Limitation on stress and stability of barrel vault elements are imposed according to the provisions of the AISC-ASD [15] as follows:

The allowable tensile stresses for tension members are calculated by

$$\sigma_i^+ = 0.6F_y \quad (6.4)$$

where F_y stands for the yield strength.

The allowable stress limits for compression members are calculated depending on two possible failure modes of the members known as elastic and inelastic buckling. Thus

$$\sigma_i^- = \begin{cases} \left[\left(1 - \frac{\lambda_i^2}{2C_c^2} \right) F_y \right] / \left[\frac{5}{3} + \frac{3\lambda_i}{8C_c} - \frac{\lambda_i^3}{8C_c^3} \right] & \text{for } \lambda_i < C_c \\ \frac{12\pi^2 E}{23\lambda_i^2} & \text{for } \lambda_i \geq C_c \end{cases} \quad (6.5)$$

where E is the modulus of elasticity; λ_i is the slenderness ratio ($\lambda_i = kl_i/r_i$); C_c denotes the slenderness ratio dividing the elastic and inelastic buckling regions ($C_c = \sqrt{2\pi^2 E/F_y}$); k is the effective length factor (k is set 1 for all truss members); L_i is the member length; and r_i is the minimum radius of gyration.

AISC-ASD recommends the maximum slenderness ratio of the elements to be restricted to 300 and 200 for tension and compression members, respectively.

6.3 Design Examples

Three double-layer barrel vault problems with 384, 693, and 1536 bar elements are considered to evaluate the performance of CBO, ECBO, VPS, and MDVC-UVPS algorithms. The design variables are the cross-sectional areas of the bar elements which are selected from the list of steel pipe sections of AISC-LRFD [16]. These pipe sections are shown in Table 6.1. ST, EST, and DEST abbreviations stand for standard weight, extra strong, and double-extra strong, respectively. Each example has been solved 30 times independently and a maximum of 1000 iterations is considered as the termination condition. A population of 20 particles is considered

Table 6.1 The steel pipe sections

No.	Type	Nominal diameter (in)	Area (in ²)	Moment of inertia (in ⁴)	Gyration radius (in)
1	ST	1/2	0.25	0.017	0.2608
2	EST	1/2	0.32	0.02	0.2500
3	ST	3/4	0.33	0.037	0.3333
4	EST	3/4	0.43	0.045	0.3224
5	ST	1	0.49	0.087	0.4197
6	EST	1	0.64	0.11	0.4073
7	ST	1 1/4	0.67	0.19	0.5399
8	ST	1 1/2	0.8	0.31	0.6229
9	EST	1 1/4	0.88	0.24	0.5241
10	EST	1 1/2	1.07	0.67	0.7889
11	ST	2	1.07	0.39	0.6045
12	EST	2	1.48	0.87	0.7658
13	ST	2 1/2	1.7	1.54	0.9515
14	ST	3	2.23	3.02	1.1637
15	EST	2 1/2	2.25	1.92	0.9238
16	DEST	2	2.66	1.31	0.7018
17	ST	3 1/2	2.68	4.79	1.3369
18	EST	3	3.02	3.89	1.1349
19	ST	4	3.17	7.23	1.5102
20	EST	3 1/2	3.68	6.28	1.3063
21	DEST	2 1/2	4.03	2.87	0.8439
22	ST	5	4.3	15.2	1.8801
23	EST	4	4.41	9.61	1.4762
24	DEST	3	5.47	5.99	1.0465
25	ST	6	5.58	28.1	2.2441
26	EST	5	6.11	20.7	1.8406
27	DEST	4	8.1	15.3	1.3744
28	ST	8	8.4	72.5	2.9378
29	EST	6	8.4	40.5	2.1958
30	DEST	5	11.3	33.6	1.7244
31	ST	10	11.9	161	3.6782
32	EST	8	12.8	106	2.8777
33	ST	12	14.6	279	4.3715
34	DEST	6	15.6	66.3	2.0616
35	EST	10	16.1	212	3.6287
36	EST	12	19.2	362	4.3421
37	DEST	8	21.3	162	2.7578

ST standard weight, EST extra strong, DEST double-extra strong

for each algorithm and the other algorithm parameters are set similar to the values proposed in [12–14]. The optimization algorithms are coded in MATLAB and the structures are analyzed using the direct stiffness method by our own codes.

6.3.1 A 384-Bar Double-Layer Barrel Vault

The first design problem deals with the size optimization of a spatial 384-bar barrel vault consisting of two rectangular nets as shown in Fig. 6.1. In order to make the structure stable, the angles of the bottom nets are placed at the center of one of the above nets. The two nets are connected using diagonal elements [3]. The span of the barrel vault is 24.82 m, its rise is 5.12 m and its length is 26.67 m. The depth of the structure, i.e., the distance between the top and bottom layers, is equal to 1.35 m. This structure consists of 111 pinned joints and 384 bar elements, which are grouped into 31 independent sizing variables as identified in Fig. 6.1. The structural material properties are assumed as follows: The modulus of elasticity is considered to be 30,450 ksi (210,000 MPa), the yield stress of steel is taken as 58 ksi (400 MPa), and the density of steel is equal to 0.288 lb per cubic inch (7833.413 kg/m^3). All connections are assumed as ball jointed and the supports are considered at the two external edges of the top layer of the barrel vault. Vertical concentrated loads of -20 kips (-88.964 kN) are applied to all free joints (non-support joints) of the top layer. Strength and slenderness limitations are according to AISC-ASD provision [15], which are discussed earlier. Displacement constraints of ± 0.1969 in (5 mm) are imposed on all nodes in x , y and z directions.

Table 6.2 presents the comparison of the results of different algorithms. The VPS algorithm yields the least weight for this example, which is 62,455.30 lb (28,329.24 kg). The other design weights are 69,448.52 lb (31,501.32 kg) by CBO, 62,486.02 lb (28,343.18 kg) by ECBO, and 62,735.42 lb (28,456.31 kg) by MDVC-UVPS. The best design of the VPS has been achieved in 12,780 analyses. CBO, ECBO, and MDVC-UVPS require 4320, 15,980, and 3460 structural analyses to find their optimum solutions, respectively. Figure 6.2 shows the convergence curves of the best results found by CBO, ECBO, VPS, and MDVC-UVPS.

6.3.2 A 693-Bar Double-Layer Barrel Vault

The considered 693-bar braced barrel vault consists of 259 joints and 693 members with 23 independent design variables. The free span of the barrel vault is 19.03 m, its rise is 5.75 m and its length is 22.9 m. The geometry and the member grouping scheme of the structure is shown in Fig. 6.3. The structural material properties are assumed as follows: The modulus of elasticity is taken as 29,000 ksi (203,893.6 MPa), the yield stress of steel is assumed to be 36 ksi (253.1 MPa), and the density of steel is 0.288 lb/in^3 (7833.413 kg/m^3). It is assumed that the barrel

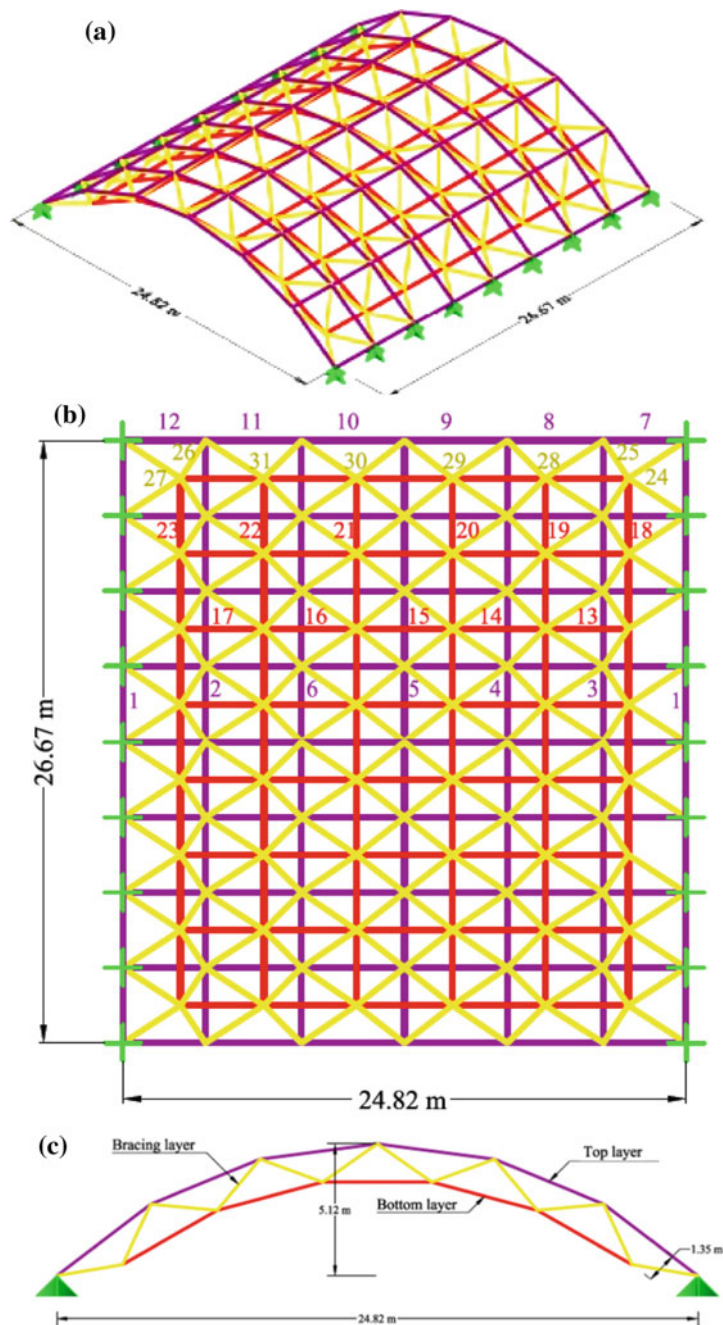


Fig. 6.1 **a** 3D view, **b** plan view with group numbers **c** flattened cross-sectional view of the 384-bar double-layer barrel vault

Table 6.2 Performance comparison for the 384-bar braced barrel vault problem

Element group	Sections			
	CBO	ECBO	VPS	MDVC-UVPS
1	ST 1/2	ST 1/2	ST 3/4	ST 1/2
2	EST 2	ST 2 1/2	EST 2 1/2	EST 2
3	EST 2	EST 2	EST 2 1/2	EST 2
4	ST 3	ST 1 1/2	EST 1 1/2	ST 1 1/2
5	DEST 2 1/2	EST 4	DEST 3	DEST 3
6	ST 2 1/2	ST 1 1/2	ST 1 1/2	ST 1 1/2
7	ST 12	ST 12	ST 12	ST 12
8	DEST 4	ST 10	EST 8	DEST 5
9	DEST 5	ST 12	EST 10	EST 10
10	ST 12	DEST 8	EST 10	EST 10
11	DEST 5	DEST 5	DEST 5	DEST 5
12	DEST 6	EST 8	DEST 5	ST 12
13	DEST 3	ST 6	ST 6	ST 6
14	EST 3 1/2	EST 3 1/2	DEST 3	ST 4
15	ST 2 1/2	ST 2 1/2	ST 2 1/2	EST 2 1/2
16	EST 6	ST 5	ST 5	ST 4
17	EST 6	EST 4	DEST 3	ST 6
18	EST 2	EST 1 1/2	EST 1 1/2	EST 1 1/2
19	EST 2	ST 1 1/4	ST 1 1/4	ST 1 1/4
20	EST 2 1/2	EST 1 1/2	EST 1 1/2	EST 1 1/2
21	EST 4	EST 1 1/2	EST 1 1/2	EST 1 1/2
22	ST 3 1/2	ST 1 1/4	EST 1 1/2	ST 1 1/4
23	EST 1 1/2	EST 1 1/2	EST 1 1/2	EST 1 1/2
24	ST 3 1/2	EST 2 1/2	EST 2 1/2	ST 3 1/2
25	ST 2 1/2	ST 2 1/2	EST 2 1/2	EST 2
26	DEST 4	ST 2 1/2	EST 1 1/2	EST 2
27	EST 3	DEST 2	ST 3	ST 3 1/2
28	EST 2	EST 1 1/2	EST 1 1/2	EST 2
29	ST 2 1/2	ST 2 1/2	EST 2	EST 2
30	ST 3	EST 1 1/2	EST 2	EST 2
31	ST 2 1/2	EST 1 1/2	EST 1 1/2	EST 2
Weight (lb)	69,448.52 (31,501.32 kg)	62,486.02 (28,343.18 kg)	62,455.30 (28,329.24 kg)	62,735.42 (28,456.31 kg)
Average optimized weight (lb)	123,397 (55,971.93 kg)	65,785 (29,839.57 kg)	67,900 (30,798.92 kg)	65,738 (29,818.26 kg)
Standard deviation on average weight (lb)	103,837 (47,099.67 kg)	3386 (1535.86 kg)	2913 (1321.31 kg)	2882 (1307.25 kg)

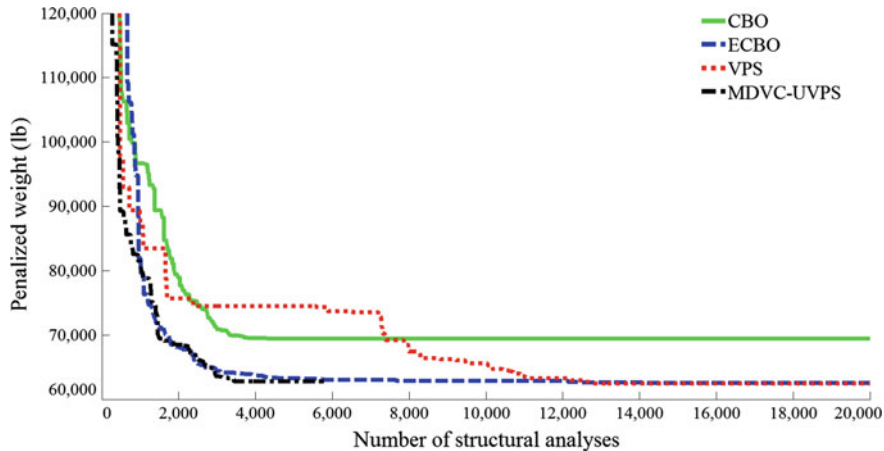


Fig. 6.2 Convergence curves for the 384-barrel vault problem

vault is loaded by uniformly distributed vertical loads applied to the top of the roof, and supports are considered at the two external edges of the top and bottom layers. The applied loads are considered as follows: a uniform dead load (DL) pressure of 35 kg/m^2 ; a positive wind load (WL) pressure of 160 kg/m^2 ; and a negative wind load (WL) pressure of 240 kg/m^2 . For design purposes, these loads are combined follows:

- Load case 1: $1.5(\text{DL} + \text{WL}) = 1.5(35 + 160) = 292.5 \text{ kg/m}^2$ (2.87 kN/m^2)
- Load case 2: $1.5(\text{DL} - \text{WL}) = 1.5(35 - 240) = -307.5 \text{ kg/m}^2$ (3.00 kN/m^2)

Stress and slenderness constraints are considered according to AISC-ASD [15] which are discussed earlier. The nodes are subjected to the displacement limits of $\pm 0.1 \text{ in}$ (0.254 cm) in every direction.

Table 6.3 presents a comparison between the obtained results. The lightest design (i.e., 9091.1 lb (4123.65 kg)) is found by MDVC-UVPS algorithm and after that the best design belongs to VPS (i.e., 9201.4 lb (4173.68 kg)). Figure 6.4 shows the convergence curves of the best results found by CBO, ECBO, VPS, and MDVC-UVPS. MDVC-UVPS converges to the optimum solution after 4120 analyses. CBO, ECBO, and VPS obtain their optimal solutions after 4400, 16,720, and 9800 analyses, respectively. Element stress ratios at the best design optimized by MDVC-UVPS are shown in Fig. 6.5. The maximum stress ratio is 81.12%.

6.3.3 A 1536-Bar Double-Layer Barrel Vault

The last design example is the size optimization of a 1536-bar double-layer barrel vault with 413 joints, a span of 40 m, a length of 50 m, and 35 independent variable

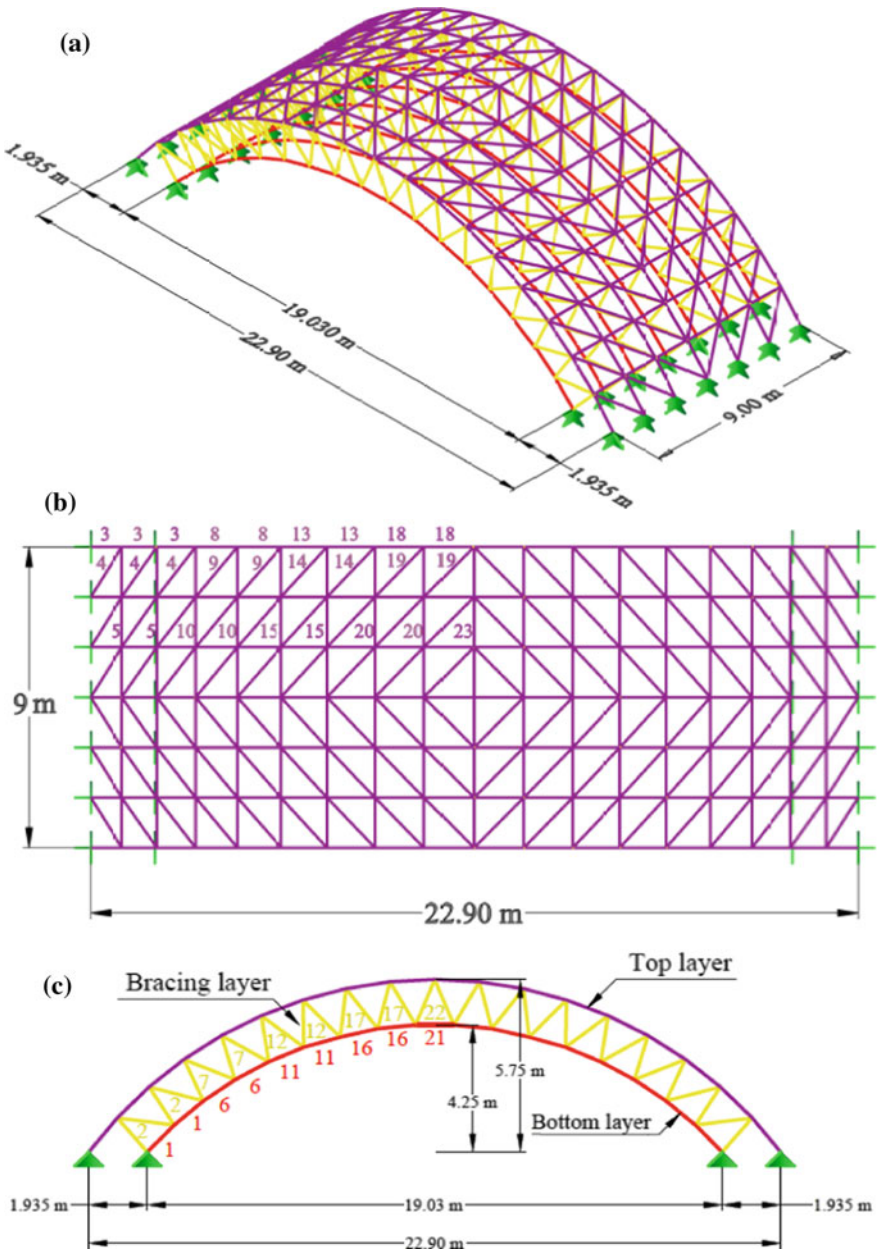


Fig. 6.3 **a** 3D view, **b** plan view with group numbers of the top layer and **c** flattened cross-sectional view with the group number of bracing and the bottom layer elements of the 693-bar double-layer barrel vault

Table 6.3 Performance comparison for the 693-barrel vault problem

Element group	Sections			
	CBO	ECBO	VPS	MDVC-UVPS
1	ST 4	ST 4	EST 3	ST 4
2	ST 1	ST 1	ST 1	ST 1
3	ST 1 1/4	ST 3/4	ST 3/4	ST 3/4
4	ST 1 1/4	ST 1	ST 1	ST 1
5	ST 3/4	ST 3/4	ST 3/4	ST 3/4
6	EST 3	ST 3	ST 3 1/2	ST 3 1/2
7	ST 1	ST 1	ST 1	ST 1
8	ST 3/4	ST 1	ST 3/4	ST 1
9	ST 1 1/2	ST 1	ST 1	ST 1
10	ST 3/4	ST 3/4	ST 3/4	ST 3/4
11	ST 3	EST 2	ST 3	EST 2 1/2
12	ST 1	ST 1 1/4	EST 1 1/4	ST 1
13	ST 1 1/4	EST 2	EST 1	ST 1 1/2
14	ST 1 1/4	ST 1	ST 1	ST 1
15	ST 3/4	ST 3/4	ST 3/4	ST 3/4
16	ST 2	ST 1	EST 1 1/2	EST 1 1/4
17	ST 1 1/2	ST 1	ST 1	ST 1
18	EST 1 1/2	ST 3	EST 1 1/2	EST 2
19	ST 1 1/2	ST 1	ST 1	ST 1
20	ST 3/4	ST 3/4	EST 3/4	ST 3/4
21	ST 2 1/2	ST 3/4	ST 1	ST 1
22	ST 1	ST 3/4	ST 1	ST 1
23	ST 3/4	ST 3/4	ST 3/4	ST 3/4
Weight (lb)	10,221.8 (4,636.53 kg)	9240.5 (4191.42 kg)	9201.4 (4173.68 kg)	9091.1 (4123.65 kg)
Average optimized weight (lb)	15,563 (7,059.26 kg)	9577 (4344.05 kg)	9823 (4455.64 kg)	9475 (4297.79 kg)
Standard deviation on average weight (lb)	3976 (1803.48 kg)	505 (229.06 kg)	598 (271.25 kg)	765 (347.00 kg)

groups [17]. The geometric details and member groups are presented in Fig. 6.6. The modulus of elasticity is taken as 30,450 ksi (210,000 MPa), the yield stress of steel is equal to 58 ksi (400 MPa), and the density of materials is considered to be 0.288 lb/in³ (7833.413 kg/m³). The supports are fixed at the two external edges of the top layer of the structure and all joints of the top layer are subjected to concentrated vertical loads of 5 kips. The design constraints (including stress and slenderness limitation) are considered according to AISC-ASD [15] which are discussed earlier. The nodal displacements are limited to ± 0.1969 in (5 mm) in every direction.

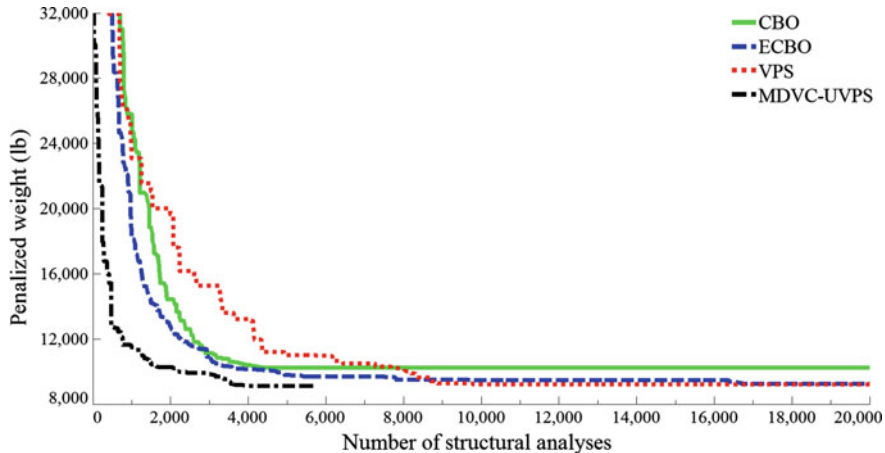


Fig. 6.4 Convergence curves for the 693-barrel vault problem

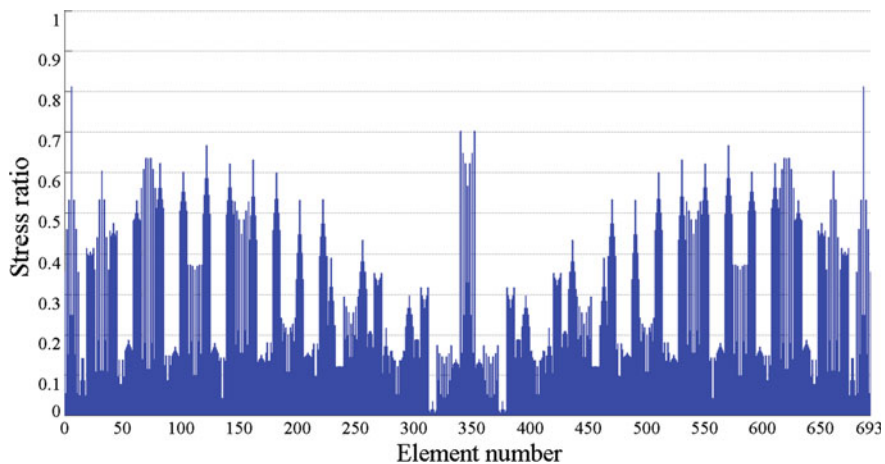


Fig. 6.5 Stress ratios for the best design obtained by MDVC-UVPS for the 693-barrel vault problem

Table 6.4 presents the results of the optimal designs of different optimization algorithms. The weight of the best result obtained by MDVC-UVPS is 122,852 lb (55,724.73 kg) that is the best among the compared methods. The average optimized weight of this method is 146,229 lb (66,328.36 kg) which is less than those of all other methods. Comparison of the convergence curves of CBO, ECBO, VPS, and MDVC-UVPS is illustrated in Fig. 6.7. MDVC-UVPS requires 4762 structural analyses to find the optimum solution while CBO, ECBO, and VPS require 4540, 15,060, and 18,080 structural analyses, respectively.

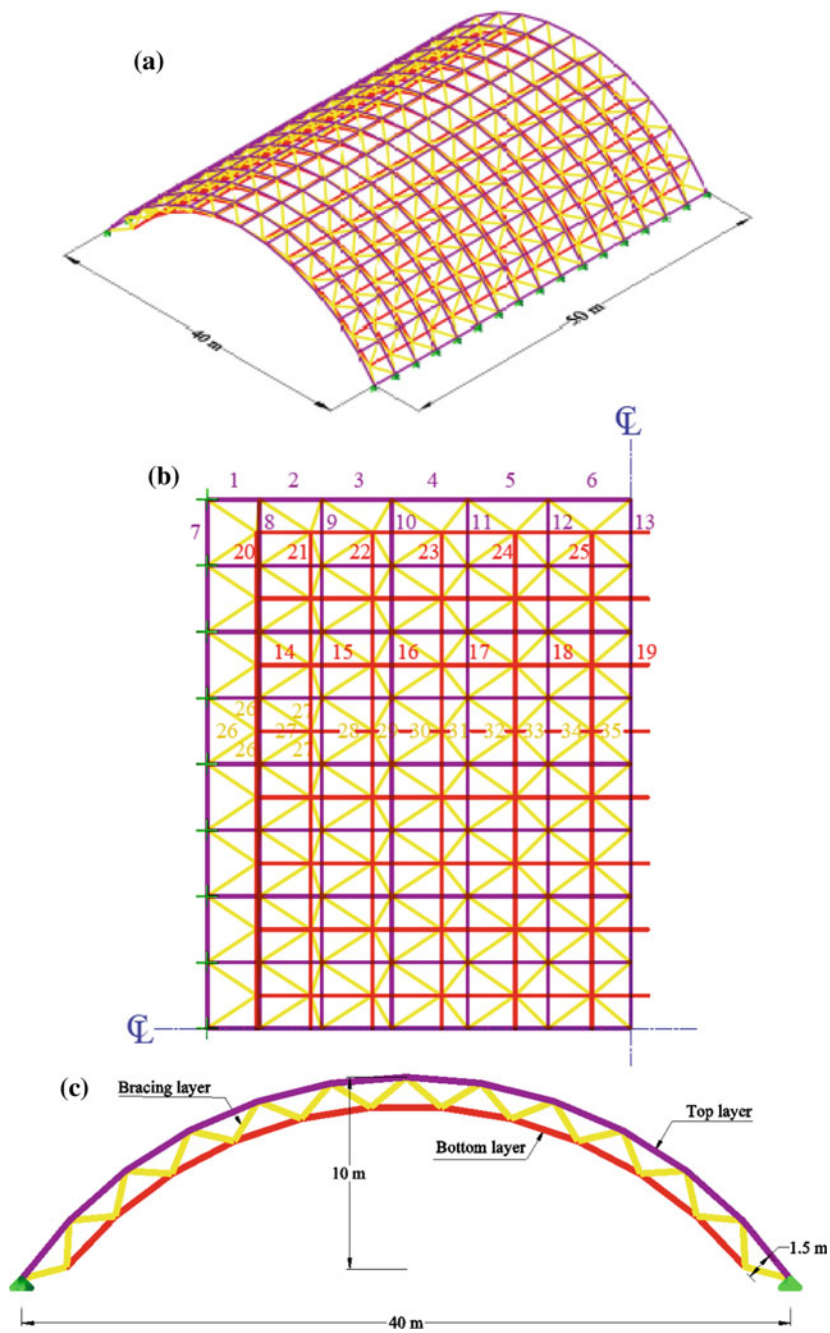


Fig. 6.6 **a** 3D view, **b** top plan view of quarter of the barrel vault with the related group numbers and **c** flattened cross-sectional view of the 1536-bar double-layer barrel vault

Table 6.4 Performance comparison for the 1536-barrel vault problem

Element group	Sections			
	CBO	ECBO	VPS	MDVC-UVPS
1	DEST 3	EST 6	DEST 4	DEST 4
2	ST 4	DEST 3	ST 3 1/2	ST 4
3	ST 4	EST 3 1/2	ST 4	EST 3 1/2
4	DEST 2 1/2	EST 4	DEST 3	EST 5
5	EST 6	DEST 4	EST 6	EST 5
6	DEST 3	DEST 5	EST 5	EST 5
7	EST 1 1/4	ST 1/2	EST 1/2	ST 1/2
8	EST 2	ST 1 1/2	EST 2	ST 1 1/2
9	EST 2 1/2	ST 1 1/2	ST 3 1/2	ST 1 1/2
10	ST 2	ST 1	ST 1 1/2	ST 1 1/4
11	EST 2	EST 1 1/2	ST 1 1/4	ST 2 1/2
12	EST 4	ST 2 1/2	ST 3	EST 2 1/2
13	ST 1 1/4	EST 3 1/2	ST 3 1/2	EST 3
14	ST 5	EST 4	ST 5	DEST 3
15	ST 8	EST 2 1/2	DEST 3	ST 6
16	ST 8	DEST 2 1/2	DEST 3	ST 5
17	EST 4	ST 3 1/2	ST 3	DEST 2 1/2
18	DEST 2 1/2	EST 1 1/2	EST 2 1/2	EST 2
19	ST 3 1/2	EST 1 1/2	EST 1 1/2	EST 2
20	EST 2	ST 1 1/2	ST 2 1/2	ST 1 1/2
21	DEST 2 1/2	ST 1 1/2	EST 1 1/2	ST 1 1/2
22	EST 2	ST 1 1/2	EST 2	ST 1 1/2
23	ST 2 1/2	ST 1 1/2	ST 1 1/2	EST 2
24	ST 1 1/2	ST 1 1/2	DEST 2 1/2	ST 1 1/2
25	EST 2 1/2	ST 1 1/2	ST 1 1/2	EST 2
26	ST 3 1/2	DEST 2	ST 3	ST 2 1/2
27	EST 2	EST 1 1/2	ST 1 1/2	EST 1 1/2
28	EST 2	ST 1 1/2	ST 1 1/2	ST 1 1/2
29	EST 1 1/2	EST 1 1/2	EST 2	ST 1 1/2
30	ST 2	ST 1 1/4	ST 2	EST 1 1/2
31	EST 1 1/2	ST 2 1/2	EST 1 1/2	EST 1 1/2
32	ST 3 1/2	ST 1 1/4	EST 1 1/2	ST 2
33	EST 2	EST 2	ST 1 1/2	EST 1 1/2
34	ST 2	ST 1 1/2	EST 1 1/2	ST 2
35	EST 1 1/2	EST 1 1/2	ST 1 1/2	ST 2
Weight (lb)	152,229 (69,049.91 kg)	128,111 (58,110.17 kg)	129,117 (58,566.49 kg)	122,852 (55,724.73 kg)
Average optimized weight (lb)	215,621 (97,804.04 kg)	149,002 (67,586.17 kg)	147,089 (66,718.45 kg)	146,229 (66,328.36 kg)
Standard deviation on average weight (lb)	36,322 (16,475.38 kg)	16,775 (7,609.01 kg)	14,644 (6,642.41 kg)	14,552 (6600.68 kg)

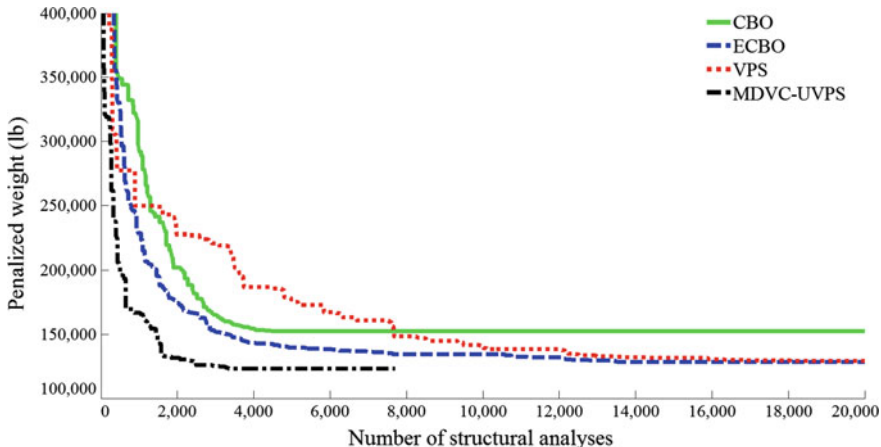


Fig. 6.7 Convergence curves for the 1536-barrel vault problem

6.4 Concluding Remarks

Barrel vaults are effective semicylindrical structural systems that are commonly used to provide long-span and economical roofs for multipurpose facilities including warehouses, rail stations, pools, sport centers, airplane hangars, and community centers.

In this chapter, three barrel vault optimization problems with discrete variables are considered under stress, stability, and displacement limitations. In the 384-bar barrel vault problem, the design found by the ECBO, VPS, and MDVC-UVPS are approximately identical and are about 10% lighter than the result obtained by CBO. In the 693-bar barrel vault problem, the design obtained by MDVC-UVPS is 12.4, 1.6, and 1.2% lighter than the best design achieved by the CBO, ECBO, and VPS, respectively. These values are 24, 4.3, and 5 for the 1536-bar barrel vault problem. A suitable average optimized weight and also an acceptable standard deviation from the mean value of the independent runs show the robustness of the proposed algorithms. Also, comparison of the convergence curves indicates that the MDVC-UVPS comes close to the optimum design rapidly.

References

1. Makowski ZS (2006) Analysis, design and construction of braced barrel vaults. Elsevier Applied Science Publishers, London, New York
2. Kaveh A, Mirzaei B, Jafarvand A (2014) Optimal design of double layer barrel vaults using improved magnetic charged system search. Asian J Civil Eng 15(1):135–154
3. Kaveh A, Moradveisi M (2016) Optimal design of double-layer barrel vaults using CBO and ECBO algorithms. Iran J Sci Technol, Trans Civil Eng 40(3):167–178

4. Hasançebi O, Kazemzadeh Azad S (2015) Adaptive dimensional search: a new metaheuristic algorithm for discrete truss sizing optimization. *Comput Struct* 154:1–16
5. Kaveh A, Eftekhari B (2012) Optimal design of double layer barrel vaults using an improved hybrid big bang-big crunch method. *Asian J Civil Eng* 13:465–487
6. Kaveh A, Farahani M, Shojaei N (2012) Optimal design of barrel vaults using charged search system. *Int J Civil Eng* 10:301–308
7. Hasançebi O, Çarbaş S (2011) Ant colony search method in practical structural optimization. *Int J Optim Civil Eng* 1:91–105
8. Hasançebi O, Çarbaş S, Saka MP (2011) A reformulation of the ant colony optimization algorithm for large scale structural optimization. In: Proceedings of the second international conference on soft computing technology in civil, structural and environmental engineering, Civil-Comp Press, Stirlingshire
9. Hasançebi O, Kazemzadeh Azad S (2013) Reformulations of big bang-big crunch algorithm for discrete structural design optimization. *World Acad Sci Eng Technol* 74
10. Hasançebi O, Kazemzadeh Azad S (2013) Discrete size optimization of steel trusses using a refined big bang–big crunch algorithm. *Eng Optimiz* 46(1):61–83
11. Kaveh A, Mahdavi VR (2014) Colliding bodies optimization: a novel meta-heuristic method. *Comput Struct* 139:18–27
12. Kaveh A, Ilchi Ghazaan M (2014) Enhanced colliding bodies optimization for design problems with continuous and discrete variables. *Adv Eng Softw* 77:66–75
13. Kaveh A, Ilchi Ghazaan M (2016) Vibrating particles system algorithm for truss optimization with multiple natural frequency constraints. *Acta Mech* 228(1):307–332
14. Kaveh A, Ilchi Ghazaan M (2018) A new hybrid meta-heuristic algorithm for optimal design of large-scale dome structures. *Eng Optimiz* 50(2):235–252
15. American Institute of Steel Construction (AISC) (1989) Manual of steel construction: allowable stress design, Chicago, USA
16. American Institute of Steel Construction (AISC) (1994) Manual of steel construction load resistance factor design, Chicago, USA
17. Kaveh A, Mahjoubi S (2018) Optimum design of double-layer barrel vaults by lion pride optimization algorithm. *Structures* 13:213–229

Chapter 7

Optimal Design of Dome-Shaped Trusses



7.1 Introduction

Domes are one of the oldest and well-established structural forms and have been used in architecture since the earliest times. These structures are of special interest to engineers as they enclose large spaces with small surfaces and have proven to be very economical in terms of consumption of constructional materials [1]. The main aim of this chapter is frequency constraint optimization of dome truss structures; however, all the domes are also optimized considering strength, stability, and displacement constraints. Structural optimization considering natural frequency constraints is believed to represent nonlinear and non-convex search spaces with several local optima [2]. In this class of problems, large generalized eigenproblems should be solved in order to find the natural frequencies of the structure. The size of the structure affects the dimensions of the matrices involved and thus the required computational time and effort. On the other hand, as the number of optimization variables increases, more and more structural analyses are needed to be performed in order to reach a near-optimal solution [3].

Structural optimization considering natural frequency constraints has been studied since the 1980s [2] and was approached using mathematical programming and meta-heuristic algorithms. Lin et al. [4] studied the minimum weight design of structures under simultaneous static and dynamic constraints proposing a bi-factor algorithm based on the Kuhn–Tucker criteria. Konzelman [5] considered the problem using some dual methods and approximation concepts for structural optimization. Grandhi and Venkaya [6] utilized an optimality criterion based on uniform Lagrangian density for resizing and scaling procedure to locate the constraint boundary. Wang et al. [7] proposed an optimality criteria algorithm for combined sizing–layout optimization of three-dimensional truss structures. In this method, the sensitivity analysis helps to determine the search direction and the optimal solution is achieved gradually from an infeasible starting point with a minimum weight increment, and the structural weight is indirectly minimized.

Sedaghati [8] utilized a new approach using combined mathematical programming based on the Sequential Quadratic Programming (SQP) technique and a finite element solver based on the integrated force method. Lingyun et al. [9] combined the simplex search method and the Niche Genetic Hybrid Algorithm (NGHA) for mass minimization of structures with frequency constraints. Gomes [10] used the Particle Swarm Optimization (PSO) algorithm to study simultaneous layout and sizing optimization of truss structures with multiple frequency constraints. Kaveh and Zolghadr [11] hybridized Charged System Search and Big Bang-Big Crunch with trap recognition capability (CSS-BBBC) to solve layout and sizing optimization problems of truss structures with natural frequency constraints. Miguel and Fadel Miguel [12] employed Harmony Search (HS) and Firefly Algorithm (FA) to study simultaneous layout and sizing optimization of truss structures with multiple frequency constraints. A hybrid Optimality Criterion (OC) and Genetic Algorithm (GA) method was used by Zuo et al. [13] for truss optimization with frequency constraints. Kaveh and Javadi [14] utilized a hybridization of Harmony search, Ray optimizer, and Particle Swarm Optimization algorithm (HRPSO) for weight minimization of trusses under multiple natural frequency constraints. Kaveh and Ilchi Ghazaan [15] employed Particle Swarm Optimization with an Aging Leader and Challengers (ALC-PSO) and HALC-PSO that transplants a harmony search-based mechanism to ALC-PSO as a variable constraint handling approach to optimize truss structures with frequency constraints. Hosseinzadeh et al. [16] used hybrid Electromagnetism-like mechanism algorithm and Migration Strategy (EM-MS) for layout and size optimization of truss structures with multiple frequency constraints.

7.2 Frequency Constraint Optimization Problem

In this chapter, the main aim of the optimization problem is to minimize the weight of the structure under multiple frequency constraints while the design variables are only the cross-sectional areas of bars (sizing optimization). Each variable should be chosen within a permissible range.

The mathematical formulation can be expressed as follows:

$$\begin{aligned}
 & \text{Find} && \{X\} = [x_1, x_2, \dots, x_{ng}] \\
 & \text{to minimize} && W(\{X\}) = \sum_{i=1}^{ng} x_i \sum_{j=1}^{\text{nm}(i)} \rho_j L_j \\
 & \text{subjected to:} && \begin{cases} \omega_j \leq \omega_j^* \\ \omega_k \geq \omega_k^* \\ x_{i\min} \leq x_i \leq x_{i\max} \end{cases} \quad (7.1)
 \end{aligned}$$

where $\{X\}$ is a vector containing the design variables; $W(\{X\})$ presents the weight of the structure; ng is the number of design groups; $\text{nm}(i)$ is the number of members for

the i th group; ρ_j and L_j denote the material density and the length of the j th member, respectively. ω_j is the j th natural frequency of the structure and ω_j^* is its upper bound; ω_k is the k th natural frequency of the structure and ω_k^* is its lower bound; $x_{i\min}$ and $x_{i\max}$ are the lower and upper bounds of the design variable x_i , respectively.

For constraint handling, a penalty approach is utilized. For this purpose, the objective function (Eq. 7.1) is redefined as follows:

$$P(\{X\}) = (1 + \varepsilon_1 \cdot v)^{\varepsilon_2} \times W(\{X\}) \quad (7.2)$$

where $P(\{X\})$ is the penalized cost function or the objective function to be minimized and v denotes the sum of the violations of the design constraints. In this chapter, ε_1 is set to unity and ε_2 is calculated by

$$\varepsilon_2 = 1.5 + 1.5 \times \frac{\text{iter}}{\text{iter}_{\max}} \quad (7.3)$$

where iter is the current iteration number and iter_{max} is the total number of iterations for optimization process.

7.3 Design Examples

The efficiencies of CBO, ECBO, VPS, and MDVC-UVPS are studied through three dome truss structures. These examples contain

- A 600-bar dome truss
- A 1180-bar dome truss
- A 1410-bar dome truss

Two constraint cases are considered for each example. In Case 1, natural frequency constraints are incorporated. In Case 2, limitation on stresses and stability of truss elements are considered according to the provisions of the ASD-AISC [17] as follows.

The allowable tensile stresses for tension members are calculated by

$$\sigma_i^+ = 0.6F_y \quad (7.4)$$

where F_y stands for the yield strength.

The allowable stress limits for compression members are calculated depending on two possible failure modes of the members known as elastic and inelastic buckling. Thus

$$\sigma_i^- = \begin{cases} \left[\left(1 - \frac{\lambda_i^2}{2C_c^2} \right) F_y \right] / \left(\frac{5}{3} + \frac{3\lambda_i}{8C_c} - \frac{\lambda_i^3}{8C_c^3} \right) & \text{for } \lambda_i < C_c \\ \frac{12\pi^2 E}{23\lambda_i^2} & \text{for } \lambda_i \geq C_c \end{cases} \quad (7.5)$$

where E is the modulus of elasticity; λ_i is the slenderness ratio ($\lambda_i = kl_i/r_i$); C_c denotes the slenderness ratio dividing the elastic and inelastic buckling regions ($C_c = \sqrt{2\pi^2 E/F_y}$); k is the effective length factor (k is set to 1 for all truss members); l_i is the member length; and r_i is the minimum radius of gyration.

In this design code provisions, the maximum slenderness ratio is limited to 300 for tension members, and this limit is recommended to be 200 for compression members. Nodal displacements in all the coordinate directions must be less than ± 8 cm.

7.3.1 A 600-Bar Dome Truss

The 600-bar single-layer dome structure is schematized in Fig. 7.1. The entire structure is composed of 216 nodes and 600 elements. Figure 7.2 shows a substructure in more detail for nodal numbering and coordinates. Each of the elements of this substructure is considered as a design variable. Thus, this is a size optimization problem with 25 variables. The elastic modulus is 200 GPa and the material density is 7850 kg/m³ for all elements. The yield stress of steel is taken as 400 MPa. A nonstructural mass of 100 kg is attached to all free nodes. The dome is considered to be subjected to vertical loading at all the unsupported joints for the second constraint case. According to symmetry, one only needs to define loading conditions of the labeled nodes shown in Fig. 7.2. These loads are -100, -500, -1500, -2500, -3500, -4500, -5500, -5000, and 0 kN, respectively. The allowable minimum and maximum cross-sectional areas of all elements are set to 1×10^{-4} and 100×10^{-4} m², respectively. There are two constraints on the

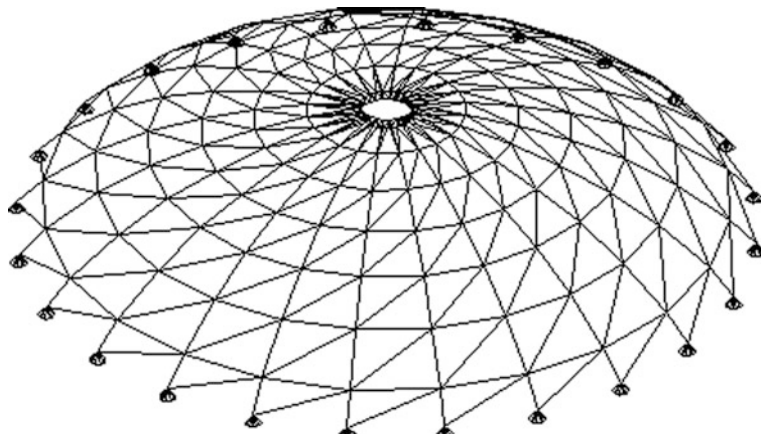


Fig. 7.1 Schematic of the 600-bar dome truss

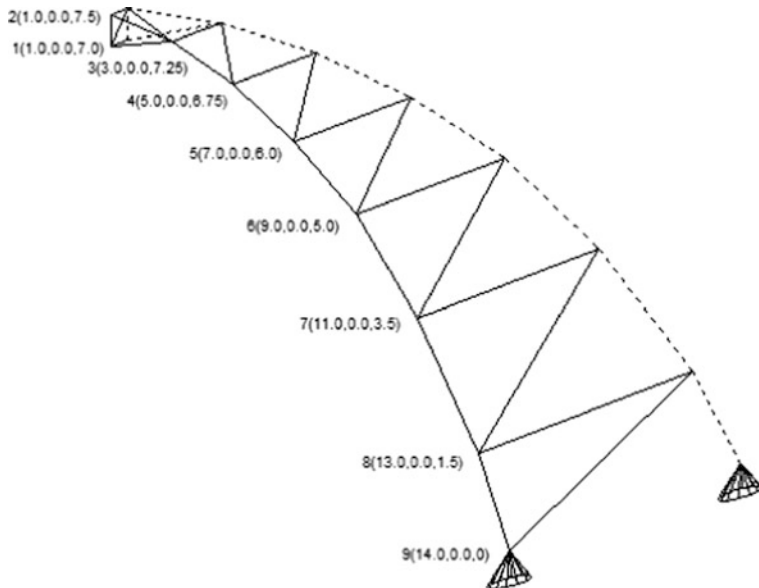


Fig. 7.2 Details of a substructure of the 600-bar dome truss

natural frequencies, which are $\omega_1 \geq 5$ and $\omega_3 \geq 7$ Hz. In order to optimize this structure by MDVC-UVPS, two stages are considered. The design variable configuration utilized for the first stage is listed as follows: [7 10 13], [16 19 22], [9 12 15], [18 21 24], [11 14 17], [20 23 25], [1 3 4 6], and [2 5 8]. Thus eight variables are used in the first stage.

7.3.1.1 Constraint Case 1

Table 7.1 presents the optimum designs obtained by CBO, ECBO [18], VPS [19], and MDVC-UVPS [20]. It can be seen that the best design was found by MDVC-UVPS. Also, the average optimized weight and standard deviation on average weight of this method are the lowest which are 6119.95 and 16.23 kg. Table 7.2 reports the natural frequencies of the optimized structures and it is clear that none of the frequency constraints are violated. Convergence histories for these techniques are depicted in Fig. 7.3. The required structural analyses to achieve the best designs by the CBO, ECBO, VPS, and MDVC-UVPS, respectively, are 17,940, 19,020, 25,040, and 17,513 analyses, respectively. It should be noted that MDVC-UVPS obtained the best design of VPS after 10,295 analyses.

Table 7.1 Performance comparison for the 600-bar dome truss problem—constraint case 1

Element number (nodes)	Areas (cm ²)			
	CBO	ECBO [18]	VPS [19]	MDVC-UVPS [20]
1 (1–2)	1.2404	1.4305	1.3155	1.2575
2 (1–3)	1.3797	1.3941	1.2299	1.3466
3 (1–10)	5.2597	5.5293	5.5506	4.9738
4 (1–11)	1.2658	1.0469	1.3867	1.4025
5(2–3)	17.2255	16.9642	17.4275	17.3802
6 (2–11)	38.2991	35.1892	40.1430	37.9742
7(3–4)	12.2234	12.2171	12.8848	13.0306
8 (3–11)	15.4712	16.7152	15.5413	15.9209
9 (3–12)	11.1577	12.5999	12.2428	11.9419
10 (4–5)	9.4636	9.5118	9.3776	9.1643
11 (4–12)	8.8250	8.9977	8.6684	8.4332
12 (4–13)	9.1021	9.4397	9.1659	9.2375
13 (5–6)	6.8417	6.8864	7.1664	7.2213
14 (5–13)	5.2882	4.2057	5.2170	5.2142
15 (5–14)	6.7702	7.2651	6.5346	6.7961
16 (6–7)	5.1402	6.1693	5.4741	5.2078
17 (6–14)	5.1827	3.9768	3.6545	3.4586
18 (6–15)	7.4781	8.3127	7.6034	7.6407
19 (7–8)	4.5646	4.1451	4.2251	4.3690
20 (7–15)	1.8617	2.4042	1.9717	2.1237
21 (7–16)	4.8797	4.3038	4.5107	4.5774
22 (8–9)	3.5065	3.2539	3.5251	3.4564
23 (8–16)	2.4546	1.8273	1.9255	1.7920
24 (8–17)	4.9128	4.8805	4.7628	4.8264
25 (9–17)	1.2324	1.5276	1.6854	1.7601
Weight (kg)	6182.01	6171.51	6120.01	6115.10
Average optimized weight (kg)	6226.37	6191.50	6158.11	6119.95
Standard deviation on average weight (kg)	60.12	39.08	28.49	16.23

Table 7.2 Natural frequencies (Hz) evaluated at the optimum designs of the 600-bar dome truss problem

Frequency number	Natural frequencies (Hz)			
	CBO	ECBO [18]	VPS [19]	MDVC-UVPS [20]
1	5.000	5.002	5.000	5.000
2	5.000	5.003	5.000	5.000
3	7.000	7.001	7.000	7.000
4	7.000	7.001	7.000	7.000
5	7.001	7.002	7.000	7.000

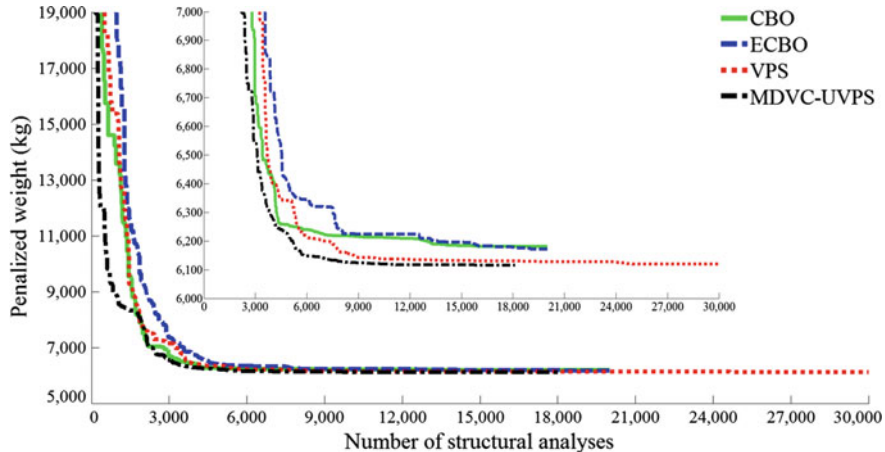


Fig. 7.3 Convergence curves for the 600-bar dome truss problem—constraint case 1

7.3.1.2 Constraint Case 2

The results found by the proposed algorithms are summarized in Table 7.3. MDVC-UVPS achieves the lightest design (i.e., 7338.37 kg). It also has better performance in terms of the average optimized weight and the standard deviation on average weight, which are 7694.13 and 122.67 kg, respectively. The best designs obtained by CBO, ECBO, and VPS are 7464.76, 7463.78, and 7379.63 kg, respectively. The maximum stress ratios for the best designs of CBO, ECBO, VPS, and MDVC-UVPS are 99.99, 98.89, 99.99, and 99.99%, respectively. The required numbers of structural analyses to achieve the best design by CBO, ECBO, VPS, and MDVC-UVPS are 18,520, 16,400, 18,720, and 15,406 analyses, respectively.

7.3.2 A 1180-Bar Dome Truss

For the second example, size optimization of a 1180-bar dome truss structure is considered. The configuration of the structure is depicted in Fig. 7.4. The structure consists of 400 nodes and 1180 elements. A substructure is illustrated in Fig. 7.5 in more detail for nodal numbering. Each of the elements of this substructure is considered as a design variable. Thus, this is a size optimization problem with 59 variables. Table 7.4 summarizes the coordinates of the nodes in Cartesian coordinate system. The elastic modulus is 200 GPa and the material density is 7850 kg/m³ for all elements. The yield stress of steel is taken as 400 MPa. A nonstructural mass of 100 kg is attached to all free nodes. The dome is considered to be subjected to vertical loading at all the unsupported joints for the second constraint case. According to symmetry, only we need to define loading conditions of labeled nodes

Table 7.3 Performance comparison of the 600-bar dome truss problem—constraint case 2

Element number (nodes)	Areas (cm ²)			
	CBO	ECBO	VPS	MDVC-UVPS
1 (1–2)	1.0007	1.1545	1.1552	1.0023
2 (1–3)	2.6144	4.6875	4.5998	4.5959
3 (1–10)	1.0267	1.4021	1.1522	5.368
4 (1–11)	1.0036	1.0025	1.0004	1.0208
5(2–3)	4.5976	4.8782	4.611	4.5967
6 (2–11)	1.1161	2.7684	1.3882	1.3896
7(3–4)	4.752	5.1739	4.752	4.8037
8 (3–11)	4.7657	4.7672	5.0116	4.7688
9 (3–12)	4.6437	1.4847	1.5148	1.4038
10 (4–5)	5.0566	5.7881	5.4851	5.0869
11 (4–12)	5.8028	5.7286	5.5706	5.576
12 (4–13)	8.041	3.8644	3.4961	3.4982
13 (5–6)	6.5194	6.2631	6.0269	6.0143
14 (5–13)	7.588	6.8744	6.8286	7.0211
15 (5–14)	4.688	4.7951	4.686	4.6903
16 (6–7)	7.0441	7.0731	7.0437	7.0399
17 (6–14)	8.463	8.5365	9.257	8.5434
18 (6–15)	5.7627	5.7799	5.8364	5.7635
19 (7–8)	8.5035	8.814	8.5035	8.5032
20 (7–15)	10.9017	10.9549	10.839	10.8387
21 (7–16)	7.7492	7.8738	7.7491	7.7481
22 (8–9)	6.1231	6.2894	6.0047	6.0053
23 (8–16)	13.7034	13.6983	13.6386	13.6388
24 (8–17)	5.4526	5.4853	5.4506	5.4509
25 (9–17)	12.4331	12.5248	12.4329	12.4327
Weight (kg)	7464.76	7463.78	7379.63	7338.37
Average optimized weight (kg)	8093.16	7739.41	7701.80	7694.13
Standard deviation on average weight (kg)	934.45	154.61	487.09	122.67

shown in Fig. 7.5. These loads are $-1000, -2500, -3500, -3500, -3500, -2000, -1000, -100, -500, 0, -2000, -3000, -3500, -3500, -2500, -1500, -100, -200, -500$, and -200 kN, respectively. The allowable minimum and maximum cross-sectional areas of all elements are set to 1×10^{-4} and 100×10^{-4} m², respectively. There are two constraints on the natural frequencies, which are $\omega_1 \geq 7$ and $\omega_3 \geq 9$ Hz. This problem is optimized in three stages by MDVC-UVPS. The numbers of design variables considered in the first and second stages are 8 and 18, respectively. These DVCs contain

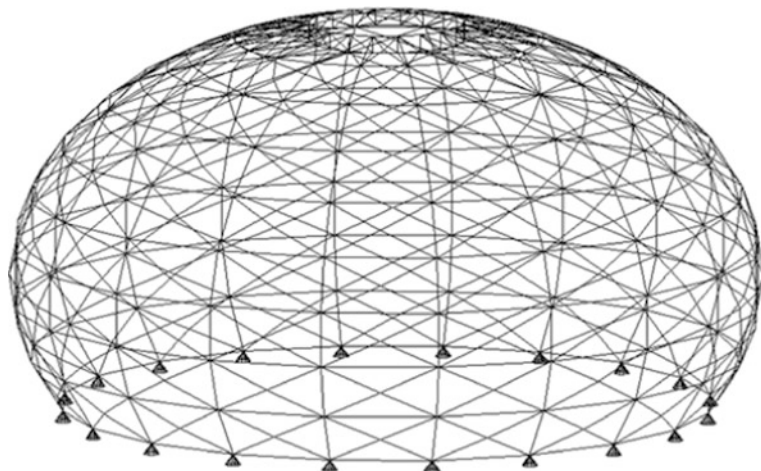


Fig. 7.4 Schematic of the 1180-bar dome truss

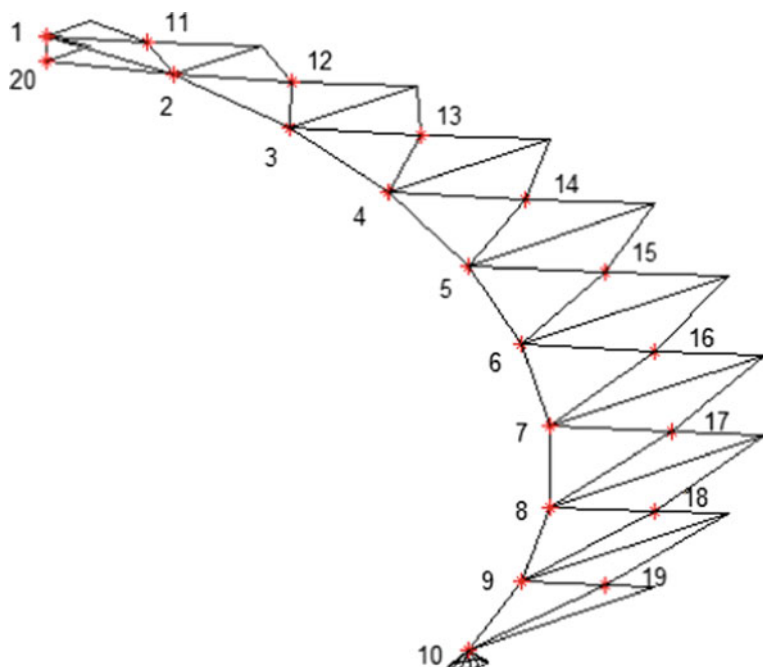


Fig. 7.5 Details of a substructure of the 1180-bar dome truss

Table 7.4 Coordinates of the nodes of the 1180-bar dome truss problem

Node number	Coordinates (x, y, z)	Node number	Coordinates (x, y, z)
1	(3.1181, 0.0, 14.6723)	11	(4.5788, 0.7252, 14.2657)
2	(6.1013, 0.0, 13.7031)	12	(7.4077, 1.1733, 12.9904)
3	(8.8166, 0.0, 12.1354)	13	(9.9130, 1.5701, 11.1476)
4	(11.1476, 0.0, 10.0365)	14	(11.9860, 1.8984, 8.8165)
5	(12.9904, 0.0, 7.5000)	15	(13.5344, 2.1436, 6.1013)
6	(14.2657, 0.0, 4.6358)	16	(14.4917, 2.2953, 3.1180)
7	(14.9179, 0.0, 1.5676)	17	(14.8153, 2.3465, 0.0)
8	(14.9179, 0.0, -1.5677)	18	(14.4917, 2.2953, -3.1181)
9	(14.2656, 0.0, -4.6359)	19	(13.5343, 2.1436, -6.1014)
10	(12.9903, 0.0, -7.5001)	20	(3.1181, 0.0, 13.7031)

Stage 1: [1 6 11 15 19]; [23 27 31 35]; [4 10 14 18 22]; [26 30 34 38 40]; [2 7 41 42 8 12 43 44 13 16 45 46]; [17 20 47 48 21 24 49 50 25 28 51 52]; [29 32 53 54 33 36 55 56 37 39 57 58]; [3 5 9 59].

Stage 2: [1 6 11]; [15 19]; [23 27]; [31 35]; [4 10]; [14 18 22]; [26 30]; [34 38 40]; [2 7 41 42]; [8 12 43 44]; [13 16 45 46]; [17 20 47 48]; [21 24 49 50]; [25 28 51 52]; [29 32 53 54]; [33 36 55 56]; [37 39 57 58]; [3 5 9 59].

7.3.2.1 Constraint Case 1

Table 7.5 presents a comparison between the results of the optimal designs. MDVC-UVPS obtained the lightest design compared to other methods that is 37,451.77 kg. Moreover, the average optimized weight and the standard deviation on average weight of MDVC-UVPS are less than those of all other methods which are 37,545.53 and 64.85 kg. Table 7.6 shows the optimized structural frequencies (Hz) for various methods. None of the frequency constraints were violated. The MDVC-UVPS algorithm requires 19,391 structural analyses to find the optimum solution while CBO, ECBO, and VPS require 19,960, 19,860, and 24,780 structural analyses, respectively. MDVC-UVPS obtained the best design of ECBO after 5873 analyses. The amount of saving in structural analyses at each iteration of the MDVC-UVPS is shown in Fig. 7.6.

7.3.2.2 Constraint Case 2

Table 7.7 lists the optimal designs found by different methods. MDVC-UVPS obtained the lightest design compared to other methods that is 17,909.10 kg. Moreover, the average optimized weight and the standard deviation on average weight of MDVC-UVPS (18,417.05 and 427.44 kg) are less than those of the other methods. The best designs found by the CBO, ECBO, and VPS are 19,869.30,

Table 7.5 Performance comparison for the 1180-bar dome truss problem—constraint case 1

Element number (nodes)	Areas (cm ²)			
	CBO	ECBO [18]	VPS [20]	MDVC-UVPS [20]
1 (1–2)	13.0171	7.6678	6.8743	7.3691
2 (1–11)	10.4346	11.1437	10.0230	9.3399
3 (1–20)	3.0726	1.8520	4.4140	2.7203
4 (1–21)	12.6969	14.5563	13.5515	13.2822
5 (1–40)	3.5654	4.9499	1.8303	3.6758
6 (2–3)	6.5190	6.8095	7.0824	6.1391
7 (2–11)	7.4233	6.6803	6.3960	7.0964
8 (2–12)	6.3471	6.7889	6.5646	6.0208
9 (2–20)	2.3013	1.0630	2.3705	2.1225
10 (2–22)	12.1936	9.1602	13.2621	12.3488
11 (3–4)	7.2877	6.9891	7.0922	6.8578
12 (3–12)	7.0961	6.9881	6.8079	5.7773
13 (3–13)	6.5669	6.9555	6.3815	6.9931
14 (3–23)	7.8257	7.5443	7.3122	7.3355
15 (4–5)	8.6812	9.5431	8.7221	10.5464
16 (4–13)	5.7888	6.9123	6.3680	6.9589
17 (4–14)	21.1342	8.9891	7.3159	8.0977
18 (4–24)	10.0502	6.8926	11.5749	7.7738
19 (5–6)	12.9279	12.6128	14.7985	12.4614
20 (5–14)	9.3212	8.1983	5.5174	7.8154
21 (5–15)	10.1260	11.8358	15.7381	10.2039
22 (5–25)	10.1358	9.7321	8.3419	8.9262
23 (6–7)	15.8585	19.1650	17.5000	16.5275
24 (6–15)	9.9672	10.4682	10.3084	9.0166
25 (6–16)	14.8493	14.1178	15.1958	13.8204
26 (6–26)	11.4909	11.14567	10.9395	11.4021
27 (7–8)	26.2359	23.4125	24.9421	24.2631
28 (7–16)	13.8812	15.5167	13.9614	14.5494
29 (7–17)	18.8857	16.6613	18.4153	17.7753
30 (7–27)	14.0257	15.9631	14.4945	15.4594
31 (8–9)	33.8826	37.0532	36.3529	34.1372
32 (8–17)	25.7142	22.2937	19.6608	19.1254
33 (8–18)	24.8644	22.7409	23.7259	24.1954
34 (8–28)	19.8498	23.5624	22.0297	21.5899
35 (9–10)	53.2630	47.7652	47.3286	49.4717
36 (9–18)	22.7771	22.5066	22.9442	26.2915
37 (9–19)	35.4230	34.6418	30.8229	33.7558
38 (9–29)	57.5480	31.6492	33.1098	29.7608

(continued)

Table 7.5 (continued)

Element number (nodes)	Areas (cm ²)			
	CBO	ECBO [18]	VPS [20]	MDVC-UVPS [20]
39 (10–19)	35.1385	32.7268	32.5526	34.0489
40 (10–30)	10.7300	1.05206	1.7363	1.0024
41 (11–21)	9.2401	11.3681	11.5271	9.0344
42 (11–22)	5.2661	6.5512	8.4571	7.5316
43 (12–22)	6.2415	6.3619	5.4136	6.3726
44 (12–23)	4.4768	5.9296	7.1832	5.7643
45 (13–23)	8.8846	7.8739	5.4066	6.7270
46 (13–24)	7.3710	6.2794	6.2534	6.7021
47 (14–24)	8.2595	7.6206	6.9383	7.8082
48 (14–25)	7.6091	7.2937	10.6872	8.1225
49 (15–25)	11.3030	10.5783	12.8005	10.1777
50 (15–26)	13.8381	10.1173	10.2216	10.1825
51 (16–26)	13.3654	15.1088	11.5330	13.4590
52 (16–27)	13.1836	12.8251	11.6918	13.9788
53 (17–27)	13.5793	17.4375	20.7566	18.1070
54 (17–28)	10.0628	20.1153	18.1341	19.2212
55 (18–28)	24.1197	24.2121	28.2882	23.4359
56 (18–29)	24.2604	23.3175	24.2023	27.6479
57 (19–29)	34.1389	34.6196	48.0180	33.6805
58 (19–30)	38.0340	35.2970	35.6517	35.7035
59 (20–40)	2.6689	8.8569	5.5956	4.7617
Weight (kg)	40,985	37,984.39	38,699.14	37,451.77
Average optimized weight (kg)	42,019.10	38,042.15	38,861.82	37,545.53
Standard deviation on average weight (kg)	655.72	101.43	385.41	64.85

Table 7.6 Natural frequencies (Hz) evaluated at the optimum designs of the 1180-bar dome truss problem

Frequency number	Natural frequencies (Hz)			
	CBO	ECBO [18]	VPS [20]	MDVC-UVPS [20]
1	7.000	7.000	7.000	7.000
2	7.001	7.001	7.001	7.001
3	9.000	9.000	9.000	9.000
4	9.000	9.000	9.000	9.000
5	9.005	9.064	9.177	9.005

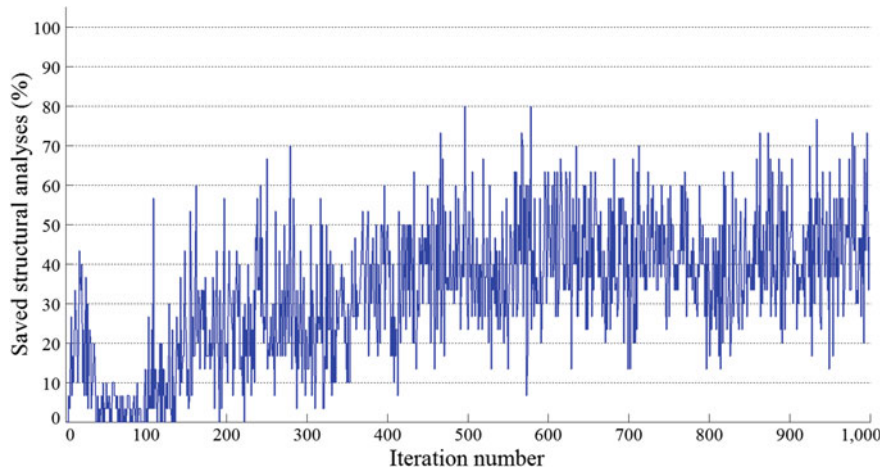


Fig. 7.6 Saving in structural analyses using the MDVC-UVPS algorithm in the 1180-bar dome truss problem—constraint case 1

18,860.43, and 18,903.65 kg, respectively. The maximum stress ratios for the best designs of CBO, ECBO, VPS, and MDVC-UVPS are 81.11, 86.52, 93.50, and 99.99%, respectively. Convergence history diagrams are depicted in Fig. 7.7. MDVC-UVPS requires 14,456 structural analyses to find the optimum solution while CBO, ECBO, and VPS require 18,220, 19,740, and 19,880 structural analyses, respectively.

Table 7.7 Performance comparison of the 1180-bar dome truss problem—constraint case 2

Element number (nodes)	Areas (cm^2)			
	CBO	ECBO	VPS	MDVC-UVPS
1 (1–2)	4.8705	5.9493	5.7015	9.4521
2 (1–11)	7.3783	5.1128	7.2102	3.8492
3 (1–20)	1.2699	1.7992	1.0055	8.1978
4 (1–21)	6.1376	5.4755	3.4166	4.2423
5 (1–40)	3.542	4.6291	3.8978	8.1978
6 (2–3)	6.1148	7.084	5.1114	9.4521
7 (2–11)	5.4713	6.473	5.064	3.8492
8 (2–12)	9.4118	7.1685	5.1467	4.8473
9 (2–20)	9.6458	11.6397	9.7255	8.1978
10 (2–22)	4.7464	6.5289	4.6638	4.2423
11 (3–4)	9.2156	9.4237	9.7013	9.4521
12 (3–12)	6.9436	5.8957	10.1884	4.8473
13 (3–13)	5.1492	5.4008	8.9843	5.5341
14 (3–23)	4.0869	5.4558	4.5727	7.112

(continued)

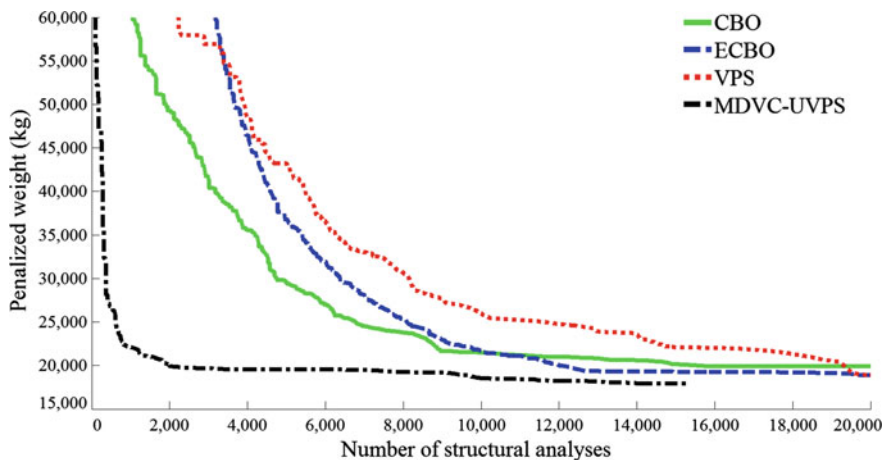
Table 7.7 (continued)

Element number (nodes)	Areas (cm^2)			
	CBO	ECBO	VPS	MDVC-UVPS
15 (4–5)	11.5998	8.9965	11.7971	9.4449
16 (4–13)	8.1323	6.7849	6.6183	5.5341
17 (4–14)	6.194	8.0975	7.0562	7.4661
18 (4–24)	5.8227	6.7986	6.3479	7.112
19 (5–6)	11.8302	10.7667	14.1573	9.4449
20 (5–14)	7.7969	7.5666	8.1737	7.4661
21 (5–15)	8.2957	7.9201	7.4761	7.4775
22 (5–25)	7.5279	7.3118	7.3921	7.112
23 (6–7)	12.7894	11.8195	10.3913	10.9878
24 (6–15)	7.3903	7.4026	7.0689	7.4775
25 (6–16)	8.0166	7.7645	8.2977	7.4749
26 (6–26)	8.5456	8.5533	8.2033	8.7224
27 (7–8)	12.2363	12.0751	11.6556	10.9878
28 (7–16)	8.1607	8.2215	9.6521	7.4749
29 (7–17)	8.6099	4.9116	4.4503	7.5663
30 (7–27)	9.9546	10.417	10.9239	8.7224
31 (8–9)	17.7962	17.8845	11.1662	11.0094
32 (8–17)	9.4484	7.9859	7.7067	7.5663
33 (8–18)	6.1548	5.2099	4.5083	4.1094
34 (8–28)	10.1519	8.8044	8.8879	8.7309
35 (9–10)	12.0321	11.7072	11.3688	11.0094
36 (9–18)	4.0536	5.4377	6.8448	4.1094
37 (9–19)	4.9601	8.8425	4.6168	3.8898
38 (9–29)	8.42	8.5341	8.3597	8.7309
39 (10–19)	9.6607	3.7971	3.7932	3.8898
40 (10–30)	1.0388	1.0996	1.0000	8.7309
41 (11–21)	5.25	5.9873	5.7214	3.8492
42 (11–22)	10.7763	4.4572	4.1908	3.8492
43 (12–22)	13.2206	5.2111	6.1135	4.8473
44 (12–23)	10.7522	10.7124	7.8898	4.8473
45 (13–23)	5.5857	8.5213	5.6613	5.5341
46 (13–24)	8.4136	5.7257	5.6122	5.5341
47 (14–24)	6.1712	6.9778	6.5029	7.4661
48 (14–25)	8.5468	7.2017	10.5263	7.4661
49 (15–25)	9.1846	7.4758	9.4067	7.4775
50 (15–26)	8.6247	8.028	7.2511	7.4775
51 (16–26)	8.0938	8.5583	7.949	7.4749
52 (16–27)	8.7015	8.3535	9.3917	7.4749
53 (17–27)	4.5706	4.6425	7.7928	7.5663

(continued)

Table 7.7 (continued)

Element number (nodes)	Areas (cm^2)			
	CBO	ECBO	VPS	MDVC-UVPS
54 (17–28)	7.623	7.729	7.6062	7.5663
55 (18–28)	4.2279	5.3966	7.1012	4.1094
56 (18–29)	5.8307	5.1474	8.1847	4.1094
57 (19–29)	6.6752	7.3322	7.8282	3.8898
58 (19–30)	5.1712	5.5059	6.0886	3.8898
59 (20–40)	17.8857	2.7226	8.2244	8.1978
Weight (kg)	19,869.30	18,860.43	18,903.65	17,909.10
Average optimized weight (kg)	22,973.72	19,768.86	20,483.73	18,417.05
Standard deviation on average weight (kg)	3793.88	1195.92	1033.38	427.44

**Fig. 7.7** Convergence curves for the 1180-bar dome truss problem—constraint case 2

7.3.3 A 1410-Bar Dome Truss

Figure 7.8 shows the 1410-bar double-layer dome truss structure. The entire structure is composed of 390 nodes and 1410 elements. Figure 7.9 shows a sub-structure in more detail for nodal numbering. Each of the elements of this sub-structure is considered as a design variable. Thus, this is a size optimization problem with 47 variables. Table 7.8 presents the coordinates of the nodes in Cartesian coordinate system. The elastic modulus is 200 GPa and the material density is 7850 kg/m^3 for all elements. The yield stress of steel is taken as 400 MPa. A nonstructural mass of 100 kg is attached to all free nodes. The dome is

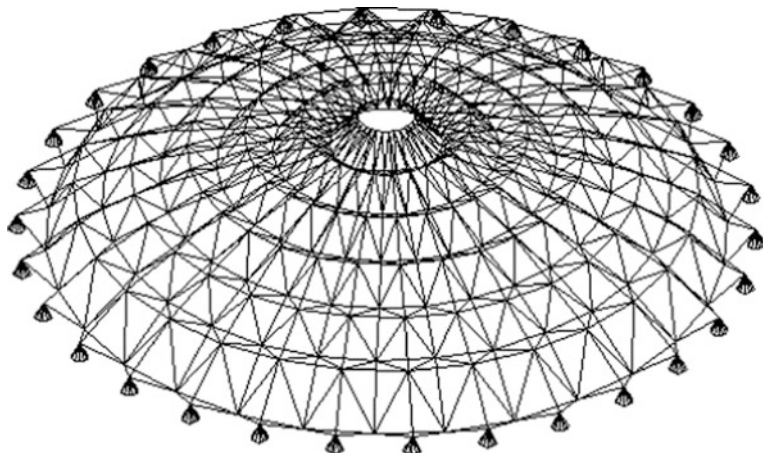


Fig. 7.8 Schematic of the 1410-bar dome truss

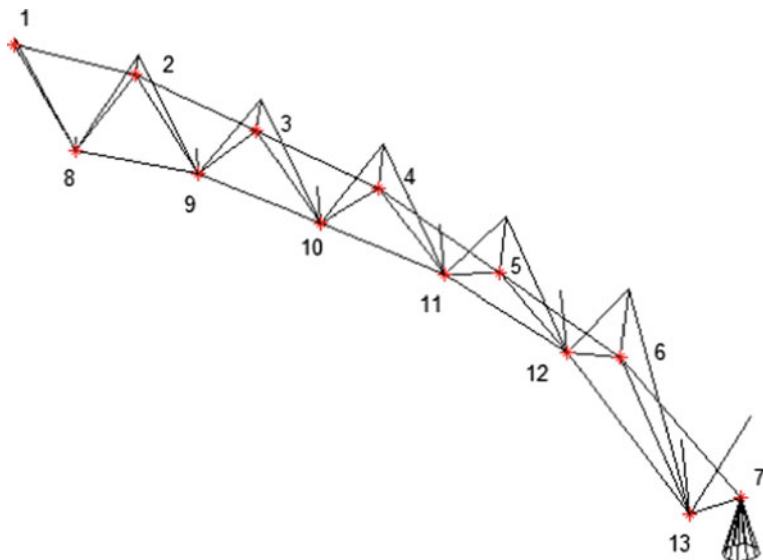


Fig. 7.9 Details of a substructure of the 1410-bar dome truss

considered to be subjected to vertical loading at all the unsupported joints for the second constraint case. According to symmetry, only we need to define loading conditions of labeled nodes shown in Fig. 7.9. These loads are -200 , -600 , -1000 , -1500 , -2000 , -2500 , 0 , -400 , -1000 , -1200 , -1500 , -2000 , and -1000 kN, respectively. The allowable minimum and maximum cross-sectional areas of all elements is set to 1×10^{-4} and $100 \times 10^{-4} \text{ m}^2$, respectively. There are two

Table 7.8 Coordinates of the nodes of the 1410-bar double-layer dome truss problem

Node number	Coordinates (x, y, z)	Node number	Coordinates (x, y, z)
1	(1.0, 0.0, 4.0)	8	(1.989, 0.209, 3.0)
2	(3.0, 0.0, 3.75)	9	(3.978, 0.418, 2.75)
3	(5.0, 0.0, 3.25)	10	(5.967, 0.627, 2.25)
4	(7.0, 0.0, 2.75)	11	(7.956, 0.836, 1.75)
5	(9.0, 0.0, 2.0)	12	(9.945, 1.0453, 1.0)
6	(11.0, 0.0, 1.25)	13	(11.934, 1.2543, -0.5)
7	(13.0, 0.0, 0.0)		

constraints on the natural frequencies, which are $\omega_1 \geq 7$ and $\omega_3 \geq 9$ Hz. Three stages with 10, 20, and 47 variables are considered to optimize this example by MDVC-UVPS. These DVCs contain

Stage 1: [3 7 11 15 19 23]; [1 4 8 12 16 20]; [28 32 36 40 44 47]; [25 29 33 37 41]; [2 26 5 27]; [6 30 9 31]; [10 34 13 35]; [14 38 17 39]; [18 42 21 43]; [22 45 24 46].

Stage 2: [3 7 11]; [15 19 23]; [1 4 8]; [12 16 20]; [28 32]; [36 40 44 47]; [25 29]; [33 37 41]; [2 26]; [5 27]; [6 30]; [9 31]; [10 34]; [13 35]; [14 38]; [17 39]; [18 42]; [21 43]; [22 45]; [24 46].

7.3.3.1 Constraint Case 1

Table 7.9 summarizes the results obtained by CBO, ECBO [18], VPS [20], and MDVC-UVPS [20] methods. MDVC-UVPS has a better performance in terms of the best weight, average optimized weight, and standard deviation on average

Table 7.9 Performance comparison for the 1410-bar dome truss problem—constraint case 1

Element number (nodes)	Areas (cm^2)			
	CBO	ECBO [18]	VPS [20]	MDVC-UVPS [20]
1 (1–2)	1.0073	7.7765	5.6333	5.8499
2 (1–8)	2.5808	6.2173	4.7628	4.5115
3 (1–14)	24.3407	23.9162	37.7385	19.4823
4 (2–3)	6.6750	11.2399	7.4927	8.8480
5 (2–8)	3.8881	2.5775	3.1824	5.0084
6 (2–9)	5.0607	1.8559	1.0193	1.3568
7 (2–15)	78.9781	16.9202	8.9475	17.4331
8 (3–4)	9.2944	13.7947	10.4272	9.1098
9 (3–9)	2.6585	5.4502	4.1398	2.8712
10 (3–10)	3.5399	2.9751	3.1408	3.5473
11 (3–16)	10.2473	13.7811	15.4194	12.3768
12 (4–5)	9.6820	9.3870	8.9931	10.1099

(continued)

Table 7.9 (continued)

Element number (nodes)	Areas (cm^2)			
	CBO	ECBO [18]	VPS [20]	MDVC-UVPS [20]
13 (4–10)	2.4435	2.3499	3.1988	2.5797
14 (4–11)	5.0637	4.9125	7.1565	5.8381
15 (4–17)	12.9434	11.8755	17.8564	13.6402
16 (5–6)	6.9073	8.8668	9.2685	9.9096
17 (5–11)	3.1808	3.6304	3.3221	3.6543
18 (5–12)	5.9622	6.2651	6.1486	6.1529
19 (5–18)	13.3195	15.1030	8.4422	11.2448
20 (6–7)	13.2136	13.1091	12.8578	13.1071
21 (6–12)	5.4405	5.2940	5.8031	5.2361
22 (6–13)	8.4703	5.9929	7.5484	7.0691
23 (6–19)	1.8700	1.0000	1.4805	2.0015
24 (7–13)	5.5203	4.9879	4.5332	4.7178
25 (8–9)	2.4492	3.1780	2.0347	2.6101
26 (8–14)	2.2150	5.9226	5.8589	4.5434
27 (8–15)	3.1193	2.4607	2.4401	4.6174
28 (8–21)	8.7508	7.5710	6.9250	9.6758
29 (9–10)	5.1195	4.8616	3.3875	3.6296
30 (9–15)	3.8508	1.5956	1.5024	1.4891
31 (9–16)	4.4435	4.9084	4.0498	3.4020
32 (9–22)	9.1339	11.6118	11.0886	6.2153
33 (10–11)	5.7811	5.2554	5.4639	5.9308
34 (10–16)	3.4510	2.8687	2.8459	3.2334
35 (10–17)	1.8344	2.3286	2.3136	2.7173
36 (10–23)	2.7952	1.6159	3.4370	1.3932
37 (11–12)	7.2668	6.9795	8.0225	6.5660
38 (11–17)	4.7761	5.3159	5.8009	4.8170
39 (11–18)	3.3394	2.9915	4.4004	3.2626
40 (11–24)	1.0001	1.0018	1.0005	1.0165
41 (12–13)	7.3874	4.1091	7.7222	7.2529
42 (12–18)	7.3114	6.0130	5.2574	5.9226
43 (12–19)	4.8773	5.8695	4.5055	5.3115
44 (12–25)	1.0000	1.0000	1.0005	1.0010
45 (13–19)	7.9928	7.7041	7.9383	7.7499
46 (13–20)	3.4989	3.7600	4.7805	4.7836
47 (13–26)	2.0951	1.0006	1.0054	1.0035
Weight (kg)	11,102.84	10,739.19	10,491.83	10,345.12
Average optimized weight (kg)	12,359.41	10,812.20	10,936.34	10,393.83
Standard deviation on average weight (kg)	251.88	64.91	158.39	39.15

Table 7.10 Natural frequencies (Hz) evaluated at the optimum designs of the 1410-bar dome truss problem

Frequency number	Natural frequencies (Hz)			
	CBO	ECBO [18]	VPS [20]	MDVC-UVPS [20]
1	7.000	7.008	7.001	7.000
2	7.001	7.008	7.002	7.001
3	9.000	9.001	9.000	9.000
4	9.000	9.012	9.000	9.000
5	9.000	9.012	9.000	9.000

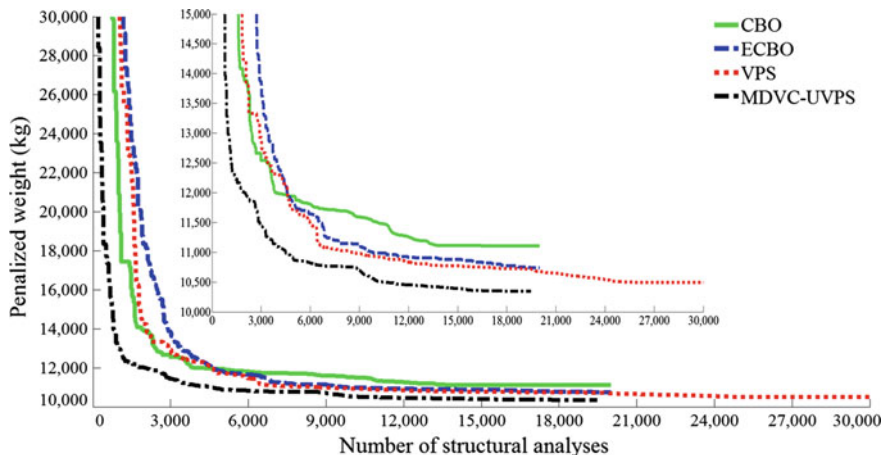


Fig. 7.10 Convergence curves for the 1410-bar dome truss problem—constraint case 1

weight that, respectively, are 10,345.12, 10,393.83, and 39.15 kg, respectively. Table 7.10 reports the natural frequencies of the optimized structures and it is clear that none of the frequency constraints are violated. Convergence histories for VPS and MDVC-UVPS are depicted in Fig. 7.10. The required numbers of structural analyses to achieve the best designs by the CBO, ECBO, VPS, and MDVC-UVPS, respectively, are 19,000, 19,420, 25,700, and 17,750 analyses, respectively. MDVC-UVPS obtained the best design of VPS after 10,697 analyses.

7.3.3.2 Constraint Case 2

Table 7.11 presents the optimum designs obtained by the proposed algorithms. The lightest design (i.e., 7661.64 kg) is achieved by MDVC-UVPS algorithm after 16,308 analyses. The best designs obtained by CBO, ECBO, and VPS are 8413.46, 7860.01, and 7848.68 kg, respectively. These values are found after 18,940,

Table 7.11 Performance comparison of the 1410-bar dome truss problem—constraint Case 2

Element number (nodes)	Areas (cm ²)			
	CBO	ECBO	VPS	MDVC-UVPS
1 (1–2)	5.1214	5.217	4.6048	4.8489
2 (1–8)	2.2479	2.213	1.5208	1.5104
3 (1–14)	1	4.0413	1.4229	4.3939
4 (2–3)	5.6721	5.3523	4.785	4.8489
5 (2–8)	2.5777	2.8635	2.3714	2.3413
6 (2–9)	1.6817	1.8832	2.2803	1.6246
7 (2–15)	1.4126	1.0007	6.0836	4.3939
8 (3–4)	6.8558	6.4681	5.037	4.8489
9 (3–9)	2.1922	1.2068	2.1952	2.1707
10 (3–10)	2.0673	1.738	1.6864	1.6765
11 (3–16)	8.9218	12.5144	2.9786	4.3939
12 (4–5)	6.4513	6.3101	5.8296	7.6688
13 (4–10)	2.5147	1.7218	2.4275	2.4287
14 (4–11)	2.3745	2.4362	4.4668	1.8282
15 (4–17)	4.273	3.5615	3.0016	5.5832
16 (5–6)	6.5994	6.1832	6.1684	7.6688
17 (5–11)	3.3831	2.7977	2.5737	2.5749
18 (5–12)	2.7308	4.1412	4.5709	3.6629
19 (5–18)	8.5163	4.1542	4.2362	5.5832
20 (6–7)	7.834	7.9148	8.7333	7.6688
21 (6–12)	3.6101	5.894	3.3266	3.7234
22 (6–13)	5.0307	3.3083	5.439	3.1638
23 (6–19)	6.127	6.6223	5.8551	5.5832
24 (7–13)	3.8352	3.6804	3.7713	3.64
25 (8–9)	5.3726	4.8207	4.6028	6.1741
26 (8–14)	2.0258	1.5864	1.5129	1.5104
27 (8–15)	5.5215	2.5913	2.3505	2.3413
28 (8–21)	3.6576	1.0843	4.334	4.0242
29 (9–10)	5.638	5.9325	8.0424	6.1741
30 (9–15)	1.7705	3.0351	1.5699	1.6246
31 (9–16)	2.3381	1.2356	2.5573	2.1707
32 (9–22)	3.316	1.708	7.4354	4.0242
33 (10–11)	6.4184	4.8743	4.8246	6.3156
34 (10–16)	5.0152	3.429	1.6796	1.6765
35 (10–17)	2.9268	1.9623	3.3532	2.4287
36 (10–23)	5.7701	2.7079	2.4308	4.8511
37 (11–12)	8.4621	5.0557	5.1426	6.3156
38 (11–17)	1.925	4.1289	1.9981	1.8282
39 (11–18)	3.0442	3.4292	2.5741	2.5749

(continued)

Table 7.11 (continued)

Element number (nodes)	Areas (cm ²)			
	CBO	ECBO	VPS	MDVC-UVPS
40 (11–24)	4.4108	4.9348	3.491	4.8511
41 (12–13)	8.4293	7.3564	6.3216	6.3156
42 (12–18)	2.295	4.4329	3.7521	3.6629
43 (12–19)	4.1246	3.3212	7.627	3.7234
44 (12–25)	5.3458	4.9391	4.8609	4.8511
45 (13–19)	3.199	3.7342	7.1805	3.1638
46 (13–20)	4.0629	4.1154	3.7848	3.64
47 (13–26)	3.6865	5.0799	3.7592	4.8511
Weight (kg)	8413.46	7860.01	7848.68	7661.64
Average optimized weight (kg)	9932.11	8250.20	8959.27	8106.52
Standard deviation on average weight (kg)	1726.69	409.09	1277.34	244.08

19,840, and 19,860 analyses. MDVC-UVPS obtained values for average optimized weight and standard deviation on average weight which are equal to 8106.52 and 244.08 kg, respectively. The maximum values of the stress ratio for CBO, ECBO, VPS, and MDVC-UVPS are 96.96, 99.41, 99.53, and 99.99%, respectively.

7.4 Concluding Remarks

Structural optimization with multiple natural frequency constraints is a highly nonlinear and non-convex dynamic optimization problem since weight reduction conflicts with the frequency constraints. Moreover, determining the optimum design of large-scale structures is known as one of the difficult and complex optimization problems. In this chapter, the performances of CBO, ECBO, VPS, and MDVC-UVPS algorithms were compared through three dome truss structures with dynamic frequency constraints. Moreover, all the examples are designed based on strength, stability, and displacement constraints to evaluate the performance of the algorithms in another type of optimization problem. MDVC-UVPS converged to better designs in all of the test problems. Also, the average weights and standard deviations found by this method in the independent optimization runs were lower in all of the benchmark examples indicating that the search reliability of the proposed method is superior. Apart from these characteristics, MDVC-UVPS needs fewer structural analyses to obtain the best design of other algorithms. Comparison of the convergence curves showed that the intermediate designs found by this algorithm were usually better than those found by CBO, ECBO, and VPS.

References

1. Lan TT (2005) Space frame structures. *Handbook of structural Engineering*. CRC Press, Boca Raton, FL, pp 24–31
2. Bellagamba L, Yang TY (1981) Minimum mass truss structures with constraints on fundamental natural frequency. *AIAA J* 19:1452–1458
3. Kaveh A, Zolghadr A (2016) Optimal design and analysis of large-scale domes with frequency constraints. *Smart Struct Syst* 18(4):733–754
4. Lin JH, Chen WY, Yu YS (1982) Structural optimization on geometrical configuration and element sizing with static and dynamic constraints. *Comput Struct* 15:507–515
5. Konzelman CJ (1986) Dual methods and approximation concepts for structural optimization. M.Sc. Thesis, Department of Mechanical Engineering, University of Toronto, Canada
6. Grandhi RV, Venkayya VB (1988) Structural optimization with frequency constraints. *AIAA J* 26:858–866
7. Wang D, Zha W, Jiang J (2004) Truss optimization on shape and sizing with frequency constraints. *AIAA J* 42:622–630
8. Sedaghati R (2005) Benchmark case studies in structural design optimization using the force method. *Int J Solids Struct* 42:5848–5871
9. Lingyun W, Mei Z, Guangming W, Guang M (2005) Truss optimization on shape and sizing with frequency constraints based on genetic algorithm. *Comput Mech* 35:361–368
10. Gomes HM (2011) Truss optimization with dynamic constraints using a particle swarm algorithm. *Expert Syst Appl* 38:957–968
11. Kaveh A, Zolghadr A (2012) Truss optimization with natural frequency constraints using a hybridized CSS-BBBC algorithm with trap recognition capability. *Comput Struct* 102–103:14–27
12. Miguel LFF, Fadel Miguel LF (2012) Shape and size optimization of truss structures considering dynamic constraints through modern meta-heuristic algorithms. *Expert Syst Appl* 39:9458–9467
13. Zuo W, Bai J, Li B (2014) A hybrid OC–GA approach for fast and global truss optimization with frequency constraints. *Appl Soft Comput* 14:528–535
14. Kaveh A, Javadi SM (2014) Shape and size optimization of trusses with multiple frequency constraints using harmony search and ray optimizer for enhancing the particle swarm optimization algorithm. *Acta Mech* 225:1595–1605
15. Kaveh A, Ilchi Ghazaan M (2015) Hybridized optimization algorithms for design of trusses with multiple natural frequency constraints. *Adv Eng Softw* 79:137–147
16. Hosseini zadeh Y, Taghizadieh N, Jalili S (2016) Hybridizing electromagnetism-like mechanism algorithm with migration strategy for layout and size optimization of truss structures with frequency constraints. *Neural Comput Appl* 27(4):953–971
17. American Institute of Steel Construction (AISC) (1989) *Manual of steel construction: allowable stress design*, Chicago, USA
18. Kaveh A, Ilchi Ghazaan M (2017) Optimal design of dome truss structures with dynamic frequency constraints. *Struct Multidiscip Optim* 53(3):605–621
19. Kaveh A, Ilchi Ghazaan M (2016) Vibrating particles system algorithm for truss optimization with multiple natural frequency constraints. *Acta Mech* 228(1):307–322. (Published online, 1–16)
20. Kaveh A, Ilchi Ghazaan M (2018) A new hybrid meta-heuristic algorithm for optimal design of large-scale dome structures. *Eng Optimiz* 50(2):235–252

Chapter 8

Optimal Design of Steel Lattice Transmission Line Towers



8.1 Introduction

Lattice towers are used for power lines of all voltages and are the most common type for high-voltage transmission lines. The design optimization of these structures has always been a difficult task due to a large number of design variables. Some studies have already been performed in the context of optimization of transmission line tower structures. For instance, Rao [1] utilized a derivative-free nonlinear optimization technique for minimum weight design of high-voltage transmission line towers under a set of control parameters, including geometrical parameters as well as tensions in conductors and ground-wires. Kaveh et al. [2] employed a migration genetic algorithm for optimization of transmission towers and they trained neural networks as analyzers to take part of the computational load. Paris et al. [3] studied the shape optimization of a transmission line tower, subjected to multiple load cases and code constraints. Guo and Li [4] presented an adaptive genetic algorithm for different optimization models of steel transmission towers considering size, layout, and topology design variables. Chunming et al. [5] utilized a genetic algorithm for optimization of a transmission tower, where cross-sectional areas and material types of the members were selected as design variables. Tort et al. [6] integrated the simulated annealing optimization algorithm into the commercial PLS-TOWER software to optimize steel lattice towers for minimum weight using both size and layout design variables.

In this chapter, the efficiency of Colliding Bodies Optimization (CBO) [7], Enhanced Colliding Bodies Optimization (ECBO) [8], Vibrating Particles System (VPS) [9], and a hybrid algorithm called MDVC-UVPS [10] are investigated in optimum design of three latticed steel towers. The procedure considers discrete values of cross-sectional areas.

8.2 Optimal Design of Transmission Line Towers

For the sizing optimization of transmission line towers, the cross-section areas of truss bars are often considered as discrete design variables; therefore, all of them are selected from a list of discrete cross sections based on production standards. The optimization problem aims to minimize the weight of the structure while satisfying strength and serviceability requirements.

Size optimization of a transmission line tower with its members being collected in ng design groups can be formulated as follows:

$$\begin{aligned} \text{Find} \quad & \{X\} = [x_1, x_2, \dots, x_{ng}] \\ \text{to minimize} \quad & W(\{X\}) = \sum_{i=1}^{ng} x_i \sum_{j=1}^{\text{nm}(i)} \rho_j L_j \\ \text{subjected to:} \quad & \begin{cases} g_j(\{X\}) \leq 0, \quad j = 1, 2, \dots, nc \\ x_{i\min} \leq x_i \leq x_{i\max} \end{cases} \end{aligned} \quad (8.1)$$

where $\{X\}$ is the vector containing the design variables; $W(\{X\})$ presents the weight of the structure; $\text{nm}(i)$ is the number of members for the i th group; ρ_j and L_j denote the material density and the length of the j th member, respectively. $x_{i\min}$ and $x_{i\max}$ are the lower and upper bounds of the design variable x_i , respectively. $g_j(\{X\})$ denotes the j th design constraint; and nc is the number of constraints.

For constraint handling, a penalty approach is utilized. For this purpose, the objective function (Eq. 8.1) is redefined as follows:

$$P(\{X\}) = (1 + \varepsilon_1 v)^{\varepsilon_2} \times W(\{X\}) \quad (8.2)$$

where $P(\{X\})$ is the penalized cost function or the objective function to be minimized and v denotes the sum of the violations of the design constraints. Here, ε_1 is set to unity and ε_2 is calculated by

$$\varepsilon_2 = 1.5 + 1.5 \times \frac{\text{iter}}{\text{iter}_{\max}} \quad (8.3)$$

where iter is the current iteration number and iter_{\max} is the total number of iterations of the optimization process.

8.3 Design Problems

The following three benchmark structural examples are considered in this section:

- A 47-bar power transmission tower
- A 160-bar power transmission tower
- A 244-bar power transmission tower

The design variables are the cross-sectional areas of the bar element and in all problems, solution candidates are allowed to select discrete values from a permissible list of cross sections (real numbers are rounded to the nearest integer in each iteration). Each example has been solved thirty times independently and a maximum of 1000 iterations is considered as the termination condition. A population of 20 particles is considered for each algorithm and the other algorithm parameters are set similar to the values proposed in [8–10]. The optimization algorithms are coded in MATLAB and the structures are analyzed using the direct stiffness method by our own codes.

8.3.1 A 47-Bar Power Transmission Tower

The first design example demonstrated in Fig. 8.1 has 47 members and 22 nodes. The cross-sectional areas of the members were categorized into 27 groups, as follows: (1) $A_1 = A_3$, (2) $A_2 = A_4$, (3) $A_5 = A_6$, (4) A_7 , (5) $A_8 = A_9$, (6) A_{10} , (7) $A_{11} = A_{12}$, (8) $A_{13} = A_{14}$, (9) $A_{15} = A_{16}$, (10) $A_{17} = A_{18}$, (11) $A_{19} = A_{20}$, (12) $A_{21} = A_{22}$, (13) $A_{23} = A_{24}$, (14) $A_{25} = A_{26}$, (15) A_{27} , (16) A_{28} , (17) $A_{29} = A_{30}$, (18) $A_{31} = A_{32}$, (19) A_{33} , (20) $A_{34} = A_{35}$, (21) $A_{36} = A_{37}$, (22) A_{38} , (23) $A_{39} = A_{40}$, (24) $A_{41} = A_{42}$, (25) A_{43} , (26) $A_{44} = A_{45}$, and (27) $A_{46} = A_{47}$. The cross-sectional areas were chosen from the 64 discrete values listed in Table 8.1. The material of the members has a Young's modulus of 206.842 kN/mm² (30,000 ksi) and a density of 8303.97 kg/m³ (0.3 lb/in³). The nodes of structure are subjected to a combination of three loading cases: (1) 6.0 kips acting in the positive x -direction and 14.0 kips acting in the negative y -direction at nodes 17 and 22, (2) 6.0 kips acting in the positive x -direction and 14.0 kips acting in the negative y -direction at node 17, and (3) 6.0 kips acting in the positive x -direction and 14.0 kips acting in the negative y -direction at node 22. The first loading case corresponds to the load applied by the two power lines to the tower at an angle, while the second and third loading cases occur when one of the two lines snaps.

Both stress and buckling constraints should be satisfied for all of the members of the tower. Allowable tensile and compressive stresses are taken as 137.895 MPa (20 ksi) and 103.421 MPa (15.0 ksi), respectively. Moreover, the Euler buckling compressive stress for a member with a cross-sectional area of A_i is calculated as follows:

$$\sigma_i^{cr} = \frac{-KEA_i}{L_i^2} \quad i = 1, 2, 3, \dots, 47 \quad (8.4)$$

where K is a constant parameter that should be selected based on the type of the cross-sectional geometry; E is the Young's modulus of the material; and L_i is the length of member i . The buckling constant K is assumed as 3.96 [11].

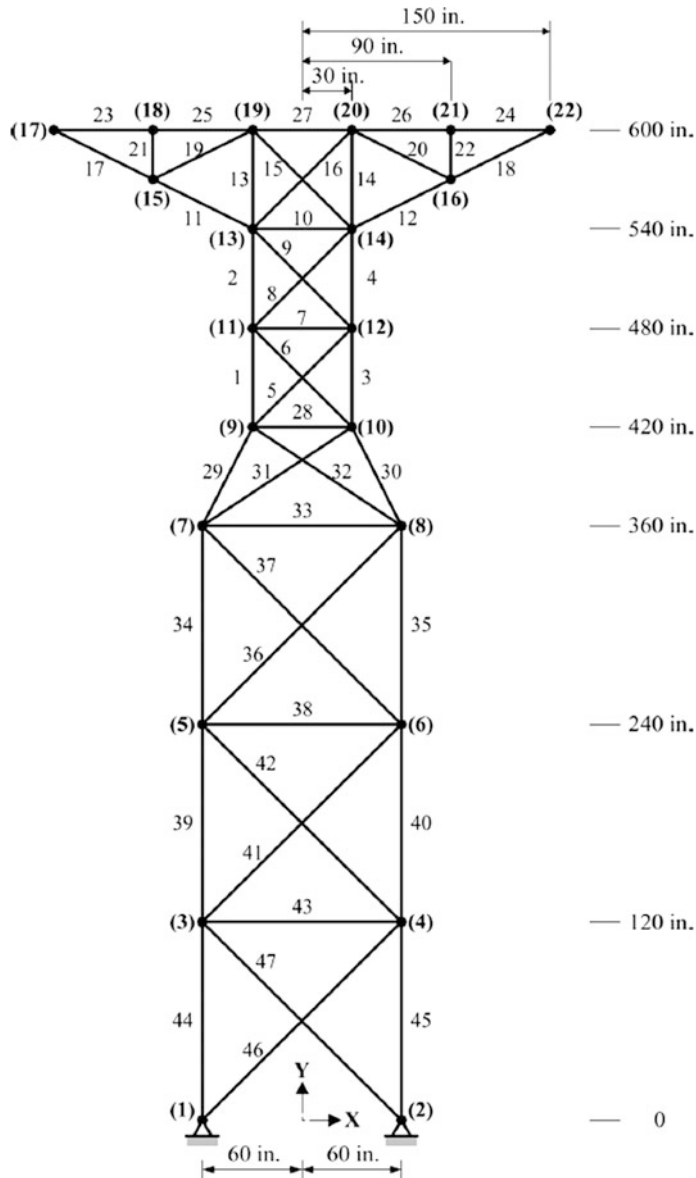


Fig. 8.1 Schematic of the 47-bar power transmission tower

Table 8.2 shows the optimum designs found by different algorithms. The lightest design (i.e., 2374.09 lb) is achieved by MDVC-UVPS algorithm after 4867 analyses. The weights of the best designs obtained by CBO, ECBO, and VPS are 2386.44, 2375.35, and 2374.81 lb, respectively. These values are found after 9760,

Table 8.1 List of available cross-sectional areas for the 47-bar power transmission tower problem

No.	Area (mm ²)	Area (in. ²)	No.	Area (mm ²)	Area (in. ²)	No.	Area (mm ²)	Area (in. ²)	No.	Area (mm ²)	Area (in. ²)
1	71,6130	0.1110	17	1008,3850	1.5630	33	2477,4140	3.8400	49	7419,43	11.5001
2	90,9680	0.1410	18	1045,1590	1.6200	34	2496,7690	3.8700	50	8709,66	13.5000
3	126,4510	0.1960	19	1161,2880	1.8000	35	2503,2210	3.8800	51	8967,724	13.9000
4	161,2900	0.2500	20	1283,8680	1.9900	36	2696,7690	4.1800	52	9161,272	14.2000
5	198,0640	0.3070	21	1374,1910	2.1300	37	2722,5750	4.2200	53	9999,98	15.5000
6	252,2580	0.3910	22	1535,4810	2.3800	38	2896,7680	4.4900	54	10,322,56	16.0000
7	285,1610	0.4420	23	1690,3190	2.6200	39	2961,2480	4.5899	55	10,903,2	16.9000
8	363,2250	0.5630	24	1696,7710	2.6300	40	3096,7680	4.8000	56	12,129,01	18.8000
9	388,3860	0.6020	25	1858,0610	2.8800	41	3206,4450	4.9700	57	12,838,68	19.9000
10	494,1930	0.7660	26	1890,3190	2.9300	42	3303,2190	5.1200	58	14,193,52	22.0000
11	506,4510	0.7850	27	1993,5440	3.0900	43	3703,2180	5.7400	59	14,774,16	22.9000
12	641,2890	0.9940	28	729,0310	1.1300	44	4658,0550	7.2200	60	15,806,42	24.5000
13	645,1600	1.0000	29	2180,6410	3,3800	45	5141,9250	7.9700	61	17,096,74	26.5000
14	792,2560	1.2280	30	2238,7050	3.4700	46	5503,2150	8.5300	62	18,064,48	28.0000
15	816,7730	1.2660	31	2290,3180	3,5500	47	5999,9880	9.3000	63	19,354,8	30.0000
16	939,9980	1,4570	32	2341,9310	3,6300	48	6999,9860	10.8500	64	21,612,86	33.5000

Table 8.2 Performance comparison for the 47-bar power transmission tower problem

Design variable	Areas (in. ²)			
	CBO	ECBO	VPS	MDVC-UVPS
1	3.84	3.84	3.84	3.84
2	3.38	3.38	3.38	3.38
3	0.785	0.766	0.766	0.766
4	0.196	0.111	0.111	0.111
5	0.994	0.785	0.785	0.785
6	1.8	1.99	1.99	1.99
7	2.13	2.13	2.13	2.13
8	1.228	1.228	1.228	1.228
9	1.563	1.563	1.563	1.563
10	2.13	2.13	2.13	2.13
11	0.111	0.111	0.111	0.111
12	0.111	0.141	0.111	0.111
13	1.8	1.8	1.8	1.8
14	1.8	1.8	1.8	1.8
15	1.563	1.457	1.457	1.457
16	0.442	0.442	0.442	0.563
17	3.63	3.63	3.63	3.63
18	1.457	1.457	1.457	1.457
19	0.307	0.307	0.307	0.25
20	3.09	3.09	3.09	3.09
21	1.266	1.266	1.266	1.228
22	0.307	0.307	0.307	0.391
23	3.84	3.84	3.84	3.84
24	1.563	1.563	1.563	1.563
25	0.111	0.111	0.111	0.111
26	4.59	4.59	4.59	4.59
27	1.457	1.457	1.457	1.457
Weight (lb)	2386.44	2375.35	2374.81	2374.09
Average optimized weight (lb)	2462.76	2415.51	2415.07	2413.46
Standard deviation on average weight (lb)	44.79	41.01	35.65	38.21

$$1 \text{ in.}^2 = 6.4516 \text{ cm}^2$$

16,240, and 15,540 analyses. The average optimized weight and standard deviation on average weight achieved by MDVC-UVPS are 2413.46 and 38.21 lb, respectively. Figure 8.2 shows the convergence curves of the best results found by CBO, ECBO, VPS, and MDVC-UVPS.

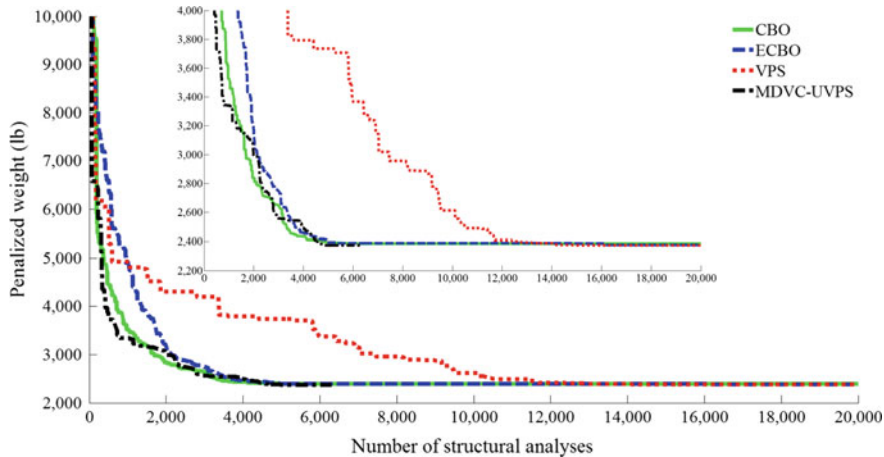


Fig. 8.2 Convergence curves for the 47-bar power transmission tower problem

8.3.2 A 160-Bar Power Transmission Tower

The second design example is the 160-bar tower structure shown in Fig. 8.3. The members of the structure are categorized into 38 design groups. The geometrical information including member's connectivity, design groups, and coordinates of nodes can be found in [12]. The material of the members has a Young's modulus of 2.047×10^6 kgf/cm² and a density of 7850 kg/m³. This tower is subjected to the combination of eight loading conditions as listed in Table 8.3. Moreover, the design constraints consist of buckling stresses of the structural members. For a member under compressive force, the buckling stress can be calculated as follows:

For $kl/r \leq 120$

$$\sigma_{\text{all}} = 1300 - \frac{(kl/r)^2}{24} \quad (8.5)$$

and if $kl/r > 120$, then

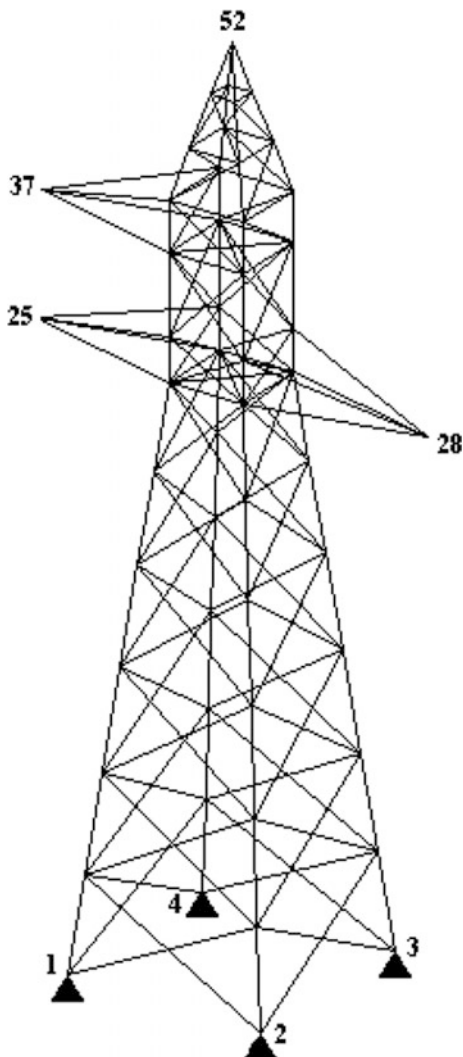
$$\sigma_{\text{all}} = 1300 - \frac{(kl/r)^2}{24} \quad (8.6)$$

where k is effective length factor, r is radius of gyration, and l is length of member. For all truss members, k is equal to unity.

For this design example, the available 42 sections and their radius of gyrations are as follows:

$D = \{1.84, 2.26, 2.66, 3.07, 3.47, 3.88, 4.79, 5.27, 5.75, 6.25, 6.84, 7.44, 8.06, 8.66, 9.40, 10.47, 11.38, 12.21, 13.79, 15.39, 17.03, 19.03, 21.12, 23.20, 25.12, 27.50, 29.88, 32.76, 33.90, 34.77, 39.16, 43.00, 45.65, 46.94, 51.00, 52.10, 61.82, 61.90, 68.30, 76.38, 90.60, 94.13\}$ (cm²).

Fig. 8.3 Schematic of the 160-bar bar power transmission tower



$$r = \{0.47, 0.57, 0.67, 0.77, 0.87, 0.97, 0.97, 1.06, 1.16, 1.26, 1.15, 1.26, 1.36, 1.46, 1.35, 1.36, 1.45, 1.55, 1.75, 1.95, 1.74, 1.94, 2.16, 2.36, 2.57, 2.35, 2.56, 2.14, 2.33, 2.97, 2.54, 2.93, 2.94, 2.94, 2.92, 3.54, 3.96, 3.52, 3.51, 3.93, 3.92, 3.92\} \text{ (cm).}$$

The optimal designs found by different methods are presented in Table 8.4. The weight of the best result obtained by MDVC-UVPS is 1336.71 kg that is the best among the compared methods. The average optimized weight of this method is 1364.56 kg, which is less than those of all other methods. Comparison of the convergence rates of CBO, ECBO, VPS, and MDVC-UVPS is illustrated in Fig. 8.4. MDVC-UVPS requires 4518 structural analyses to find its optimum

Table 8.3 Loading conditions for the 160-bar power transmission tower problem

Condition	Node	F _x	F _y	F _z	Condition	Node	F _x	F _y	F _z
1	52	-868	0	-491	5	52	-917	0	-491
	37	-996	0	-546		37	-951	0	-546
	25	-1091	0	-546		25	-1015	0	-546
	28	-1091	0	-546		28	-636	0	-428
2	52	-493	1245	-363	6	52	-917	1259	-491
	37	-996	0	-546		37	-572	0	-428
	25	-1091	0	-546		25	-1015	1303	-546
	28	-1091	0	-546		28	-1015	0	-546
3	52	-917	0	-491	7	52	-917	0	-491
	37	-951	0	-546		37	-951	0	-546
	25	-1015	0	-546		25	-1015	0	-546
	28	-1015	0	-546		28	-636	1303	-428
4	52	-917	0	-546	8	52	-498	1460	-363
	37	-572	1259	-428		37	-951	0	-546
	25	-1015	0	-546		25	-1015	0	-546
	28	-1015	0	-546		28	-1015	0	-546

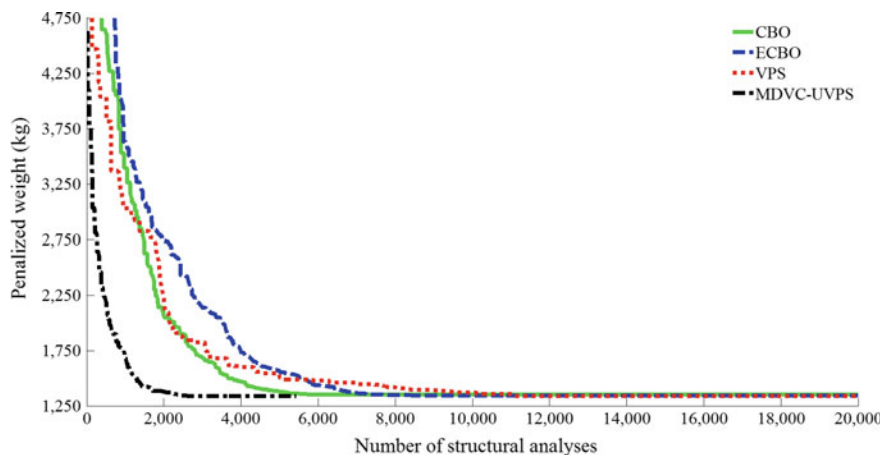
Table 8.4 Performance comparison for the 160-bar power transmission tower problem

Design variable	Areas (cm ²)			
	CBO	ECBO	VPS	MDVC-UVPS
1	19.03	19.03	19.03	19.03
2	5.27	5.27	5.27	5.27
3	19.03	19.03	19.03	19.03
4	5.27	5.27	5.27	5.27
5	19.03	19.03	19.03	19.03
6	5.75	5.75	5.75	5.75
7	15.39	15.39	15.39	15.39
8	5.75	5.75	5.75	5.75
9	13.79	13.79	13.79	13.79
10	5.75	5.75	5.75	5.75
11	5.75	5.75	5.75	5.75
12	12.21	12.21	13.79	12.21
13	6.25	6.25	6.25	6.25
14	5.75	5.75	5.75	5.75
15	4.79	3.88	2.66	3.88
16	6.25	7.44	7.44	7.44
17	4.79	1.84	1.84	1.84
18	8.66	8.66	8.66	8.66
19	2.66	2.66	2.66	2.66
20	3.07	3.07	3.07	3.07

(continued)

Table 8.4 (continued)

Design variable	Areas (cm^2)			
	CBO	ECBO	VPS	MDVC-UVPS
21	2.66	2.66	2.66	2.66
22	8.06	8.06	8.06	8.06
23	5.75	5.27	5.27	5.75
24	6.25	7.44	6.25	6.25
25	6.25	5.75	5.75	5.75
26	1.84	1.84	1.84	1.84
27	4.79	4.79	4.79	5.27
28	2.66	2.66	2.66	2.66
29	3.47	3.47	3.47	3.47
30	1.84	1.84	1.84	1.84
31	2.26	2.26	2.26	2.26
32	3.88	3.88	3.88	3.88
33	1.84	1.84	1.84	1.84
34	1.84	1.84	1.84	1.84
35	3.88	3.88	3.88	3.88
36	1.84	1.84	1.84	1.84
37	1.84	1.84	1.84	1.84
38	3.88	3.88	3.88	3.88
Weight (kg)	1350.37	1339.17	1337.44	1336.71
Average optimized weight (kg)	1403.97	13,776.26	1375.51	1364.56
Standard deviation on average weight (kg)	215.11	109.83	125.43	73.46

**Fig. 8.4** Convergence curves for the 160-bar power transmission tower problem

solution while CBO, ECBO, and VPS require 5820, 11,420, and 11,080 structural analyses, respectively.

8.3.3 A 244-Bar Power Transmission Tower

The 244-bar transmission tower shown in Fig. 8.5 is studied as the final design problem to demonstrate the efficiency of the compared algorithms. Members of the structure are categorized into 26 groups as given by Saka [13]. The cross-sectional areas were chosen from the 45 discrete values listed in Table 8.5. The modulus of elasticity and yield stress of steel are assumed to be 210 kN/mm^2 and 233.3 N/mm^2 ,

Fig. 8.5 Schematic of the 244-bar bar power transmission tower

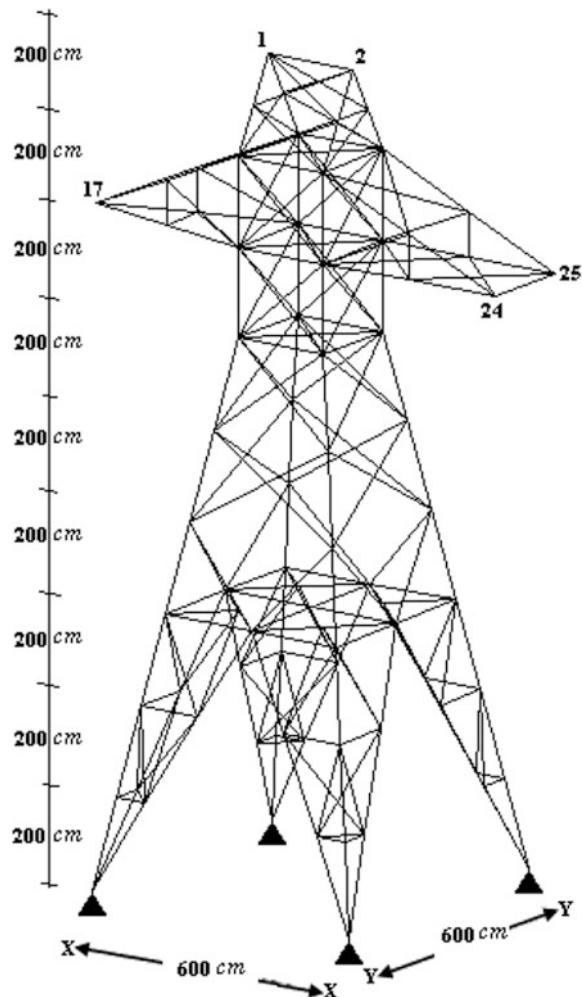


Table 8.5 List of available cross sections for the 244-bar power transmission tower problem

No.	Section	A_{in}^2 (mm ²)	r in. (mm)	Num.	Section	A_{in}^2 (mm ²)	r in. (mm)
1	L 6 × 6 × 1	11.0 (7096.76)	1.17 (29.72)	24	L 3 1/2 × 3 1/2 × 1/2	3.25 (2096.77)	0.683 (17.35)
2	L 6 × 6 × 7/8	9.73 (6277.41)	1.17 (29.72)	25	L 3 1/2 × 3 1/2 × 7/16	2.87 (1851.61)	0.684 (17.37)
3	L 6 × 6 × 3/4	8.44 (5445.15)	1.17 (29.72)	26	L 3 1/2 × 3 1/2 × 3/8	2.48 (1600.00)	0.687 (17.45)
4	L 6 × 6 × 5/8	7.11 (4587.09)	1.18 (29.97)	27	L 3 1/2 × 3 1/2 × 5/16	2.09 (1348.38)	0.690 (17.53)
5	L 6 × 6 × 9/16	6.43 (4148.38)	1.18 (29.97)	28	L 3 1/2 × 3 1/2 × 1/4	1.69 (1090.32)	0.694 (17.63)
6	L 6 × 6 × 1/2	5.75 (3709.67)	1.18 (29.97)	29	L 3 × 3 × 1/2	2.75 (1774.19)	0.584 (14.83)
7	L 6 × 6 × 7/16	5.06 (3264.51)	1.19 (30.23)	30	L 3 × 3 × 7/16	2.43 (1567.74)	0.585 (14.86)
8	L 6 × 6 × 3/8	4.36 (2812.90)	1.19 (30.23)	31	L 3 × 3 × 3/8	2.11 (1361.29)	0.587 (14.91)
9	L 6 × 6 × 5/16	3.65 (2354.83)	1.20 (30.48)	32	L 3 × 3 × 5/16	1.78 (1148.38)	0.589 (14.96)
10	L 5 × 5 × 7/8	7.98 (5148.38)	0.973 (24.71)	33	L 3 × 3 × 1/4	1.44 (929.03)	0.592 (15.04)
11	L 5 × 5 × 3/4	6.94 (4477.41)	0.975 (24.77)	34	L 3 × 3 × 3/16	1.09 (703.22)	0.596 (15.14)
12	L 5 × 5 × 5/8	5.86 (3780.64)	0.978 (24.84)	35	L 2 1/2 × 2 1/2 × 1/2	2.25 (1451.61)	0.487 (12.37)
13	L 5 × 5 × 1/2	4.75 (3064.51)	0.983 (24.97)	36	L 2 1/2 × 2 1/2 × 3/8	1.73 (1116.13)	0.487 (12.37)
14	L 5 × 5 × 7/16	4.18 (2696.77)	0.986 (25.04)	37	L 2 1/2 × 2 1/2 × 5/16	1.46 (94.33)	0.489 (12.42)
15	L 5 × 5 × 3/8	3.61 (2339.03)	0.990 (25.15)	38	L 2 1/2 × 2 1/2 × 1/4	1.19 (76.74)	0.491 (12.47)
16	L 5 × 5 × 5/16	3.03 (1954.83)	0.944 (25.25)	39	L 2 1/2 × 2 1/2 × 3/16	0.902 (581.93)	0.495 (12.57)
17	L 4 × 4 × 3/4	5.44 (3509.67)	0.778 (19.76)	40	L 2 × 2 × 3/8	1.36 (87.42)	0.389 (9.88)
18	L 4 × 4 × 5/8	4.61 (2974.19)	0.779 (19.79)	41	L 2 × 2 × 5/16	1.15 (74.93)	0.390 (9.91)
19	L 4 × 4 × 1/2	3.75 (2419.35)	0.782 (19.86)	42	L 2 × 2 × 1/4	0.938 (605.16)	0.391 (9.93)
20	L 4 × 4 × 7/16	3.31 (2135.48)	0.785 (19.94)	43	L 2 × 2 × 3/16	0.715 (461.29)	0.394 (10.00)
21	L 4 × 4 × 3/8	2.86 (1845.16)	0.788 (20.02)	44	L 2 × 2 × 1/8	0.484 (312.26)	0.398 (10.11)
22	L 4 × 4 × 5/16	2.40 (1548.38)	0.791 (20.09)	45	L 1 1/4 × 1 1/4 × 3/16	0.434 (280.00)	0.244 (6.198)
23	L 4 × 4 × 1/4	1.94 (1251.61)	0.795 (20.19)				

Table 8.6 The load cases and displacement bounds for the 244-bar bar power transmission tower problem

Loading conditions	Joint number	Loads (kN)		Displacement limitations (mm)	
		X	Z	X	Z
1	1	10	-30	45	15
	2	10	-30	45	15
	17	35	-90	30	15
	24	175	-45	30	15
	25	175	-45	30	15
2	1	-	-360	45	15
	2	-	-360	45	15
	17	-	-180	30	15
	24	-	-90	30	15
	25	-	-90	30	15

respectively [14]. The load cases considered and the bounds imposed on the displacements are shown in Table 8.6. Values of the allowable tensile and compressive stresses are calculated based on ASD-AISC code [15]. Moreover, as per the recommendation of ASD-AISC, the maximum slenderness ratios are set to 200 and 300 for compression and tension members, respectively.

Table 8.7 shows the comparison of the results of different algorithms. MDVC-UVPS algorithm yields the least volume design for this example, which is 0.755011 m^3 . The other designs are 0.813555 m^3 by CBO, 0.768159 m^3 by ECBO, and 0.764982 m^3 by VPS. The best design of the hybrid method has been achieved after 6665 analyses. CBO, ECBO, and VPS require 30,000, 4020, 9260, and 19,480 structural analyses to find their optimum solutions, respectively. Figure 8.6 shows the convergence curves of the best results found by CBO, ECBO, VPS, and MDVC-UVPS.

8.4 Concluding Remarks

In this chapter, size optimization of transmission line towers under multiple loading cases is studied. Three steel lattice towers with 26, 27, and 38 discrete variables are considered. Numerical results demonstrate that the MDVC-UVPS achieved the lightest designs in all examples. The average and standard deviation values achieved from independent runs also confirm the efficiency of the hybrid method in optimal design of real-size structures. Moreover, comparison of the convergence curves and the required structural analyses indicate that MDVC-UVPS comes close to the optimum design rapidly.

Table 8.7 Performance comparison for the 244-bar power transmission tower problem

Design variable	Sections			VPS	MDVC-UVPS
	CBO	ECBO	VPS		
1	L 1 1/4 × 1 1/4 × 3/16	L 1 1/4 × 1 1/4 × 3/16	L 1 1/4 × 1 1/4 × 3/16	L 1 1/4 × 1 1/4 × 3/16	L 1 1/4 × 1 1/4 × 3/16
2	L 4 × 4 × 1/4				
3	L 2 × 2 × 1/4				
4	L 4 × 4 × 5/16	L 3 × 3 × 7/16	L 3 × 3 × 3/8	L 3 × 3 × 3/8	L 5 × 5 × 7/16
5	L 3 × 3 × 7/16	L 2 × 2 × 3/8	L 2 1/2 × 2 1/2 × 3/8	L 2 1/2 × 2 1/2 × 3/8	L 2 × 2 × 3/8
6	L 5 × 5 × 7/8	L 5 × 5 × 7/8	L 5 × 5 × 5/16	L 4 × 4 × 3/4	L 4 × 4 × 3/4
7	L 1 1/4 × 1 1/4 × 3/16	L 1 1/4 × 1 1/4 × 3/16	L 1 1/4 × 1 1/4 × 3/16	L 1 1/4 × 1 1/4 × 3/16	L 1 1/4 × 1 1/4 × 3/16
8	L 4 × 4 × 3/4	L 5 × 5 × 3/8	L 5 × 5 × 7/16	L 4 × 4 × 3/4	L 4 × 4 × 3/4
9	L 2 × 2 × 1/4				
10	L 2 × 2 × 3/8				
11	L 3 1/2 × 3 1/2 × 5/16	L 5 × 5 × 3/4	L 5 × 5 × 3/8	L 5 × 5 × 1/2	L 5 × 5 × 1/2
12	L 5 × 5 × 3/4	L 4 × 4 × 5/8	L 4 × 4 × 5/8	L 4 × 4 × 3/8	L 4 × 4 × 3/8
13	L 2 1/2 × 2 1/2 × 3/8	L 2 × 2 × 1/4			
14	L 2 × 2 × 1/8				
15	L 6 × 6 × 3/4	L 6 × 6 × 5/8	L 6 × 6 × 7/8	L 6 × 6 × 3/4	L 6 × 6 × 3/4
16	L 3 1/2 × 3 1/2 × 5/16	L 3 1/2 × 3 1/2 × 5/16	L 3 1/2 × 3 1/2 × 5/16	L 3 1/2 × 3 1/2 × 5/16	L 3 1/2 × 3 1/2 × 5/16
17	L 2 × 2 × 1/8				
18	L 2 × 2 × 1/8				
19	L 3 × 3 × 3/8	L 3 × 3 × 3/8	L 2 1/2 × 2 1/2 × 1/2	L 3 × 3 × 3/8	L 3 × 3 × 3/8
20	L 6 × 6 × 5/8	L 6 × 6 × 9/16	L 6 × 6 × 1/2	L 6 × 6 × 9/16	L 6 × 6 × 9/16
21	L 3 × 3 × 3/16				
22	L 2 × 2 × 1/4				
23	L 2 × 2 × 1/4				
24	L 2 × 2 × 1/8				
25	L 1 1/4 × 1 1/4 × 3/16	L 1 1/4 × 1 1/4 × 3/16	L 1 1/4 × 1 1/4 × 3/16	L 1 1/4 × 1 1/4 × 3/16	L 1 1/4 × 1 1/4 × 3/16
26	L 1 1/4 × 1 1/4 × 3/16	L 1 1/4 × 1 1/4 × 3/16	L 1 1/4 × 1 1/4 × 3/16	0.764982	0.755011
Volume (m ³)	0.813555	0.768159	0.833456	0.818619	
Average optimized volume (m ³)	0.899143	0.830075	0.1207	0.1053	
Standard deviation on average volume (m ³)	0.1462	0.1184			

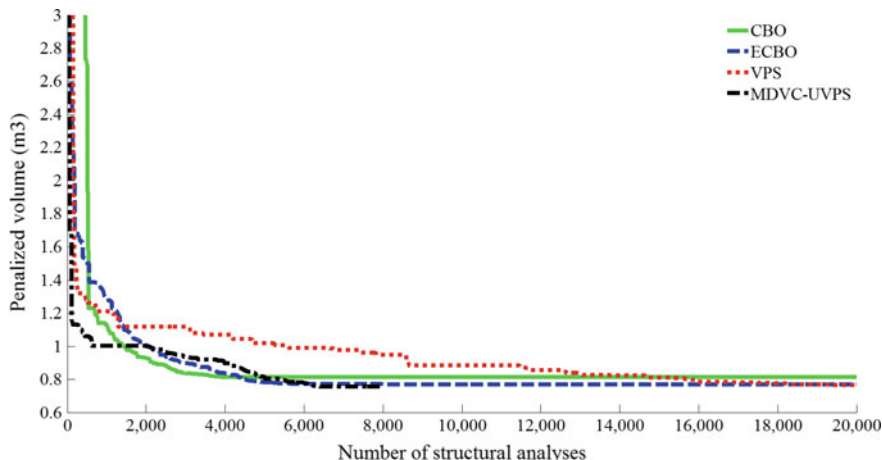


Fig. 8.6 Convergence curves for the 244-bar bar power transmission tower problem

References

1. Rao GV (1995) Optimum designs for transmission line towers. *Comput Struct* 57(1):81–92
2. Kaveh A, Gholipour Y, Rahami H (2008) Optimal design of transmission towers using genetic algorithm and neural networks. *Int J Space Struct* 23(1):1–9
3. París J, Martínez S, Navarrina F, Colominas I, Casteleiro M (2010) Structural optimization of high tension towers. In: 2nd International conference on engineering optimization, Portugal
4. Guo HY, Li ZL (2011) Structural topology optimization of high-voltage transmission tower with discrete variables. *Struct Multidiscip Optim* 43(6):851–861
5. Chunming W, Tingting S, Bin M, Jing G (2012) Research on the optimal layout of high strength steel in the transmission tower. *Phys Procedia* 33:619–625
6. Tort C, Şahin S, Hasançebi O (2017) Optimum design of steel lattice transmission line towers using simulated annealing and PLS-TOWER. *Comput Struct* 15(179):75–94
7. Kaveh A, Mahdavi VR (2014) Colliding bodies optimization: a novel meta-heuristic method. *Comput Struct* 139:18–27
8. Kaveh A, İlchi Ghazaan M (2014) Enhanced colliding bodies optimization for design problems with continuous and discrete variables. *Adv Eng Softw* 77:66–75
9. Kaveh A, İlchi Ghazaan M (2016) Vibrating particles system algorithm for truss optimization with multiple natural frequency constraints. *Acta Mech* 228(1):307–332
10. Kaveh A, İlchi Ghazaan M (2018) A new hybrid meta-heuristic algorithm for optimal design of large-scale dome structures. *Eng Optimiz* 50(2):235–252
11. Lee KS, Geem ZW, Lee SH, Bae KW (2005) The harmony search heuristic algorithm for discrete structural optimization. *Eng Optimiz* 37(7):663–684
12. Groenwold AA, Stander N, Snyman JA (1999) A regional genetic algorithm for the discrete optimal design of truss structures. *Int J Numer Methods Eng* 44:749–766
13. Saka MP (1990) Optimum design of pin-jointed steel structures with practical applications. *J Struct Eng* 116(10):2599–2620
14. Togan V, Daloglu AT (2006) Optimization of 3D trusses with adaptive approach in genetic algorithms. *Eng Struct* 28(7):1019–1027
15. American Institute of Steel Construction (AISC) (1998) Manual of steel construction: allowable stress design, Chicago, USA

Chapter 9

Optimal Seismic Design of 3D Steel Frames



9.1 Introduction

Steel buildings are preferred in residential as well as commercial buildings because of being super-quick to build on-site, as a great deal of work can be prefabricated at the factory. Moreover, these structures are flexible, which makes them quite suitable structures for resisting dynamic forces such as earthquake loads. Design of frame structures necessitates the selection of steel sections for its columns and beams from a standard steel section tables such that the frame satisfies the serviceability and strength requirements specified by the code of practice while the economy is taken into account in the overall or material cost of the frame.

Sizing optimization of frame structures which are complicated optimization problems was studied by many researchers. Hasançebi et al. [1] utilized seven meta-heuristic search algorithms (genetic algorithms, simulated annealing, evolution strategies, particle swarm optimizer, tabu search, ant colony optimization, and harmony search) to optimize real-size rigidly connected steel frames. Evolution strategies approach has been the most effective algorithm amongst the seven and simulated annealing could be considered as the second winner of this performance competition. Aydogdu and Saka [2] used ant colony optimization for optimum design of irregular steel space frames including element warping effect. Kaveh and Zakian [3] employed Charged System Search (CSS) and Improved Harmony Search (IHS) algorithms for optimal design of steel frames under seismic loading. The results show that the performance of the CSS is better than that of the IHS considering the same number of structural analyses. Hasançebi and Carbas [4] examined Bat Inspired (BI) algorithm in the context of discrete size optimization of real-size steel frames designed for minimum weight. The numerical results of the BI algorithm are compared to the previously reported solutions using different meta-heuristics in the literature and indicate robustness and efficiency of the BI algorithm for this class of problems. Talatahari et al. [5] combined the Eagle Strategy algorithm with Differential Evolution (ES-DE) to minimize the weight of

steel frames. The optimized designs obtained by the proposed algorithm are better than those found by the standard differential evolution algorithm and also very competitive with literature. The overall convergence behavior is significantly enhanced by the hybrid optimization strategy. Artar and Daloglu [6] used a method based on genetic algorithm for minimum weight design of composite steel frames with semirigid connections and column bases. Their results show that consideration of the contribution of concrete on the behavior of the floor beams enables a lighter and more economical design for steel frames with semirigid connections and column bases. Kaveh et al. [7] employed cuckoo search algorithm to optimize steel frame structures under seismic loading based on response spectral and equivalent static analyses. The effect of lateral seismic loading distribution on the achieved optimum designs was also investigated. Results show similar weights for optimum designs using spectral and equivalent static analyses; however, different material distribution and seismic behaviors are observed. Carbas [8] enhanced the performance of the firefly algorithm by suggesting two new expressions for the attractiveness and randomness parameters of the algorithm and optimized two steel space frame design examples by this method. Kaveh and Bolandgerami [9] indicated the efficiency of the cascade enhanced colliding body optimization for optimum design of large-scale space steel frames. Kaveh et al. [10] employed nine meta-heuristic algorithms to study the effect of the change in the ductility type on the structural weight. Results show that the Ordinary Moment Frame (OMF) can produce lighter designs in most cases, in spite of larger base shear. Kaveh et al. [11] studied three different types of lateral resisting steel moment frames consisting of ordinary moment frame, intermediate moment frame, and special moment frame. Optimum seismic design was performed for 3D steel moment frames with different types of lateral resisting systems.

The contribution of this chapter is concerned with optimization of steel frames under seismic loads based on response spectral. Frame members are selected from available set of steel sections for producing practically acceptable designs according to Load and Resistance Factor Design-American Institute of Steel Construction (LRFD-AISC) specification. Three irregular steel frame problems are considered to evaluate the performance of the CBO, ECBO, VPS and MDVC-UVPS algorithms [12].

9.2 Optimum Design Problem of Steel Space Frame

Structural optimization aims to design structure with minimum weight or minimize an objective function corresponding to minimal cost of the structure, while the corresponding design constraints are satisfied. The design constraints and objective function for investigated problems are explained in the following subsections.

9.2.1 Design Constraints

The design should be carried out in such a way that the frame satisfies the following constraint:

1. Strength constraints: Each frame member should have sufficient strength to resist the internal forces developed due to factored external loading.
2. Serviceability constraints: Beam deflections and lateral displacement of the frame should be less than the limits specified in the code.
3. Geometric constraints: Three types of geometric constraints are considered to satisfy practical requirements. The first type ensures that the depths of the W-shaped sections selected for the columns of two consecutive stories should be either equal to each other or the one in the above story should be smaller than the one in the below story. The second and third types of constraint make sure that if a beam is connected to flange of a column, the flange width of the beam should be less than or equal to the flange width of the column in the connection and if a beam is connected to the web of a column, the flange width of the beam should be less than or equal to $(D - 2t_b)$, where D and t_b are the depth and the flange thickness of the W-shaped section selected for column, respectively. Figure 9.1 and the following formula clarify the geometric constraints.

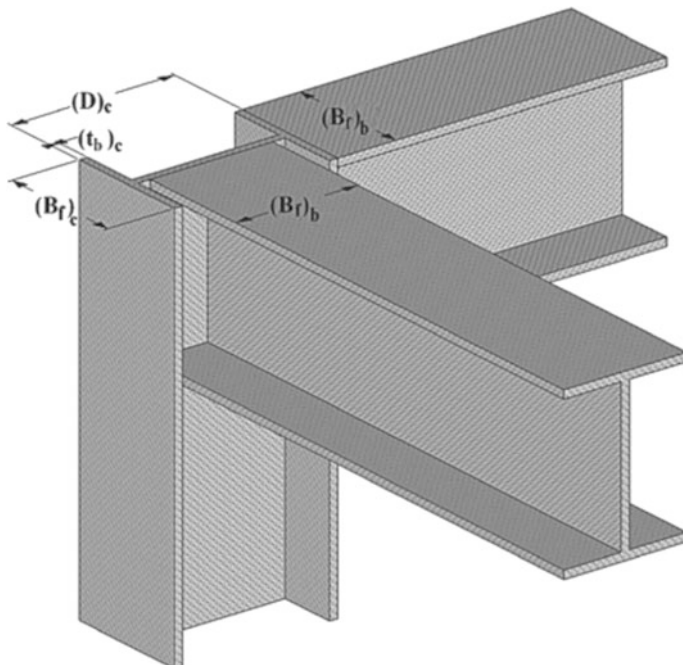


Fig. 9.1 Beam–column geometric constraints

$$\frac{(D)_i}{(D)_{i-1}} \leq 1 \quad i = 2, \dots, n_s \quad (9.1)$$

$$\frac{(B_f)_{bi}}{(B_f)_{ci}} \leq 1 \quad i = 1, \dots, n_f \quad (9.2)$$

$$\frac{(B_f)_{bi}}{(D)_i - 2(t_b)_i} \leq 1 \quad i = 1, \dots, n_w \quad (9.3)$$

where n_s , n_f , and n_w are the number of stories, the total number of joints where beams are connected to the flange of a column, and the total number of joints where beams are connected to the web of a column, respectively. $(B_f)_{bi}$ and $(B_f)_{ci}$ are the flange width of W-section selected for the beam and column at joint i , respectively.

9.2.2 The Objective Function

Sizing optimization of a steel frame with its members being collected in ng design groups can be formulated as follows:

$$\begin{aligned} \text{Find} \quad & \{X\} = [x_1, x_2, \dots, x_{ng}] \\ \text{to minimize} \quad & W(\{X\}) = \sum_{i=1}^{ng} x_i \sum_{j=1}^{\text{nm}(i)} \rho_j L_j \\ \text{subjected to:} \quad & \begin{cases} g_j(\{X\}) \leq 0, \quad j = 1, 2, \dots, nc \\ x_{i\min} \leq x_i \leq x_{i\max} \end{cases} \end{aligned} \quad (9.4)$$

where $\{X\}$ is the vector containing the design variables; $W(\{X\})$ presents the weight of the structure; $\text{nm}(i)$ is the number of members for the i th group; ρ_j and L_j denote the material density and the length of the j th member, respectively. $x_{i\min}$ and $x_{i\max}$ are the lower and upper bounds of the design variable x_i , respectively. $g_j(\{X\})$ denotes design constraints; and nc is the number of the constraints.

For constraints handling, a penalty approach is utilized. For this purpose, the objective function (Eq. 9.4) is redefined as follows:

$$P(\{X\}) = (1 + \varepsilon_1 v)^{\varepsilon_2} \times W(\{X\}) \quad (9.5)$$

where $P(\{X\})$ is the penalized cost function or the objective function to be minimized and v denotes the sum of the violations of the design constraints. In this chapter, ε_1 is set to unity and ε_2 is calculated by

$$\varepsilon_2 = 1.5 + 1.5 \times \frac{\text{iter}}{\text{iter}_{\max}} \quad (9.6)$$

where iter is the current iteration number and iter_{\max} is the total number of iterations for optimization process.

9.3 Design Examples

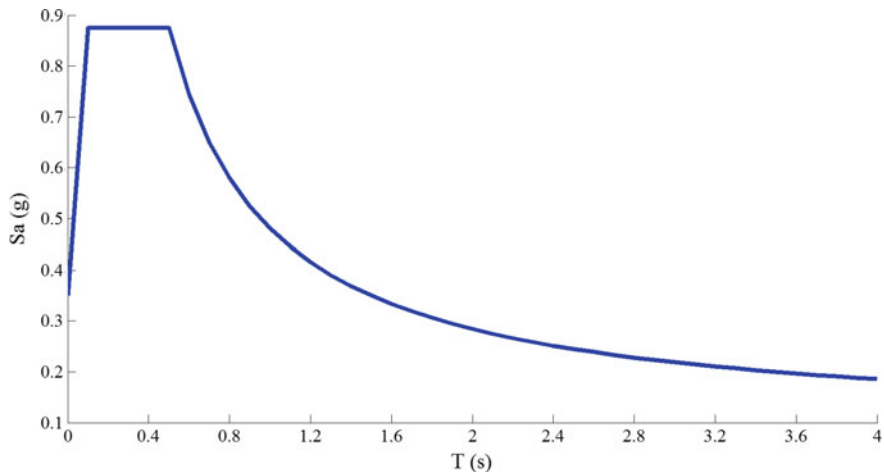
Optimum seismic designs of three steel space frames are investigated in this section. These design examples contain:

- The four-story 132-member steel frame
- The four-story 428-member steel frame
- The twelve-story 276-member steel frame

The algorithms select suitable sections from the complete W-section list given in AISC which consists of 273 sections starting from W6 × 8.5 to W14 × 730. These sections with their properties are used to prepare a design pool. The sequence numbers assigned to this pool that are sorted with respect to the area of sections are considered as design variables. In other words, the design variables represent a selection from a set of integer numbers between 1 and 273. A population of 20 agents is used for all the algorithms. In the first and the last two examples, the optimization process is terminated after 150 and 200 iterations, respectively.

The frames are subjected to gravity and earthquake loads and are designed according to the LRFD-AISC design criteria [13]. Load combinations recommended by ASCE 7–10 are considered in Ref. [14] and the frames are Intermediate Moment Frames (IMF). The gravity loads are as follows: the design dead load is 2.88 kN/m², the design live load is 2.39 kN/m², and the ground snow load is 0.755 kN/m² [15]. Iran has a long history of seismicity and has experienced destructive earthquakes since ancient times. The history and the existence of faults indicate the seismicity of metropolitan Tehran and this city are considered as high seismicity area. Therefore, the response spectrum function of Tehran is utilized in this study [16]. Figure 9.2 shows the design response spectrum as acceleration versus period. The details of this figure are reported in Table 9.1. Occupancy importance and redundancy factor are considered as 1. Modal and directional combinations of response spectrum load cases are performed by CQC and SRSS methods, respectively. In all the seismic load combinations, 100% of the design seismic force for one direction is added to the 30% of the design seismic force for the perpendicular direction. The vertical seismic load effect is also considered (S_{Ds} is set to 1.05). For the first two examples, story drift is limited to 8.75 cm and for the last problem, it is limited to 7 cm.

In the following examples, the height of each story is taken as 3.5 m and each frame member is modeled as a line element. A992 steel is used with modulus of elasticity equal to $E = 200$ GPa, yield stress of $F_y = 250$ MPa, and weight per unit volume of $\rho = 7850$ kgf/m³. Direct analysis and general second-order methods are used for the models. *Tau-b fixed* is employed for stiffness reduction method.

**Fig. 9.2** Design response spectrum**Table 9.1** Design response spectrum details

T (S)	Sa (g)	T (S)	Sa (g)
0.000	3.432	2.000	2.789
0.100	8.580	2.100	2.697
0.150	8.580	2.200	2.613
0.200	8.580	2.300	2.537
0.300	8.580	2.400	2.467
0.400	8.580	2.500	2.402
0.500	8.580	2.600	2.343
0.600	7.293	2.700	2.288
0.700	6.374	2.800	2.237
0.800	5.684	2.900	2.189
0.900	5.148	3.000	2.145
1.000	4.719	3.100	2.104
1.100	4.368	3.200	2.065
1.200	4.076	3.300	2.028
1.300	3.828	3.400	1.994
1.400	3.616	3.500	1.961
1.500	3.432	3.600	1.931
1.600	3.271	3.700	1.902
1.700	3.129	3.800	1.874
1.800	3.003	3.900	1.848
1.900	2.890	4.000	1.823

9.3.1 A Four-Story 132-Member Steel Frame

The plan and 3D views of the first example are shown in the Figs. 9.3 and 9.4, respectively. This is an irregular steel frame with 70 joints and 132 members which are collected in 16 independent design variables. The member grouping is given in Table 9.2. In order to optimize this structure by MDVC-UVPS, three stages are considered. The design variable configuration utilized for the first and second stages are listed as follows: first stage: [1 2 3 4], [5 6 7 8], [9 10 11 12], and [13 14 15 16]; second stage: [1 2], [3 4], [5 6], [7 8], [9 10], [11 12], [13 14], and [15 16].

The optimal designs found by the different algorithms are compared in Table 9.3 that shows also the corresponding structural weights and required number of structural analyses. The MDVC-UVPS obtained 304.89 kN after 1775 analyses which is better than 362.83 kN found by CBO after 2900 analyses, 325.98 kN achieved by ECBO after 2740 analyses and 349.83 kN obtained by VPS after 2720 analyses. The maximum values of the stress ratio for CBO, ECBO, VPS, and MDVC-UVPS are 85, 95, 95, and 98%, respectively. Convergence history diagrams are depicted in Fig. 9.5. It can be seen that the intermediate designs found by MDVC-UVPS are always better than those found by other algorithms.

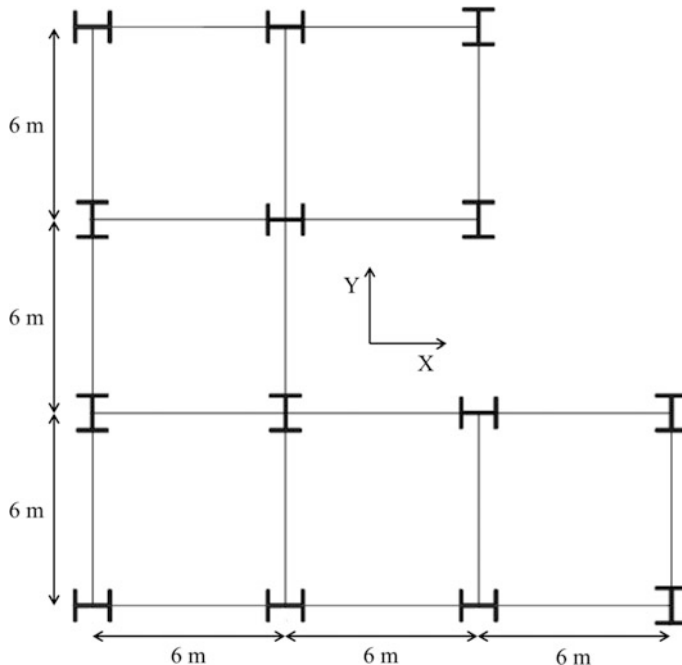


Fig. 9.3 Plan view of the four-story 132-member steel frame problem

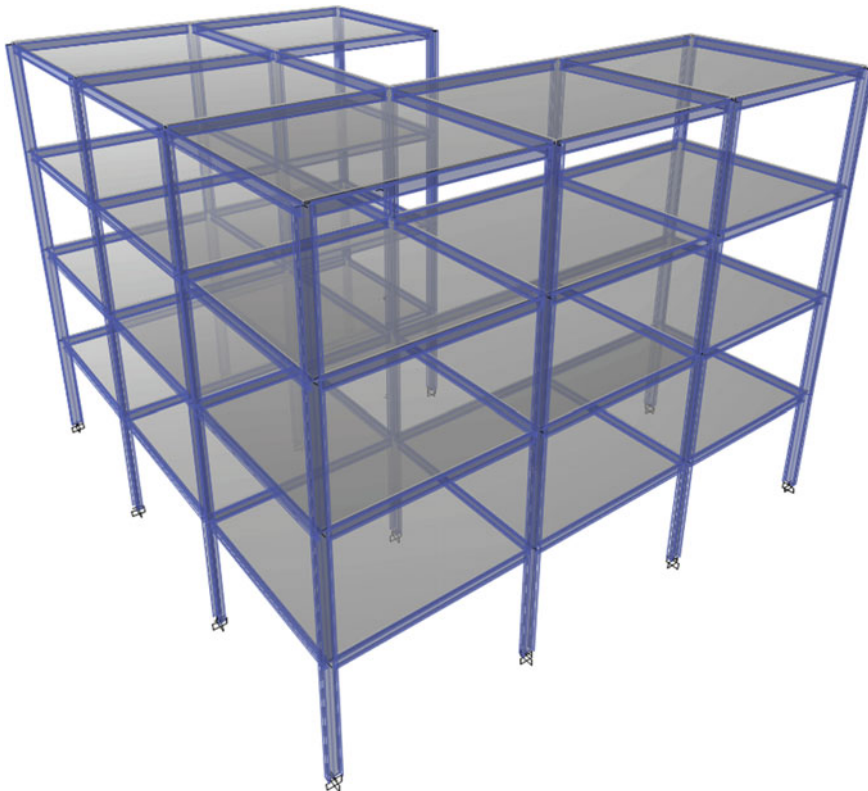


Fig. 9.4 3D view of the four-story 132-member steel frame problem with a U-shape form

Table 9.2 Member grouping of the four-story 132-member steel frame problem

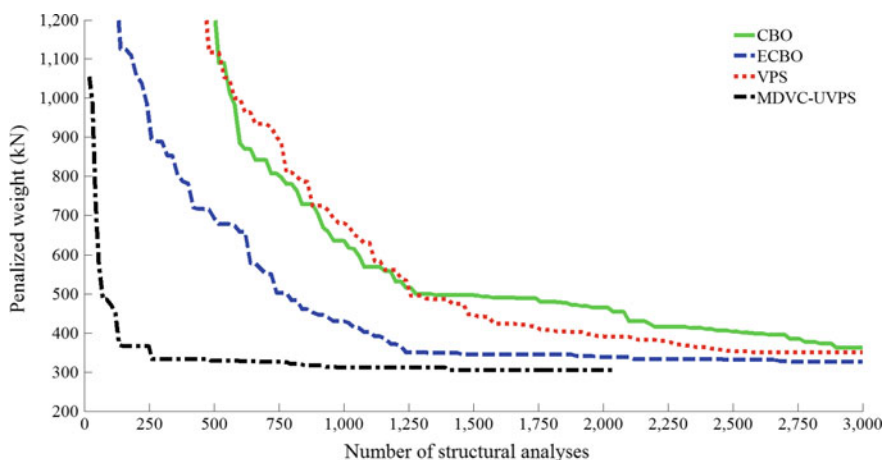
Story	Corner column	Side column	Side beam	Inner beam
1	1	5	9	13
2	2	6	10	14
3	3	7	11	15
4	4	8	12	16

9.3.2 A Four-Story 428-Member Steel Frame

The second design example is selected as a space four-story steel frame with 215 joints and 428 members. Figures 9.6 and 9.7 show the plan and 3D views of the structure. This is a size optimization problem with 20 variables and the member grouping of the frame members is listed in Table 9.4. Three stages with 5, 10, and 20 variables are considered by MDVC-UVPS algorithm. These DVCs are as

Table 9.3 Performance comparison of the four-story 132-member steel frame problem

Element group	Optimal W-shaped sections			
	CBO	ECBO	VPS	MDVC-UVPS
1	W21 × 68	W18 × 60	W18 × 97	W18 × 55
2	W14 × 82	W16 × 45	W18 × 86	W18 × 46
3	W14 × 74	W12 × 50	W18 × 76	W16 × 67
4	W14 × 99	W10 × 88	W16 × 77	W14 × 48
5	W16 × 50	W21 × 55	W18 × 50	W24 × 55
6	W14 × 68	W18 × 65	W16 × 57	W16 × 57
7	W12 × 58	W12 × 45	W12 × 50	W16 × 50
8	W10 × 88	W12 × 53	W12 × 58	W14 × 48
9	W14 × 22	W16 × 26	W14 × 22	W16 × 26
10	W12 × 26	W16 × 26	W12 × 26	W16 × 26
11	W14 × 22	W12 × 26	W14 × 22	W8 × 21
12	W10 × 22	W8 × 24	W10 × 22	W10 × 22
13	W12 × 30	W14 × 26	W14 × 26	W16 × 26
14	W14 × 26	W8 × 28	W12 × 30	W16 × 31
15	W12 × 22	W10 × 22	W12 × 19	W10 × 22
16	W6 × 25	W12 × 22	W12 × 22	W14 × 22
Weight (kN)	362.83	325.98	349.83	304.89
Number of structural analyses	2900	2740	2720	1775

**Fig. 9.5** Convergence curves for the four-story 132-member steel frame problem

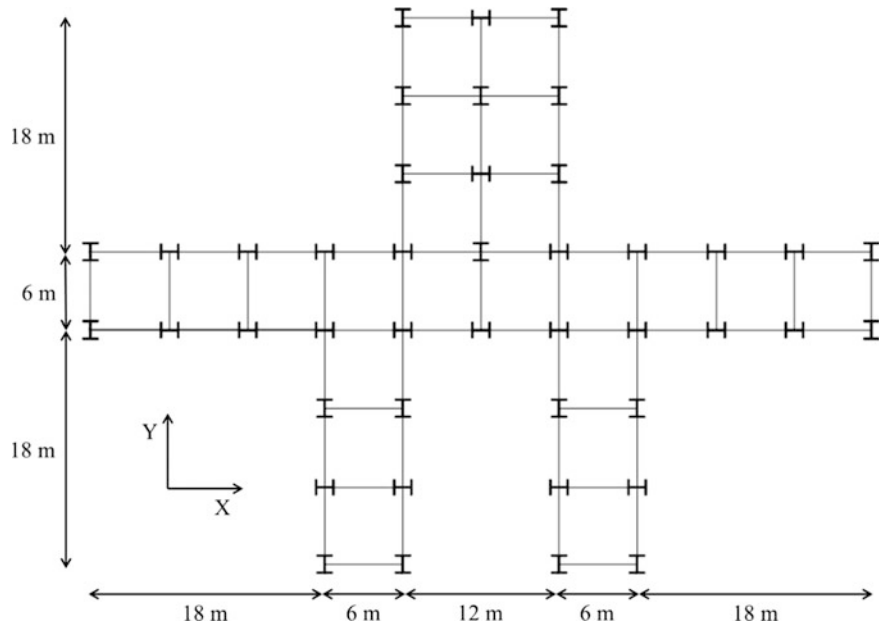


Fig. 9.6 Plan view of the four-story 428-member steel frame problem

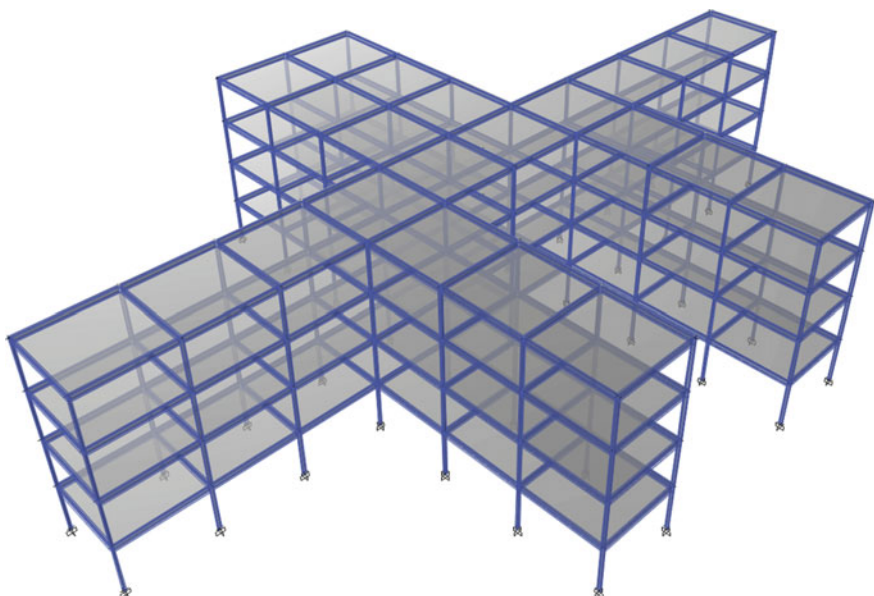


Fig. 9.7 3D view of the four-story 428-member steel frame problem with one plane of symmetry

Table 9.4 Member grouping of the four-story 428-member steel frame problem

Story	Corner column	Side column	Inner column	Side beam	Inner beam
1	1	5	9	13	17
2	2	6	10	14	18
3	3	7	11	15	19
4	4	8	12	16	20

Table 9.5 Performance comparison of the four-story 428-member steel frame problem

Element group	Optimal W-shaped sections			
	CBO	ECBO	VPS	MDVC-UVPS
1	W30 × 90	W14 × 61	W27 × 84	W16 × 50
2	W21 × 83	W12 × 58	W14 × 68	W14 × 68
3	W14 × 68	W12 × 53	W14 × 68	W14 × 53
4	W14 × 90	W10 × 54	W12 × 72	W14 × 48
5	W14 × 38	W24 × 62	W18 × 65	W21 × 68
6	W14 × 61	W21 × 68	W18 × 65	W21 × 68
7	W12 × 87	W18 × 60	W18 × 60	W21 × 50
8	W12 × 53	W16 × 67	W16 × 36	W16 × 45
9	W18 × 106	W40 × 167	W24 × 62	W27 × 84
10	W16 × 100	W40 × 149	W24 × 62	W18 × 65
11	W16 × 89	W36 × 160	W14 × 74	W18 × 86
12	W14 × 82	W33 × 169	W14 × 61	W14 × 211
13	W14 × 26	W16 × 26	W16 × 26	W14 × 26
14	W10 × 19	W12 × 30	W12 × 26	W14 × 26
15	W24 × 55	W16 × 26	W14 × 30	W16 × 26
16	W5 × 16	W12 × 30	W12 × 30	W14 × 26
17	W16 × 31	W12 × 26	W16 × 26	W12 × 26
18	W12 × 35	W12 × 30	W10 × 26	W12 × 26
19	W8 × 24	W10 × 26	W12 × 22	W12 × 22
20	W16 × 31	W10 × 22	W10 × 22	W8 × 21
Weight (kN)	1247.72	1170.9	1115.68	1064.17
Number of structural analyses	3700	3660	3520	1931

follows: first stage: [1 2 3 4], [5 6 7 8], [9 10 11 12], [13 14 15 16], and [17 18 19 20]; second stage: [1 2], [3 4], [5 6], [7 8], [9 10], [11 12], [13 14], [15 16], [17 18], and [19 20].

Table 9.5 presents the optimum designs obtained by proposed algorithms. The lightest design (i.e., 1064.17 kg) is achieved by MDVC-UVPS algorithm after 1931 analyses. The best designs obtained by the CBO, ECBO, and VPS are 1247.72,

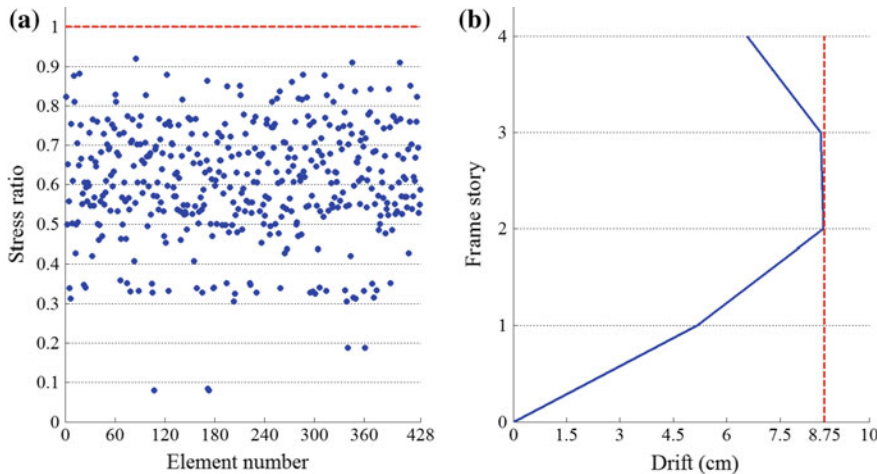


Fig. 9.8 Constraint margins for the best design obtained by MDVC-UVPS algorithm in the four-story 428-member steel frame problem: **a** element stress ratio and **b** story drift

1170.9 and 1115.68 kN, respectively. These values are found after 3700, 3660 and 3520 analyses. Figure 9.8 demonstrates the existing stress ratios and inter-story drifts for the best designs of MDVC-UVPS. The maximum stress ratio is 93% while maximum drift is 8.71 cm. The maximum stress ratios for the best designs of the CBO, ECBO, and VPS are 87, 80, and 90%, respectively.

9.3.3 A Twelve-Story 276-Member Steel Frame

The plan and 3D views of the twelve-story frame in Figs. 9.9 and 9.10 show an irregular steel space frame composed of 130 joints and 276 members. All members are categorized into 24 design groups. The member grouping is given in Table 9.6. Three stages with 8, 16, and 24 variables are considered by MDVC-UVPS algorithm. These DVCs are as follows: first stage [1 2 3 4], [5 6], [7 8 9 10], [11 12], [13 14 15 16], [17 18], [19 20 21 22], and [23 24]; second stage: [1 2], [3 4], [5], [6], [7 8], [9 10], [11], [12], [13 14], [15 16], [17], [18], [19 20], [21 22], [23], and [24].

In Table 9.7, the minimum weight designs of the twelve-story 276-member steel frame problem obtained by the proposed algorithms are compared. The MDVC-UVPS obtained the lightest design compared to other methods that is 1644.31 kN. This algorithm requires 1576 structural analyses to find the optimum solution while CBO, ECBO, and VPS require 3580, 3140, and 3440 structural analyses, respectively. The maximum values of the stress ratio for the CBO, ECBO, VPS, and MDVC-UVPS are 84, 97, 79, and 94%, respectively. Convergence history diagrams are depicted in Fig. 9.11 and demonstrated that the intermediate designs found by MDVC-UVPS are always better than those found by other

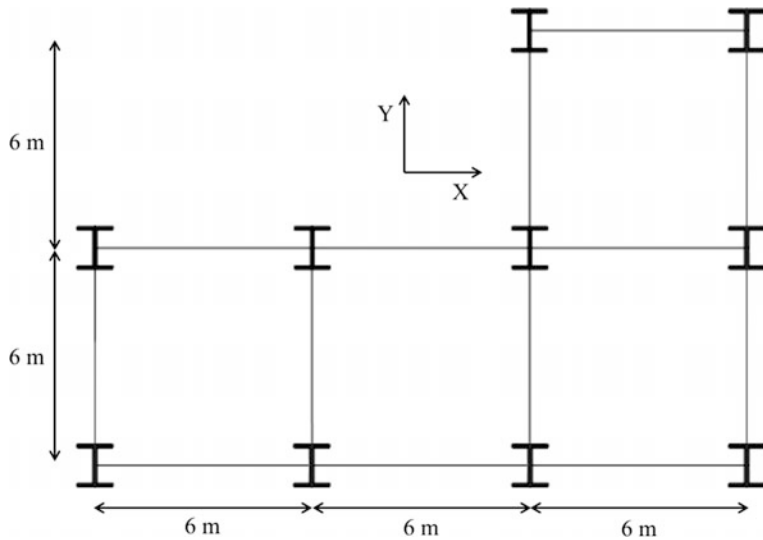


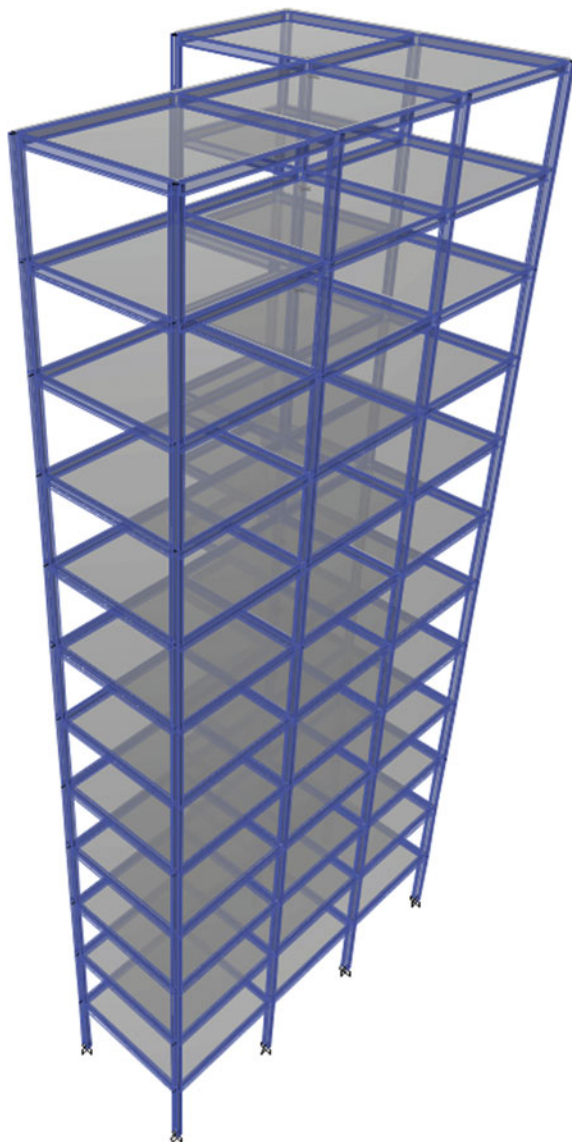
Fig. 9.9 Plan view of the twelve-story 276-member steel frame problem

algorithms. The amount of saving in structural analyses in each iteration of the MDVC-UVPS is shown in Fig. 9.12.

9.4 Concluding Remarks

Optimum design of real-size steel space frames under design code provisions is a complicated optimization problem due to the presence of large numbers of highly nonlinear constraints and discrete design variables. Main purpose of this chapter is to propose a suitable meta-heuristic optimization algorithm for optimum design of this class of problems. Three irregular steel frame optimization problems are considered and the stress constraints of LRFD-AISC, maximum lateral displacement constraints, and geometric constraints are imposed on all frames. Numerical results demonstrate that the MDVC-UVPS achieves the lightest designs in all the considered examples. This algorithm also shows a good convergence rate and comes close to the optimum design rapidly. In the first example, the best weight found by this method is 19, 7, and 14% lighter than the weight of the best design obtained using the CBO, ECBO, and VPS, respectively. In the second example, the optimum

Fig. 9.10 3D view of the twelve-story 276-member steel frame problem with corner shaped form



design produced by the hybrid method is 17, 10, and 5% lighter than the ones attained by other techniques, respectively. These values are, respectively, 15, 11, and 4% for the last example. Besides, average computational time required for MDVC-UVPS is about 35% less than the other algorithms.

Table 9.6 Member grouping of the twelve-story 276-member steel frame problem

Story	Corner column	Side column	Side beam	Inner beam
1–2	1	7	13	19
3–4	2	8	14	20
5–6	3	9	15	21
7–8	4	10	16	22
9–10	5	11	17	23
11–12	6	12	18	24

Table 9.7 Performance comparison of the twelve-story 276-member steel frame problem

Element group	Optimal W-shaped sections			
	CBO	ECBO	VPS	MDVC-UVPS
1	W30 × 173	W33 × 130	W33 × 141	W33 × 118
2	W27 × 194	W24 × 162	W33 × 130	W21 × 101
3	W24 × 146	W24 × 146	W33 × 118	W14 × 132
4	W24 × 131	W18 × 192	W30 × 132	W14 × 99
5	W16 × 67	W14 × 120	W14 × 68	W14 × 90
6	W14 × 145	W10 × 100	W12 × 79	W12 × 170
7	W36 × 231	W33 × 152	W33 × 201	W40 × 235
8	W33 × 241	W33 × 152	W30 × 211	W40 × 199
9	W27 × 258	W27 × 194	W30 × 191	W36 × 232
10	W24 × 306	W27 × 194	W27 × 194	W33 × 221
11	W14 × 176	W24 × 335	W24 × 335	W33 × 169
12	W12 × 230	W24 × 250	W24 × 250	W27 × 217
13	W16 × 40	W21 × 57	W21 × 57	W21 × 62
14	W16 × 36	W18 × 65	W16 × 67	W24 × 62
15	W16 × 45	W21 × 55	W21 × 55	W21 × 55
16	W18 × 40	W21 × 55	W18 × 65	W18 × 60
17	W16 × 45	W14 × 48	W12 × 50	W16 × 31
18	W8 × 21	W12 × 50	W12 × 53	W14 × 48
19	W27 × 217	W16 × 40	W16 × 40	W18 × 40
20	W24 × 250	W16 × 40	W16 × 45	W16 × 45
21	W36 × 182	W12 × 53	W12 × 53	W12 × 53
22	W33 × 169	W12 × 50	W12 × 50	W12 × 50
23	W8 × 31	W40 × 264	W27 × 129	W33 × 141
24	W12 × 26	W8 × 67	W8 × 67	W12 × 35
Weight (kN)	1896.06	1824.64	1716.41	1644.31
Number of structural analyses	3580	3140	3440	1576

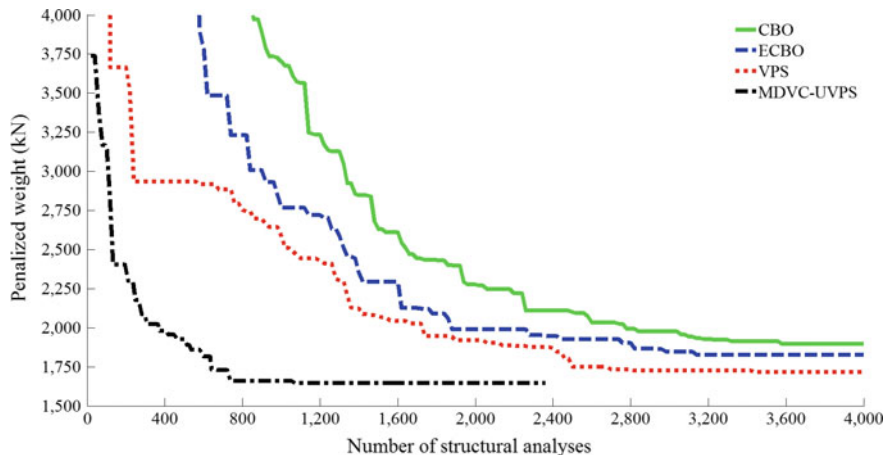


Fig. 9.11 Convergence curves for the twelve-story 276-member steel frame problem

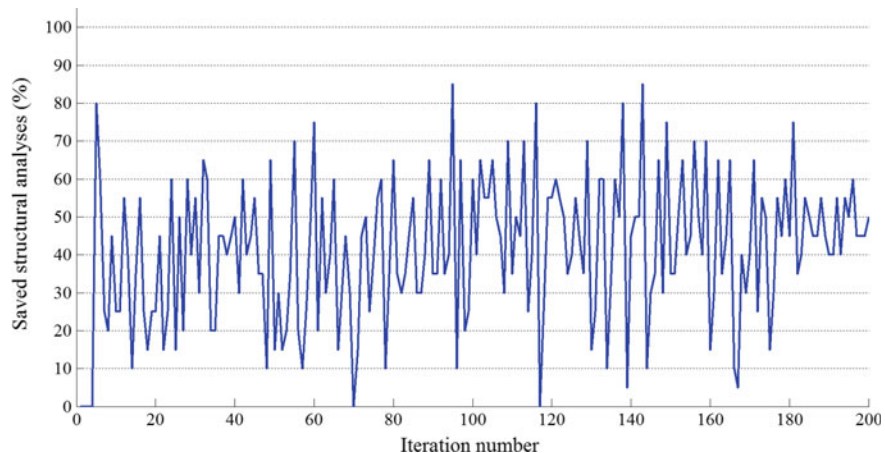


Fig. 9.12 Saving in structural analyses using the MDVC-UVPS algorithm in the twelve-story 276-member steel frame problem

References

- Hasançebi O, Çarbaş S, Doğan E, Erdal F, Saka MP (2010) Comparison of non-deterministic search techniques in the optimum design of real size steel frames. *Comput Struct* 88 (17):1033–1048
- Aydogdu I, Saka MP (2012) Ant colony optimization of irregular steel frames including elemental warping effect. *Adv Eng Softw* 44(1):150–169
- Kaveh A, Zakian P (2013) Optimal design of steel frames under seismic loading using two meta-heuristic algorithms. *J Construct Steel Res* 82:111–130

4. Hasançebi O, Carbas S (2014) Bat inspired algorithm for discrete size optimization of steel frames. *Adv Eng Softw* 67:173–185
5. Talatahari S, Gandomi AH, Yang XS, Deb S (2015) Optimum design of frame structures using the eagle strategy with differential evolution. *Eng Struct* 9:16–25
6. Artar M, Daloglu AT (2015) Optimum design of composite steel frames with semi-rigid connections and column bases via genetic algorithm. *Steel Compos Struct* 19(4):1035–1053
7. Kaveh A, Bakhshpoori T, Azimi M (2015) Seismic optimal design of 3D steel frames using cuckoo search algorithm. *Struct Des Tall Special Build* 24(3):210–227
8. Carbas S (2016) Design optimization of steel frames using an enhanced firefly algorithm. *Eng Optim* 48(12):2007–2025
9. Kaveh A, Bolandgerami A (2017) Optimal design of large-scale space steel frames using cascade enhanced colliding body optimization. *Struct Multidiscip Optim* 55(1):237–256
10. Kaveh A, Ghafari MH, Gholipour Y (2017) Optimum seismic design of steel frames considering the connection types. *J Construct Steel Res* 130:79–87
11. Kaveh A, Ghafari MH, Gholipour Y (2017) Optimal seismic design of 3D steel moment frames: different ductility types. *Struct Multidiscip Optim* 56(6):1353–1367
12. Kaveh A, Ilchi Ghazaan M (2018) Optimum seismic design of 3D irregular steel frames using modern meta-heuristic algorithms. *J Comput Civil Eng*, 32(3), 04018015
13. AISC 360-10 (2010) Specification for structural steel buildings. American Institute of Steel Construction, Chicago, Illinois 60601-1802, USA
14. ASCE 7-10 (2010) Minimum design loads for building and other structures, Chicago, USA
15. Aydoğdu İ, Akin A, Saka MP (2016) Design optimization of real world steel space frames using artificial bee colony algorithm with levy flight distribution. *Adv Eng Softw* 92:1–14
16. ICSRDB (2015) Iranian code of practice for seismic resistant design of buildings (Standard 2800), 4rd edn, PN S 253, Building and Housing Research Center of Iran

Appendix A

Configuration Processing

A.1 Introduction

For large systems, configuration processing is one of the most tedious and time-consuming parts of the analysis. Different methods have been proposed for configuration processing and data generation, among which the formex algebra of Nooshin [1, 2] is perhaps the most general tool for this purpose. Behravesh et al. [3] employed set theory and showed that some concepts of set algebra can be used to build up a general method for describing the interconnection patterns of structural systems. There are many other references on the field of data generation; however, most of them are prepared for specific classes of problem. For example, many algorithms have been developed and successfully implemented on mesh or grid generation, a complete review of which may be found in a paper by Thacker [4] and a book by Thomson et al. [5].

Graph theoretical methods for the formation of structural and finite element models are developed by Kaveh [6, 7]. In all these methods, a submodel is expressed in algebraic form and then the functions are used for the formation of the entire model. The main functions employed consist of translation, rotation, reflection, and projection, or combination of these functions. On the other hand, many structural models can be viewed as the graph products of two or three subgraphs, known as their generators. Many properties of structural models can be obtained by considering the properties of their generators. This simplifies many complicated calculations, particularly in relation with eigen solution of regular structures, as shown by Kaveh and Rahami [8, 9] and Kaveh and Mirzaie [10]. Four undirected and directed graph products are presented in [11] for the formation of structural models. The undirected products are extensively used in graph theory and combinatorial optimization, however, the directed products are more suitable for the formation of practical structural models.

Different structures are studied in this book and all of them, except the 3D frames, are analyzed using the direct stiffness method by our own codes. In this appendix, MATLAB codes for generation of the coordinates and connectivities of three different types of structures utilized in this book are developed. These

structures consist of a 1016-bar double-layer grid, a 693-bar double-layer barrel vault, and a 600-bar dome truss. Using the concepts employed in these codes, all the structures studied in the book can be simply generated.

A.2 Examples

In this section, configuration processing of three types of space structures are discussed in detail. These structures are as follows:

- A double-layer grid
- A double-layer barrel vault
- A double-layer dome.

A.2.1 Example 1

Consider a double-layer grid as shown in Fig. A.1. It is a 40×40 m grid with certain bays of equal length in two directions and the height is equal to 3 m. The structure consists of 1016 members and 320 joints. The geometry and the member's labels of the structure are depicted in Fig. A.2. The MATLAB code for generation of coordinates and connectivities of this grid is listed below.

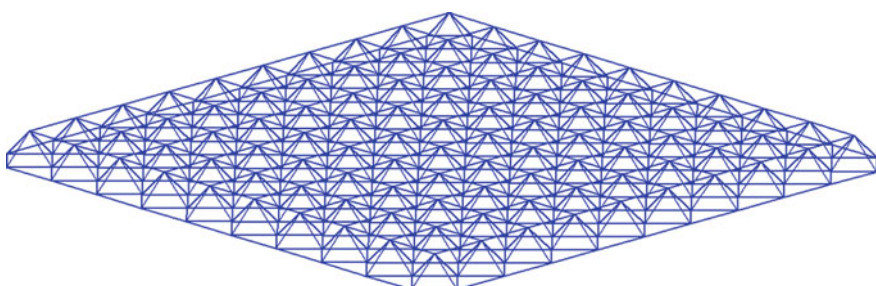


Fig. A.1 3D view of the 1016-bar double-layer grid

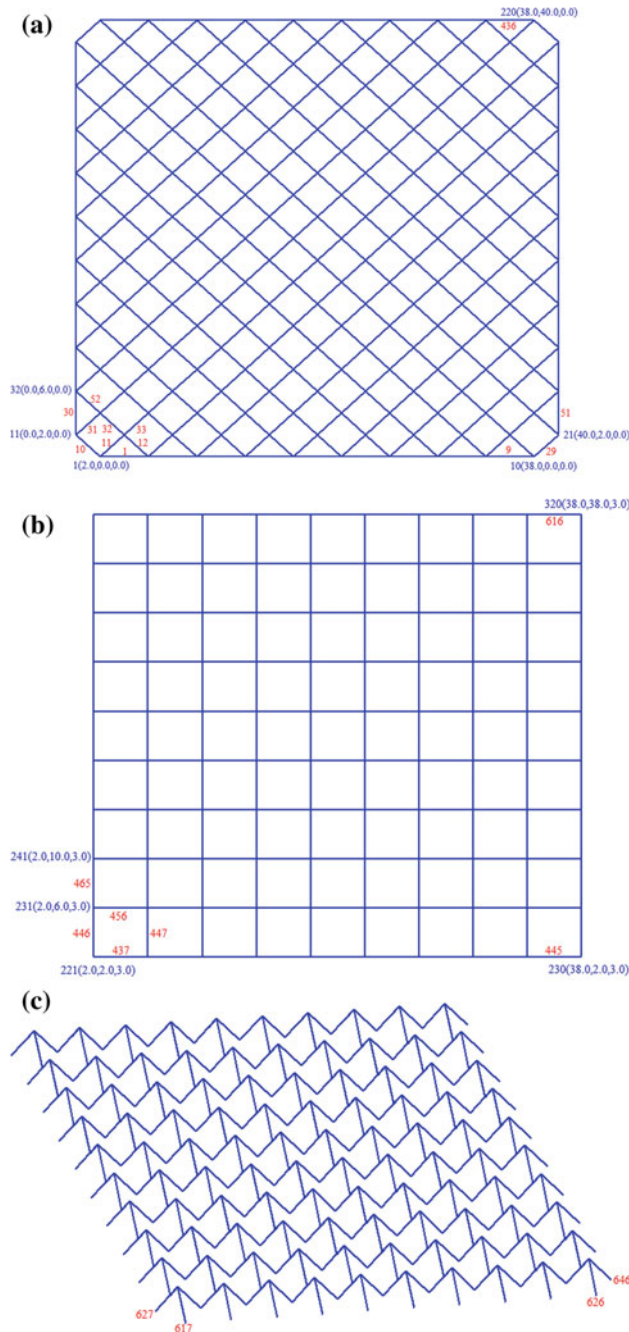


Fig. A.2 **a** bottom layer, **b** top layer, and **c** web members of the 1016-bar double-layer grid

```
% MATLAB codes for generation of coordinates and connectivities
% example1.m

% NUM_X: number of parts in x direction bottom top layer
% NUM_Y: number of parts in y direction bottom top layer
% LEN_X: length of bays in x direction
% LEN_Y: length of bays in y direction

NUM_X = 10;
NUM_Y = 10;
LEN_X = 4;
LEN_Y = 4;

% Node coordinates of bottom-layer
%   nodes: node coordinates
nodes = [];
for ny=1:NUM_Y
    x = [LEN_X / 2 + LEN_X * (0:NUM_X-1), LEN_X * (0:NUM_X)];
    y = [repmat(LEN_Y * (ny-1), 1, NUM_X), repmat(LEN_Y / 2 + LEN_Y *
        (ny - 1), 1, NUM_X + 1)];
    z = zeros(1, 2 * NUM_X + 1);
    nodes = [nodes; [x; y; z]'];
end
nodes = [nodes; [LEN_X / 2 + LEN_X * (0:NUM_X-1); repmat(LEN_Y * NUM_Y, 1,
    NUM_X); zeros(1,NUM_X) ]'];

% Node coordinates of top-layer
xTop = LEN_X/2 + repmat(LEN_X * (0:NUM_X-1), 1, NUM_Y);
yTop = LEN_Y/2 + reshape(repmat(LEN_Y * (0:NUM_Y-1), NUM_X, 1), [], 1)';
zTop = repmat(3, 1, NUM_X * NUM_Y);
nodes = [nodes; [xTop; yTop; zTop]'];

% Bottom-layer elements
%   elements: connections at elements
elements = [];
elements = [elements; [1:NUM_X-1; 2:NUM_X]'];
for ny=1:NUM_Y
    firstNodeBottomRow = (2 * NUM_X + 1) * (ny - 1) + 1;
    firstNodeTopRow = (2 * NUM_X + 1) * (ny - 1) + NUM_X + 1;
    for nx=1:NUM_X
        elements = [elements; [firstNodeBottomRow + nx - 1, firstNodeTopRow +
            nx - 1]];
    end
end
```

```

elements = [elements; [firstNodeBottomRow + nx - 1, firstNodeTopRow +
nx]];
end
for nx=1:NUM_X+1
if nx ~= 1
elements = [elements; [firstNodeTopRow + nx - 1,
firstNodeTopRow + nx - 1 + NUM_X]];
elseif ny ~= NUM_Y
elements = [elements; [firstNodeTopRow, firstNodeTopRow +
(2 * NUM_X + 1)]];
end
if nx ~= NUM_X+1
elements = [elements; [firstNodeTopRow + nx - 1,
firstNodeTopRow + nx - 1 + NUM_X + 1]];
elseif ny ~= NUM_Y
elements = [elements; [firstNodeTopRow + NUM_X, firstNodeTopRow +
NUM_X + (2 * NUM_X + 1)]];
end
end
elements = [elements; (2 * NUM_X + 1) * NUM_Y + [1:NUM_X-1; 2:NUM_X]'];

% Top-layer elements
firstNodeTopLayer = (2 * NUM_X + 1) * NUM_Y + NUM_X + 1;
for ny=1:NUM_Y
firstNode = firstNodeTopLayer + (ny - 1) * NUM_X;
elements = [elements; [firstNode:firstNode+NUM_X-2;
firstNode+1:firstNode+NUM_X-1']];
if ny ~= NUM_Y
elements = [elements; [firstNode:firstNode+NUM_X-1;
firstNode+NUM_X:firstNode+2*NUM_X-1']];
end
end

% Web elements
for ny=1:NUM_Y
firstNodeBot = (2 * NUM_X + 1) * (ny - 1) + 1;
firstNodeTop = firstNodeTopLayer + (ny - 1) * NUM_X;
elements = [elements; [firstNodeBot:firstNodeBot+NUM_X-1;
firstNodeTop:firstNodeTop+NUM_X-1']];
for nx=1:NUM_X
elements = [elements; [firstNodeBot + NUM_X + nx - 1, firstNodeTop +

```

```

nx - 1]];
elements = [elements; [firstNodeBot + NUM_X + nx, firstNodeTop + nx -
1]];
end
elements = [elements; [firstNodeBot+2*NUM_X+1:firstNodeBot+3*NUM_X;
firstNodeTop:firstNodeTop+NUM_X-1']];
end

```

A.2.2 Example 2

The double-layer barrel vault presented in Fig. A.3 consists of 693 members and 259 joints. The geometry and the member's labels of the structure are shown in Fig. A.4.

In geometry, a circular segment is a region of a circle which is “cut off” from the rest of the circle by a chord. Let R be the radius of the circle, θ the central angle, c the chord length, s the arc length, h the height of the segment, and d the height of the triangular portion (Fig. A.5); therefore, we have

$$R = h + d = \frac{h}{2} + \frac{c^2}{8h} \quad (\text{A.1})$$

$$\theta = 2 \arctan \frac{c}{2d} \quad (\text{A.2})$$

For the top layer of the barrel vault, $h_T = 5.75$ m and $c_T = 22.9$ m. Therefore, R_T and θ_T are 14.275 m and 1.862 rad, respectively. For the bottom layer, $h_B = 4.25$ m and $c_B = 19.03$ m. Thus, R_B and θ_B are 12.776 m and 1.680 rad, respectively.

The connections at elements and node coordinates of the double-layer barrel vault can be generated by the following MATLAB code.

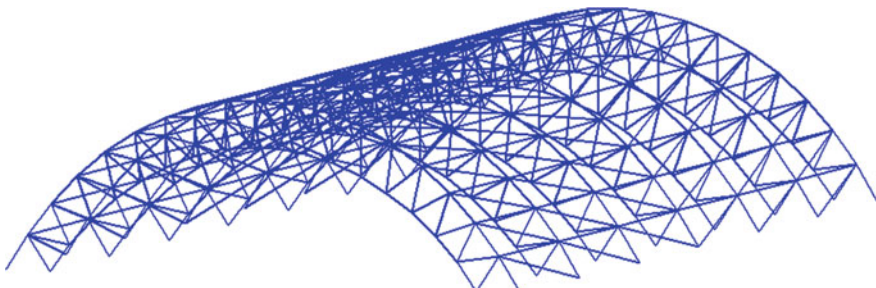


Fig. A.3 3D view of the 693-bar double-layer barrel vault

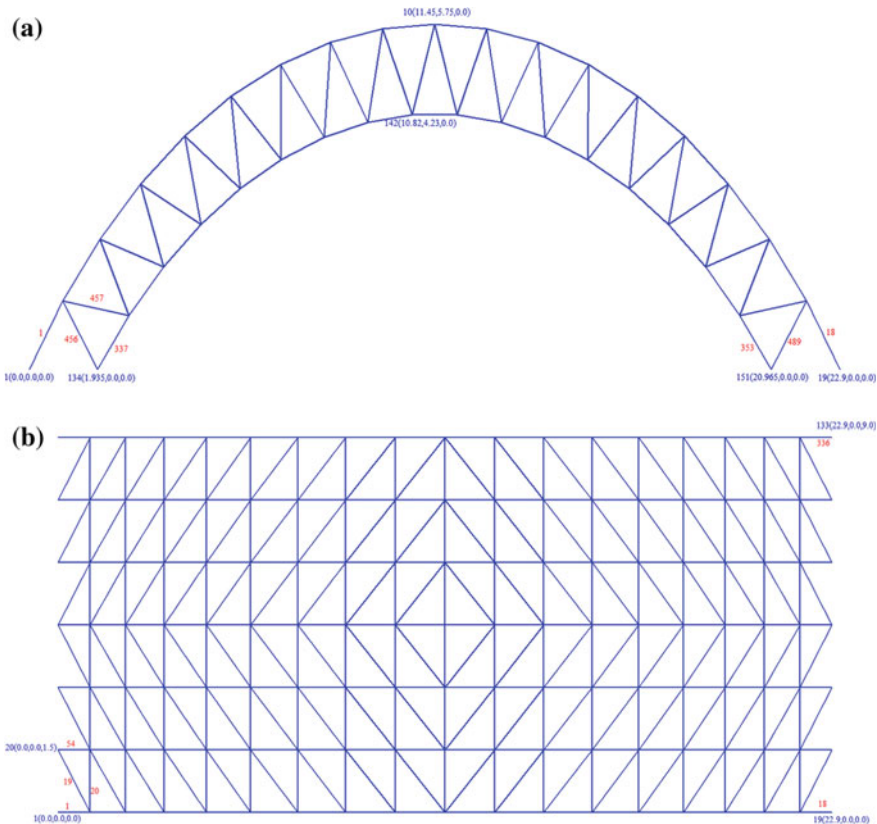


Fig. A.4 **a** flatten cross-sectional view and **b** plan view of the 693-bar double-layer barrel vault

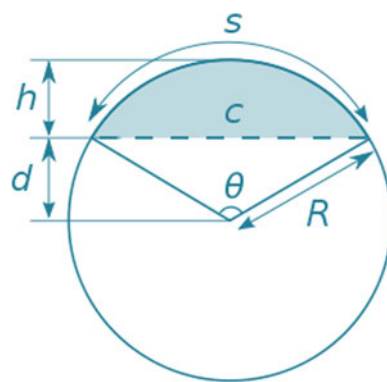


Fig. A.5 A circular segment is enclosed between a chord (the dashed line) and the arc whose endpoints equal the chord

```
% MATLAB codes for generation of coordinates and connectivities
% example2.m

%NUM_X: number of bays in x direction for top layer
%NUM_Z: number of bays in z direction
NUM_X = 18;
NUM_Z = 6;

% Node coordinates of top-layer
% H_TOP: height of segment for top layer
% C_TOP: chord length for top layer
% R_TOP: radius of circle for top layer
% THETA_TOP: central angle for top layer
% nodes: node coordinates

H_TOP = 5.75;
C_TOP = 22.9;
R_TOP = (H_TOP/2) + (C_TOP^2)/(8*H_TOP);
THETA_TOP = 2 * atan(C_TOP/(2*(R_TOP-H_TOP)));
nodes = [];
for nz=1:NUM_Z+1
    x = sin(THETA_TOP/2) - cos((pi - THETA_TOP)/2 + (0:NUM_X) *
        (THETA_TOP / NUM_X));
    y = -cos(THETA_TOP/2) + sin((pi - THETA_TOP)/2 + (0:NUM_X) *
        (THETA_TOP / NUM_X));
    nodes = [nodes; [R_TOP * x; R_TOP * y; repmat(9 / NUM_Z * (nz - 1), 1,
        NUM_X+1)']];
end

% Node coordinates of bottom-layer
% H_BOT: height of segment for bottom layer
% C_BOT: chord length for bottom layer
% R_BOT: radius of circle for bottom layer
% THETA_BOT: central angle for bottom layer

H_BOT = 4.25;
C_BOT = 19.03;
R_BOT = (H_BOT/2) + (C_BOT^2)/(8*H_BOT);
THETA_BOT = 2 * atan(C_BOT/(2*(R_BOT-H_BOT)));
for nz=1:NUM_Z+1
    x = sin(THETA_BOT/2) - cos((pi - THETA_BOT)/2 + (0:NUM_X-1) *
        (THETA_BOT / (NUM_X - 1)));
    y = -cos(THETA_BOT/2) + sin((pi - THETA_BOT)/2 + (0:NUM_X-1) *
        (THETA_BOT / (NUM_X - 1)));
    nodes = [nodes; [1.935 + R_BOT * x; R_BOT * y; repmat(9 / NUM_Z *
```

```

        (nz - 1), 1, NUM_X)]'];
end

% Top-layer elements
%   elements: connections at elements
elements = [];
for nz=1:NUM_Z+1
    firstNode = (nz - 1) * (NUM_X + 1) + 1;
    elements = [elements; [firstNode:firstNode+NUM_X-1;
                           firstNode+1:firstNode+NUM_X']];
if nz < NUM_Z+1
    for nx=1:NUM_X
        if (nx <= NUM_X/2 && nz <= NUM_Z/2) ||
           (nx > NUM_X/2 && nz > NUM_Z/2)
            elements = [elements; [firstNode + nx, firstNode + nx +
                                   NUM_X]];
        else
            elements = [elements; [firstNode + nx - 1, firstNode + nx +
                                   NUM_X + 1]];
        end
        if nx ~= NUM_X
            elements = [elements; [firstNode + nx, firstNode + nx +
                                   NUM_X + 1]];
        end
    end
end
elements = [elements; [firstNode + nx - 1, firstNode + nx +
                       NUM_X + 1]];
end

% Bottom-layer elements
for nz=1:NUM_Z+1
    firstNode = (NUM_X + 1) * (NUM_Z + 1) + (nz - 1) * NUM_X + 1;
    elements = [elements; [firstNode:firstNode+NUM_X-2;
                           firstNode+1:firstNode+NUM_X-1']];
end

% Web elements
for nz=1:NUM_Z+1
    firstNodeBot = (NUM_X + 1) * (NUM_Z + 1) + (nz - 1) * NUM_X + 1;
    firstNodeTop = (nz - 1) * (NUM_X + 1) + 1;
    for nx=1:NUM_X-1
        elements = [elements; [firstNodeBot + nx - 1, firstNodeTop + nx]];
        elements = [elements; [firstNodeBot + nx, firstNodeTop + nx]];
    end
end

```

A.2.3 Example 3

The dome truss shown in Fig. A.6 consists of 600 elements and 216 joints. Fig. A.7 presents a substructure in more detail for nodal numbering and coordinates. The following MATLAB code is developed to generate the dome from its substructure.

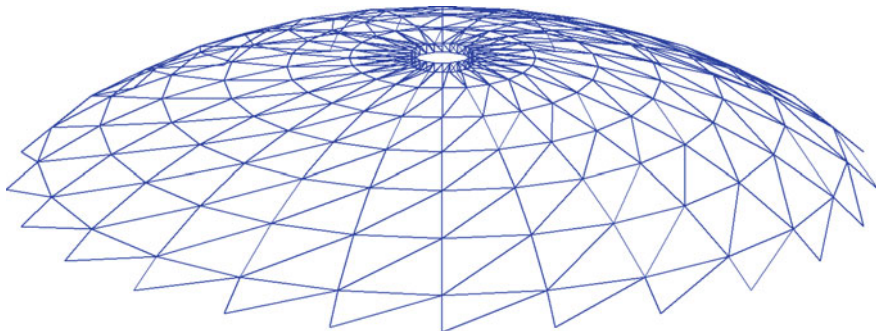
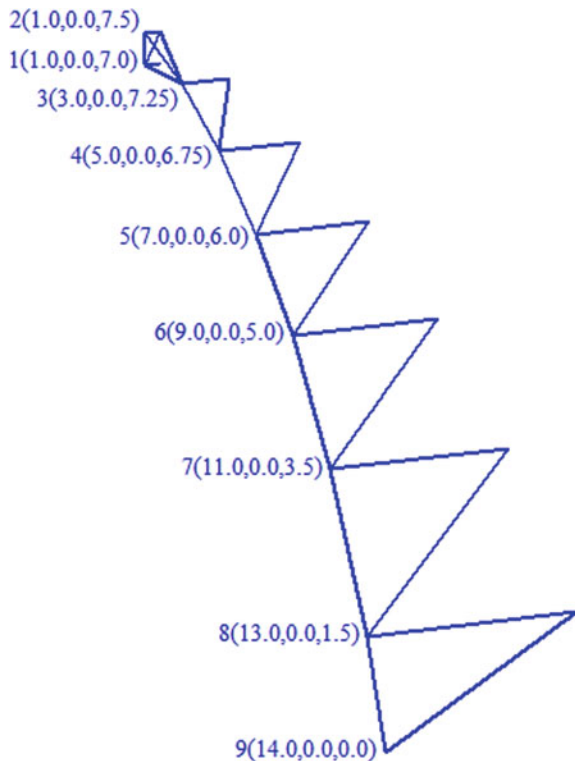


Fig. A.6 3D view of the 600-bar dome truss

Fig. A.7 A substructure of the 600-bar dome truss



```
% MATLAB codes for generation of coordinates and connectivities
% example3.m

% NUM_S: number of substructures
% NUM_NODE: number of substructure nodes
% THETA: angle of revolution
% RADIUS: distance of the the substructure nodes from z axis
% % Z_COORDS: z coordinates of substructure nodes

NUM_S = 24;
NUM_NODE = 9;
THETA = 2 * pi / NUM_S;
RADIUS = [1 1 3 5 7 9 11 13 14];
Z_COORDS = [7 7.5 7.25 6.75 6 5 3.5 1.5 0];

% Node coordinates
%   nodes: node coordinates
nodes = [];
for ns=1:NUM_S
    nodes = [nodes; [RADIUS * cos((ns-1) * THETA); RADIUS * sin((ns-1) *
    THETA); Z_COORDS]'];
end

% Elements
%   elements: connections at elements
elements = [];
for ns=1:NUM_S
    firstNodeCur = (ns - 1) * NUM_NODE + 1;
    if ns ~= NUM_S
        firstNodeNext = firstNodeCur + NUM_NODE;
    else
        firstNodeNext = 1;
    end
    elements = [elements; [firstNodeCur:firstNodeCur+NUM_NODE-2;
        firstNodeCur+1:firstNodeCur+NUM_NODE-1']];
    elements = [elements; [firstNodeCur, firstNodeCur + 2]];
    elements = [elements; [firstNodeCur:firstNodeCur+NUM_NODE-2;
        firstNodeNext:firstNodeNext+NUM_NODE-2']];
    elements = [elements; [firstNodeCur+2:firstNodeCur+NUM_NODE-1;
        firstNodeNext+1:firstNodeNext+NUM_NODE-2']];
    elements = [elements; [firstNodeCur, firstNodeNext + 1]];
end
```

References

1. Nooshin H (1975) Algebraic representation and processing of structural configurations. *Comput Struct* 5(2):119–130
2. Nooshin H (1984) Formex configuration processing in structural engineering. Elsevier Applied Science Publishers Ltd, Essex, U.K.
3. Behravesh A, Kaveh A, Nani M, Sabet S (1988) A set theoretical approach for configuration processing. *Comput Struct* 30(6):1293–1302
4. Thacker WC (1980) A brief review of techniques for generating irregular computational grids. *Int J Numer Methods Eng* 15(9): 1335–1341
5. Thompson JF, Warsi ZU, Mastin CW (1985) Numerical grid generation: foundations and applications. Elsevier, Amsterdam
6. Kaveh A (1993) A graph-theoretical approach to configuration processing. *Comput Struct* 48 (2):357–363
7. Kaveh A (2004) Structural mechanics: graph and matrix methods. 3rd edn. Research Studies Press, Somerset, UK
8. Kaveh A, Rahami H (2006) Block diagonalization of adjacency and Laplacian matrices for graph product; applications in structural mechanics. *Int J Numer Methods Eng* 68(1):33–63
9. Kaveh A, Rahami H (2005) A unified method for eigendecomposition of graph products. *Int J Numer Methods Biomed Eng* 21(7):377–388
10. Kaveh A, Mirzaie R (2008) Minimal cycle basis of graph products for the force method of frame analysis. *Int J Numer Methods Biomed Eng* 24(8):653–669
11. Kaveh A, Kohestani K (2008) Graph products for configuration processing of space structures. *Comput Struct* 86(11–12):1219–1231